



**UNIVERSITY OF
BIRMINGHAM**

**CLUTTER ANALYSIS AND SIMULATION IN FORWARD
SCATTER MICRO RADAR NETWORK**

By

Nor Ayu Zalina Binti Zakaria

**A thesis submitted to School of Electronic, Electrical and
Computer Engineering of The University of Birmingham**

for the degree of

DOCTOR OF PHILOSOPHY

2016

UNIVERSITY OF
BIRMINGHAM

University of Birmingham Research Archive

e-theses repository

This unpublished thesis/dissertation is copyright of the author and/or third parties. The intellectual property rights of the author or third parties in respect of this work are as defined by The Copyright Designs and Patents Act 1988 or as modified by any successor legislation.

Any use made of information contained in this thesis/dissertation must be in accordance with that legislation and must be properly acknowledged. Further distribution or reproduction in any format is prohibited without the permission of the copyright holder.

Abstract

Over the past few years, numbers of research have been carried out to investigate the clutter characteristic especially for conventional monostatic and bistatic radar detection (mostly in maritime and airborne using Ultra Wide Band radar and Synthetic Aperture Radar) and not specifically on Forward Scatter Radar (FSR). FSR provides an efficient approach for detection of stealth target, simplicity of the hardware design, increase the power budget and work in all weather operation. One of the limitations in forward scatter radar is the range resolution. Clutter mainly from the surrounding vegetation is picked up from a large area illuminated by transmitter and receiver which is located on the ground. Vegetation clutter is a significant factor that limits the performance of ground based Forward Scatter Radar.

In this research, the analysis is focused on clutter on ground-based Forward Scatter Micro Radar system network where the clutter characteristics are studied for different environmental conditions such as different land sites, wind and weather conditions for different carrier frequencies. These comprehensive analyses are used eventually to determine the clutter characteristics and are used for clutter modelling in order to create similar clutter-like signal that can be used to develop a synthetic environment for Forward Scatter Radar detection performance analysis in the future.

Three main works have been done; 1) real measurements to determine clutter characteristic for FSR based on statistical analysis from a number of experiments; 2) modelling and simulation of clutter signal based on real signal characteristics and 3) the comparison of simulated and measured signals.

Acknowledgements

First of all, I am really grateful and thanks to Allah the Al-Mighty who gave me the strength and guided me throughout my PhD journey and my life. Then I would like to express my sincere gratitude to my supervisors Prof. Mike Cherniakov and Dr Marina Gashinova for the continuous support of my PhD study and related research. Their patience, motivation, guidance and criticism helped me to overcome many problems not only towards my research and writing of this thesis but as well as in my life at the time. I could not have imagined having a better supervisors and mentor for my PhD study.

I would also like to thank my fellow friends in Microwave Integrated System Laboratory, you know who you are; for the great years we spent together especially Dr Vladimir Sizov. Thank you for the encouragement, helpful discussion and companion during my measurements in rainy, foggy and cold weather. I will never forget that.

My sincere thanks to my grant sponsors, University of Birmingham and University Technology MARA who have provided financial support throughout my study and made this opportunity possible.

Last but not the least, I would like to thank my family, my parents for always supporting me spiritually throughout PhD journey and my life in general. My husband Mohd Ali Supian, my kids Emir Zikry, Erisyazara and Eizara, thanks for your patience and endless support. Love you all and this thesis is dedicated to you all.

Table of Contents

CHAPTER 1: INTRODUCTION	1
1.1 Background	1
1.2 Motivation for The Present Work	3
1.3 Problem Statement and Original Work	5
1.4 Thesis Organisation	7
 CHAPTER 2: BASIC PRINCIPLE OF FORWARD SCATTER RADAR	 8
2.9 Introduction	8
2.9 Radar Overview	8
2.9 Basic System Configurations	10
2.9 Forward Scatter Radar	12
2.9 Forward Scatter Radar Basis Equations	14
2.5.1 Doppler Relationships	15
2.5.2 Radar Cross Section	18
2.9 Current Studies On Forward Scatter Radar	19
2.9 Clutter	23
2.7.1 Volume Distributed Clutter	23
2.7.2 Surface Distributed Clutter	24
2.7.3 Foliage Clutter	25
2.7.4 Clutter Modelling Approach	26
2.9 Current Studies on Radar Clutter	27
2.9 Summary	29
 CHAPTER 3: EXPERIMENTAL DATA COLLECTION	 31
3.1 Introduction	31

3.2	Experimental Set Up	31
3.3	Hardware Assembly	36
3.4	Measurement Test Sites	39
3.5	Method of Measurements	50
3.6	Measurements	51
3.7	Data Processing	60
3.8	Summary	65

CHAPTER 4: EXPERIMENTAL CLUTTER ANALYSIS **66**

4.1	Introduction	66
4.2	Physical Model of Vegetation Clutter	66
4.2.1	Pendulum Experiment	67
4.3	Introduction to Clutter Properties	71
4.3.1	Signal Standard Deviation	71
4.3.2	Power Spectral Density	71
4.3.3	Probability Density Function	72
4.3.4	Cumulative Distribution Function	74
4.3.5	Dynamic Range	74
4.4	Results from Different Clutter properties	75
4.4.1	Clutter Versus Test Sites	77
4.4.2	Clutter Versus Carrier Frequencies	79
4.4.3	Clutter Versus Baselines	80
4.4.4	Clutter Versus Different Weather	81
4.5	Clutter Results Based on Different Wind Speed from Short Term Measurement	83
4.5.1	Doppler Signal Output for Low Wind Speed	84
4.5.2	Doppler Signal Output for Medium Wind Speed	90
4.5.3	Doppler Signal Output for Strong Clutter	96
4.5.4	Doppler Signal Output for Very Strong Clutter	101
4.5.5	Summary of Clutter Results Based on Different Wind Speeds	107
4.6	Clutter Results Based on Signal's Standard Deviation from Long Term Measurement	101

4.6.1	64 MHz Channel	112
4.6.2	135 MHz Channel	114
4.6.3	173 MHz Channel	115
4.6.4	434 MHz Channel	117
4.6.5	Summary of Clutter Results Based on Signal Standard Deviation	119
4.7	Summary	123
CHAPTER 5: EMPIRICAL MODEL OF CLUTTER		124
5.1	Introduction	124
5.2	The Model Structure	124
5.2.1	Stage 1: Generating Stationary Clutter	126
5.2.2	Stage 2: Generating Time Varying Envelope of Non-stationary Clutter	128
5.2.3	Stage 3: Generating Gaussian Noise	131
5.3	Clutter Generation	132
5.4	Modelled Clutter Parameter Estimation	133
5.4.1	Simulated Low Clutter Strength	133
5.4.2	Simulated Medium Clutter Strength	139
5.4.3	Simulated Strong Clutter Strength	144
5.4.4	Simulated Very Strong Clutter Strength	149
5.5	Comparison of The Empirical Model and The Recorded Clutter	154
5.5.1	Simulated Versus Measured Clutter for Different Clutter Strengths	155
5.5.2	Simulated Versus Measured Clutter for Different Frequencies	160
5.6	Summary	164
CHAPTER 6: CONCLUSION AND FUTURE WORK		165
REFERENCES		169

APPENDIX A:	174
Hardware Description	
Matlab Programs	
APPENDIX B:	198
Explanation of Data processing	
Databases for Long Term and Short Term Measurement	
APPENDIX C:	228
Publications	

List of Figures

CHAPTER 1: INTRODUCTION

Figure 1.1: The concept of the FSR micro-sensors radar network	2
Figure 1.2: Clutter characteristic analysis and simulation for FSR micro sensor flowchart	6

CHAPTER 2: BASIC PRINCIPLE OF FORWARD SCATTER RADAR

Figure 2.1: Radar principle	10
Figure 2.2: Radar system configurations, (a) monostatic radar, (b) bistatic radar, (c) multistatic radar and (d) forward scatter radar	11
Figure 2.3: Illustration of FSR	13
Figure 2.4: Illustration of sound waves for a moving target (Doppler effect)	16
Figure 2.5: Doppler effect for moving target in target trajectory and the total received power	17
Figure 2.6: FSR target detection and classification block diagram	20

CHAPTER 3: EXPERIMENTAL DATA COLLECTION

Figure 3.1: Testing equipment, (a) 3-channels equipment, (b) 4-channels equipment	32
Figure 3.2: Simplified hardware block-diagram	33
Figure 3.3: 3 channels and 4-channels equipment position during the experiment	34
Figure 3.4: Helical monopole antennas	35
Figure 3.5: Directional Yagi antenna on tripod	35
Figure 3.6: 4-channels transmitter and receiver modules assembly	36
Figure 3.7: 4-channels equipment assembly in the container	37
Figure 3.8: FSR equipment and video camera and on positions (left – receiver; right – transmitter, in the middle – video camera and IR projector, one of four)	38

Figure 3.9: Central post (left – FSR data acquisition and video surveillance computers; right – receiving antennas for wireless cameras and weather station	38
Figure 3.10: Airfield test site	40
Figure 3.11: Shenneleys Park test site	41
Figure 3.12: Metchley lane sport pitch site	42
Figure 3.13: Roke Manor test site	43
Figure 3.14: Long term trials position in Horton Grange	44
Figure 3.15: Botanical garden in the University of Birmingham	45
Figure 3.16: Lickey Hills Country Park test site	46
Figure 3.17: Cleehill test site	47
Figure 3.18: Malvern Hills test site	48
Figure 3.19: Portable weather station on the roof of Land Rover	52
Figure 3.20: (a) Portable station wind station (b) Roof top wind station	53
Figure 3.21: Wind Speed Comparison between roof top station and portable station in three different wind conditions; (a) Strong (b) Medium (c) low	54
Figure 3.22: Example equipment position of short measurement in Botanical garden with 100 m baseline	56
Figure 3.23: Test site in Horton Grange (View from position of camera 2)	58
Figure 3.24: Test site in Horton Grange (View from all cameras)	59
Figure 3.25: Database Test site in Horton Grange Form	60
Figure 3.26: Real signal processing program layout using Matlab software	62
Figure 3.27: Example of 64 MHz output results	63
Figure 3.28: Main program of long term measurement (run_all_measured_ cluttersignal.mat)	64

CHAPTER 4: EXPERIMENTAL CLUTTER ANALYSIS

Figure 4.1: Vegetation model as number of pendulums	68
Figure 4.2: Pendulum oscillating results for three different frequencies and magnitude of oscillation	69
Figure 4.3: Results from Doppler return model from 30 pendulums, (a) topology, (b) signal's return model, and (c) PSD	70

Figure 4.4: Weibull distribution graph with shape factor n	73
Figure 4.5: Clutter record (a) 64 MHz non-stationary clutter, (b) Clutter envelope PSD, (c) Clutter signal PSD	76
Figure 4.6: Clutter power versus frequency and leakage level versus frequency and range	77
Figure 4.4: Clutter power spectrum for different test sites	79
Figure 4.8: Clutter power spectrum for different carrier frequencies	80
Figure 4.9: Clutter power spectrum for different baseline distances	81
Figure 4.10: PSD for clutter during snow and rainy day	82
Figure 4.5: Clutter power spectrum for different wind speeds	83
Figure 4.6: Measured Doppler signals at 64 MHz, 135 MHz, 173 MHz and 434 MHz	84
Figure 4.7: Envelopes for all signal frequencies	86
Figure 4.8: Power Spectral Density for clutter envelopes with 0.1 cut-off frequency (a) normalized (b) absolute value	87
Figure 4.9: PSD of clutter signals for all frequency channels at MHz, 135 MHz, 173 MHz and 434 MHz for low clutter	87
Figure 4.16: (a) PSD comparison for low clutter for all frequency channels, (b) Cumulative distribution for all frequency channels	88
Figure 4.17: Weibull Distribution of a measured clutter at 64 MHz, 135 MHz, 173 MHz, and 434 MHz	89
Figure 4.18: Measured Doppler signals at 64 MHz, 135 MHz, 173 MHz and 434 MHz for medium clutter	91
Figure 4.19: Envelopes for all signal frequencies for medium clutter	92
Figure 4.20: Power Spectral Density for clutter envelopes 0.1 cut-off frequency (a) normalized (b) absolute value for medium clutter	93
Figure 4.10: PSD of clutter signals for all frequency channels at MHz, 135 MHz, 173 MHz and 434 MHz for low clutter	94
Figure 4.11: (a) PSD comparison for medium clutter for all frequency channels, (b) Cumulative distribution for all frequency channels	94
Figure 4.12: Weibull Distribution of a measured clutter at 64 MHz, 135 MHz, 173 MHz and 434 MHz	95

Figure 4.13: Measured Doppler signals at 64 MHz, 135 MHz, 173 MHz and 434 MHz for strong clutter	96
Figure 4.25: Envelopes for all signal frequencies for strong clutter	98
Figure 4.26: Power Spectral Density for clutter envelopes 0.1 cut-off frequency normalized (b) absolute value for strong clutter	98
Figure 4.27: PSD of clutter signals for all frequency channels at 64 MHz, 135 MHz, 173 MHz and 434 MHz for strong clutter	99
Figure 4.28: (a) PSD comparison for strong clutter for all frequency channels, (b) Cumulative distribution for all frequency channels	100
Figure 4.29: Distribution Weibull Distribution of a measured clutter at 64 MHz, 135 MHz, 173 MHz and 434 MHz for strong clutter	101
Figure 4.14: Measured Doppler signals at 64 MHz, 135 MHz, 173 MHz and 434 MHz for very strong clutter	102
Figure 4.15: Envelopes for all signal frequencies for very strong clutter	103
Figure 4.16: Power Spectral Density for clutter envelopes 0.1 cut-off frequency (a) normalized (b) absolute value for very strong clutter	104
Figure 4.17: PSD of clutter signals for all frequency channels at MHz, 135 MHz, 173 MHz and 434 MHz for very strong clutter	105
Figure 4.18: (a) PSD comparison for very strong clutter for all frequency channels, (b) Cumulative distribution for all frequency channels	106
Figure 4.19: Weibull Distribution of a measured clutter at 64 MHz, 135 MHz, 173 MHz and 434 MHz for very strong clutter	106
Figure 4.36: Doppler signal standard deviation value for different wind Speed	107
Figure 4.37: Envelopes for all wind conditions for (a) 64 MHz, (b) 135 MHz, (c) 173 MHz, and (d) 434 MHz frequency channel	108
Figure 4.38: PSD comparison for all wind conditions for (a) 64 MHz, (b) 135 MHz, (c) 173 MHz, and (d) 434 MHz frequency Channel	109
Figure 4.39: Distribution of standard deviation, minimum and maximum signal envelopes and the shape factors for 64 MHz frequency channel	112
Figure 4.40: Histograms of standard deviation, minimum and maximum signal envelopes and the shape factors for 64 MHz frequency channel	113

Figure 4.41: Distribution of standard deviation, minimum and maximum signal envelopes and the shape factors for 135 MHz frequency channel	114
Figure 4.20: Histograms of standard deviation, minimum and maximum signal envelopes and the shape factors for 135 MHz frequency channel	115
Figure 4.21: Distribution of standard deviation, minimum and maximum signal envelopes and the shape factors for 173 MHz frequency channel	116
Figure 4.22: Histograms of standard deviation, minimum and maximum signal envelopes and the shape factors for 173 MHz frequency channel	117
Figure 4.23: Distribution of standard deviation, minimum and maximum signal envelopes and the shape factors for 434 MHz frequency channel	118
Figure 4.46: Histogram of standard deviation, minimum and maximum signal envelopes and the shape factors for 434 MHz frequency channel	119
Figure 4.47: Dynamic range for low, medium, strong and very strong clutter signals	121
Figure 4.48: (a) Standard deviation CDF for all channels, (b) Weibull shape factor CDF for all channels	122
Figure 4.49: (a) Envelope's minimum values CDF for all channels, (b) Envelope's maximum values CDF for all channels	122

CHAPTER 5: EMPIRICAL MODEL OF CLUTTER

Figure 5.1: Vegetation clutter simulation model block diagram	126
Figure 5.2: Generating stationary clutter	126
Figure 5.3: Stationary clutter Simulated for 64 MHz	127
Figure 5.4: Stationary clutter for all clutter conditions	128
Figure 5.5: Develop clutter's envelope	128
Figure 5.6: Clutter's envelope for 64 MHz low clutter	129
Figure 5.7: 64 MHz clutter's envelope varies from low to very strong clutter powers	130
Figure 5.8: 64 MHz normalised non-stationary clutter varies from low to very strong clutter	131
Figure 5.9: Added noise to simulated clutter	131
Figure 5.10: 64 MHz Non-stationary clutters varies from low to very strong clutter	132
Figure 5.11: Simulated non-stationary low clutter power for all frequency Channels	134

Figure 5.12: Clutter's envelope for all frequency channels	135
Figure 5.13: Normalised and absolute value clutter's envelope PSD for all frequency Channels	136
Figure 5.14: PSD for all frequency channels for low clutter	137
Figure 5.15: (a) PSD comparison for low clutter, (b) Cumulative distribution for all Frequencies	137
Figure 5.16: Weibull's distribution for all frequencies	138
Figure 5.17: Simulated non-stationary medium clutter power for all frequency channels	139
Figure 5.18: Simulated medium clutter's envelope for all frequency channels	141
Figure 5.19: Normalised and absolute clutter's envelope PSD for all frequency channels	141
Figure 5.20: PSD for all frequency channels for medium clutter	142
Figure 5.21: (a) PSD comparison for medium clutter, (b) Cumulative distribution for all frequencies	143
Figure 5.22: Weibull's distribution for all frequencies	144
Figure 5.23: Simulated non-stationary strong clutter power for all frequency channels	145
Figure 5.24: Simulated strong clutter's envelope for all frequency channels	146
Figure 5.25: Normalised clutter's envelope PSD for all frequency channels	147
Figure 5.26: (a) PSD comparison for strong clutter, (b) Cumulative distribution for all frequencies	147
Figure 5.27: PSD for all frequency channels for strong clutter	148
Figure 5.28: Weibull's distribution for all frequencies	149
Figure 5.29: Simulated non-stationary very strong clutter power for all frequency channels	150
Figure 5.30: Very strong clutter's envelope for all frequency channels	151
Figure 5.31: Normalised clutter's envelope PSD for all frequency channels	152
Figure 5.32: PSD for all frequency channels for very strong clutter	153
Figure 5.33: (a) PSD comparison for very strong clutter, (b) Cumulative distribution for all frequencies	153
Figure 5.34: Weibull's distribution for all frequencies	154
Figure 5.35: 64 MHz simulated and measured clutter envelopes	156
Figure 5.36: 135 MHz simulated and measured clutter envelopes	157
Figure 5.37: 173 MHz simulated and measured clutter envelopes	157

Figure 5.38: 434 MHz simulated and measured clutter envelopes	158
Figure 5.39: Simulated and measured clutter PSD for 64 MHz	159
Figure 5.40: Simulated and measured clutter PSD for 135 MHz	159
Figure 5.41: Simulated and measured clutter PSD for 173 MHz	160
Figure 5.42: Simulated and measured clutter PSD for 434 MHz	160
Figure 5.43: Simulated low clutter for different frequency channels	161
Figure 5.44: Measured low clutter for different frequency channels	161
Figure 5.45: Simulated and measured low clutter PSD	162
Figure 5.46: Simulated very strong clutter for different frequency channels	163
Figure 5.47: Measured very strong clutter for different frequency channels	163
Figure 5.48: Simulated and measured very strong clutter PSD	164

List of Tables

CHAPTER 4: EXPERIMENTAL DATA COLLECTION

Table 3.1: 3-channels (transmitter and receiver) and 4-channels (transmitter and receiver) equipment's operating frequency with output power	33
Table 3.2: Measurement sites comparison	49

CHAPTER 4: EXPERIMENTAL CLUTTER ANALYSIS

Table 4.1: Measured low clutter strength for different frequencies	85
Table 4.2: Measured very strong clutter strength for different frequencies	91
Table 4.3: Measured very strong clutter strength for different frequencies	97
Table 4.4: Measured very strong clutter strength for different frequencies	103
Table 4.5: Measured clutter parameters for different clutter strengths (based on wind speed)	110
Table 4.6: Measured clutter parameters for different clutter strengths (based on signal standard deviation)	120

CHAPTER 5: EMPIRICAL MODEL OF CLUTTER

Table 5.1: Low clutter parameters for simulated low clutter power	134
Table 5.2: Medium clutter parameters for simulated clutter power	140
Table 5.3: Strong clutter parameters for simulated clutter power	146
Table 5.4: Very strong clutter parameters for all frequencies	151
Table 5.5: Simulated clutter parameters for different wind conditions	155

Glossary of Abbreviations

FSR	Forward Scatter Radar
SAR	Synthetic Aperture Radar
RCS	Radar Cross Section
EM	Electromagnetic
CST	Computer Simulation Technology
DEM	Digital Elevation Method
PCA	Principle Component Analysis
ADC	Analog Digital Converter
ATC	Automatic Target Detection
USB	Universal Serial Bus
MISL	Microwave Integrated System Laboratory
MIMO	Multiple Input Multiple Output
SCR	Signal to Clutter Ratio
STD	Standard Deviation
Rx	Receiver
MHz	Megahertz
dBm	Milidecibel
BNC	Bayonet Neill–Concelman
PCB	Printed Circuit Board
EECE	Electronic, Electrical and Computer Engineering
PC	Personal Computer
PSD	Power Spectral Density
PDF	Power Density Function

CHAPTER 1

INTRODUCTION

1.1 Background

Research on Forward Scatter Radar (FSR) has begun many decades ago. Forward scatter radar can be categorised as a bistatic radar when the bistatic angle between the transmitter and receiver near 180° [1-3]. It provides an efficient approach for detection of so-called “difficult” targets which can be characterised either by low radar cross section (RCS) or low speed, small target and it is a potential countermeasure to stealth aircraft [4].

The performance of FSR under a variety of environmental conditions and targets for the radar system is very important. A radar signal usually contains a target signal embedded into a strong background (noise and clutter) signal. This will limit the performance of any Doppler radar. In order to estimate the performance under these conditions, general analysis of Doppler target returns from the real measurements, interference signals, noise and clutter must be implemented. These involve processing and analysing real data, as well as performing computer simulations.

High power level of non-stationary clutter is one of crucial problem in radar detection. Thus performance of the FSR depends on signal-to-clutter ratio and on specific characteristics of clutter such as caused by foliage or wind [5, 6]. Despite of its importance, FS clutter analysis is still waiting its elaborate investigation.

The concept of Forward Scatter Micro-sensors Radar network for situational awareness in ground operation was explained in detail in [7,8]. This type of radar network is used in this research due to its robustness, easy deployment and low maintenance [9]. The network consists of number of nodes separated short-range transmitter/receiver pairs (micro-sensors), operating in forward scatter configuration intended for the detection and/or recognition of moving ground targets such as personnel and vehicles entering into protected area and crossing the radar node's baselines as shown in Figure 1.1. FSR utilizes continuous wave operation.

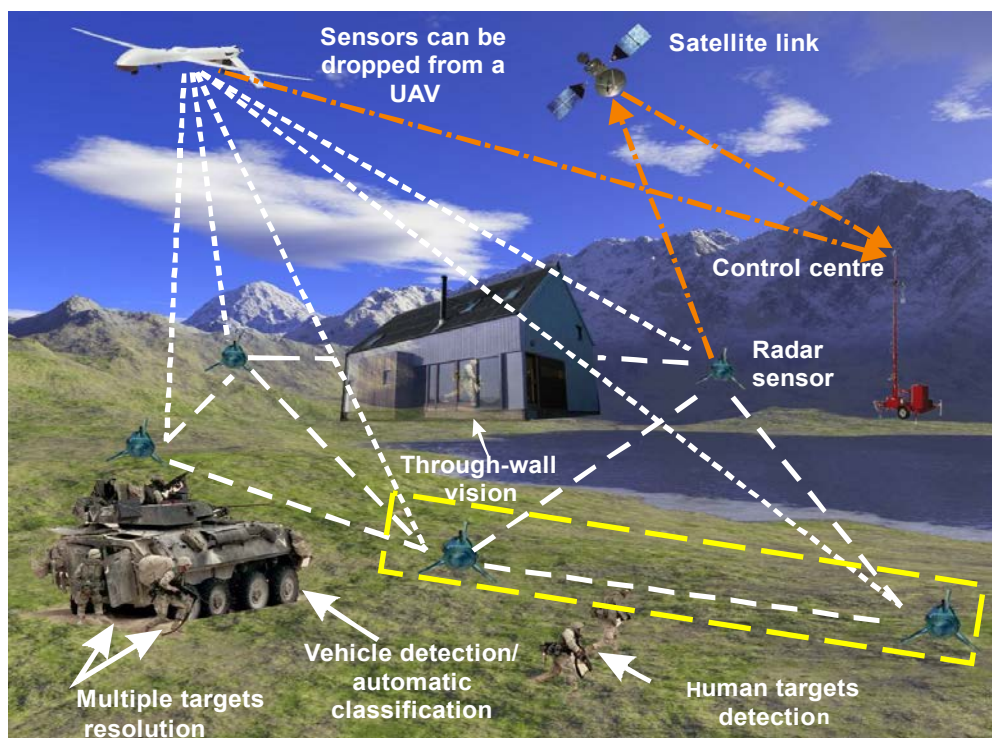


Figure 1.2 The concept of the FSR micro-sensors radar network

The proposed method of micro-sensors delivery and spreading over the area of interest is a free drop from UAV. After the drop, sensors are situated directly on the ground in random positions and, therefore, have random antenna orientations. This defines the requirements of the sensors' operational characteristics, such as using the VHF band for network communication and radar operation and exploitation of omni-directional antennas [10].

Vegetation may surround the radar position and be presented in close proximity to Tx/Rx and directly on the baseline. The clutter is collected from a large volume, where spatially distributed clutter sources may be generally considered as obstacles forming the backscatter, bistatic and forward scatter signal interference which can mask the useful target signals [9, 11] and cause essential errors in target classification and detection. For this specific radar configuration FSR micro-sensors operate within a volume of distributed vegetation scatterers and theoretical or empirical clutter models established for monostatic radars should additionally be validated for FSR [10].

1.2 Motivation for The Present Work

Clutter is one of the most significant problem in FSR detection. Over the past few years, numbers of research have been carried out to investigate clutter especially for conventional monostatic and bistatic radar but not specifically on Forward Scatter Radar (FSR). Moreover, clutter is a complex issue, that depends on the parameters such as the surrounding environment and wind. Therefore, this complex problem merit's special analysis like long term investigation to analyse and understand the characteristics of the clutter.

Forward scatter radar is well known for its simplicity in hardware design, increase the power budget and robustness to stealth technology [12-14]. The peculiarity of FSR system is the absence of range resolution and clutter is picked up from the large area illuminated by transmitter and receiver antennas. This makes the clutter issue more critical in comparison with monostatic radars [9,10]. In FSR the target can only be detected if it is moving within the sensor area due to the changes in its Doppler signature. If the area is surrounded by the vegetation, it can mask the target signal and the performance of detection of the system will be reduced [11]. Besides that, the researchers stated that by using micro sensors FSR network, the sensor antennas are placed directly on the ground surface with few hundred meters of baseline length. The clutter from the surrounding foliage will be considered as volume distributed scatterers that may produce clutter exceeding the target signal. Here the effect of clutter in FSR is analysed and proved the foliage clutter existence in FSR detection. Simple model has been proposed and used to predict the clutter properties.

In our research, we concentrate on the vegetation clutter analysis in ground-based for Forward Scatter Micro Radar Network. None of the above references were dedicated to analyse the characteristic of ground-based clutter for FSR system. This leaves the open space to do further research study for the particular area and the need to contribute more especially the analysis of real measurements of clutter in area varying from flat surface to dense wood. Furthermore, the analysis is supported by the simulated clutter-like signal that can be benefited for developing synthetic environment.

1.3 Problem Statement and Original Work

In this research, the analysis is focused on clutter in ground-based Forward Scatter Micro Radar system network where the effect of clutter and clutter characteristics are studied for different environmental conditions such as different land sites, wind conditions and weather conditions for different carrier frequencies. This comprehensive analysis is eventually used for modelling of clutter in order to create similar clutter-like signals that can be used to develop synthetic environment for Forward Scatter Radar detection performance analysis.

To achieve this aim, few new studies are conducted as below:

- Real measurements on sites for clutter and human as a target.
- Analysis of data collections from several sites with different landscapes (varying from concrete runway to dense woodlands)
- Analysis of data collections for different carrier frequencies in VHF/UHF band (64 MHz, 135 MHz, 173 MHz and 434 MHz)
- Analysis of data collections for different wind speeds.
- Analysis and estimation of clutter characteristics for development of clutter modelling using Matlab simulation.
- Comparison between measured and simulated clutter.
- Generate signals as a base for the synthetic environment for FSR.

This research is based on statistical approaches on different environments varying from flat surfaces to dense woods. Furthermore, multiple measurements are carried out in each landscape with different weather conditions and wind speeds.

Before the work begins, preliminary studies of wind condition have been made to analyse the effect of wind speed to the result. Besides that, measurements with few targets such as human and fox also have been studied. All possible scenarios in radar detection are included in order to understand the characteristic of clutter for each scenario with or without a target.

The summarized workflow is shown in Figure 1.2.

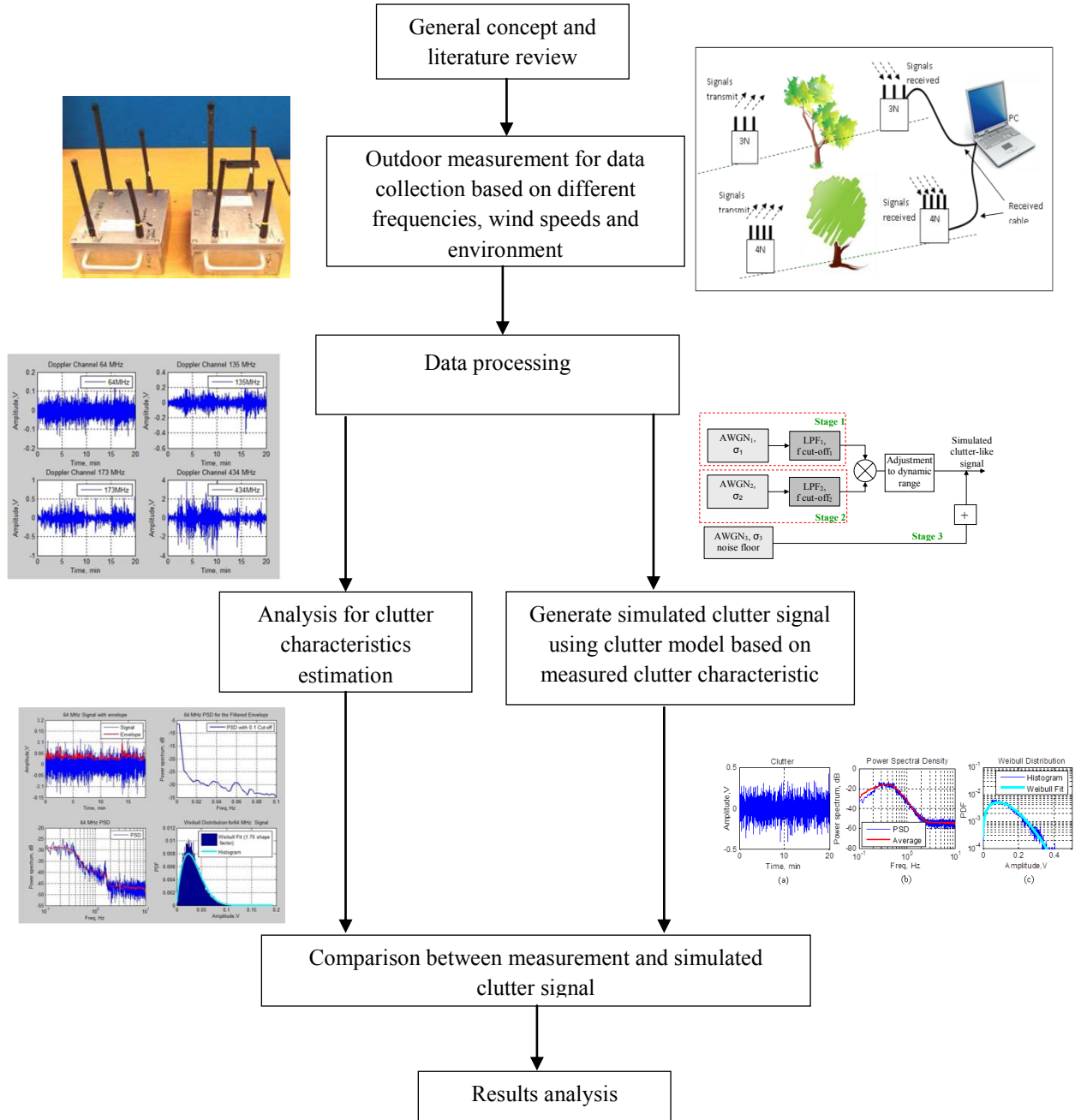


Figure 1.2: Clutter characteristic analysis and simulation for FSR micro sensor flowchart

1.4 Thesis Organisation

This thesis is divided into six chapters, including Chapter 1 for the introduction and the organisation of the thesis. In Chapter 2, brief overview about radar technology, including basic system configuration of bistatic and monostatic radar. Then followed by the introduction of Forward Scatter Radar (FSR) basis equation, comprising Doppler relationships and radar cross section (RCS). Next is the reviews of the recent publications on FSR. The second part in Chapter 2, is about clutter which includes an overview about clutter and the reviews from publication papers related to radar clutter in FSR.

In Chapter 3, the experimental set up for data collections are described. This includes hardware assembly, measurement test sites, methods of data collection (short term and long term measurement) data processing and analysis. Chapter 4 continues with an experimental clutter analysis. Results from the measurements are analysed based on three different methods. First, clutter results from different parameters (different test sites, carrier frequencies, baselines and weathers), second clutter analysis based on different wind speed from short term measurement and third clutter analysis based on clutter's standard deviation (STD) from long term measurement.

While in Chapter 5, described empirical models of clutter. This includes the explanation of the clutter model structure and simulated clutter results using Matlab program based on the parameters from the measurement results. Next is the comparison of the empirical model with measured results. Finally, Chapter 6, is the summary of the work completed, conclusion and the future work.

CHAPTER 2

BASIC PRINCIPLES OF FORWARD SCATTER RADAR

2.1 Introduction

In this chapter radar theory is described briefly beginning with radar overview and history. Then different types of radar such as monostatic and bistatic are discussed, followed by the background of Forward Scatter Radar (FSR) as well as the FSR principle and system. Next discussed on the advantages and disadvantages of FSR. This is to give the reader ideas on the basis of FSR including the FSR Radar Cross Section (RCS), Doppler Effect in FSR and current studies on FSR. In the next part of this chapter, is about the clutter which includes different type of clutters and the review of the existing radar clutter.

2.2 Radar Overview

The word RADAR is an acronym taken from Radio Detection and Ranging. It was named in the year 1941 replacing the words, RDF stands for Range and Direction Finding used in the United Kingdom [15,16].

Historically, radar has been designed and developed by several scientists and engineers since 1904. It was recorded that Christian Hülsmeyer is the first person who used radio waves to detect the presence of metallic objects and was patented in April the same year. Then later in August 1917, Nicola Tesla established the principles of frequency and power level for the first primitive radar units. In 1934, an American Dr. Robert M. Page from Naval Research Laboratory tested the first monopulse radar then continued by the Germans, French and British was the first to use radar as a defence system developed by Robert Watson-Watt team in 1935 leading to the first development of the first real radars [15,16] before the Second World War. The work in designing and developing of radars is still continuing until today.

Radar is a sensing device that is used for detecting, locating, tracking and recognizing moving or fixed objects such as vehicles, ships, aircraft, spacecraft, weather and terrain at various distances and places [15]. Figure 2.1 shows the basic principle of radar where the electromagnetic signals are transmitted from the radar antenna within the antenna beam region where the targets are expected. When the signals come into contact with any object (target), they reflect back to the transmitter. These reflected signals are analysed to determine the target. The time delay between the transmitted time and the received time are used to determine the distance of the target. If the target is moving away or towards the transmitter, the reflected signals will have a different frequency from the transmitted signal earlier. This is called the Doppler shift.

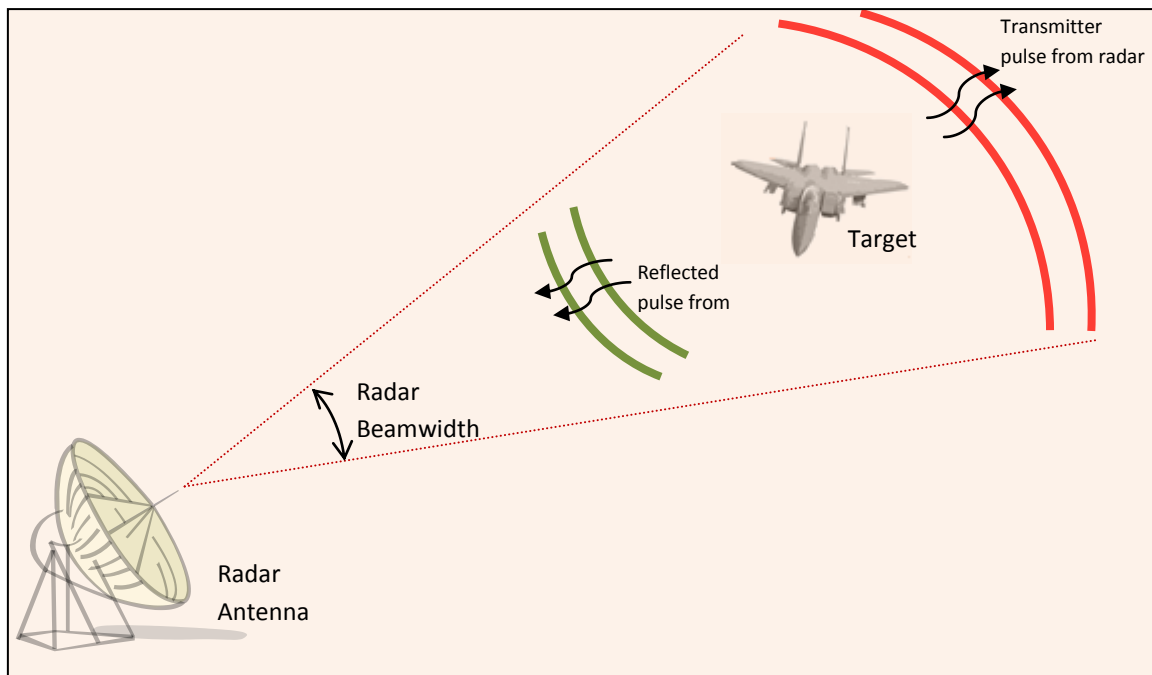


Figure 2.1: Radar principle

2.3 Basic System Configurations

Radar can be categorised into three different configurations. These include monostatic, bistatic and multistatic radar. In monostatic radar, the radar antenna is used for both transmit and receive signal. For bistatic radar, the transmitter and receiver are using different sets of antennas which are allocated in two different places. Furthermore, multistatic radar refers to a radar system that consist of one transmitter and several distributed receivers with joint processing information [17]. All these configurations are shown in Figure 2.2.

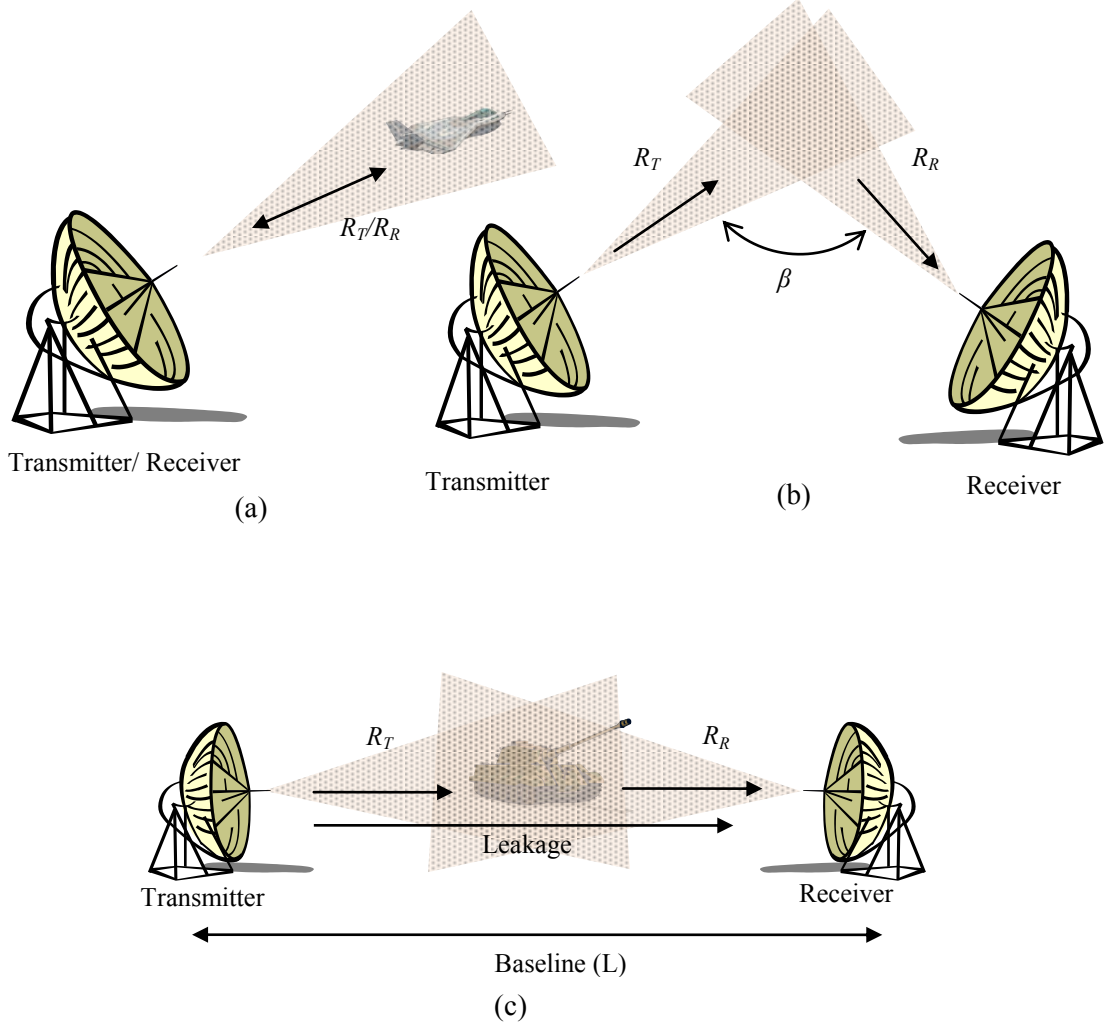


Figure 2.2: Radar system configurations, (a) monostatic radar, (b) bistatic radar, and (c) forward scatter radar

In this research, we concentrate on Forwards Scatter Radar which belong to a special bistatic radar configuration. In bistatic radar, the maximum angle between the transmit signal rays, R_T and the receive signal, R_R are called as bistatic angle, β . The bistatic angle has a limit from zero to 180° with $0^\circ \leq \beta \leq 180^\circ$. If $\beta < 90^\circ$, the radar is stated to use the reflection phenomenon of an electromagnetic wave on a target, may be termed as backscattering radar. While radar at $90^\circ < \beta \leq 180^\circ$ phenomenon, is stated to use the diffraction phenomenon of an electromagnetic wave on a target may be termed as forward scattering radar [4]. The

configuration of forward scatter radar is shown in Figure 2.2 (d) where the transmitter and the receiver are separated in a distance called as baseline.

2.4 Forward Scatter Radar

Forward scatter radars are designed to detect targets crossing the baseline between the transmitter and receiver or moving nearby the baseline area. Its act like a fence-like configuration. The illustration of FSR is shown in Figure 2.3 where the transmitter (Tx) and the receiver (Rx) are separated within a distance called as baseline (L). Target that crosses the baseline or near FSR region will be detected.

FSR can be classified as the bistatic radar as the bistatic angle approaches 180° [1, 2]. The research on FSR especially on ground based micro sensor FSR network has been carried out recently by MISL research group at University of Birmingham [1,4,7].

FSR gives advantages including robustness to stealth technology where FS RCS is independent from radar absorbing material (RAM) coating or the shape that can reflect the signal away from the receiver. Besides that, it used continuous wave (CW) radiation which usually employed using less radiated power, so that a simpler hardware design for transmitter and receiver could be used as compared to monostatic pulse radar since it did not require a modulator or high voltage. The system also offers increase in power budget because of its one way propagation and a reduction of signal fluctuation compared to monostatic radar, as the signal is defined by shadow contour in FSR [4]. Furthermore deployable FSR network can be exploited as an efficient electronic barrier for using separately or along with other existing

systems. Due to its simplicity in hardware design, FSR network can be deployed anywhere to create a network.

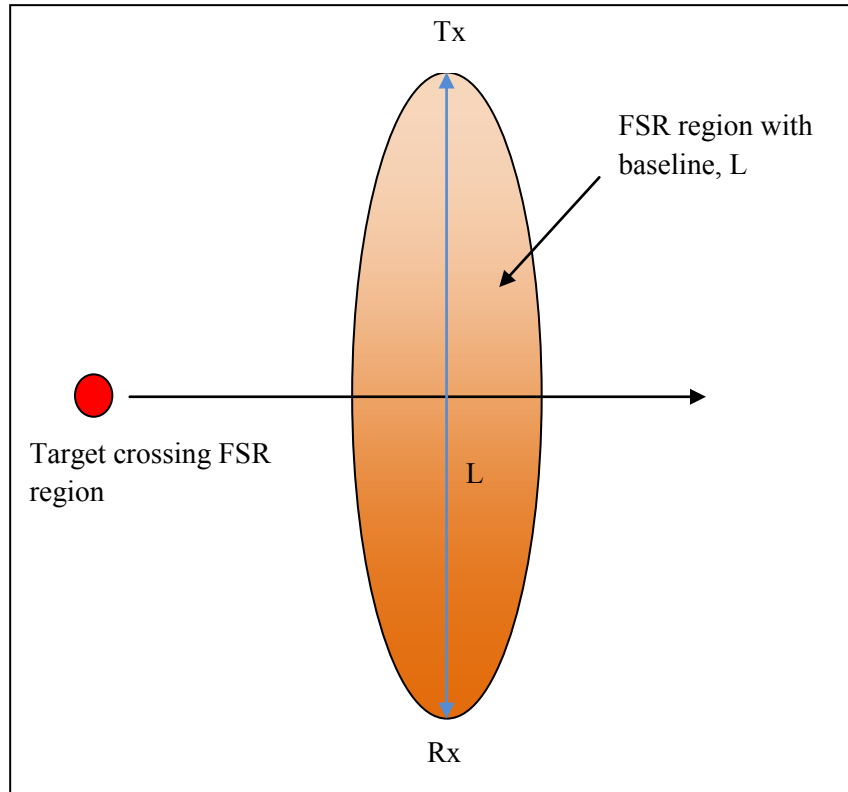


Figure 2.3: Illustration of FSR [17]

Besides that, FSR also has some disadvantages. The absence of range resolution made it difficult to detect static targets. Target detection is possible only when the target is moving by selecting its Doppler signature. The surrounding vegetation also can mask the useful target signals [9]. Other than that, interference and jamming from nearby will affect the received signals. More on basics of FSR can be found in [4,18].

2.5 Forward Scatter Radar Basis Equations

The FSR basic equation includes the relationship between the transmit and receive signal including the gains for both antennas and the range of the target. The equation can be expressed as below [1,2,19]:

$$P_R = \frac{P_T G_T G_R^2 \sigma}{(4\pi)^3 R_T^2 R_R^2} \quad (2.1)$$

where P_R and P_T are the received power and the transmitted power while G_T and G_R are the transmitted and received antenna gain in the target's direction. Whereas λ is the wavelength and σ is the target radar cross section. While R_T and R_R are the range from the transmitter to the target and from the receiver to the target respectively.

Propagation losses always present in radar. By considering the losses for transmit, L_T and receive transmission, L_R for the case of perfect conductive ground, the losses can be written as below [20]:

$$L_T \approx \frac{h_T^2 h_{tg}^2}{d_T^4} \text{ and } L_R \approx \frac{h_{tg}^2 h_R^2}{d_R^4} \quad (2.2)$$

Then the FSR range equation can be written as [20]:

$$P_R = P_T G_T G_R \frac{4\pi\sigma}{2} L_T L_R \quad (2.3)$$

where h_T and h_R are the transmitter and receiver elevations respectively, h_{tg} is the height of the target center, d_T and d_R is the transmitter and receiver separation respectively. According to 2-ray model, power degrades as a function of $1/d^4$.

2.5.1 Doppler Relationships

In radar system, the signal that is transmitted from the transmitter will reflect and scatter when it interacts with any vegetation in surrounding or any target. The received signal will contain a lot of information which includes the target signal with clutter in surrounding. Any activity or movement from example human, vehicle or animal within the area with constant velocity, will shift the carrier frequency [21] of the transmitted signal. The changes in frequency are called as Doppler effect or Doppler shift named after Austrian physician Christian Doppler who proposed the theory in 1842 [16,22,23].

The close example of Doppler effect is the sound of an ambulance's siren. When the ambulance approaches or passes an observer, the received frequency is higher during the approach or instant passing. As the ambulance moving away from the observer, the frequency is low. An illustration in Figure 2.4 shown Doppler effect of a moving target. When the target moves to the left, the time between arrivals of successive wavefronts is reduced (high frequency). On the right side of the target (back of the target), each successive wave increased slightly (low frequency) and take a longer time compared to the left [15,22,23].

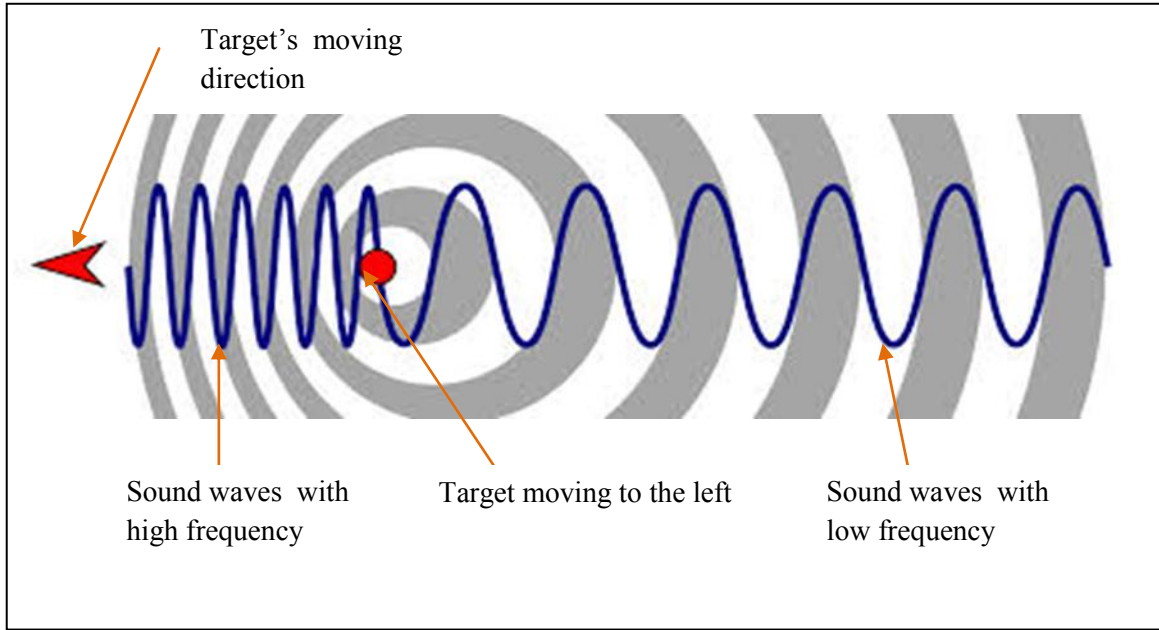


Figure 2.4: Illustration of sound waves for a moving target [15]

In Forward scatter radar (FSR) network used in this research, the transmitter and receiver are separated with a baseline distance ranging from 50 to 200 m. Any object presence near the baseline, the receiver will receive not only the signal but including the clutter. Let's assume an isotropic source act as a small target moving towards the baseline at y-axis direction with the distance d_T and d_R from the origin. The target is moving with constant velocity in x-axis direction with time, t as shown in Figure 2.5.

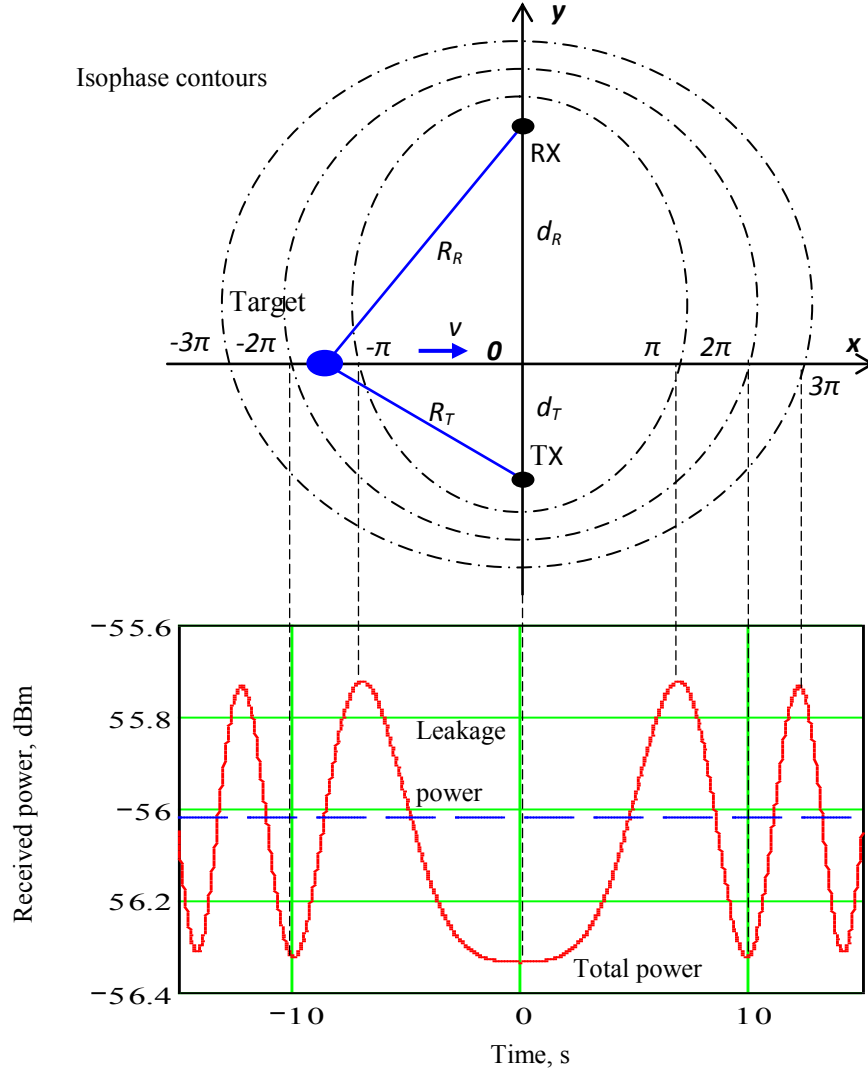


Figure 2.5: Doppler effect for moving target in target trajectory and the total received power [9]

Then assume this model is using two-dimensional (2D) with unity transmitted power, $P_T = 1\text{W}$ and using isotropic antennas for transmitter and receiver with the gain of $G_R = G_T = 1$. Furthermore, the height of the antennas and the target height are considered to be 0 m and the wave propagation is to be in free space. With these conditions, the leakage and target signal magnitudes may be written as [24]:

$$U_L = \frac{1}{4\pi d} \quad (2.4)$$

$$U_{tg} = \frac{1}{(4\pi)^2 R_T(t) R_R(t)} \sqrt{\frac{\sigma}{4\pi}} \quad (2.5)$$

where R is the distance in functions of time as the target moving with distance from transmitter to target is R_T and from target to transmitter is R_R . Thus we considered the total received signal, $u_R(t)$ [24] as:

$$u_R(t) = u_L + u_{tg}(t) \quad (2.6)$$

where u_L is the constant direct leakage signal while $u_{tg}(t)$ is the target signal which changes in time when its moving. Then by considering equation (2.3) and (2.4), the total received signal can be rewritten as:

$$u_R(t) = U_L e^{j(\omega_0 t + \varphi_L)} + U_{tg}(t) e^{j(\varphi_{tg}(t) - \varphi_L)} \quad (2.7)$$

Where φ_L and φ_{tg} are phases of the leakage rays and target respectively in geometry system [4] respectively with the equations as:

$$\varphi_L = 2\pi d / \quad (2.8)$$

$$\varphi_{tg} = \frac{2\pi[R_T(t) + R_R(t)]}{\lambda} \quad (2.9)$$

2.5.2 Radar Cross Section

Radar cross section (RCS) can be defined as the detectability measurement of a radar for an object. The larger the RCS of certain object, the easier it will be detected. RCS is depending on the size and the ability of a target to reflect the radar energy from its body [25]. In this research, RCS pattern in FSR is studied briefly especially for human as a target (detail study is not required as it is not the main part in this research) and to analyse the effect of clutter on target detection. RCS can be calculated as [26],

$$\sigma = \lim_{r \rightarrow \infty} 4\pi r^2 \frac{|E_s|^2}{|E_i|^2}$$

(2.10)

where E_s and E_i are the far field scattered and incident electric field intensities, respectively.

2.6 Current Studies On Forward Scatter Radar

Recently, research on FSR has been carried out enormously. These show the rising interest on this topic. It includes study on the readiness of FSR network for ground target detection mainly on coordinates estimation, speed estimation and automatic target classification [4-7, 11, 12, 14, 20, 30-39]

In paper [31], the feasibility study of FSR Micro sensors in detection and classification of ground targets has been carried out. The network of compact deployable FSR micro sensor which act as a situation awareness system are used to detect target when it crosses the baseline between transmitter and receiver. The recorded data are then process for classification analysis.

While in Forward Scattering Radar: current and future application [36], this paper described the further research study on FSR ground target classification [31]. Here, the process of target detection and classification method is described in detail. Different car's dimensions are used to capture the sample waveforms in both frequency and time domains for detection. Then Principle Component Analysis (PCA) is used for feature extraction for the classification. From the result, FSR has potential and high sensitivity for ground target detection and classification. Figure 2.6 shows the block diagram of FSR target detection and classification process in [36].

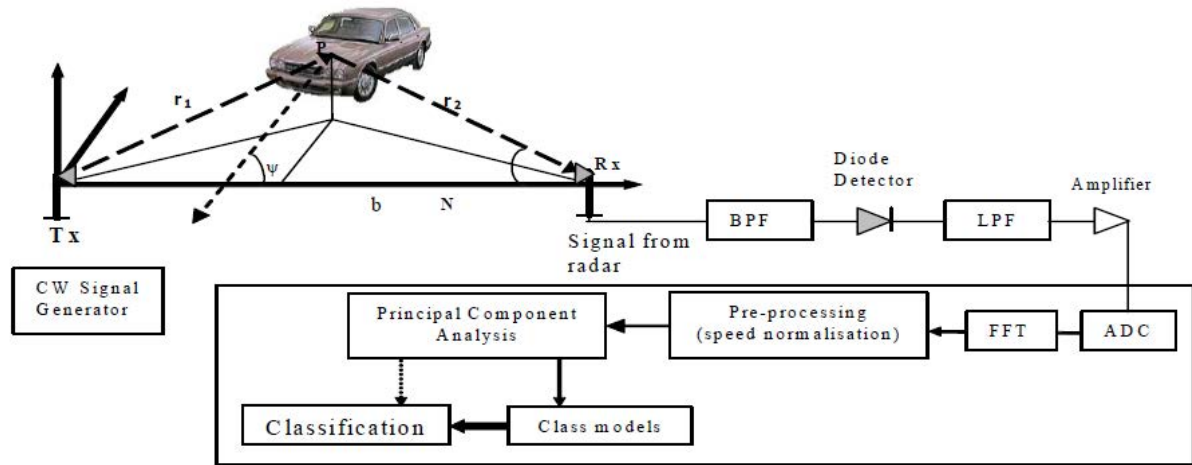


Figure 2.6: FSR target detection and classification block diagram [36]

The analysis in FSR continues with the study of target classification with different method. In [28], 850 vehicle signatures are obtained from three vehicles and classify into three conditional vehicle categories which are small, medium and large vehicle using PCA. The results show very good performance from the system with limited data for both testing and training. Then the neural network approach is used. By using this system, it will trained and ‘learned’ about the problem and predict classification [28]. Hence, it proved based on the results that FSR system has a potential to be used as the ground target detection and classification.

Furthermore, besides target detection and classification, research in speed estimation of target in FSR is also have been carried out in [37]. The aim in this research is to estimate the speed estimation of a vehicle when it crosses the FSR sensor. An algorithm is developed based on the value of standard deviation. The vehicle speed was measured by making comparison between the time-domain signatures with the estimated speed of vehicle captured from the video footage. As a result, the standard deviation for each signal is unique and shows better accuracy [37].

Next is the paper on FSR power budget analysis for ground targets [20]. This paper focused on the power budget analysis for ground FSR target detection with different FSR configuration. The configuration includes: the radar antennas are positioned directly on the ground (ground reflection must be considered) and the targets are considered with the dimensions comparable with radar operating wavelengths (from 4.5 to 0.35m). Hence the power budget analysis is important as the sensors are deployed and operate using battery. Furthermore, from the analysis, the FSR micro sensors can be served as a fence for situation awareness with long operational lifetime for detection of ground targets.

Moreover in [12], the analysis of FSR are continued, followed by the power budget analysis and potential cross range resolution. Theoretical models are then being constructed to verify the results. As the conclusion from the paper, it shows that FSR system has the ability to distinguish between two targets and does not depend on the distance of the baseline. An algorithm for detection of small targets whose signal are buried within the background of bigger targets have been developed [12].

Following the research on FSR, the next feasibility study is done on ultra wideband (UWB) FSR. In paper [38], the new UWB FSR concept is explored to look into the potential of target detection. In this paper, the researcher focused on air target detection and maritime target detection. As a result, the system demonstrates unique system properties that can be used for numerous practical applications such as: reduction in surface clutter (applicable for maritime), high immunity to multipath (can be used for situation awareness in urban areas) and essential reduction in surface clutter for air targets detection [38].

Currently, research on other influences in FSR has been carried out such as the different transmitting frequencies [39], baseline lengths [40], different ground characteristic [32] and the phenomenology of Doppler FSR. In [39], study about automatic target detection continued with two different traditional approaches; coherent and non-coherent Doppler signal processing. Coherent processing is the optimal processing that provides a maximum signal-to-noise-ratio (SNR) where the transmitting signal will act as the reference signal and compared with the received signal. While for non-coherent process, it is technically simpler and effective if the signal dominates above the noise but if SNR less than 0, the efficiency will reduce. New approach has been developed for signal detection which called as quasi-coherent processing where cross-correlation technique is used. By using multi frequencies which enables correlation of Doppler output from two different channels which can be considered as the matching waveform or as the reference signal to the first signal. This will lead to a compression of the FSR return by cross-correlation with enhance processing gain and enhanced target detection [39].

Another study about other influences in FSR is in [40], analysing the effect of different baseline lengths to the target signature. The study is based on different target crossing baseline length to the target spectra on two-ray path propagation configuration. Results show the target's spectra for different baseline become more evident when the target approaches optical approximation and the spectra stability from different frequencies can be achieved after applying with a baseline normalization process.

2.7 Clutter

The term “clutter” refers to backscattered return or echoes returned that reflects back when the electromagnetic energy is transmitted. These echoes returned from targets are undesired signal to the radar operators. There are caused by reflected signal from uneven ground and sea surfaces, precipitation due to rain droplets, snow or hail, moving animals like foxes and birds, surrounding environment such as forest, vegetation from trees and bushes. Furthermore, man-made object also can contribute clutter such as building, vehicles and aircraft [42]. Not all vegetation returns are undesired signals; remote sensing is one of the applications that used the return signals from natural vegetation as the primary target. Thus clutter can be considered as signal returns from a physical object or a group of objects which are undesired for a specific application [42].

The undesired signals can be categorized into different types of sources. Surface distributed clutter (such as ground and sea clutter) and volume distributed clutter (hail, rain, snow and chaff). All of these sources are influenced by many factors. These include the wind conditions for instance the speed and the direction, the height of ocean waves, the terrain surface for examples the dense of surrounding foliage and surface roughness [9, 42, 43].

2.7.1 Volume Distributed Clutter

In the air, the most significant problem is the clutter due to the weather. This can be produced from snow, rain, clouds, hail, dust and chaff. All of these are categories as volume clutter or atmospheric clutter. Volume clutter attenuates the radar signal and because of the limited radar power, the target detection can become worst when this atmospheric clutter exists as the frequency rises.

2.7.2 Surface Distributed Clutter

Surface clutter is generally divided into two; land clutter and sea clutter. On land it depends on the roughness of the surface and the dielectric permittivity of the soil and the dense of surrounding area (trees, buildings, atmospheric effect). The more ridged or uneven the surface, the stronger the clutter will be. While on sea surface, it depends on the polarization of the incident and reflected waves.

- **Sea Clutter**

The backscattered radar signals from the sea surfaces are called as sea clutter. Sea clutter is quite uniform over relatively large area but it is depending on the wind condition (speed and direction) which will vary with time as the wind speed and the direction change. Other than that, sea bird, white caps and concave in the sea waves may also create target-like sea returns called spikes [19, 44-48].

The performance of maritime radar such as remote sensing radar and surveillance radar are adversely affected by sea clutter. This backscattered radar signal can either be useful or just an interference to other radar's operators. Remote sensing radar signal are used for oceanographic studies and sea mapping (for sea ice detections, and collecting data on currents and waves) while surveillance radar operations are for target detections of submarines and ships [49].

- **Ground Clutter**

On land, surface clutters are based on the reflected signal from the surface of the ground back to the receiver. The clutter may be uniform over limited area but may be different from one area to another depends on the surrounding environment. This is based on the

nature of the surface (hills, flat, dense wood), its roughness, the grazing angle and the frequency [42,50]. The sources of clutter are the sum from variety of individual returns from foliage (leaves, bushes, trees which swayed and moved when it blew by the wind) and stationary sources (buildings, big tree trunk).

Foliage clutter is the main sources of clutter on ground. It can be very large and masked the targets in the received signal. This will degrade the performance of radar system for target detections and classifications. Trees and bushes consist of branches, trunk, twigs and leaves which sway by the wind. Each sway will cause varying amount of attenuation and scattering. This clutter is being considered in this research.

2.7.3 Foliage Clutter

As describe earlier, clutter is an unwanted signal that are detected by the receivers of any radar. Clutter can be in many categories such as surface distributed clutter and volume distributed clutter. In this research, it is focus on target detection on ground for forward scattering radar and this can be related to ground clutter in surface distributed clutter categories. Ground clutter is based on the reflected signals from the surrounding such as; the natures of the surface like hills, mountain and flat terrain. Besides that, the sources of clutter may also come from trees, bushes, leaves which can be called as foliage clutter or maybe from stationary sources like building [50].

Foliage clutter can be very significant and the main limiting factor in radar detection. In our research, the transmitter and receiver are located in certain baseline length ranging from 50 m to 200 m and placed on the ground. Omnidirectional antennas are used with low elevation

angle. This equipment set up is surrounded by the vegetation, foliage and the tree branches. If the wind is blowing in the area with a certain speed, the vegetation, foliage and the tree branches will sway and this can be considered as volume distributed scatterers. These will act like a clutter and will be picked up by the sensors.

2.7.4 Clutter Modelling Approach

In radar system, the return signals from target are process and analyse. The return signal will include the presence of any target and also unwanted noise such as clutter. In order to differentiate between the target and unwanted noise, a suitable processing algorithm need to be developed. A good understanding in clutter characteristic is important so that the clutter returns can be distinguished from the return signal.

The characteristics of clutter can be generalized using physical or statistical models. These models are designed to describe the numerous features of clutter. Physical model is a model that is based on a design of a scale model of the target of clutter. Example like; target miniature with the scale of $1/10^{\text{th}}$, the different roughness of ground planes mould in different size, pendulum to replicate the branches of a tree and many more. While for the statistical model is based on the repetitive experiments and statistical analysis that are carried out to study the trends of each data. Then conclusions are made based on the analysis.

Most of the researchers are preferred to do clutter analysis research using statistical model. Only few of them are using physical model. With physical model, it requires the researcher to do the designing part of the physical model involve, as well as the measurement part. This will require more time consuming on modelling different type of targets or clutter. While for

statistical modelling, the researchers only need to have a very big database with different characteristics involved to do the analysis. Few papers are described in [11, 47] as an example of these two models.

2.8 Current Studies on Radar Clutter

Studies on clutter have carried out since many years ago and generally for all types of radar. Concerned about interference for radar detection such as clutter makes researchers studied, analysed and modelled the clutter. In [19], clutter is generally distributed in spatial extent in that it is much larger in physical size than the radar resolution cell that produced large backscatter. Large clutter echoes can mask the echoes from desired targets and limit radar capability.

In [52], the knowledge of radar statistical characteristics for target to be detected is the starting point in designing a radar system. The approach to statistical characterization differs significantly depending on the radar system function. As example, it used for target classification, recognition in noise and clutter. Clutter can be very significant in any detection. A simple target detection requires different amounts of information on the target scattering properties to differentiate between the target and clutter. Clutter properties are determined by a large number of factors having different physical sense and value. Therefore, a study on the clutter characteristics is important in designing a radar system.

Research on land clutter at low grazing angles was acquired by [50]. This include the collections of land clutter data that are taken over a wide variety of terrain in a long period of time. Measurements were made at five frequencies: VHF (167 MHz), UHF (435 MHz), L

(1.23 GHz), S (3.24 GHz) and X (9.2 GHz). The radars were mobile and the antennas are mounted on a tower that could be extended to heights of 30, 60, or 100 ft. As the results, most of the significant land clutter echoes at low angles come from spatially localised or discrete vertical features such as trees, buildings, fences or high point of terrain. Low regions of terrain are shadowed at low grazing angles so that the clutter is spatially patchy. Over the range of depression angles employed in the measurements, the mean clutter strengths increased and the cell-to-cell fluctuations decreased with increasing angle. While for different weather or season, the variation of the clutter echo was found to be small and usually less than 1.5 dB for weather and 3 dB for changes in season [22].

Next paper on Statistical Analysis of Measured Radar Ground Clutter Data [53] and [20], stated that the performance of ground-based surveillance radar strongly depends on the spectral characteristics and the distribution of ground clutter. A good design of signal processing algorithm based on clutter characteristics is very important and a preliminary statistical analysis of ground clutter data is necessary. Parametric autoregressive (AR) modelling of the clutter process is developed for this purpose for gaussianity test analysis. Based on the test, incoherent analysis has been carried out by comparing the fitting of the signal distribution using Rayleigh, Weibull, log-normal and K-distribution model and the best fit has been found to be Weibull model [50, 53, 54].

In Forward Scattering Radar, studies in clutter are very minimal. Most researchers are focused on the target detection. In paper [57], clutter influenced the target classification in forward scattering radar (FSR) is studied. A simulated clutter is added to the real measured recorded signal (without any clutter) within the UHF and VHF bands. The analysis was performed on

several cases such as the speed estimation error only, the shape deformation error only and the combination of both speed estimation and shape deformation errors presented in automatic target classification (ATC) system. It shows good robustness of the speed estimation algorithm to clutter. Besides that, better ATC is achieved where the clutter influence is very minimal for low frequency and the target signature is bigger when the frequency is high. In conventional clutter-uncompensated ATC, the system achieved high classification accuracy only at high signal-to-clutter ratio (SCR) but the accuracy drops when SCR is low. With clutter-compensated ATC system where the clutter level is estimated from the received signal, very significant classification accuracy improvements for low SCR.

Another paper on clutter for forward scattering radar is Vegetation Clutter Spectral Properties in VHF/UHF Bistatic Doppler Radar [11]. In this paper, a vegetation clutter model is designed for forward scattering radar network. A physical model of pendulum is used to replicate the foliage with different resonant frequencies. From this model, predictions of clutter spectral properties are analysed and compared with the real clutter data from the measurement on different sets of frequencies in VHF and UHF bands. As a result, the clutter power spectrum width slightly increases when the carrier frequency increase. While the power spectrum density decreased with frequency. Furthermore, the clutter power also increases when the wind speed increase from low to strong wind strength as predicted theoretically. These results will be investigated further in this research.

2.9 Summary

Research in radar has been carried out long time ago since early 1900s. The interest in radar begun as the needs for defence system increased. Americans, Germans, French and British among the first scientists and engineers who developed the system. Until today, the research on radar still continues with advance technology for various radar systems including Forward Scatter Radar (FSR). As a summary, forward scatter radar offers numerous advantages with few limitations such as clutter. Clutter can be very significant in FSR especially in the presence of wind with dense vegetation in the surrounding area. Prominent studies on the characteristics of FSR clutter need to be done in order to improve the performance of the radar system.

Clutter can be the main contributor that affects the performance of radar system by masking the target detection and classification. There are few categories of clutters such as surface distributed clutter and volume distributed clutter. In this research which is focused on target detection of ground FSR, foliage clutter is the main limiting factor. This is because the transmitter and receiver are placed on the ground that surrounded by foliage which varies from as low as the grass and bushes, and as high as the trees. Current studies on radar clutter have been discussed and mainly on ground clutter for FSR.

CHAPTER 3

EXPERIMENTAL DATA COLLECTIONS

3.1 Introduction

In chapter 2 we stated all the problems and peculiarities of clutter from vegetation in radar as in general and in FSR to be more specific. The next stage is to study the behaviors and the characteristics of the clutter in different environments. In this chapter, in order to analyse the characteristics of the clutter itself, outdoor experiments have been set up and carried out in several places. The description on the test sites chosen in the experiment are described in this chapter. This is followed by description on the hardware and the method of measurement used. Last part of this chapter is the explanation on database collection format for all signal measurements is described.

3.2 Experimental Set Up

There are two sets of equipment used in this research which is 3-channels and 4-channels module equipment. These two sets of equipment consist of transmitter and receiver for each set as shown in Figure 3.1. This equipment is design and developed by Microwave Integrated

System Laboratory, University of Birmingham (MISL Group) [30]. It is used to collect FSR signals for research purposes before the real micro radar prototype is develop.

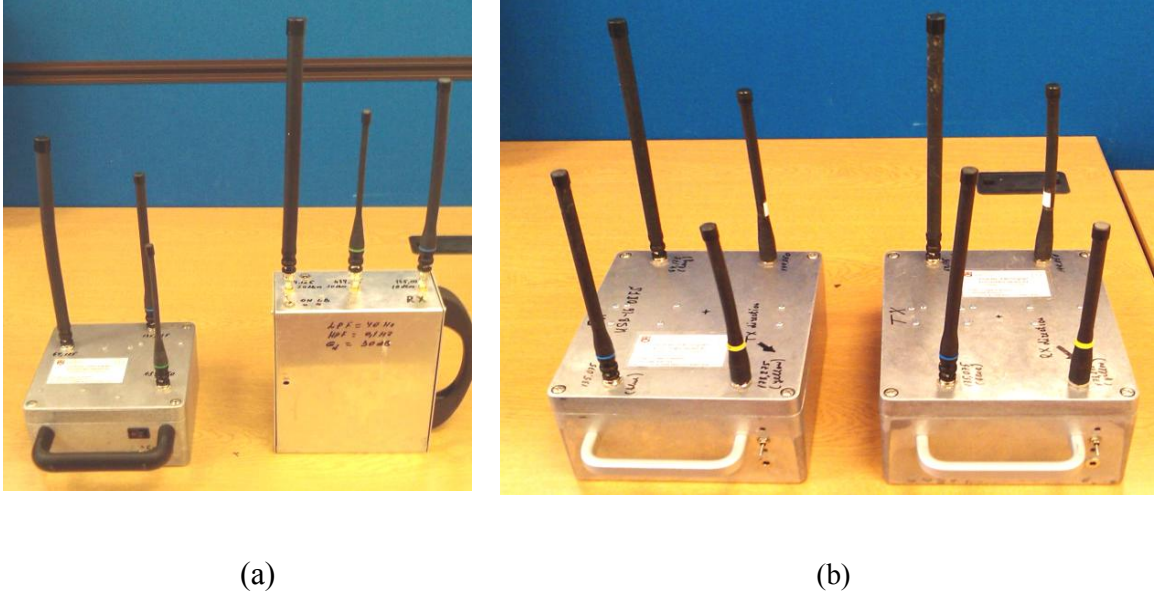


Figure 3.1: Testing equipment, (a) 3-channels equipment, (b) 4-channels equipment

The inside of the equipment can be simplified in block diagram where the signals that received by each of the operating frequency will be connected to analogue-to-digital converters (ADC). Then the digitized data are transferred to the computer by extended USB cables for database storage and for further analysis.

Figure 3.2 shows block diagram for 3-channels long term (LT) equipment (3LT TX for transmitter and 3LT RX for receiver) and 4-channels long term equipment (4LT TX for transmitter and 4LT RX for receiver). These two sets of equipment are only differed from the operating frequencies that are used. Details of the equipment's block diagrams are described in Hardware description in Appendix A.

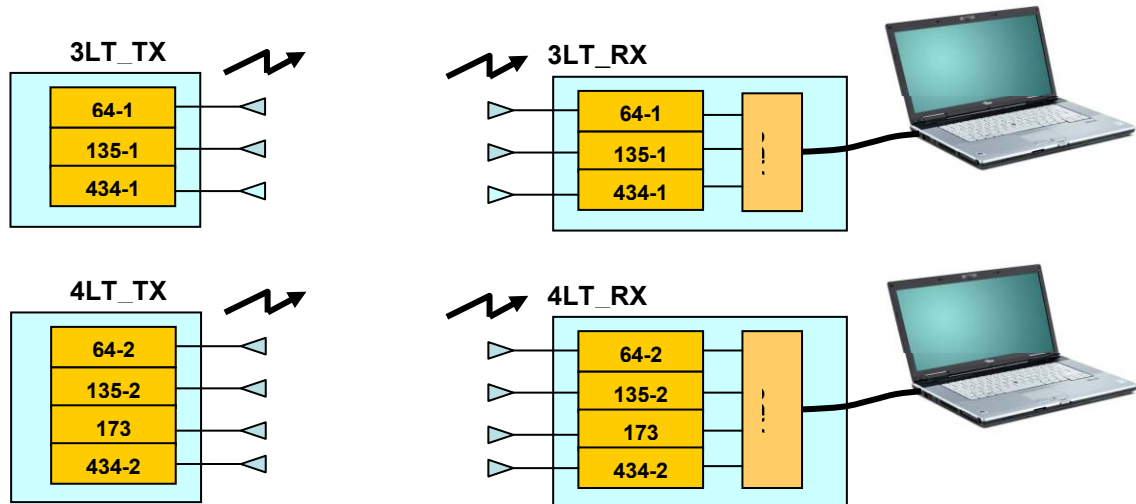


Figure 3.2: Simplified hardware block-diagram

It can be seen from Figure 3.2 where the operating frequencies for 3-channels equipment and 4-channels equipment are practically the same. The frequencies are 64 MHz, 135 MHz and 434 MHz, except for 4-channels equipment where there is one more operating frequency used which is 173 MHz. Details of each channels operating frequency with the output powers are written in Table 3.1.

Table 3.1: 3-channels (transmitter and receiver) and 4-channels (transmitter and receiver) equipment's operating frequency with output power

Equipment type	Channel	Carrier frequency, MHz	Output power, dBm
3LT_RX / 3LT_TX	64-1	64.125	20
	135-1	135.025	10
	434-1	434.450	20
4LT_RX / 4LT_TX	64-2	64.175	20
	135-2	135.075	10
	173	173.275	10
	434-2	434.600	20

Normally both equipments are running at the same time in the measurement. Both transmitters from 3-channels and 4-channels equipments will transmit signal and received by the receiver that will connected to the personal computer (see Figure 3.3). Even though sometimes the measurement of both equipments are running simultaneously, the capability of the receiver selectivity is able to work with both transmitter models at the same time. This will be an advantage for the system where it can be used for the study of space de-correlation of clutter signals and the target measurement in different FSR geometry at the same time as numbers of transmitter and receiver modules will be installed in separate places.

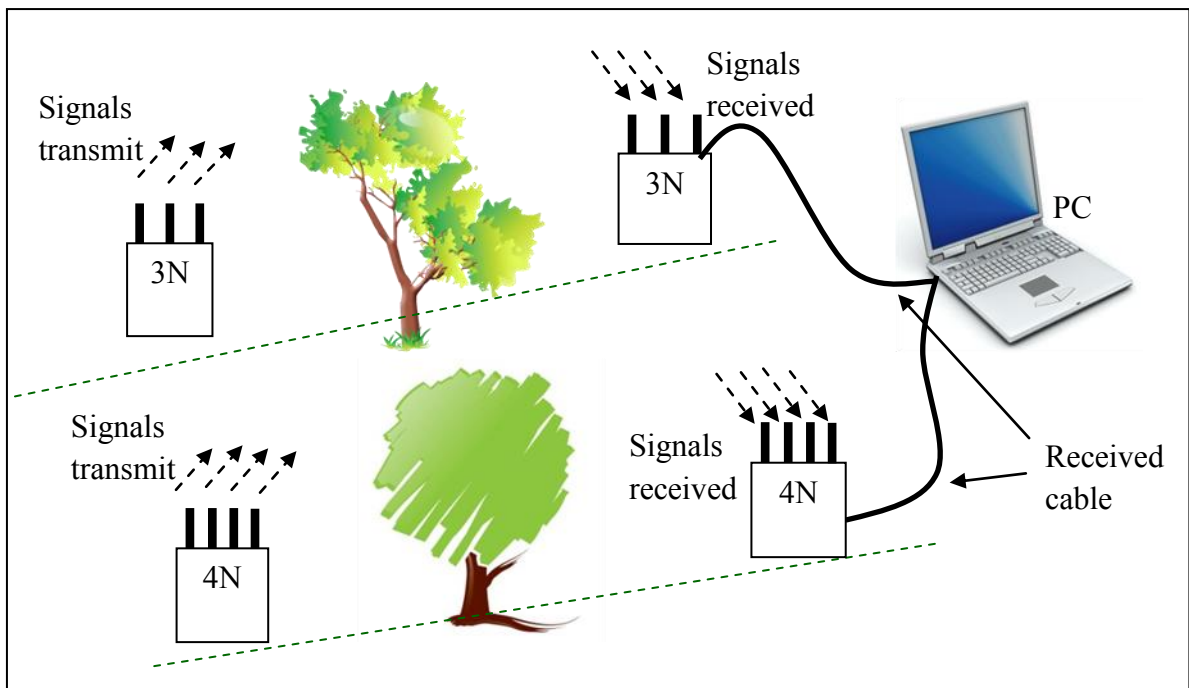


Figure 3.3: 3-channels and 4-channels equipment position during the experiment

In this experiment, helical monopole antennas are used for all frequencies in transmitter and receiver. In some specific measurements, directional antenna is also used for 434 MHz carrier frequency as well. Directional Yagi antenna is used for observation of direct signal transmission. The picture of the antennas is shown in Figure 3.4 and Figure 3.5. Multiple

frequencies are used to give any possibilities of changing the operating frequency in the equipment easily according to the trial's goal and also to analyse the effect of clutter signals on different frequencies.



Figure 3.4: Helical monopole antennas

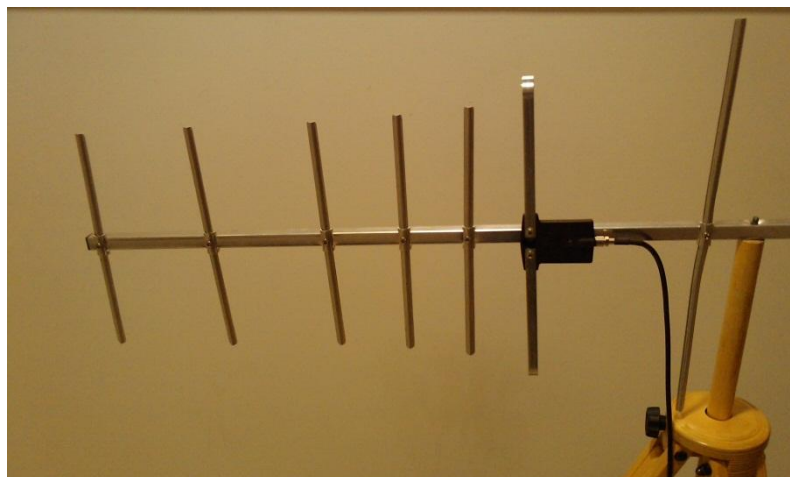


Figure 3.5: Directional Yagi antenna on tripod

3.3 Hardware Assembly

The transmitter and receiver modules are assembled as shown in Figure 3.6. In this figure, 4-channels module is used as an example. The receiver module is placed together with ADC, Doppler filter PCB and battery. Both modules are placed in a waterproof metal box. Then the BNC connectors are used for antenna's connections which are placed on top of the box. This can be seen in Figure 3.1.

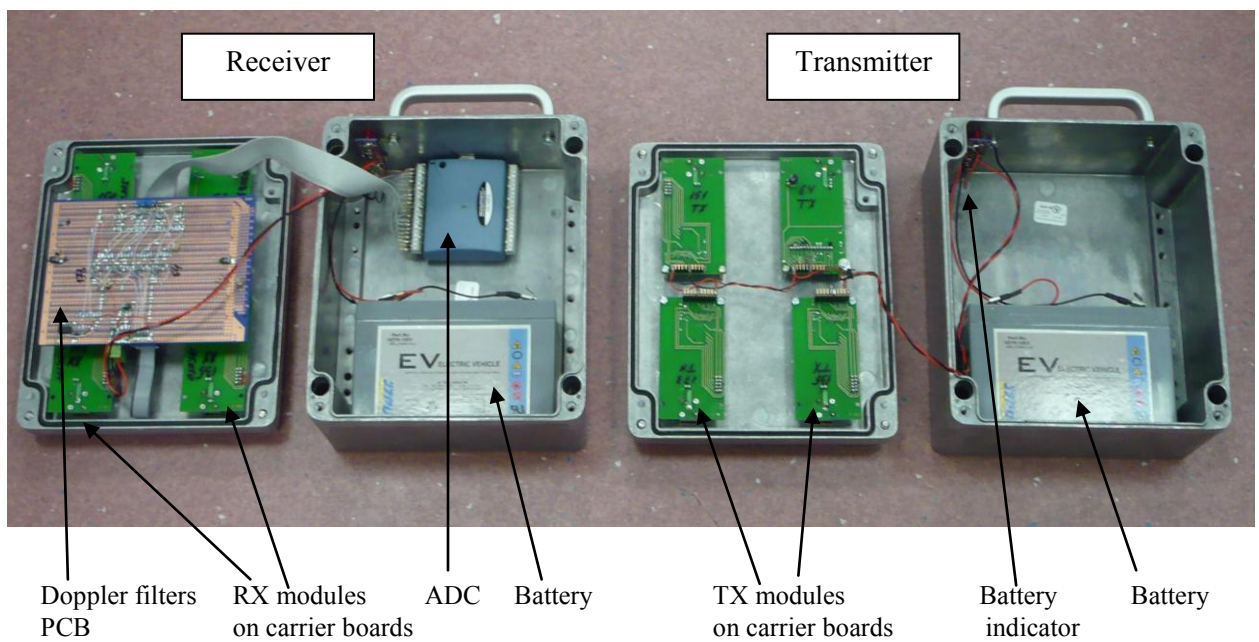


Figure 3.6: 4-channels transmitter and receiver modules assembly

There are two types of measurements involved in this research; short term measurement and long term measurement. The equipment's set up are different for both measurements. The equipment setting for short measurement is much simpler than the long term measurement. It is because for short measurement, the experiment is just in a few hours as compared with long term where the equipment is placed for several days. Proper set up need to be done to withstand the all-weather conditions such as rain.

The set up for short measurement is shown in Figure 3.3 where the equipment is placed directly on the ground, while for long term measurement; the equipment is placed in the bottom of waterproof container and the directional antenna is mounted on the top of the container as shown in Figure 3.7 and Figure 3.8. Then the equipment is connected to USB cable connector to a personal computer in central post room which is situated just next to the receiver (Figure 3.9). In this room, there are two computers used; one for the data collections and another one for the video data collections. Besides that, there is weather station (to check the weather during the measurements) and four wireless video cameras equipped with IR projector positioned at four different places around the baseline which the data from the cameras can be received via the antenna situated at the central post room as shown in Figure 3.8 and 3.9. The data from the video are recorded as a proof of any detections, that are used for the comparison with the measurement's data in data analysis.



Figure 3.7: 4-channels equipment assembly in the container



Figure 3.8: FSR equipment and video camera and on positions (left – receiver; right – transmitter, in the middle – video camera and IR projector, one of four)



Figure 3.9: Central post (left – FSR data acquisition and video surveillance computers; right – receiving antennas for wireless cameras and weather station)

3.4 Measurement Test Sites

Numbers of measurements have been done to analyse the characteristic of clutter signals.

Many factors are considered to classify different measurement test sites. These include:

- presence or absence of vegetation within and around the FSR position and the character of the vegetation;
- presence of roads, which different vehicle targets could move on;
- presence or absence of false targets (humans, vehicles, animals);
- the level of environmental noise and interferences;
- the maximum baseline distance available;
- the form of terrain (flat or rough);
- presence or absence of different obstacles, multi-path propagation, and so on.

All these factors give major impact to the received clutter signals. Each of the factors contributes different characteristics that may affect the signals, especially with the presence of wind.

There is no ideal place for all kinds of measurements. Most of the measurement test sites are chosen depends on the main goal of the trial itself. Normally the test sites replicate similar characteristic with certain places example, such as an old airfield in Tilefords in Pershore which replicate the flat terrain surface. Another example is Cleehill and Malvern Hill, which are the hilly side that replicate mountain areas. All the venues of measurement test sites are discussed as below:

i. Airfield Test Site (Flat Field)

Old airfield situated in Tilesford is one of the measurement test sites chosen due to flat surface shown in Figure 3.10. There are no multipath effect and the possibility of human and car crossing the area are very minimal. The baseline of the measurement is set to be 100 m to 500 m. There are two types of ground surface in this area: concrete, on the runway, and grass, outside the runway.



Figure 3.10: Airfield test site

We can observe that the influenced of blowing wind will have caused very strong atmospheric clutter and not from the vegetation clutter. Numbers of trials have been made in this place during the period of February to March 2009, including car targets, convoy (two cars, humans in a convoy) targets, human targets and clutter measurements.

ii. Flat Field Test Sites Surrounded by Vegetation

These two practically same sites both having flat grass field areas that surrounded by vegetation are shown in Figure 3.11 for Shenneleys Park and Figure 3.12 for Metchley Lane sport pitch site. The modules are placed in the middle of the flat field with the baseline used around 100 m to 200 m. In here vegetation clutter and environment clutter are present due to the wind. How strong it is depends on the wind blowing during that time. The stronger the wind, the stronger it will sway the branch of the trees and increase the possibility of stronger environmental clutter signal.



Figure 3.11: Shenneleys Park test site

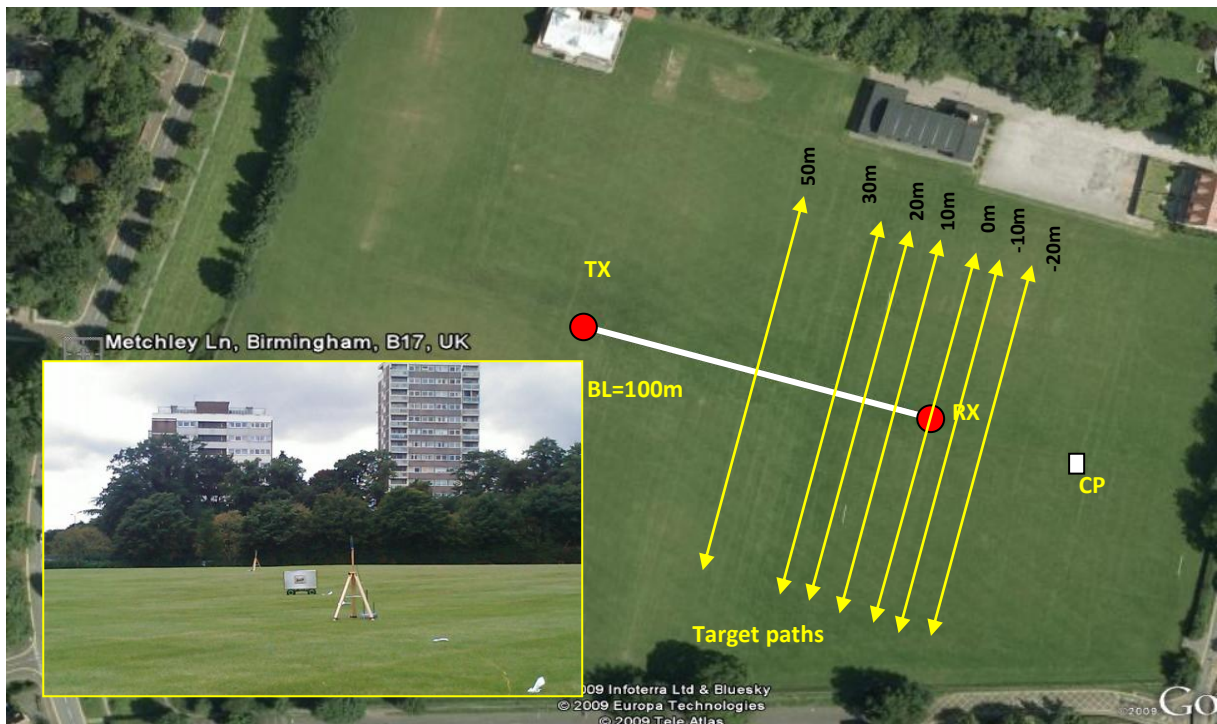


Figure 3.12: Metchley lane sport pitch site

There are disadvantages of these test sites. In Shenneleys Park, it is a public place where uncontrolled targets such as human and dogs moving around. These can create false target reply to the received signals. While for Metchley Lane sport pitch site it is near to Queen Elizabeth Hospital which create some radio interference at all frequency in VHF band. Other than that, both give good place for measurement test.

Roke Manor in Figure 3.13 is also another example of flat area surrounded by vegetation. It is situated in rural area in Southampton. It is a private area with limited access to the test site. Baseline was measured at 75 m to approximately 100 m with two sets of equipment are used. This test site is located just next to the pig farm. This will interfere the received signal as the pig moving around.



Figure 3.13: Roke Manor test site

iii. Horton Grange Test Sites (Complex Vegetation)

Horton Grange is a complex environment which is situated near EECE Department of the University of Birmingham and, consequently, is very convenient for everyday testing. It is a flat area with different kinds of vegetation such as large and small trees, bushes which is dense enough to create different scale (low, medium and strong) of vegetation clutter. This is an ideal place for vegetation clutter measurement.

Figure 3.14 shows the position of long term trials in Horton Grange where four cameras are positioned in different places to get accurate results. The disadvantage of this place is some of the signals are distorted by neighboring signals from a nearby hospital.



Figure 3.14: Long term trials position in Horton Grange

iv. Dense Vegetation Test Sites

Botanical garden is a unique place where lake and dense wood can be found in one area. It is also situated near to University of Birmingham. The dense wood located on the bank of Edgbaston Lake and when the wind blown from the lake towards the wood, the tree branches swaying with full magnitude. The highest strong wind ever recorded during the measurement is from 30 – 45 km/h speed with 200 m baseline. As a comparison from all the measurements made from all test sites, results from this test site contribute the highest vegetation clutter ever recorded because of the high wind speed during the experiment. Figure 3.15 shown Botanical Garden with the position of transmitter (TX), receiver (RX) and the personal computer (PC).



Figure 3.15: Botanical garden in the University of Birmingham

Another quite similar place used for the measurement is Lickey Hill Park. This is totally forest with two baseline positions used, one on flat surface along the ravine, and another one across the ravine. As a public park, this place has big disadvantage because a lot of people walking around and sometimes with dogs. So it is quite difficult to get clear target and just clutter signals. Please refer to Figure 3.16.



Figure 3.16: Lickey Hills Country Park test site

v. Cleehill and Malvern Hills Test Sites (Hilly Areas)

The Cleehill area shown in Figure 3.17 is an old mine with rough terrain. There is no vegetation except grass and small bushes. In here the experiment was done to analyse the effect of rough terrain if the equipment is to be placed in this kind of place in the future. This is an open area with public access. So this is disadvantage for us to do clutter measurement due to target (human and dog) passes by frequently, but it is an advantage if we want to make target measurement.

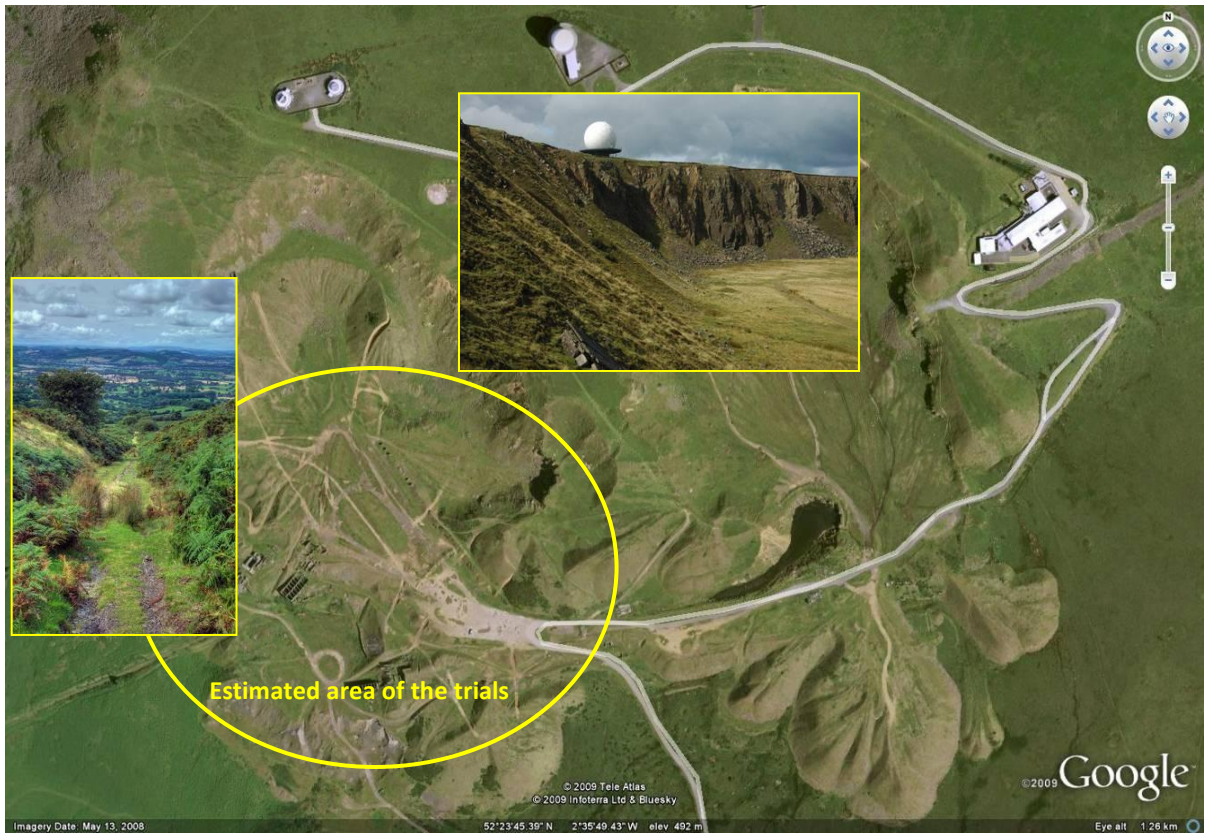


Figure 3.17: Cleehill test site

Malvern Hills as shown in Figure 3.18 is situated between Herefordshire, Gloucestershire and Worcestershire. It is a hilly terrain with small trees in few parts of the area. Same as Cleehill, Malvern Hill also an open area for public access. There are lots of people and dogs walking around on the hills and sometime walking along our baseline. Clutter measurement will not be a good idea in this place but we managed to get few data of clutter signals without any target interfering the signals.

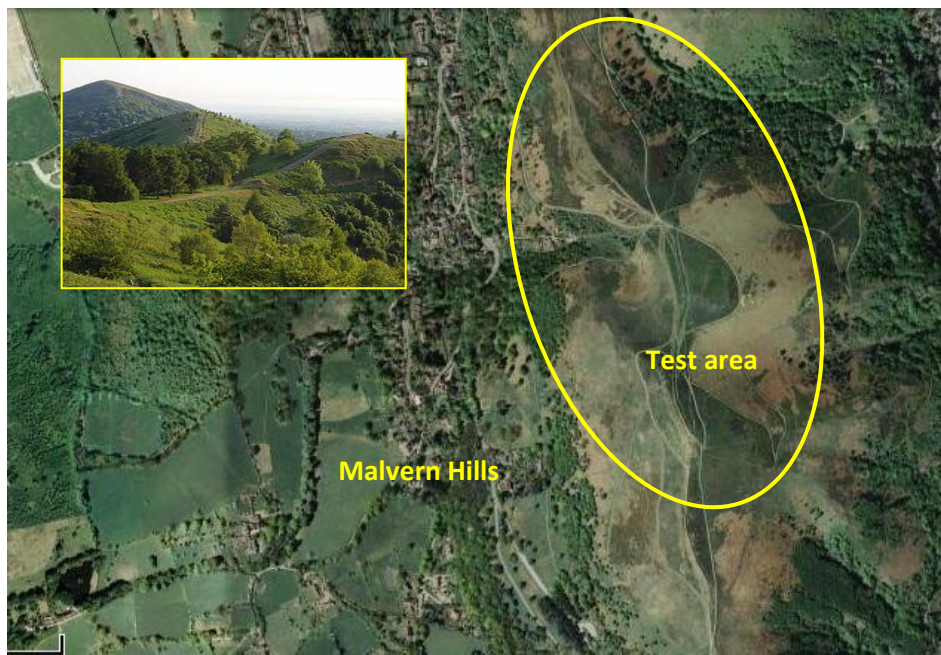


Figure 3.18: Malvern Hills test site

All test area sites are summarized in Table 3.2 for quick view. It is much easier to view in this way as a comparison between all the test sites with different characteristics such as:

- types of Terrain – flat with concrete, flat with grass, hilly, very rough, dense wood or half wood half flat (lake)
- environmental category – what type of surrounding – rural, business, urban or residential
- vegetation - types of surrounding vegetation – grass, bushes or dense wood
- maximal baseline length, m

Table 3.2: Measurement sites comparison

Test site	Figure	Terrain	Environmental category	Vegetation	Maximal baseline length, m
Old airfield, Tilesford, Pershore	3.10	Flat	Rural, with some interferences	No	500
Shenneleys Park, Birmingham	3.11	Almost flat	Residential	Surrounding	250-300
Metchley Lane Gymnastics Field, Birmingham	3.12	Flat	Residential, urban	Surrounding	250-300
Horton Grange, UoB	3.14	Almost flat	Business, urban	Complex: trees, brush	100
Botanical Garden, UoB	3.15	Almost flat	Residential	Forest and open space	200
Lickey Hills Country Park, South of Birmingham	3.16	Flat and rough	Rural	Forest	300-400
Roke Manor, Romsey, Southampton	3.13	Flat	Rural	Surrounding	60-100
Old mines, Cleehill, Shropshire	3.17	Rough, hilly	Rural	No	300
Malvern Hill, Herefordshire, Gloucestershire and Worcestershire	3.18	Rough, hilly	Rural	No	100 - 200

Among all the places that we tested for our measurements, Botanical garden contributed much higher clutter power as compared to other site such as dense wood, Shenneleys Park or even Airfield. This is because the strong wind and gale that is blowing from the open area (lake) is damped by the dense wood situated at the end of the lake. From all the places, Horton Grange is chosen as suitable test site for long term measurement because it has complex vegetation in surrounding and furthermore it is closer to University of Birmingham. As for now, there are four conditions of winds have been taken in this place such as very strong (gale), strong, medium and low wind speed.

3.5 Method of Measurements

There are lots of work has been done to analyse the effect of clutter in Forward Scattering Radar (FSR) network. In this research, FSR network is using bistatic radar system configuration where the transmitter and receiver are separated within a distance called as baseline (BL). When the transmitter or receiver is placed in certain position in the surrounding area full with vegetation and foliage that grows on or near the baseline, it will add to the target signal and sometimes can even mask it making difficult signal detection. The unwanted reflections from a vegetation creates noise-like signals that received by the receiver are what we called as clutter. The FSR network system is not robust to clutter. This contributes to the limitations of FSR system where the absence of range resolution will cause the clutter pick up from large area around the sensors. The omnidirectional antennas that are used as sensors also contribute strong clutter collections.

Vegetation and foliage are the main influence of clutter, especially in the presence of wind. Foliage such as branches and leaves from trees will sway in one fixed position. This swaying

foliage under windy condition creates additional noise in Doppler frequency band and does not have Doppler Effect nature and practically independent of radar frequency over wide range of frequency band [11].

In this research, clutter in forward scattering (FS) micro radar network for ground targets is analysed in different environment such as flat or rough ground surface, dense wood, hilly side and many more. With all these varieties of landscapes, it will cover possible scenarios of different places all over the world and analyse the effect of environment to the clutter signals. Furthermore it also covers full weather conditions such as snow, rain and windy day [8].

The FS micro radar system operates in VHF (about 60 and 150 MHz) frequency band for very rough target detection and at higher frequency in the UHF (about 400 MHz) frequency band for very precise detection. Sort-range FSR micro sensors operates at the baseline of around 50m to 200m in length. The receiver will then connect to computer for data processing.

3.6 Measurements

The main work for this research is the analysis of clutter. In these analyses, all the characteristics of the clutter signals are analysed. It is obvious, that vegetation clutter depends not only from the vegetation types and its density around the FSR position, but also from the wind speed. Stronger wind causes vegetation to sway with bigger amplitude creating bigger clutter signal. So that, to analyse clutter properties we should take into account in which weather (especially wind) conditions the measurements were done. The wind measurement experiments are carried out in Horton Grange and Gisbert Kapp Building at University of Birmingham. Results from this experiment will be used for the next analyses.

- **Wind Measurement**

The wind speed measurements are done in two different set up places in Horton Grange and Gisbert Kapp Building in the University of Birmingham. This is to compare and observe the wind speed on the ground (with surrounding trees in Horton Grange) with roof top area (open area on the top of Gisbert Kapp Building). This measurement is mainly for long term measurement which needs to be done in Horton Grange. Wind speeds give major influence to detection signal. When the wind speed is high, it will blow all the trees in surrounding areas and the branches will sway which create big clutter to the signal.

Figure 3.19 shows the experiment set up in Horton Grange. The portable wind station is placed on vehicle roof top about 2.5 m from the ground shown in Figure 3.20 (a). While Figure 3.20 (b) shows the roof top station on top of Gisbert Kapp Building. Graph in Figure 3.21 shows the comparison of wind speeds between roof top station and portable weather station in Horton Grange for low, medium and strong wind conditions.



Figure 3.19: Portable weather station on the roof of Land Rover

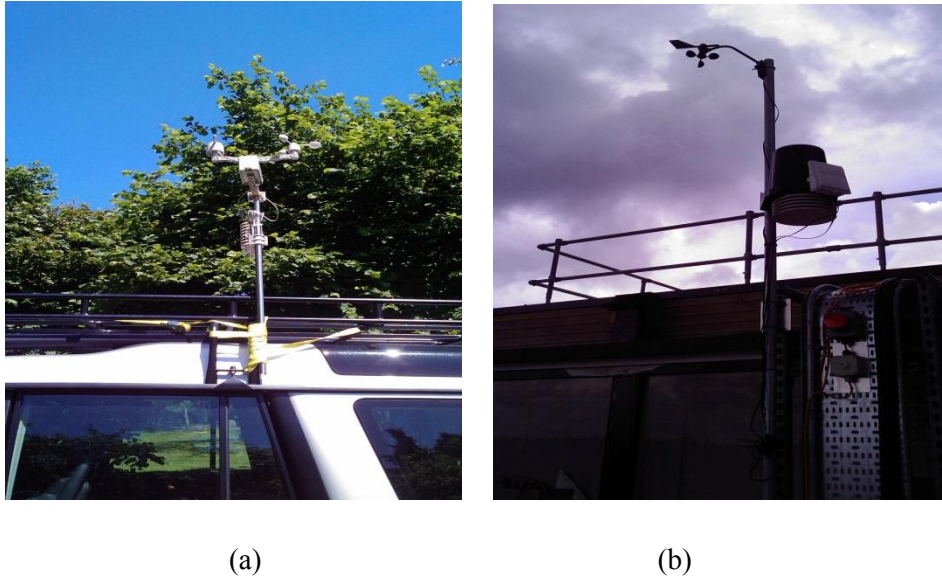


Figure 3.20: (a) Portable wind station (b) Roof top wind station

The data for the graphs are taken from two different days with three different wind conditions. Data from Figure 3.21 (a) is taken from strong windy day on 17th June 2009 where it ranges from 8 mph to 16 mph (from roof top wind station). The wind speed is quite steady within the range. While the wind speeds for the portable weather station at the same day are about 3 mph much lesser than the roof top station. This is because it is understandable that wind speed in an open area with the height of more than average height of any tree surrounding can be very high compared to the wind speed taken from just 2.5 m above ground with surrounding trees. The wind is damped by the surrounding trees.

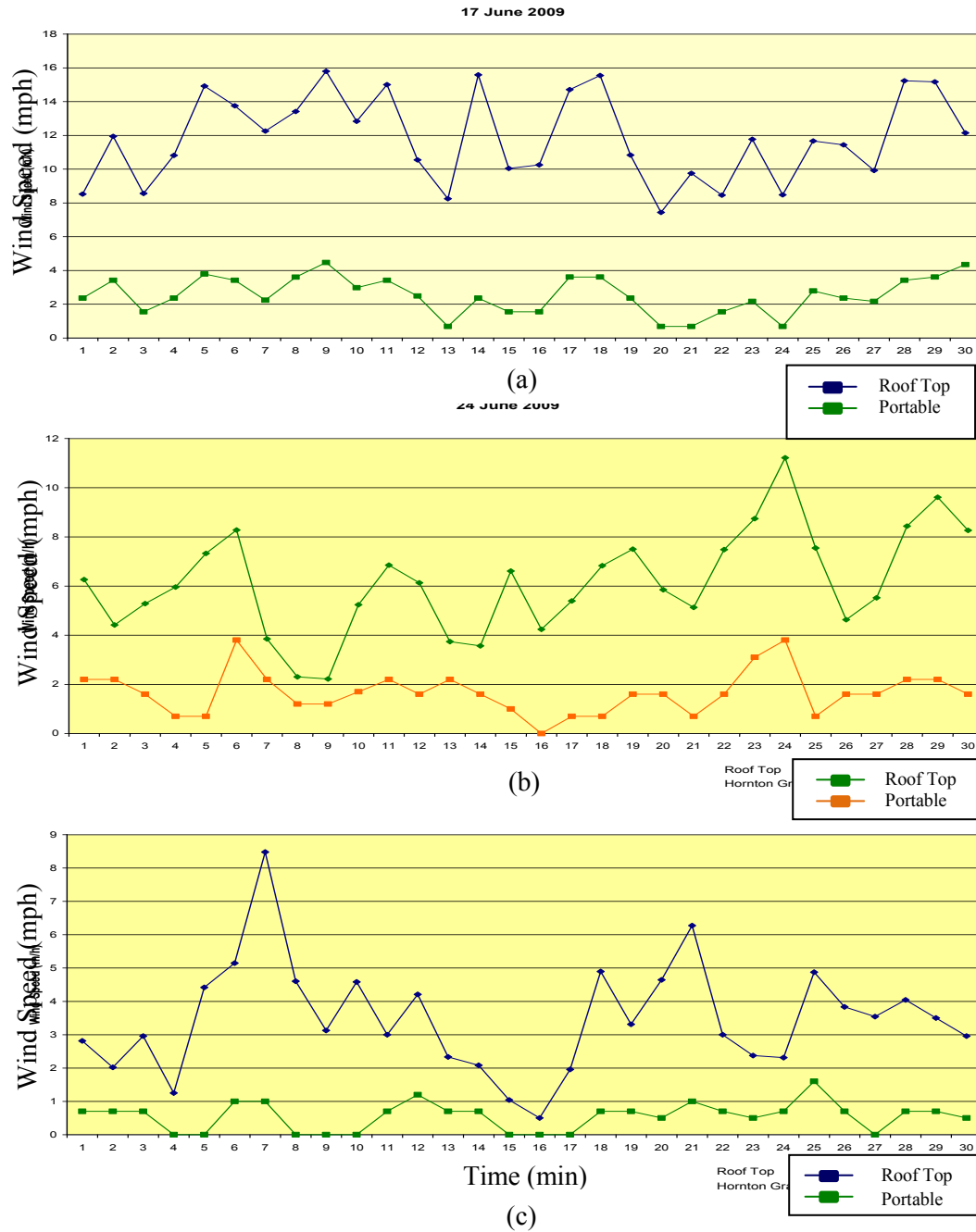


Figure 3.21: Wind Speed Comparison between roof top station and portable station in three different wind conditions; (a) Strong (b) Medium (c) Low

Figure 3.21 (b) and (c) are taken from two different wind conditions; moderate speed and slow speed respectively. From all these three graphs, it can be concluded that the trend of the wind speed of portable station and roof top station are similar and either one

of the wind stations can be used as the wind condition reference for the main experiment.

Then all the main experiments will be carried out. This will include the experiment for the target signal detection and clutter signal. The experiments are divided into two main measurements. One is the short term measurement which is mostly for target detection experiment. The measurement was done at some given weather conditions to a day of tests, but in different vegetation surrounding. The second measurement is the long term measurement which is mostly for clutter experiment. Long term tests were done in the same FSR position to examine the dependence of clutter from wind conditions and day time; and observed for a long period of time (few days) to collect clutter at different weather.

The short term measurement is done in several places such as at Shenneleys Park, Airfield, Roke Manor and many more. All together there are nine different places (as stated in Part 3.4 in this chapter). While the long term measurements are done at Horton Grange due to the complex vegetation in the surrounding area and ideal for vegetation measurement. Details of each of these measurements will be discussed in the next part.

i. Short Term Measurement

These sets of measurements have been done in few places on different days. This is to study the effect of different environments to clutter signal. The measurements have been carried out using 3-channels and 4-channels module equipments. Each measurement is set up with 20 minutes running program with baseline varies from 50 m to 200 m. All received signal will be

stored in a personal computer for further analysis on understanding the effect of clutter in the received signal.

Figure 3.22 displayed the set up position example of 3-channels and 4-channels modules in Botanical Garden in Birmingham for clutter measurement. Botanical Garden is chosen due to geographical area with a lake on one side and dense wood in the other side. This is as an example on how the experiments have been carried out for short term measurement experiment. By comparing all the results from all the measurements, Botanical Garden represent very strong clutter signal. Winds that travel from the lake surface (flat area) are blocked by dense wood. The strong clutter signals will be detected by the receiver. Details of the clutter results due to wind speed are explained in Chapter 4.

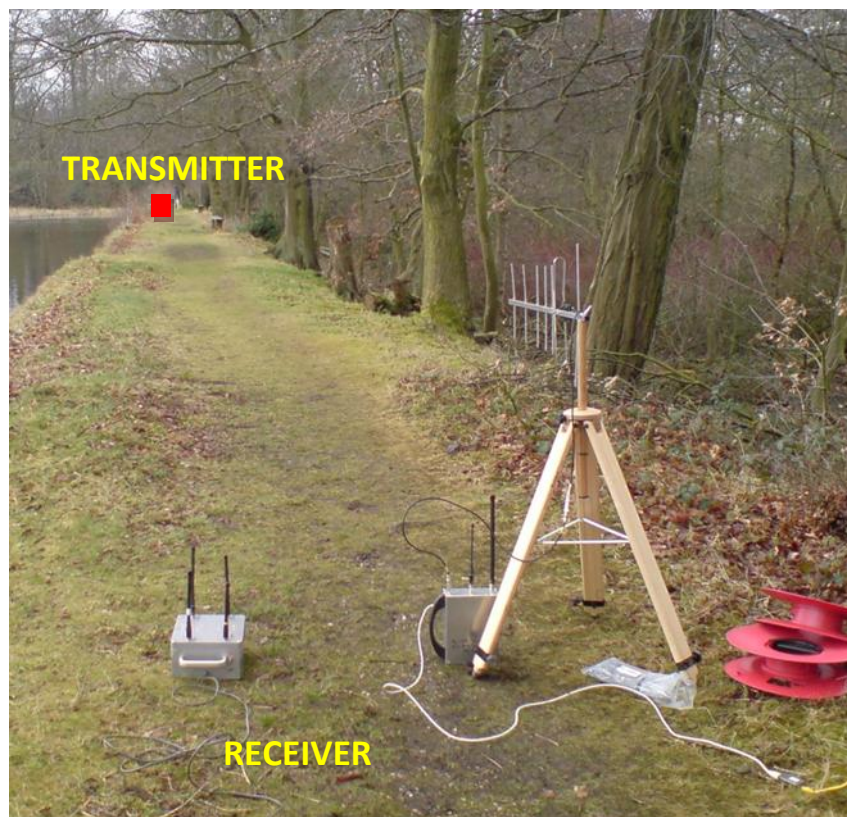


Figure 3.22: Example of equipment position of short measurement in Botanical garden with 100 m baseline

ii. Long Term Measurement

Long term measurement has been carried out in Horton Grange, Edgbaston, University of Birmingham. With long term monitoring of selected areas accompanied by video surveillance developed by Swann Communications Limited. With this video recorder, it will provide better understanding of the system functionality.

This experiment is mainly about clutter signal. The received data signal is compared with the video data. This is just to specify the system performance for 24 hours running experiment in real environment. There are two results that need to analyse in this experiment. One is to investigate any false alarm (unwanted targets) that can be detected during the 24 hours running experiments and second is totally the analysis of the clutter signal itself.

Horton Grange is chosen due to the complex environment in the surrounding area which is suitable for clutter analysis. It is a medium density wooden urban area in which different targets are expected: humans, small animals (squirrels, foxes) and birds within forward scattering radar (FSR) position as well as cars and humans moving on the roads outside the baseline in a distance 50-100 m. Total FSR baseline length is around 100 m. The experiments are conducted 24 hours. In the evening and morning time, the presence of human targets is estimated, but for night times (say, from 10 pm till 6 am) the possibilities of any human passing nearby are very minimal.

The operational area is controlled by four video cameras and illuminated by IR projectors in night times. All these four cameras are pointing directly to baseline position so any false target crossing and moving near the baseline can be seen. These include one in the middle of

the baseline (cam 1), one near the receiver (cam 2), another one facing towards the baseline (cam 3) and the last one near the transmitter (cam 4). The positions of the cameras can be referred to Figure 3.14.

The video camera will be running at the same time as the equipment running. The collected video from the wireless camera then will be transmitted to the camera receiver (using Yagi antenna) at the central post as shown in Figure 3.9. Personal computer is used to collect and store cameras video (1 frame per second). These video data are then processed which by going through it manually and compared with the Doppler data signal. Then the data of any crossing are recorded which include the time of any occurrences occurs. Figure 3.23 and Figure 3.24 shows the video display on the computer from one camera (CAM 2) and all cameras respectively using Swann software.



Figure 3.23: Test site in Horton Grange (View from position of camera 2)



Figure 3.24: Test site in Horton Grange (View from all cameras)

Then all the data from the measurement in Horton Grange are recorded in Long Term Processing Form as shown in Figure 3.25. In this form, all the video data detection and also data signal will be recorded. These include the date of the experiment, the data signal file name, the start and stop time for data taken from both data signal and video detection, then the video detection column (any detection that can be seen from the video camera), next will be the signal processing which include non-coherent and cross-correlation processing (signal processing for target detection).

Location:		Horton Grange		Baseline distance		100m	
Date:		04-05.11.2009		See table			
Wind Speed:		Sampling		20 Hz		Attenuators	
Hardware:		4LT_RX&TX		20dB 64RX		10dB 135RX	
Weather conditions:		Windy and sunny day		10dB 173RX			
Task:		Human (Alan) as a target with different crossing points on BL, different humans and animals around					
		Data time duration in one file		20 min			

Date	File name	Time		Video detections (target type)				Non-coherent			CC detections			Optimal			
		Start	Stop	CAM1	CAM2	CAM3	CAM4	64	135	173	64/135	135/173	64/173	64	135	173	Wind
04.11.09	File HG_1 Started at 10:59:32	10:59:36	11:00:00	Human P6				√	√	√	x (0.74)	√	√	To be processed in future			0,3
		11:00:10	11:00:50	VS P7	VS P7	VS P7		√	√	√	√	√	√				
		11:01:25	11:01:54	Alan P7	Alan P7	Alan P7		√	√	√	√	√	√				
		11:01:25	11:01:49				Squirrel	√	√	√	√	√	√				
		11:07:30	11:07:35	Human P6	Human P6	Human P6		√	√	√	√	√	0				
		11:09:00	11:09:19	Human P7	Human P7	Human P7		√	√	√	√	x (0.53)	√				
		11:10:46	11:10:54	Alan P6	Alan P6	Alan P6		√	√	√	√	0	√				
		11:11:53	11:12:55				Squirrel	0	√	√	0	√	0				
	HG_2 (11:19:32)	11:15:00	11:15:36	Alan P6	Alan P6	Alan P6		√	√	√	√	x (0.65)	√				0,3
		11:18:38	11:19:10	Alan P6	Alan P6	Alan P6		√	√	√	√	x (0.68)	√				
		11:20:16	11:21:33				Squirrel	0	0	0	x (0.53)	0	x (0.68)				
		11:22:48	11:23:02	Alan P5	Alan P5	Alan P5		0	√	√	x (0.53)	x (0.63)	0				
		11:25:19	11:29:52	AY + VS (adjust Cam 2)		AY + VS (adjust Cam 2)		√	√	√	√	√	√				
		11:31:30	11:34:30				Squirrel	0	0	0	√	x (0.61)	x (0.63)				
		11:38:00	11:38:20	VS P7	VS P7	VS P7		√	√	√	√	0	√				
		11:39:39	11:41:00				Squirrel	0	0	0	0	0	0				

Figure 3.25: Database Test site in Horton Grange Form

From this form the false alarm or true detection can be determined. If the signals are detected from both video and data signals, means that it is true detection but if the signal can only be detected by the data signal only and not from the video data, means that is it a false alarm.

3.7 Data Processing

Data processing is the main part of the research. In this part all the received signals either from short term measurement or long term measurement will be processed for further analysis. This includes the analysis to check the power level, power spectrum density, amplitude distribution and many more. This complicated part is divided into two main stages:

i. Stage 1: Data acquisition

This stage is the first stage of data processing part. The entire received signal will be stored in computer database that connected to the receiver. To collect the data, first the equipment (3-channels or 4-channels equipment) is connected to the computer. *Install Calc* program is used to detect the equipment. After the equipment has been detected, the Data Collection program is used to monitor the received signals. This program is developed by MISL group using Mathcad Software.

ii. Stage 2: Data analysis

There are two types of data that are analysed. One is the short measurement data and another set of data is the long term measurement data.

- **Short Term Measurement**

Short term measurement is set in several places with 20 minutes long for each data. All data are processed using Real Signal Processing program developed by using MATLAB Software. As shown in Figure 3.26 In this program all parameters such as operating frequency, equipment module (3 channels or 4 channels), sampling rate, time for each data, cut-off frequency for the filters and number of bins used for Weibull distribution are keyed in. Step-by-step instructions on how to process the data are described in Appendix B.

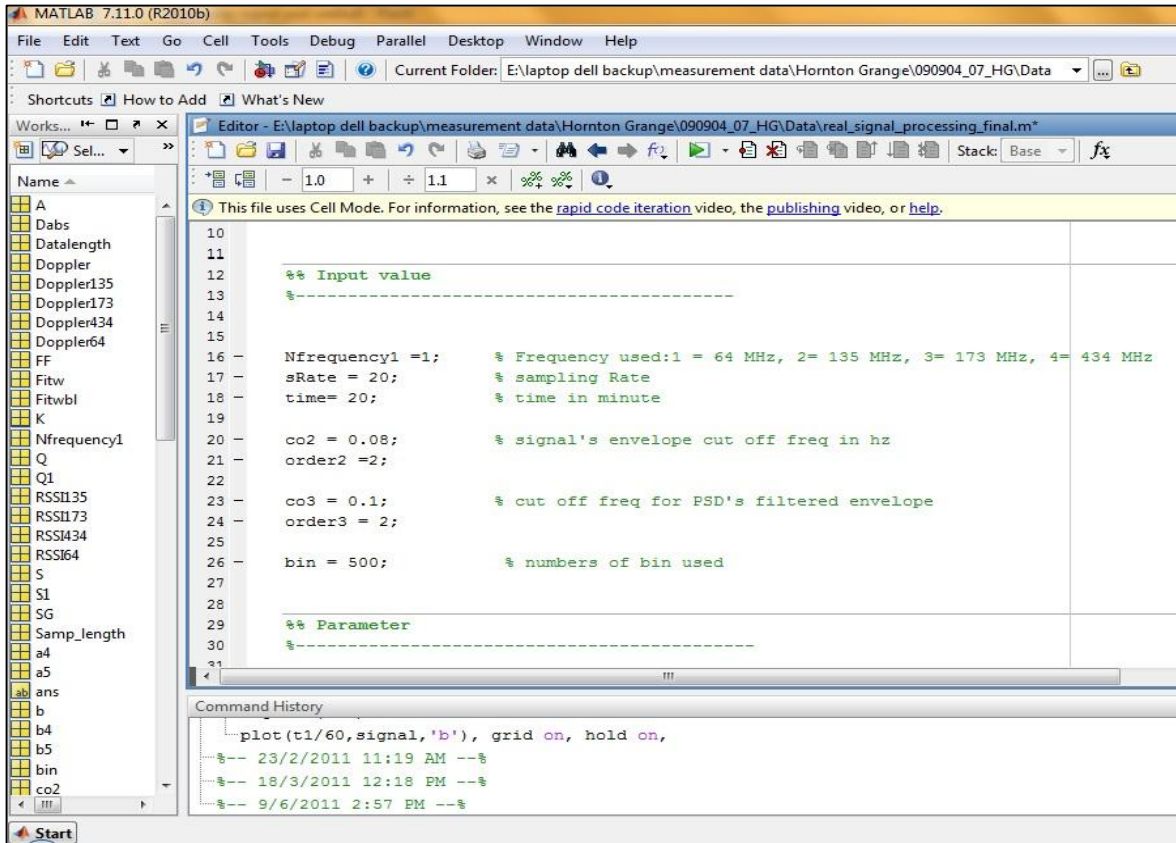


Figure 3.26: Real signal processing program layout using MATLAB Software

The output from the program, displayed the Doppler signal for four different frequencies (64 MHz, 135 MHz, 173 MHz and 434 MHz). Next will be the envelope's minimum and maximum value, (envmin, envmax), signal's standard deviation (stdsignal), signal's dynamic range of the envelope (d_range), the mean value (mu), signal's power spectral density (PSD and signal distribution). Results are displayed as shown in Figure 3.27. Figure shows the analysis for 64 MHz strong clutter strength signal with 0.1 cutoff frequency for the signal's envelope and 1.75 for Weibull's fit shape factor.

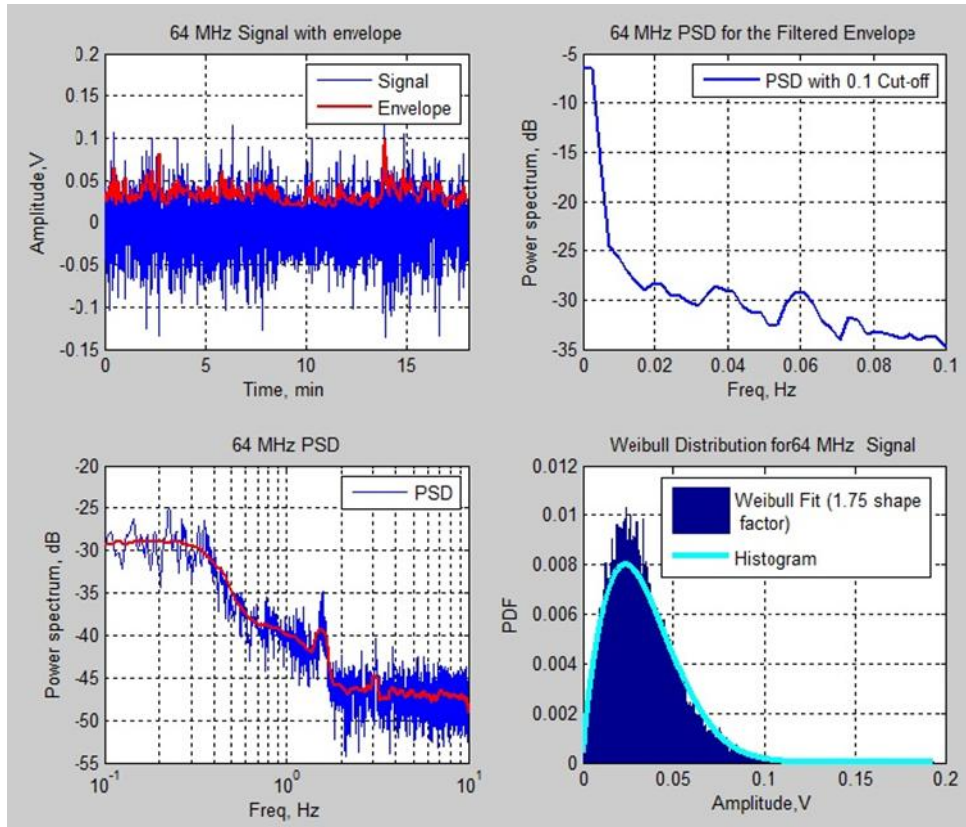


Figure 3.27: All output signals

- **Long Term Measurement**

In long term measurement the program is a bit different even though there are some part of it is still the same. In this measurement program shown in Figure 3.28, it is developed to read all the data files in one time. There is one main program and two main sub-functions. The main program is used to call the two main sub-functions and to display all the output graphs. Step-by-step instructions on how to process the data are described in Appendix B and long term measurement full program can be view in detail in Appendix A.

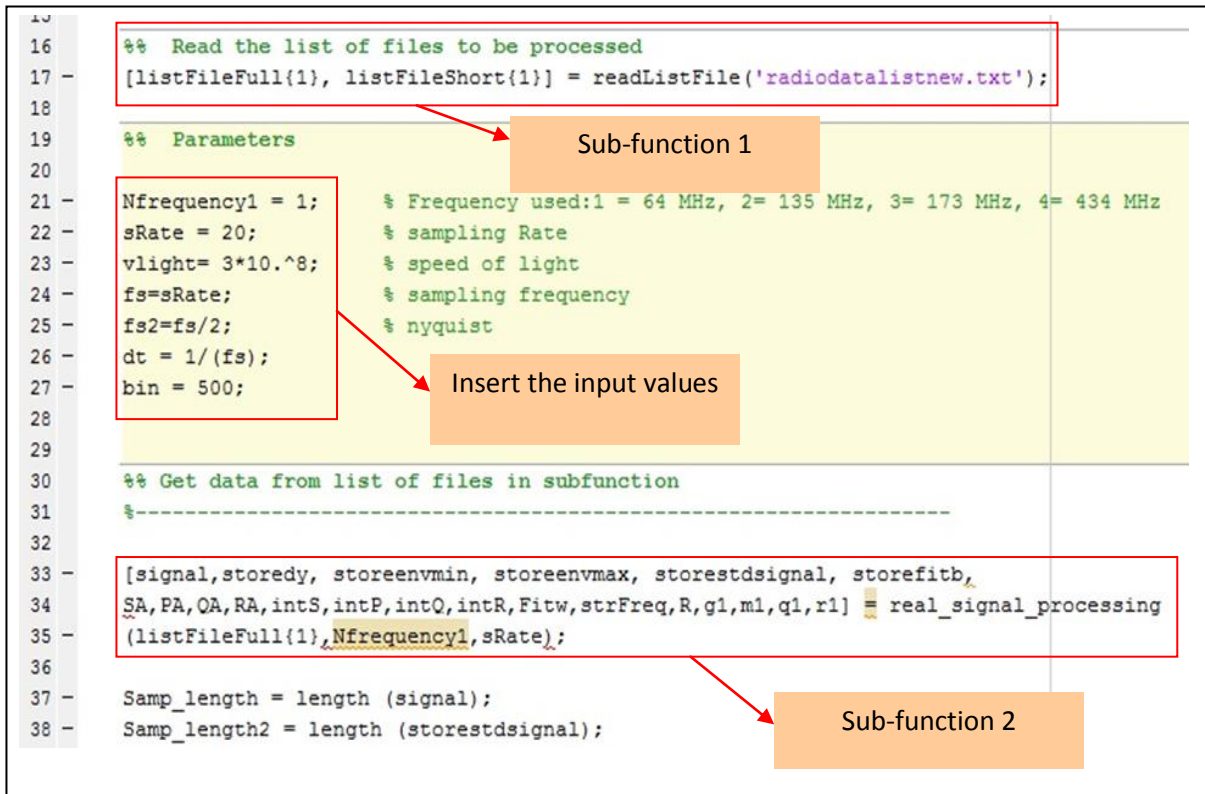


Figure 3.28: Main program of long term measurement (run_all_measured_cluttersignal.mat)

The two main sub-functions used are:

a. readListFile.mat (Sub-function 1)

This sub-function was created earlier by one of the group member in MISL Group. This function is used to call all the data file in my database. This is much simpler rather than open and analyse each files one by one. In this sub-function it will read all the data file name that is written in radiodatalist.txt file that is saved in the same folder. Radiodatalist file content all the data filenames that need to be process.

b. real_signal_processing.mat (Sub-function 2)

In this sub-function, it processes all the data file for the current directory one by one in one time. In here, the signal's STD, envelope minimum and maximum, PSD and the

shape factor will be analysed same as in short measurement program. The only difference in here is the data signals are combined among few hundreds of data files and run simultaneously. All the results will then transferred back to the main program in `run_all_measured_cluttersignal.mat`.

Details of these two stages are described in Appendix B.

3.8 Summary

In this chapter, methods of measurement used in the research are described step by step. These include short term measurement and long term measurement which are used for clutter analysis. Detailed of the programs used are attached in Appendix A. Each measurement has their own set of analysis. These analyses include the influences of different test sites to the system and different environmental conditions. Different test sites are mentioned and the comparisons between the test sites are discussed in Section 3.4. Results from the analyses will be described in Chapter 5.

CHAPTER 4

EXPERIMENTAL CLUTTER ANALYSIS

4.1 Introduction

In this chapter all the results for clutter analysis are shown. There will be a few sets of results. First is the results based on different parameters such as different test sites, baseline distances, different weather conditions and different frequencies. Second is the clutter analysis result based on different wind conditions which are categories as low, medium, strong and very strong wind conditions. Third is the clutter analysis results based on clutter power conditions categories in different frequencies and then into different clutter strength as low, medium, strong and very strong clutter power. All the characteristics such as the clutter amplitude, power spectrum, the probability density function, the cumulative distribution function and the dynamic range of the signals itself will be discussed. Before we begin with the result's analysis, first the physical model of vegetation clutter is analysed to proof the assumptions of the results. Furthermore, all the basic introduction of the characteristic will be described.

4.2 Physical Model of Vegetation Clutter

Clutter is the main factor limiting the performance of any Doppler radar especially when the radar network system is surrounded by complex vegetation. Vegetation mainly refers to

bushes and trees that are scattered in place or area that blocked the radio signal path. The branches and leaves of the trees will sway especially with the presence of wind. This will make the transmitted electromagnetic signal scatter and loss if it transmitted through bushes or trees. This situation can be modelled by physical model of vegetation clutter which is first formulated in [11]. This model is done in order to confirm the basic assumptions of the model with the real situations which are already analysed in [10]. All the characteristics of the modelled clutters are then compared with measured clutters. Then the practical approach is proceed for the non-stationary clutter simulation based on the clutter characteristics that have been analysed. This research is not under my scope of study but the results really proof that the assumptions made before is precise and can be compared with the results from my research.

4.2.1 Pendulum Experiment

Branches and leaves on trees and bushes will sway when the wind blown. The speeds of the movements are depending on the speed of the wind blown. We can see that it sways with quasi-oscillations movements with different amplitudes and periods from a stable position. As a result from this observation, we can model the foliage as a number of separate pendulums. This is shown in Figure 4.1 where the vegetation model imitating a tree.

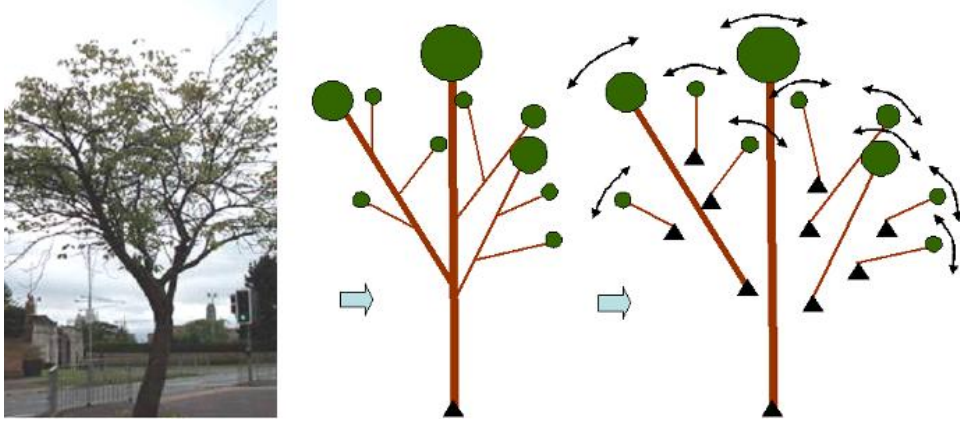


Figure 4.1: Vegetation model as number of pendulums

Before the physical experiment begin, simulation technique using oscillating target signature creation model is studied. It is done by using a pendulum as a target and this is stated clearly in [11] with results. Bistatic radar is used as a set up with 40 m baseline between transmitter and receiver. Then a pendulum which act as a small target is placed in the coordinates of (10, 30, 5) represent (x_0, y_0, z_0) coordinates in unit meters oscillates in x- axis direction with given period of time 5s and oscillation magnitude, A. This can be written in mathematical form where the target's positions are varies with time as [11]:

$$x(t) = x_0 + A \sin(2\pi t/T) \quad (4.1)$$

Two-ray path propagation model equation (explain in detail in [20]) is applied to equation (4.1) to see the outcomes of target detection for different magnitudes of oscillation. As a results described in [9], when the magnitude of pendulum increase, the magnitude of oscillations in the target signature will also increase as shown in Figure 4.2.

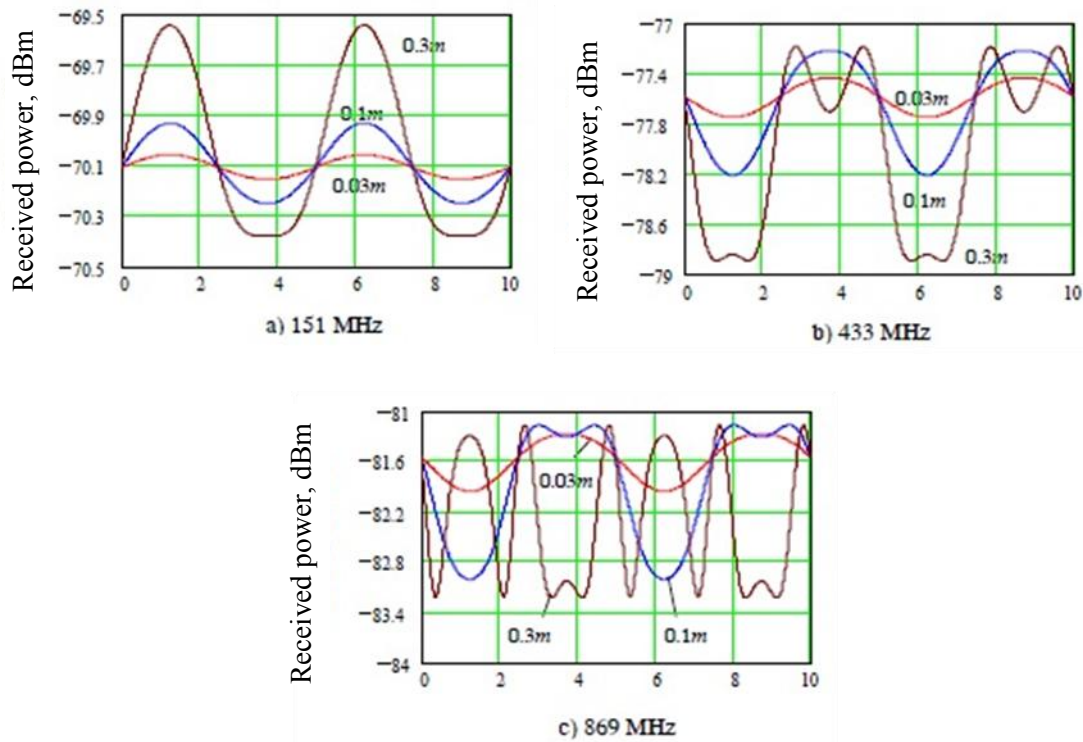
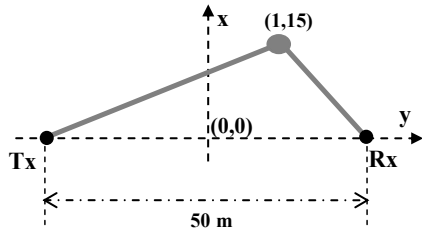


Figure 4.2: Pendulum oscillating results for three different frequencies and magnitude of oscillation [11]

Next will be the physical pendulum experiment which also describe in detail in [11, 20]. In this experiment, it is set up with FSR configuration with 9 m baseline and operating frequency of 869 MHz. A metal sphere with diameter of 21 cm is hanged as pendulum with length 2.35 m. Then the pendulum is oscillating with an initial magnitude of 1 m. A 3-D model is used as a target to create expected target signature [11, 20]. Results from the experiment show similar output as in target signature creation model. The magnitude of the pendulum increase with the increased of the target signature oscillation magnitude.

This analysis is then continued with an example of a return from Doppler receiver using numbers of pendulum imitating small bushes. Two-ray path propagation model is applied to the set of oscillators. This is to create similar tree model with branches and leaves with certain parameters. The parameters are such as uniform distributed amplitudes of mechanical

oscillation varies from 1 to 30 cm, the initial phase of the oscillation from $-\pi$ to π and uniformly distributed point of suspensions of the pendulum from 1 to 30 cm which originating with coordinate (1, 15, 1) in unit meters [10]. Figure 4.3 displayed the results of the experiment from the Doppler return of 30 pendulums for three different frequencies. From the results, it shows that the higher the frequency, the higher will be the signal's voltage amplitude and the trend of the signal's power spectral density is the same for all frequencies where it decreased with frequency.



(a)

(b)

(c)

Figure 4.3: Results from Doppler return model from 30 pendulums, (a) topology, (b) signal's return model, and (c) PSD [10]

4.3 Introduction to Clutter Properties

Clutter characteristics are the main factor that is analysed for each clutter signal. It is important to understand the clutter characteristics in order to generate clutter model so that it can be used to design a virtual radar performance system such as synthetic environment for FSR [53, 59]. These characteristics include signal standard deviation, power spectral density, probability density function, cumulative distribution function and the dynamic range. These will be described in detail next.

4.3.1 Signal Standard Deviation

The standard deviation (STD) is similar to average deviation, except the averaging is done with power instead of amplitude. It determined on how far the signal fluctuates from the mean. The equation of STD is as below: The STD can be calculated as below [24]:

$$\text{STD} = \sqrt{\frac{1}{N-1} \sum_{i=1}^N |A_i - \mu|^2}, \quad (4.2)$$

where A is the clutter signal made up of N input data and μ is the mean of A :

$$\mu = \frac{1}{N} \sum_{i=1}^N A_i \quad (4.3)$$

4.3.2 Power Spectral Density

Power spectral density (PSD) can be defined as a function which shows the power strength of the signals at various frequencies [8, 59, 60] or how the power distributed in certain frequency. Normally PSD is described as decibels per hertz (dB/Hz) and PSD is the Fourier Transform of the auto-correlation function of the signal. Let say the signal is denoted as $x(t)$

and the power spectral density is $S_x(f)$. Then the power spectral density equation can be stated as [60]:

$$S_x(f) = \lim_{T \rightarrow \infty} \frac{|F_T(f)|^2}{T} \quad (4.4)$$

Where $F_T(f)$ is the Fourier Transform of the signal with the equation as:

$$F_T(f) = \int_{-T}^T x(t) e^{-2\pi i f t} dt \quad (4.5)$$

4.3.3 Probability Density Function

Amplitude distribution of clutter is the most important property in clutter analysis. This includes the analysis of probability density function or PDF in clutter. PDF is a statistical measure of a probability distribution for a continuous random variable in a given interval. It can be represented in a PDF graph where the area in the graph indicates its variable value which is fall within the interval.

There are few models which are typically used to study clutter distribution from various research include log-normal, Rayleigh, Weibull distribution model and many more. These models have been used many years. It is stated in [50, 54, 62, 63] that from all the models that have been analysed, the best fit model for ground clutter is Weibull distribution model. It is a very flexible model distribution only by changing the shape parameter it can be fitted to various type of ground clutter. Normally for ground clutter distribution, the shape parameter (n) are varies from 1 to 2 where when $n=2$, the distribution is also considered as Rayleigh distribution. This can be seen clearly in Figure 4.4.

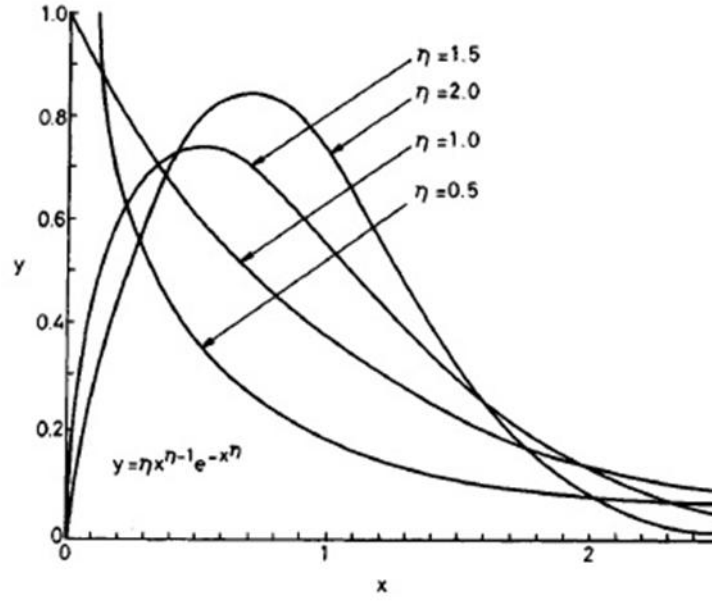


Figure 4.4: Weibull distribution graph with shape factor n [42]

The Weibull PDF can be derived as [54] :

$$p(x) = b \cdot c \cdot x^{b-1} e^{-cx^b} \quad (4.6)$$

It is considered that random variable x represents the clutter strength,

$$x = \sigma^\circ F^4 \quad (4.7)$$

where: F = pattern propagation factor

σ° = clutter coefficient

Then the value b in Weibull shape parameter form, a_w is represent as:

$$b = \frac{1}{a_w} \quad (4.8)$$

Furthermore, value c is denoted as:

$$c = \frac{\ln 2}{x_{50}^b} \quad (4.9)$$

where x_{50} is considered as the median value of clutter strength or σ_{50}° . As we substitute equation (4.9) into equation (4.6), the Weibull power density function can be rewritten as:

$$p(x) = \frac{b \cdot \ln 2 \cdot x^{b-1}}{x_{50}^b} \cdot e^{-\frac{\ln 2 \cdot x^b}{x_{50}^b}} \quad (4.10)$$

4.3.4 Cumulative Distribution Function

It is known that cumulative distribution function (CDF) is related to PDF. The Weibull cumulative distribution function equation can be represented as [65]:

$$F(x) = 1 - e^{-\frac{\ln 2 \cdot x^b}{x_{50}^b}} \quad (4.11)$$

Or it can be written as:

$$F(x) = 1 - e^{-\frac{\ln 2 \cdot x^b}{x_{50}^b}} \quad (4.12)$$

where the value b and c are the same as Weibull PDF above in equation (4.8) and equation (4.9) respectively.

4.3.5 Dynamic Range

Dynamic range can be defined as the ratio of maximum detectable value to a minimum detectable value of a parameter and in this case is maximum and minimum amplitude power of the received signal and it is expressed in dB.

Dynamic range is an important parameter in radar system. The radar receiver must have high dynamic range to detect very weak signals in the presence of very large clutter.

(4.13)

4.4 Results from Different Parameters

In this research, few preliminary analyses have been done. These include different test sites, different carrier frequencies use, various baseline distances between transmitter and receiver and different wind speeds. All these analyses are just to study and estimate the effect of various parameters to the clutter power level.

Clutter signal is a non-stationary signal that received by the receiver. The example of typical non-stationary clutter recorded for 64 MHz is displayed in Figure 4.5 (a) with clutter envelope. While examples of power spectral density for both envelope and clutter signal are shown in Figure 4.5 (b) and (c) respectively.

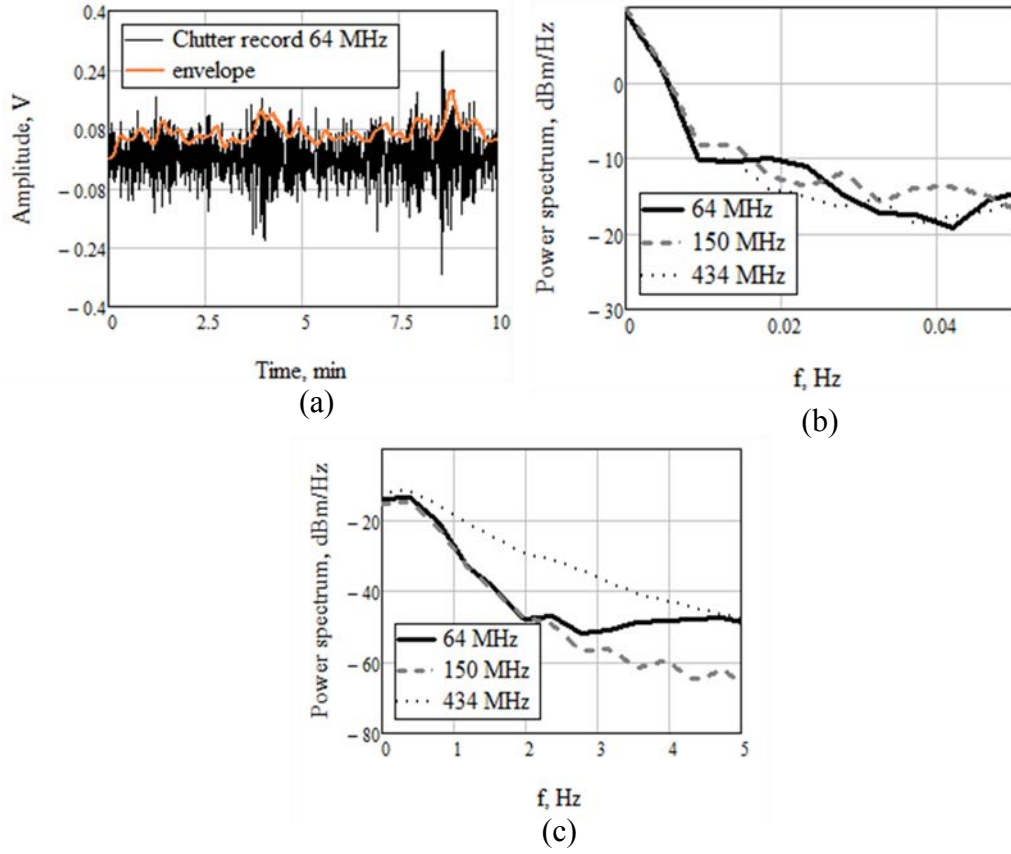


Figure 4.5: Clutter record (a) 64 MHz non-stationary clutter, (b) Clutter envelope PSD, (c) Clutter signal PSD

In the analysis, it is found out that clutter demonstrated certain invariant of clutter power spectrum and from vast majority records of different environmental conditions, the clutter power exhibits certain dependence to the frequency. If we looked into the clutter power versus frequency graphs displayed in Figure 4.6, we can see that the clutter power increased with the increased of frequencies for different baseline distance ranges and as expected the stronger the wind, the larger clutter power produced. Still in Figure 4.6 for the leakage level versus frequency graphs, leakage level of the signal is decreased with the increased in frequency and the longest baseline distance of 200 m contributes the lowest leakage level followed by 150 m, 100 m and 50 m. Moreover, for the leakage level versus baseline range,

434 MHz frequency gives the lowest leakage level followed by 151 MHz and 64 MHz as predicted. Details of these analyses are described in detail in the next section.

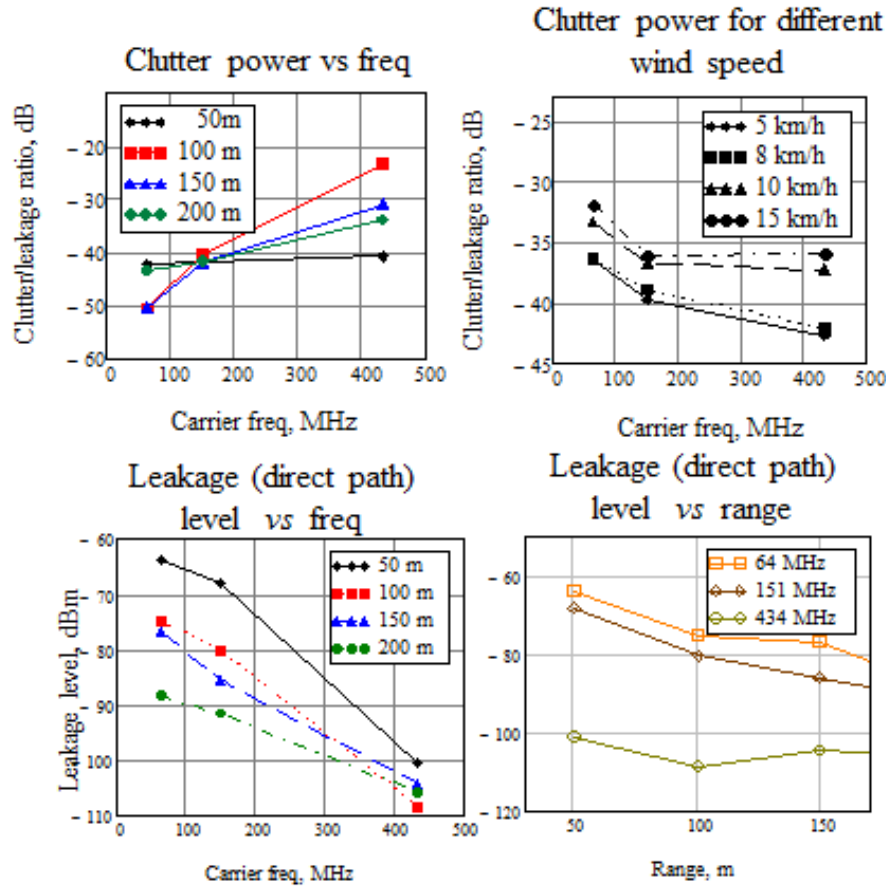


Figure 4.6: Clutter power versus frequency and leakage level versus frequency and range

4.4.1 Clutter versus Test Sites

In this research different test sites are chosen to analyse the effect of different environments and landscapes to Doppler return signals. Several places have been selected which is already described in Chapter 3, Sub-topic 3.4. There are about nine test positions that are tested in this clutter measurement. All nine places have different type of landscapes and terrain profiles which vary from dense wood in Lickey Hill to flat open space in Airfield. All the clutter signals from the vast majority of clutter measurements were then recorded and analysed.

As a result, it was found that no matter what type of landscapes and environmental conditions, the clutter still demonstrated certain invariant of power spectral density. This is shown in Figure 4.7 where the data is taken from Airfield with open space landscape, Lickey Hills with dense wood landscape and Senneleys Park with open space and vegetation in surrounding. The data are recorded during daytime and the wind speeds are varies from no wind in Airfield to slightly wind in Lickey Hills and breeze in Senneleys Park. These three major landscapes replicate the most common landscape that can be found anywhere in the world.

The figure also shows slightly increased of clutter power between Airfield to Senneleys Park. This is due to the different wind speed reading for all three places. The increased is about 10 dB for 64 MHz to approximately 40 dB for 434 MHz omnidirectional antenna. If we compared the power drop and spectrum width for different frequencies in Airfield itself, we can see that clutter power exhibit the same trend for all frequencies and not much difference between each frequency and same goes for Lickey Hills. This is because the wind speed in these two places is very low which very small amount of clutter is picked up by the receiver. Another reason is the open space landscape of Airfield and also in Lickey Hills, the wind is damped by surrounding trees. Furthermore, in Senneleys Park the difference in power drop between all four frequencies is about 10 dB to 20 dB and the spectrum width is still the same for all the frequencies.

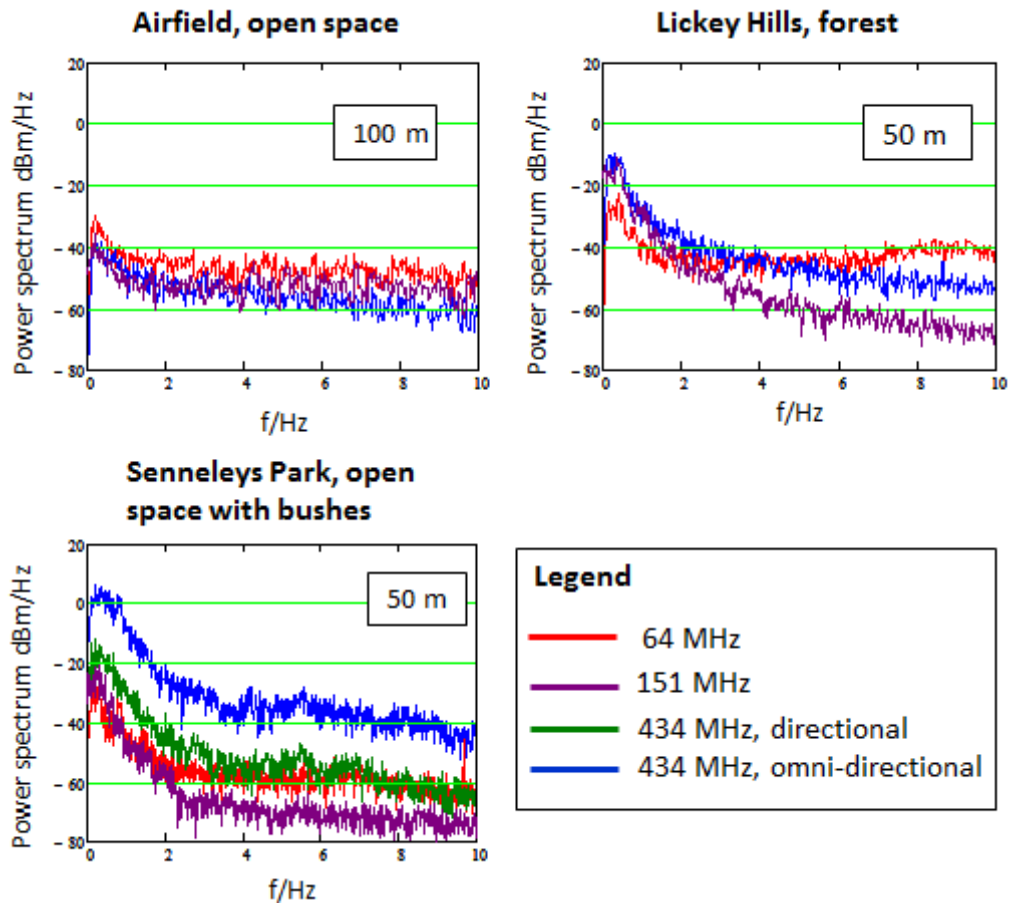


Figure 4.7: Clutter power spectrum for different test sites

4.4.2 Clutter versus Carrier Frequencies

In this research, the frequencies used are ranging from VHF to UHF. These two sets of frequencies are commonly used for communication devices. Results shown below in Figure 4.8 is taken from Senneleys Park. In this figure all four carrier frequencies PSD are displayed both in absolute values and normalised graph. We can conclude that the spectrum widths are the same at any frequencies and practically invariant of carrier frequency. This proved that the signals came from the same source at the same time. Furthermore the clutter strength is increased when the frequency is increased by 30 dB from 64 MHz to 434 MHz. In the absolute PSD graph also shown that the 434 MHz directional antenna contributed much lower

clutter as compared to 434 MHz omnidirectional antenna. This is because omnidirectional antenna can pick up clutter up to 360° in surrounding as compared to directional antenna.

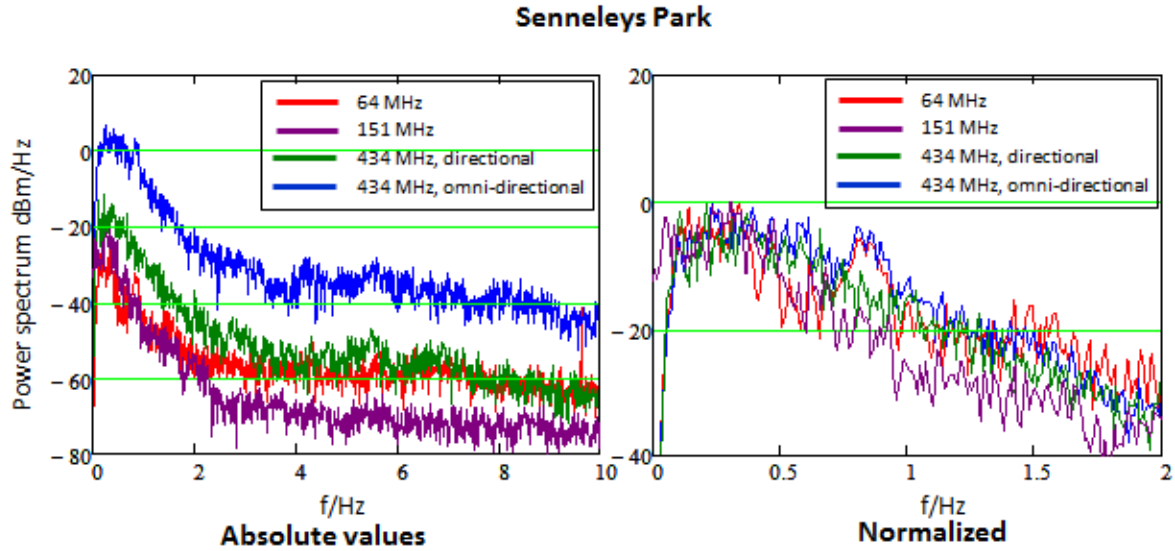


Figure 4.8: Clutter power spectrum for different carrier frequencies

4.4.3 Clutter Versus Baselines

There are three baseline distances used in this analysis to study the effect of different distances to the clutter power. The experiment was set up in Lickey Hills and Airfield with frequency ranging from 64 MHz to 434 Hz. As results, the clutter power increased with the increased of the baseline distances as shown in Figure 4.9. The increment for both Lickey Hills and Airfield are about 6 dB when the distance is doubled.

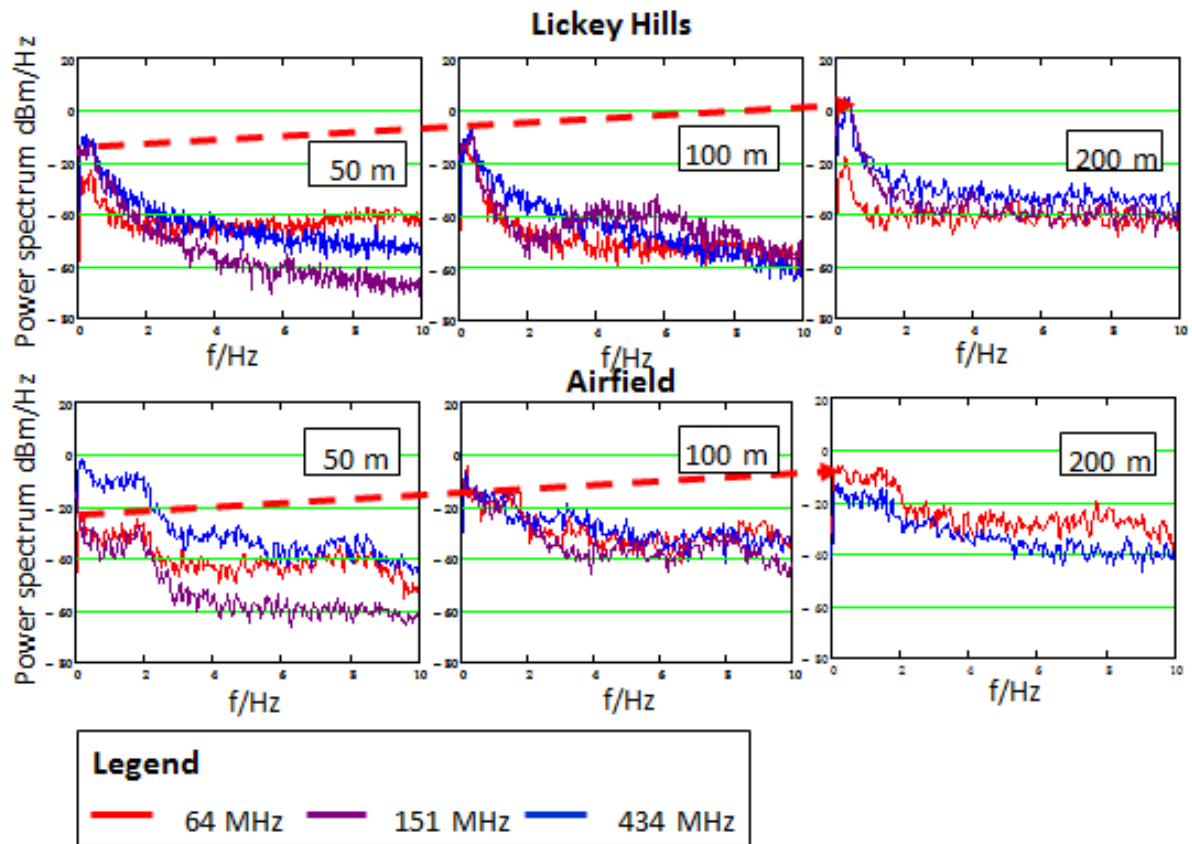


Figure 4.9: Clutter power spectrum for different baseline distances

4.4.4 Clutter Versus Different Weather

Another analysis involved in this research is to study the effect of different weather condition. The experiment took place in several day with different weather conditions such as snow, rain and windy day. These three different weather conditions are typically can be found all around the world especially windy day which normally occurs during spring and autumn. Results from these experiments are shown below in Figure 4.10 and Figure 4.11.

In Figure 4.10 it shows the PSD of clutter signal during snow with no wind and during rainy day with light wind (3-5 kmh). Both show the invariant of clutter power for different frequencies having the same spectrum width.

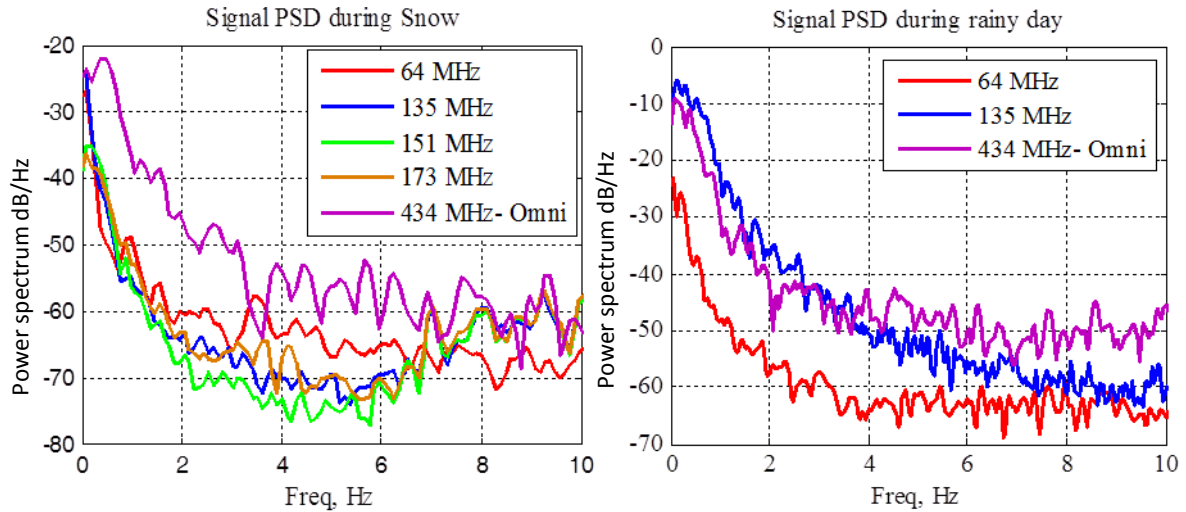


Figure 4.10: PSD for clutter during snow and rainy day

Wind records have been recorded in Airfield with three different wind conditions: no wind at all, light wind and strong wind. Figure 4.11 displayed the results. All these three conditions give three different results, where the amplitude and frequency increased with the increased of wind speed. This situation confirmed the fact that when the wind blown, all vegetation in surrounding will swayed in certain angle and this will affect the Doppler signal received by the receiver. Figure 4.11 also displayed the clutter spectrum with the width ranging from 0.4 Hz to 0.5 Hz defined by 10 dB power drop.

Compared to all other parameters, wind speed gives the most impact to clutter strength build up which will affect the performance of target detection. Details of the analysis for different wind speeds are carried out and described in details in the next section.

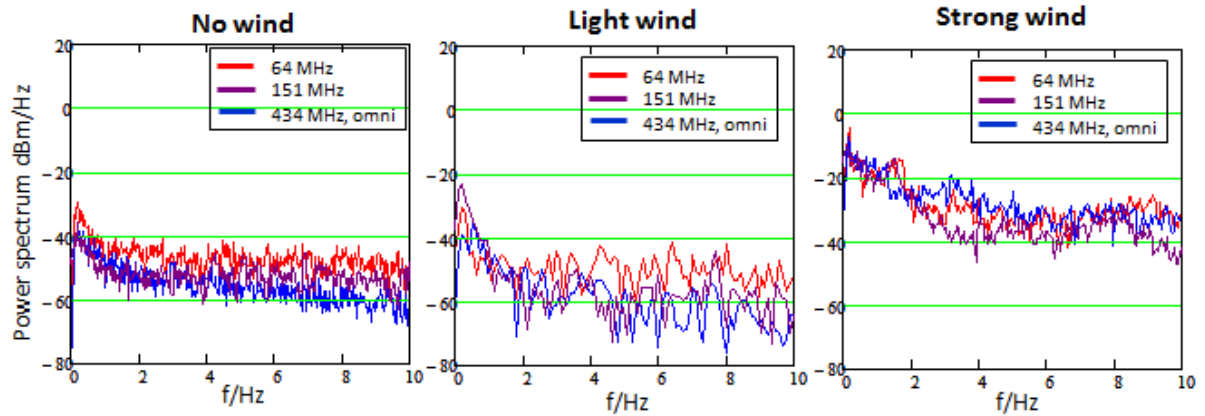


Figure 4.11: Clutter power spectrum for different wind speeds

4.5 Clutter Results Based on Different Wind Speed (Short Term Measurement)

As we can see from results in Section 4.4, the main influence to clutter build up is the wind speed as compared to others. Then the next analysis is to carry out an experiment in order to understand the characteristic of clutter power for different wind speed. The experiment took place in Horton Grange due to complex vegetation area and nearer to Electrical, Electronic and Computer Engineering School of Birmingham and also easy to access and convenient.

These data that are used in this analysis are taken from short term measurement data trial from 4th September 2009 until 7th September 2009. Within these four days, the wind speed varies from low to very strong wind conditions. The results are processed to classify the wind conditions based on four categories which are low (up to 5 mph), medium (6 – 15 mph), strong (16 - 24 mph) and very strong (gale > 25 mph) wind conditions.

4.5.1 Doppler Signal Output for Low Wind Speed

There are 180 files all together in this data trial. From all those files, file number 77 (File 77 HG 05/09/09) is chosen because it demonstrates the lowest clutter amplitudes over all the data in this data trial. During the experiment, the recorded wind speed varies from 0 to 5 mph which is considered as low wind speed.

In Figure 4.12 it shows the Doppler output signals of low wind condition for different frequency carriers (64 MHz, 135 MHz, 173 MHz and 434 MHz). From the figures we can see that the maximum amplitude of the Doppler output signal for 64 MHz channel is around 0.13 V whereas for 434 MHz, the maximum amplitude of the Doppler signal is around 0.37 V. These show that the amplitude is increased in the increments of frequencies and larger clutter power for higher frequencies.

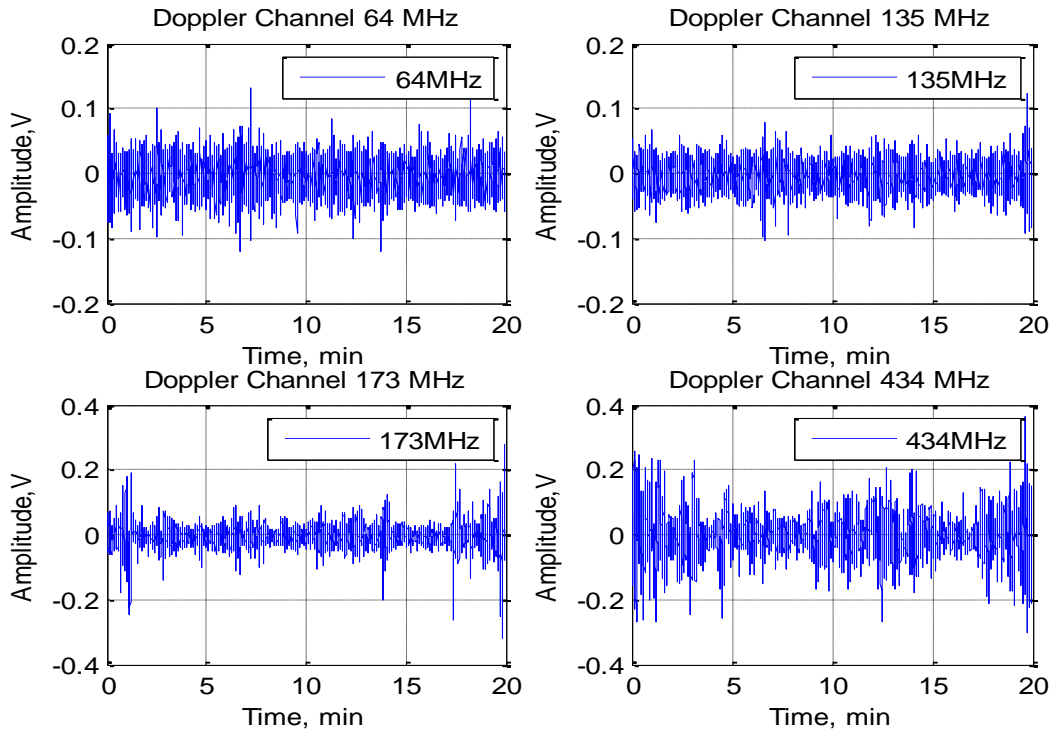


Figure 4.12: Measured Doppler signals at 64 MHz, 135 MHz, 173 MHz and 434 MHz

All the results from this file are recorded in Table 4.1. This includes the standard deviation value, minimum and maximum values of the signal's envelope and the dynamic range. From the table it is shown, when the frequency is increased, STD, amplitudes of the envelopes and the dynamic ranges are also increased. The amplitudes of the clutter power also imitate each other for the same wind condition for each frequency. The higher the frequency, the larger clutter power will be. Figure 4.13 shows the envelopes for all signal frequencies in the same source of clutter and in this case for low wind condition.

Table 4.1: Measured low clutter strength for different frequencies

Frequency	Standard Deviation	Envelope		Dynamic Range (dB)
		Min	Max	
64 MHz	0.0195	0.0138	0.0682	6.94
135 MHz	0.0171	0.0114	0.0767	8.26
173 MHz	0.0339	0.0107	0.2132	12.98
434 MHz	0.0574	0.0177	0.1926	10.38

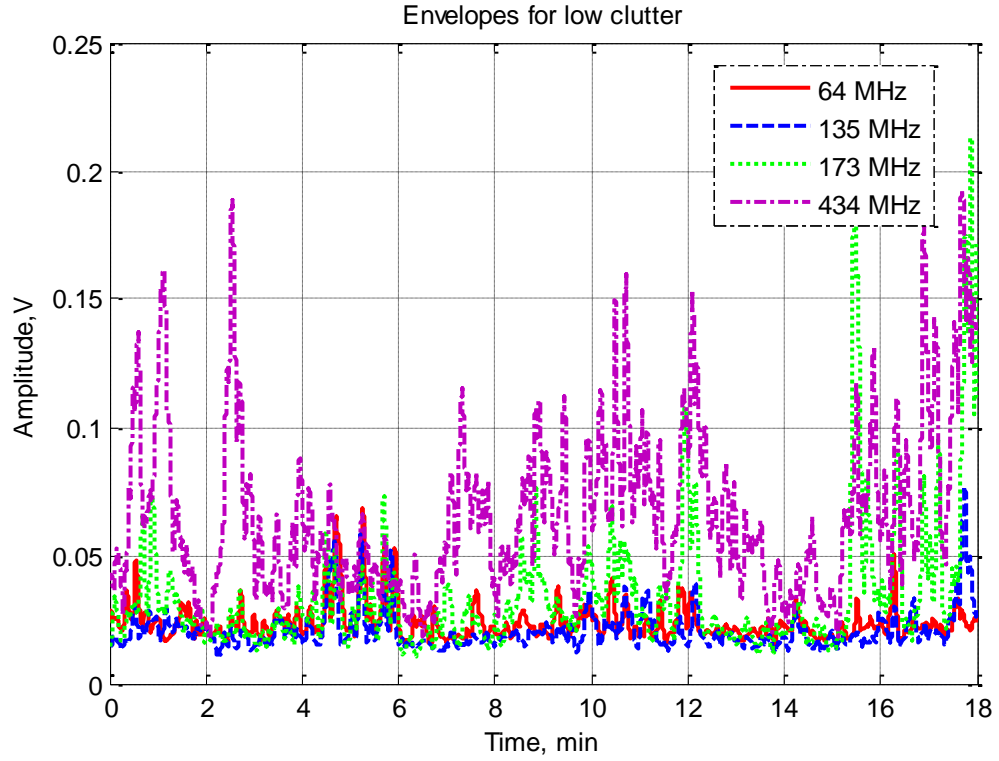


Figure 4.13: Envelopes for all signal frequencies

Another important characteristic of a signal that needs to be determined is the power spectral density (PSD). PSD shows the strength of the energy variations as a function of frequency as in Figure 4.14. In this figure, we can see two graphs, one with the normalized version and another one is the absolute value of the PSD for low wind condition, where the PSD of the envelope for each frequency channel exhibit the power drop approximately around 0.005 Hz to 0.01 Hz with second order LPF and cut-off frequency of 0.1 Hz. While in Figure 4.15 and Figure 4.16 (a) shows the PSD of the clutter signals separately for each of the frequency and combined PSD for all frequencies respectively.

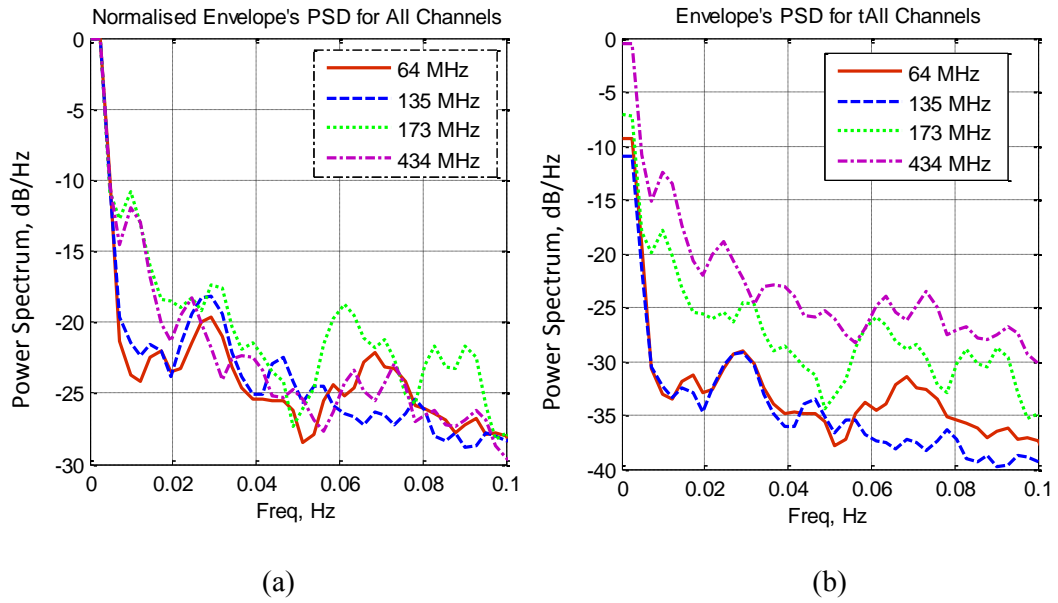


Figure 4.14: Power Spectral Density for clutter envelopes with 0.1 cut-off frequency (a) normalized (b) absolute value

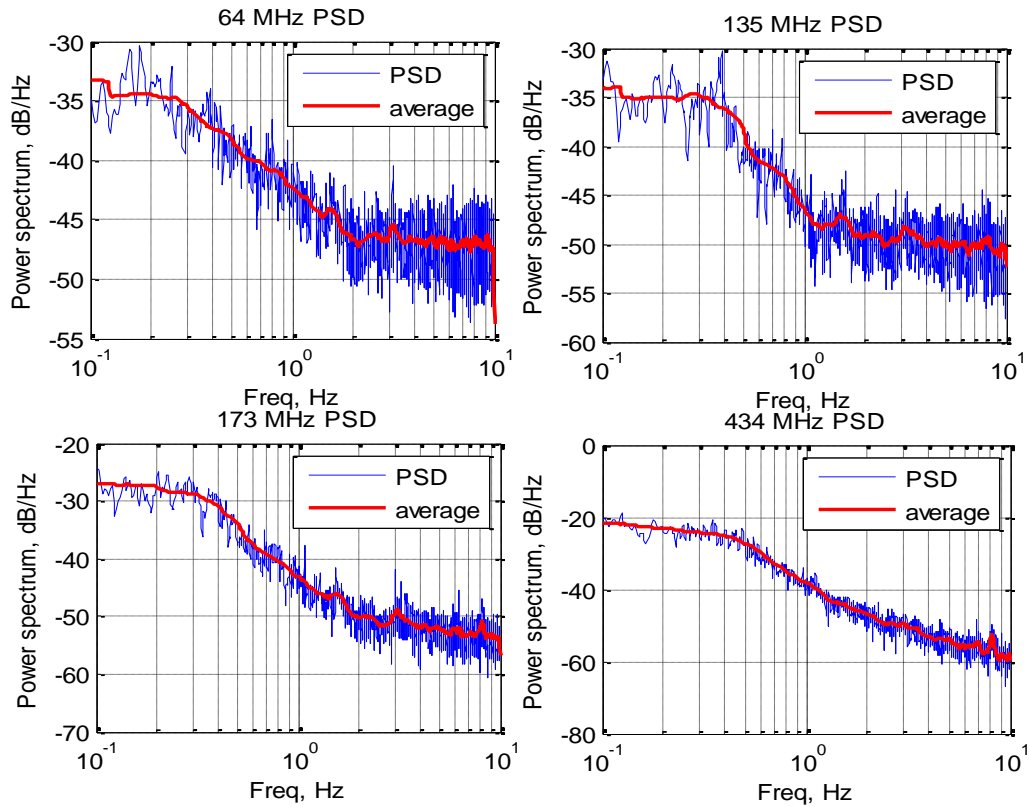


Figure 4.15: PSD of clutter signals for all frequency channels at 64 MHz, 135 MHz, 173 MHz and 434 MHz for low clutter

In Figure 4.16 (a) the spectrum width for different frequency channels which is defined by 10 dB power drop are about 0.4 to 0.5 Hz. It is displayed that for low clutter signal which is the lowest frequency channel, 64 MHz is a bit higher than 135 MHz channel and followed by 173 MHz and 434 MHz. In low wind condition, the clutter power is very small and for 64 MHz channel, the clutter signal is considered mainly from the environmental noise and thermal noise that produced by the receiver. Both these two noises contributed high power than the surrounding area which contributes higher power for 64 MHz signal as compared to 135 MHz channel. The PSD slopes drop approximately around 20 dB to 30 dB per decade for each channel.

The next graph in Figure 4.16 (b) shows the cumulative distribution function (CDF) for all frequency channels. The 64 MHz and 135 MHz channel exhibit the same trend where the CDF reached the value of 1 at approximately 0.08 V, and this is followed by 173 MHz channel and 434 channels at 0.15 V and 0.26 V respectively.

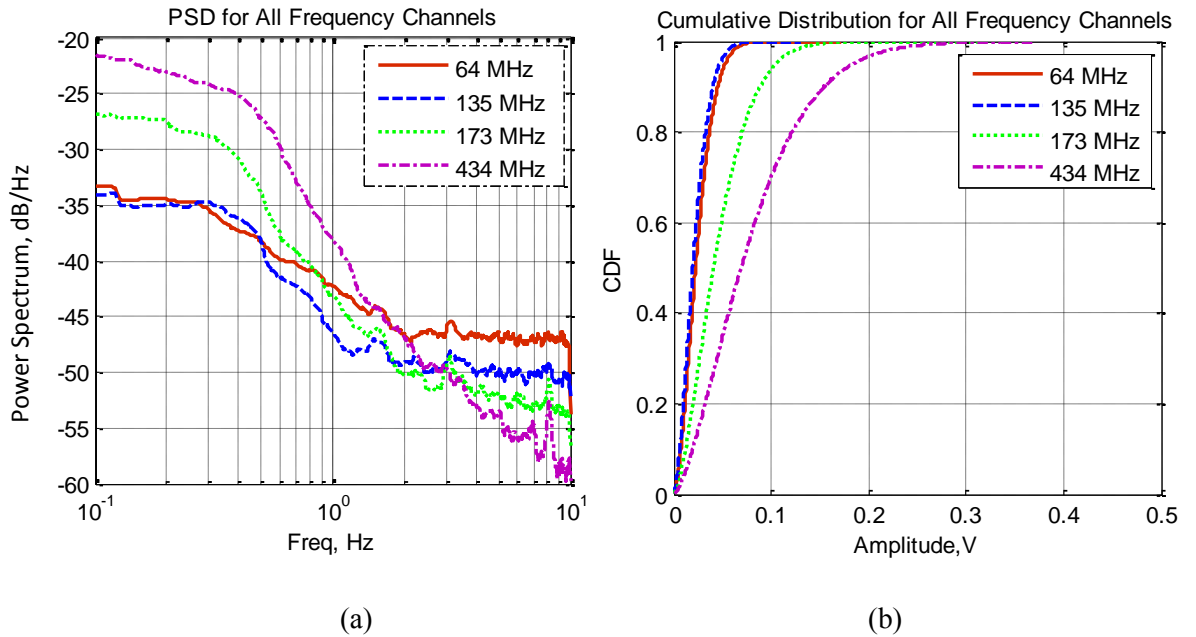


Figure 4.16: (a) PSD comparison for low clutter for all frequency channels, (b) Cumulative distribution for all frequency channels

The clutter distributions in Figure 4.17 represent the power density function (PDF) of the clutter signals for all four frequency channels. This is one of the clutter characteristic used in order to estimate system detection performance. From the figure, the histograms and the PDF fits corresponds to Weibull distribution with shape factor 2.0 for 64 MHz and 1.60 for 434 MHz channel. The lower the frequency, the closer the distribution will be to Rayleigh distribution.

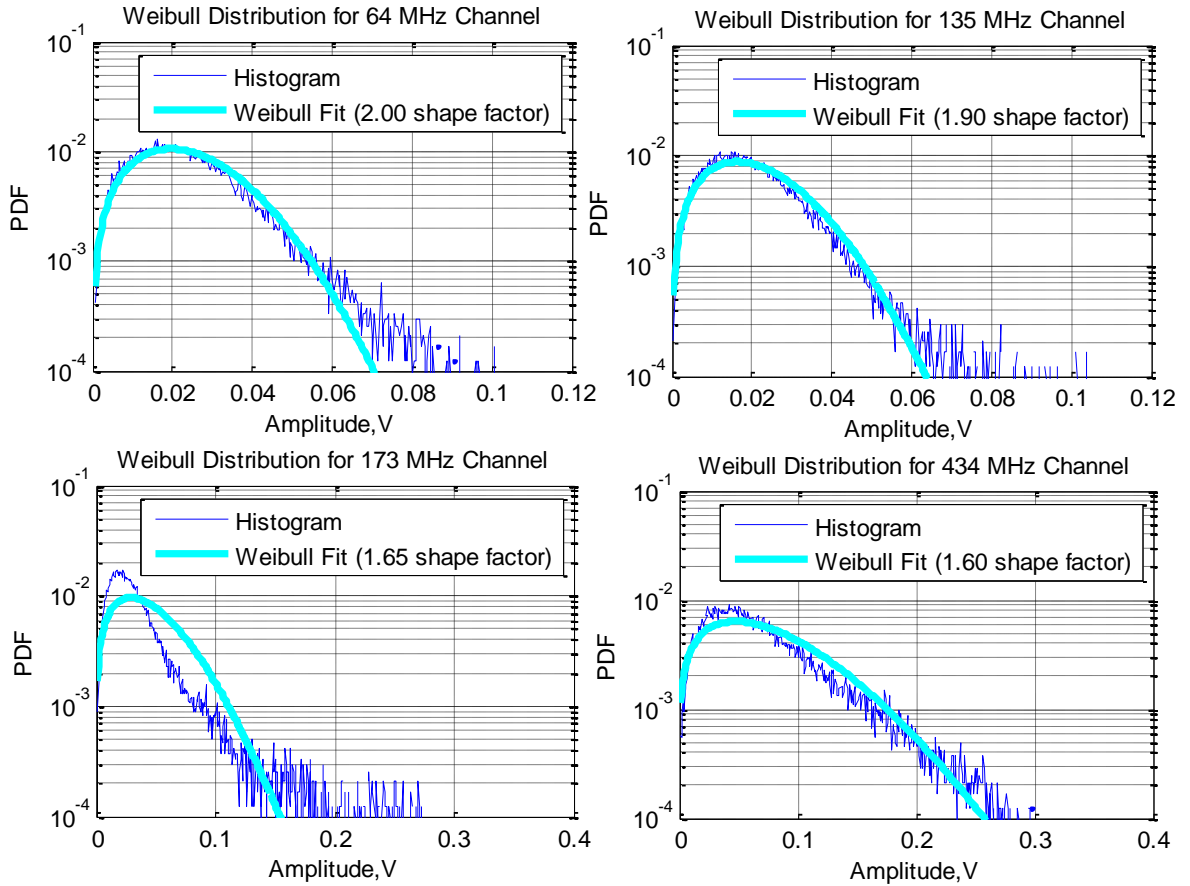


Figure 4.17: Weibull Distribution of a measured clutter at 64 MHz, 135 MHz, 173 MHz, and 434 MHz

In this research, the clutter distributions found by our FSR measurement shows the distribution are closed to Weibull distribution. As a result Weibull PDF is used in our analysis using Matlab software to display the distribution by using histograms and Weibull fits of the

clutter records. Figure 4.17 shows the example of Weibull distribution for all frequency signals.

4.5.2 Doppler Signal Output for Medium Wind Speed

File LT_32 is chosen as a medium clutter in this data analysis because it demonstrates medium range of signal's amplitude as compared to other 180 files. This data is taken from the file name of 28 HG dated on 05/09/09.

Graph in Figure 4.18 shows the Doppler signals for all frequency channels of medium wind condition. The graphs portray the same result as for low clutter condition where the highest frequency gives the highest amplitude. In this case the maximum amplitude for 64 MHz is 0.08 V. The maximum amplitude of the Doppler signal keeps increasing with the raise of frequency where the 434 MHz maximum amplitude is 0.85 V. If we compare the clutter power between low wind conditions with medium wind conditions, higher wind contributes higher clutter. Table 4.2 described the standard deviation, the envelope's minimum and maximum amplitudes, and the dynamic range of the envelopes.

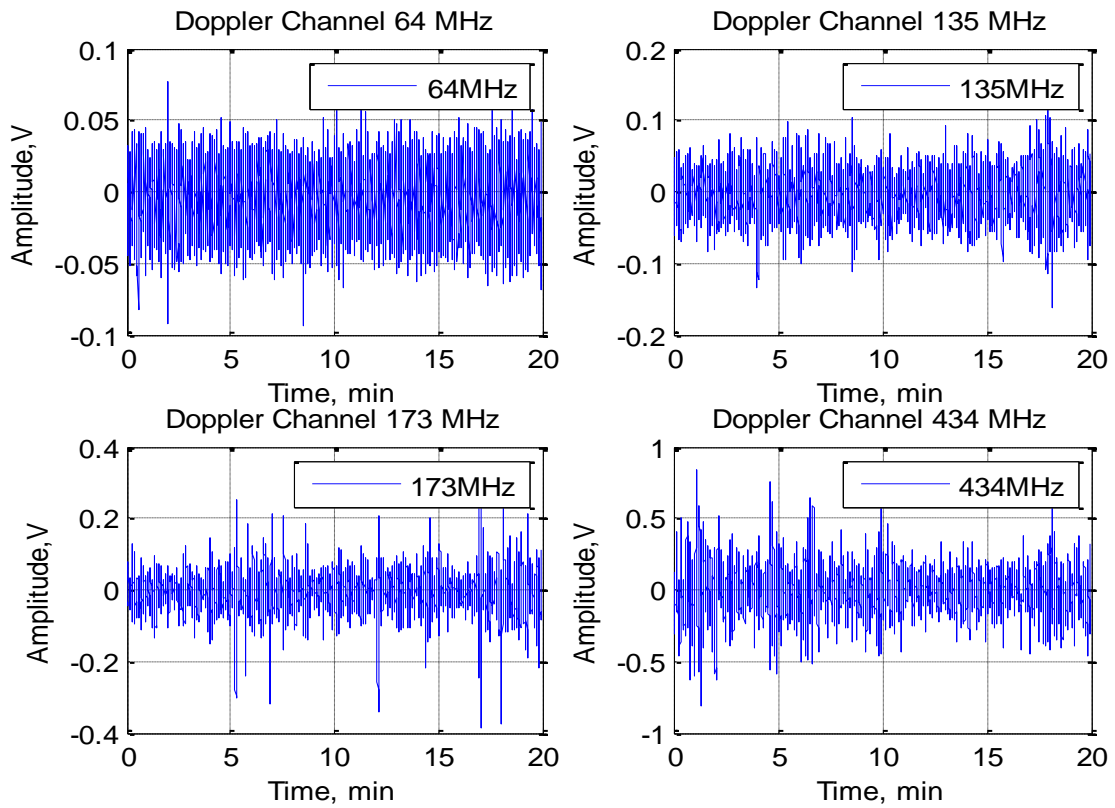


Figure 4.18: Measured Doppler signals at 64 MHz, 135 MHz, 173 MHz and 434 MHz for medium clutter

Table 4.2: Measured medium clutter strength for different frequencies

Frequency	Standard Deviation	Envelope		Dynamic Range (dB)
		Min	Max	
64 MHz	0.0163	0.0149	0.0339	3.56
135 MHz	0.0275	0.0153	0.1156	8.77
173 MHz	0.0564	0.0161	0.2731	12.29
434 MHz	0.1468	0.0554	0.5623	10.06

In Figure 4.19, it can be seen that the signal envelopes replicate each other with 64 MHz as the lowest amplitude while 434 MHz signal envelope as the highest amplitude. In this figure,

the highest amplitude for 434 MHz is 0.56 V which is slightly higher than in low wind condition where the highest amplitude for 434 MHz is 0.19 V. So the signal envelopes for medium wind condition are about 0.37 V higher, it doubles the amplitude for low wind condition.

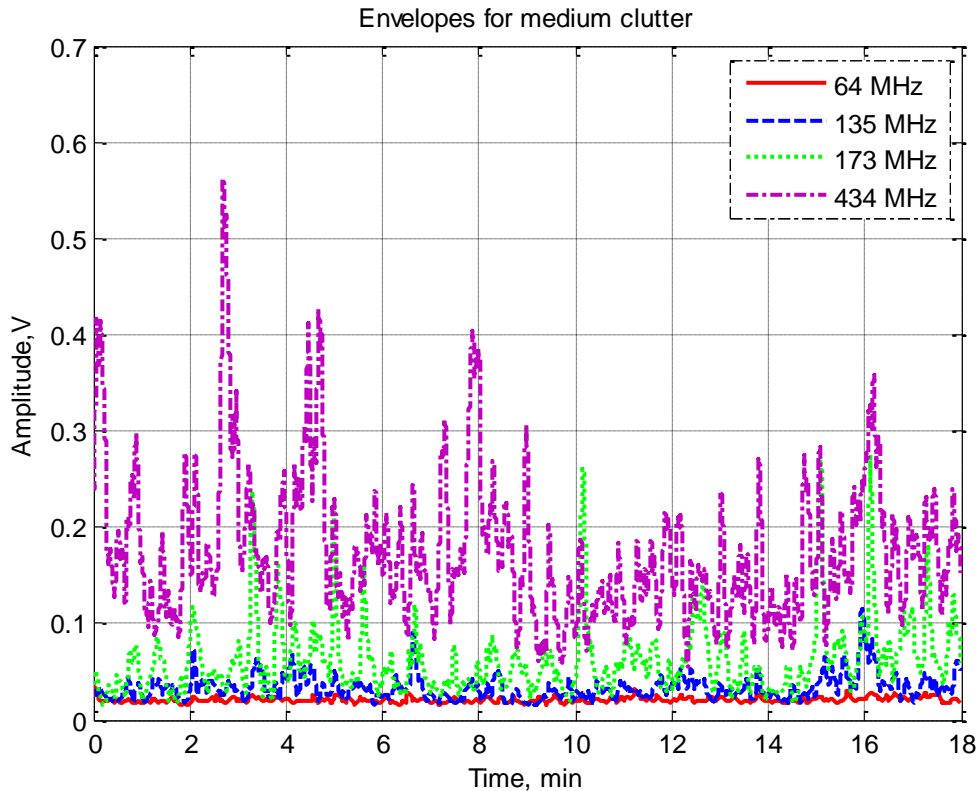


Figure 4.19: Envelopes for all signal frequencies for medium clutter

As we can see, the PSD for medium wind condition in Figure 4.20 gives the same characteristic with low wind condition. The normalized PSD shows the slopes for all frequencies drop at approximately between 0.005 Hz to 0.02 Hz which is correspond to 50 to 200 secs.

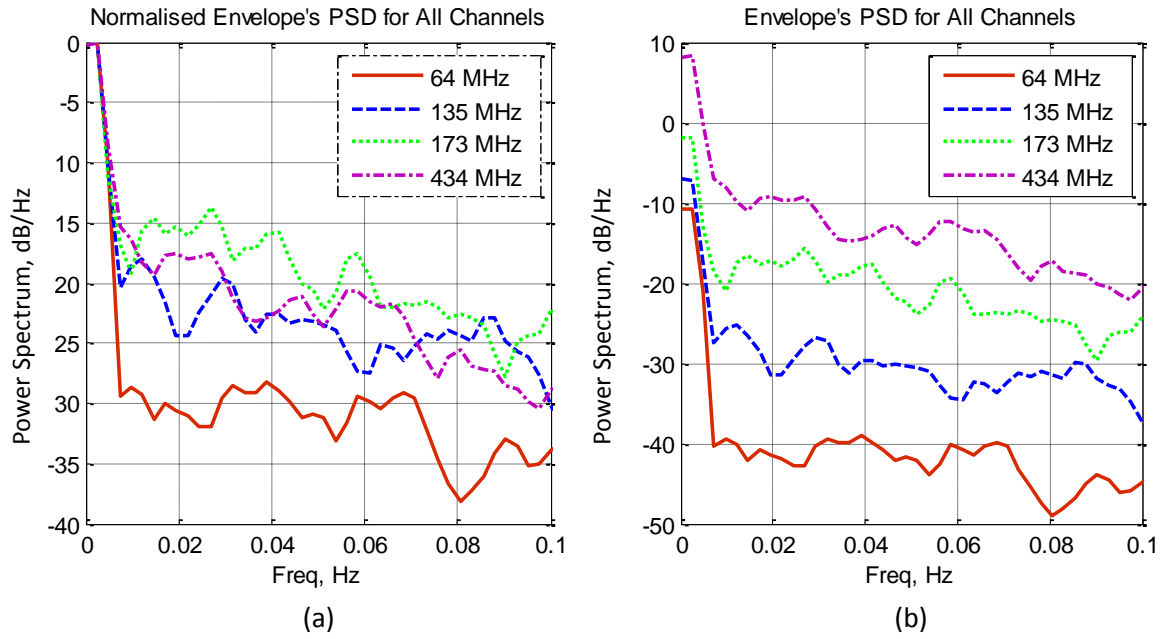


Figure 4.20: Power Spectral Density for clutter envelopes 0.1 cut-off frequency (a) normalized (b) absolute value for medium clutter

By looking at Figure 4.21 and Figure 4.22 (a), the signal PSD for medium wind condition has approximately 40 dB per decade slopes. The spectrum width with 10 dB power drop approximately around 0.4 Hz to 0.5 Hz and the total clutter power increased about 15 dB between 135 MHz and 434 MHz channels. As for the Figure 4.22 (b), it exhibits the CDF for the medium clutter signal. In this graph, the width between 64 MHz and 434 MHz for 0.8 CDF value is about 0.27 V. The width between these two channels is increased when the wind speed increased from low to much higher speeds.

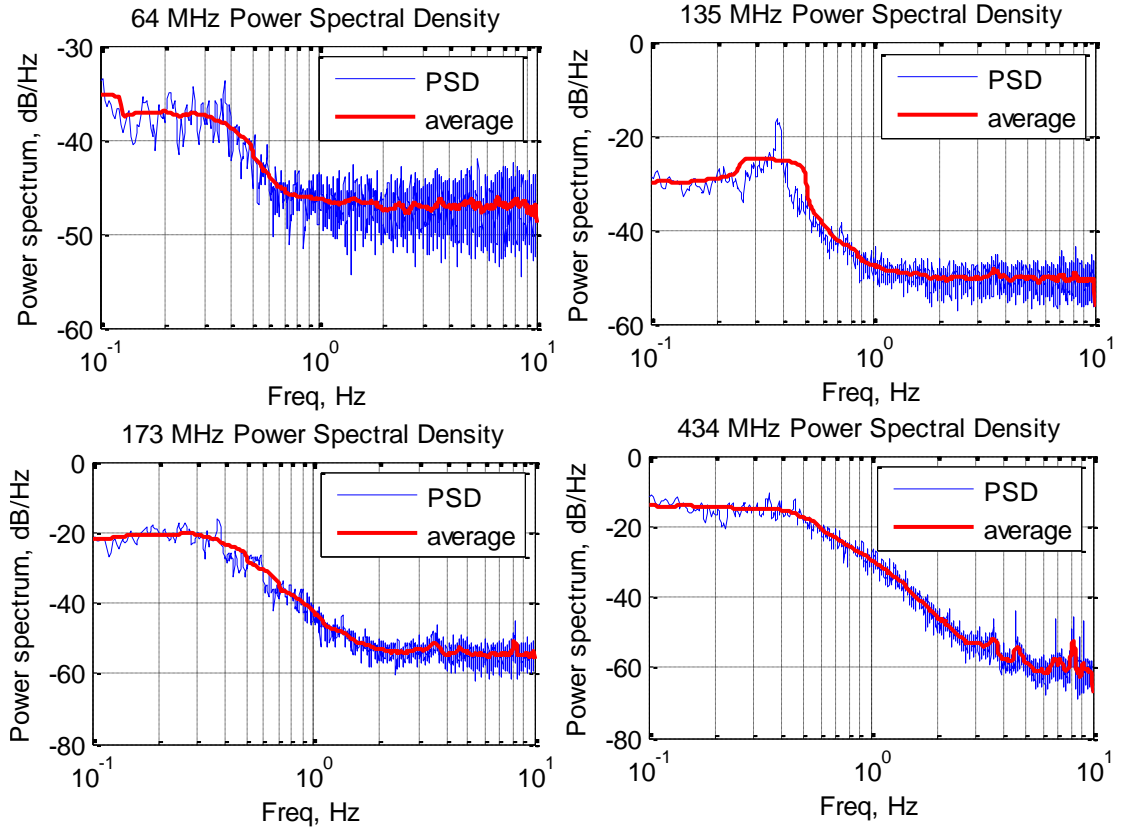


Figure 4.21: PSD of clutter signals for all frequency channels at 64 MHz, 135 MHz, 173 MHz and 434 MHz for medium clutter

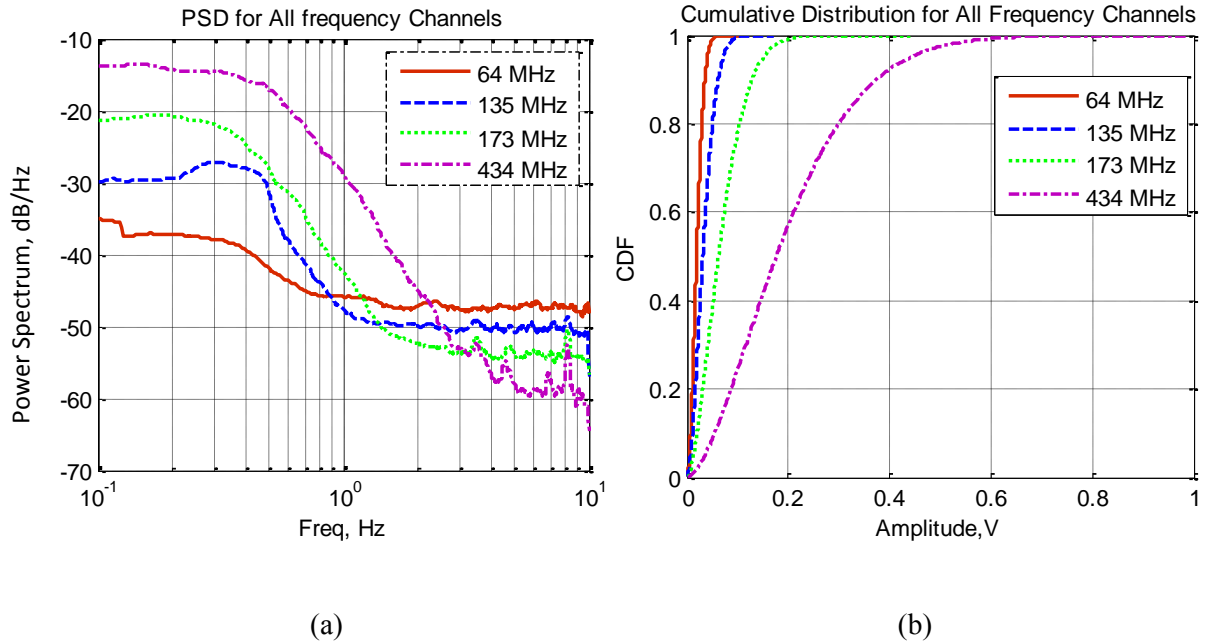


Figure 4.22: (a) PSD comparison for medium clutter for all frequency channels, (b) Cumulative distribution for all frequency channels

Next figure is the PDF distribution shown in Figure 4.23, it also exhibits the Weibull distribution with the shape factor ranging from 1.94 for 64 MHz channel to 1.60 for 434 MHz channel.

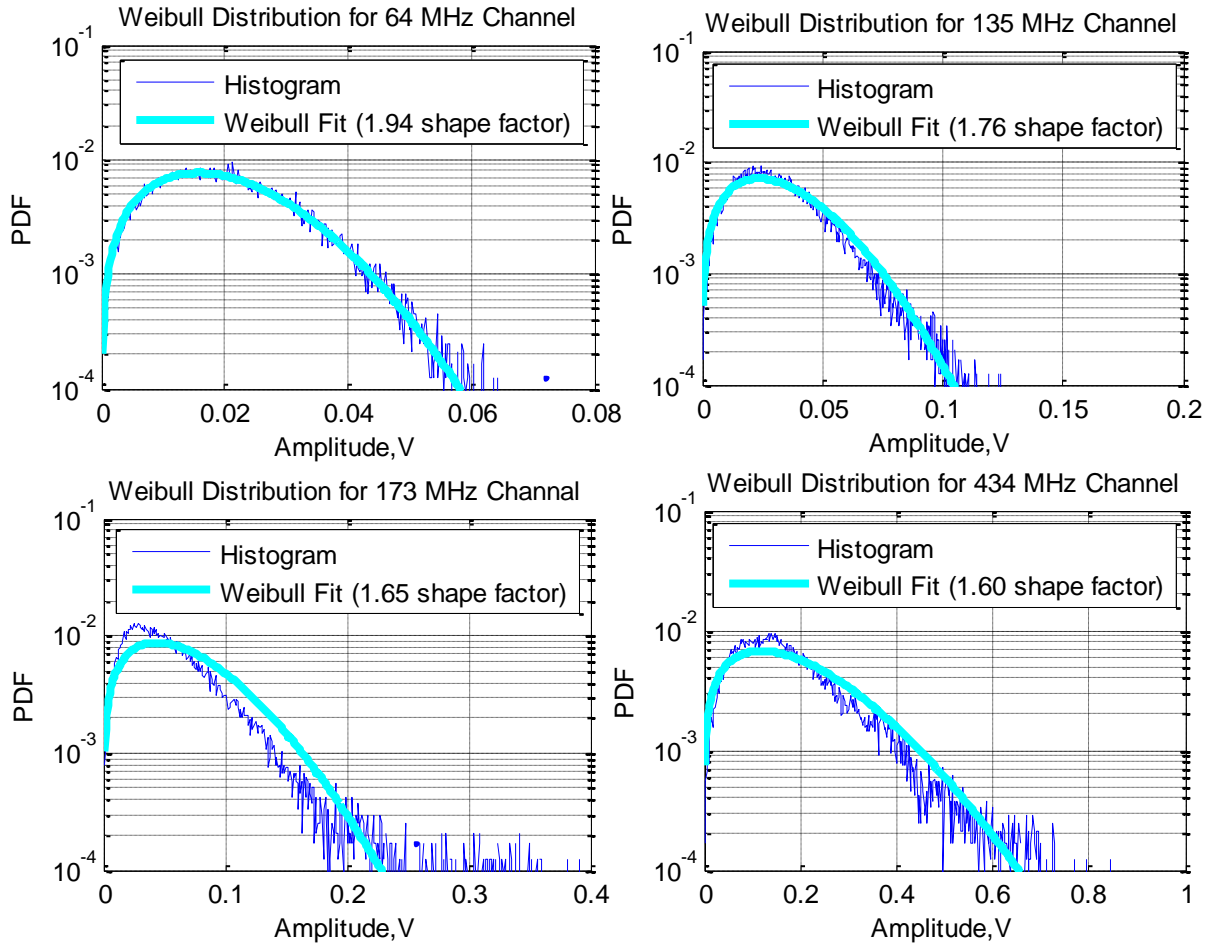


Figure 4.23: Weibull Distribution of a measured clutter at 64 MHz, 135 MHz, 173 MHz, and 434 MHz

4.5.3 Doppler Signal Output for Strong Wind Speed

The next graphs in Figure 4.24 are the Doppler signals for strong wind condition for all frequency channels. File LT_90 is chosen as strong clutter, exhibit much stronger clutter conditions as compared to medium clutter. The maximum amplitude for this clutter condition ranging from 0.13 V for 64 MHz channel up to 2.62 V for 434 MHz channel. Same goes for the value in Table 4.3 for standard deviation, minimum and maximum of signal's envelope, and the dynamic range of the envelope for each frequency channel.

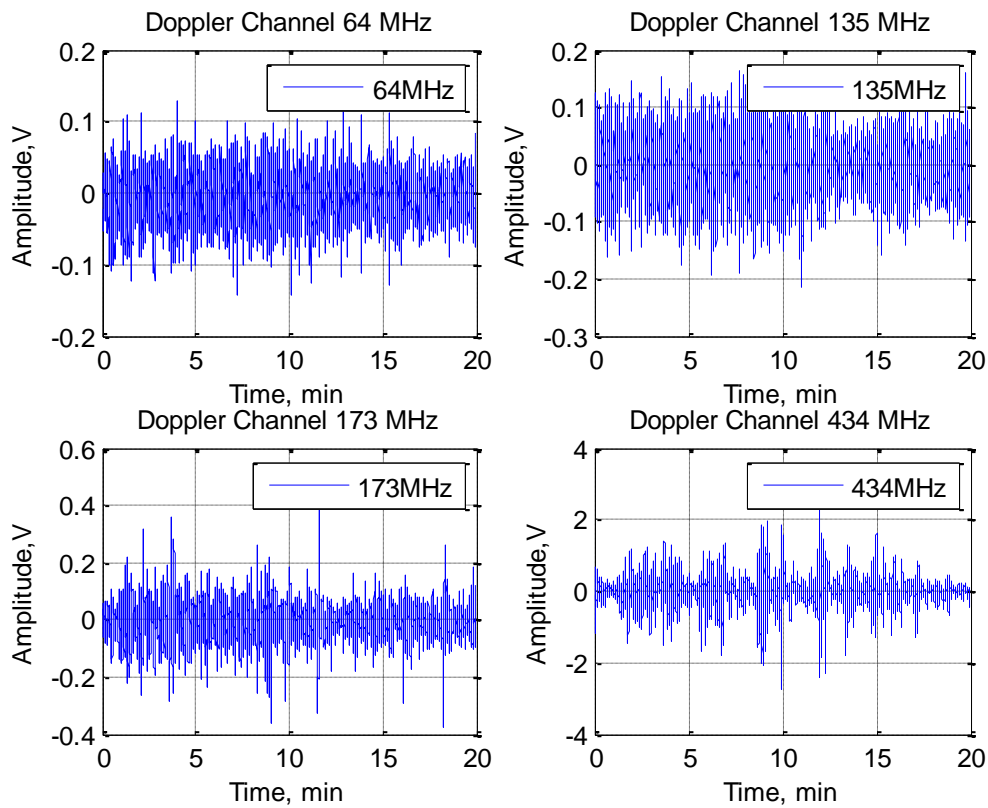


Figure 4.24: Measured Doppler signals at 64 MHz, 135 MHz, 173 MHz and 434 MHz for strong clutter

Table 4.3: Measured strong clutter strength for different frequencies

Frequency	Standard Deviation	Envelope		Dynamic Range (dB)
		Min	Max	
64 MHz	0.0293	0.0188	0.0902	6.82
135 MHz	0.0482	0.0196	0.1276	8.15
173 MHz	0.0693	0.0211	0.3727	12.47
434 MHz	0.4447	0.0803	2.0468	14.06

In strong wind condition, the amplitude of the signal envelope still shows the same pattern according to the frequencies but with this wind condition, the 64 MHz, 135 MHz and 173 MHz amplitude ranging from 0.09 V to 0.37 V in Figure 4.25. While for the 434 MHz channel, the amplitude is quite big with 2.05 V. Probably this is because 434 MHz frequency channel is very sensitive to the surrounding (higher the frequency, higher will be the sensitivity to the surrounding environment). So it picked up the sudden wind blow between 8th to 13th minute of time shown in Figure 4.25.

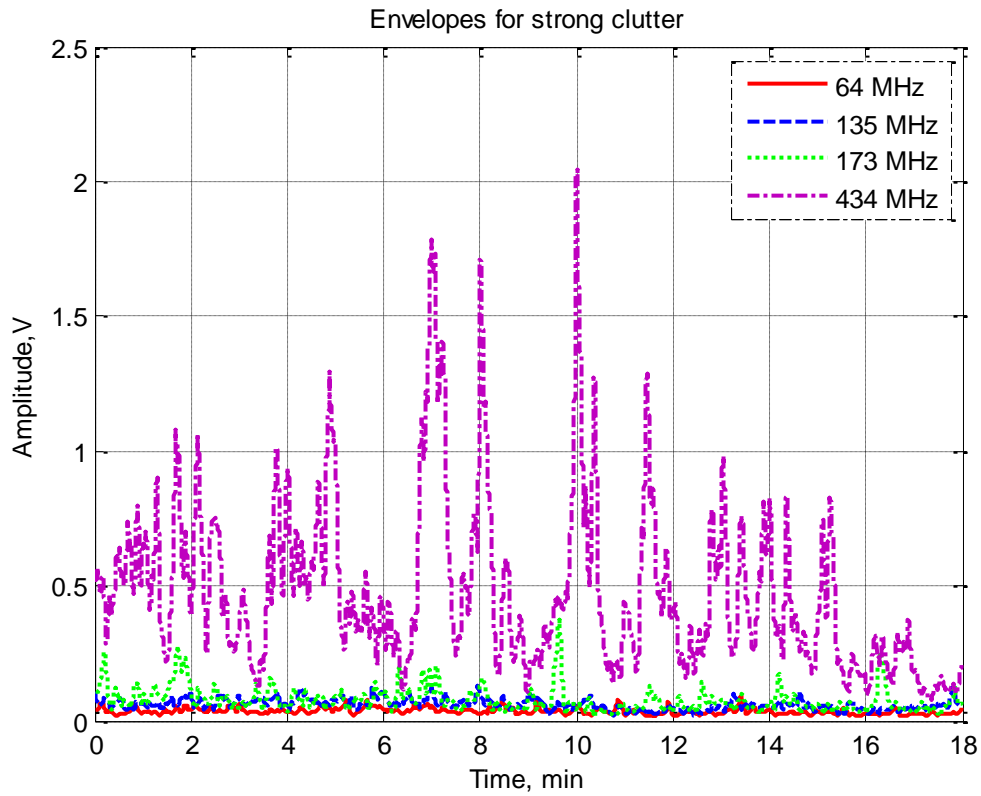


Figure 4.25: Envelopes for all signal frequencies for strong clutter

If we looked at the PSD of the envelopes in Figure 4.26 for normalized PSD, the slopes shows the cut-off of the clutter signals for each channel approximately between 0.005 to 0.01 Hz. The signal's PSD in Figure 4.27 and Figure 4.28 (a) demonstrates that the slopes of the PSD for each frequency channel approximately between 20 dB to 40 dB per decade.

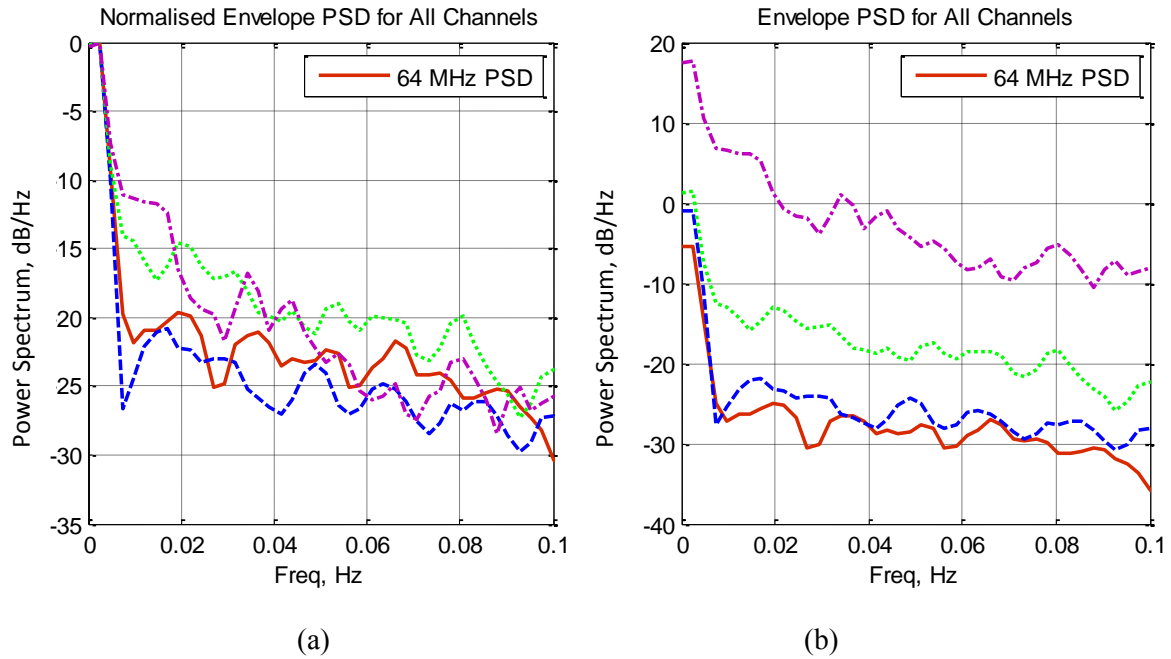


Figure 4.26: Power Spectral Density for clutter envelopes 0.1 cut-off frequency

(a) normalized (b) absolute value for strong clutter

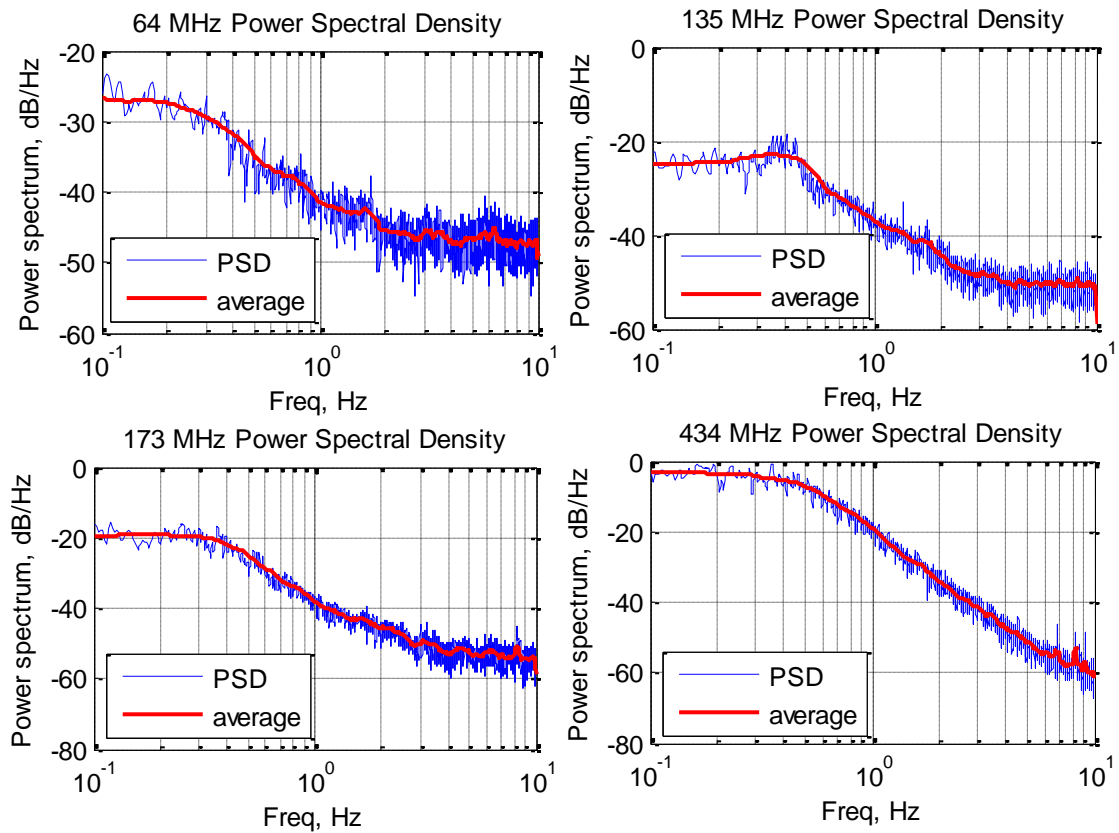


Figure 4.27: PSD of clutter signals for all frequency channels at 64 MHz, 135 MHz, 173 MHz and 434 MHz for strong clutter

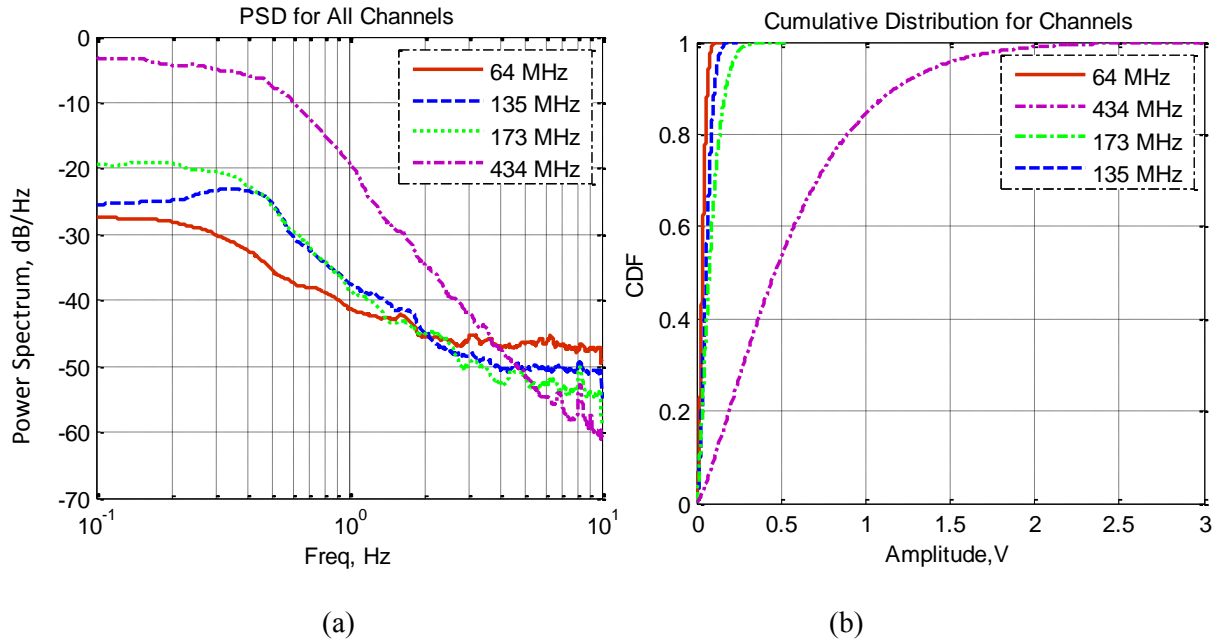


Figure 4.28: (a) PSD comparison for strong clutter for all frequency channels, (b) Cumulative distribution for all frequency channels

Figure 4.29 shows the PDF distributions for strong wind condition with the shape factor vary from 1.29 to 1.90 from the lowest frequency channel to the highest frequency channel respectively.

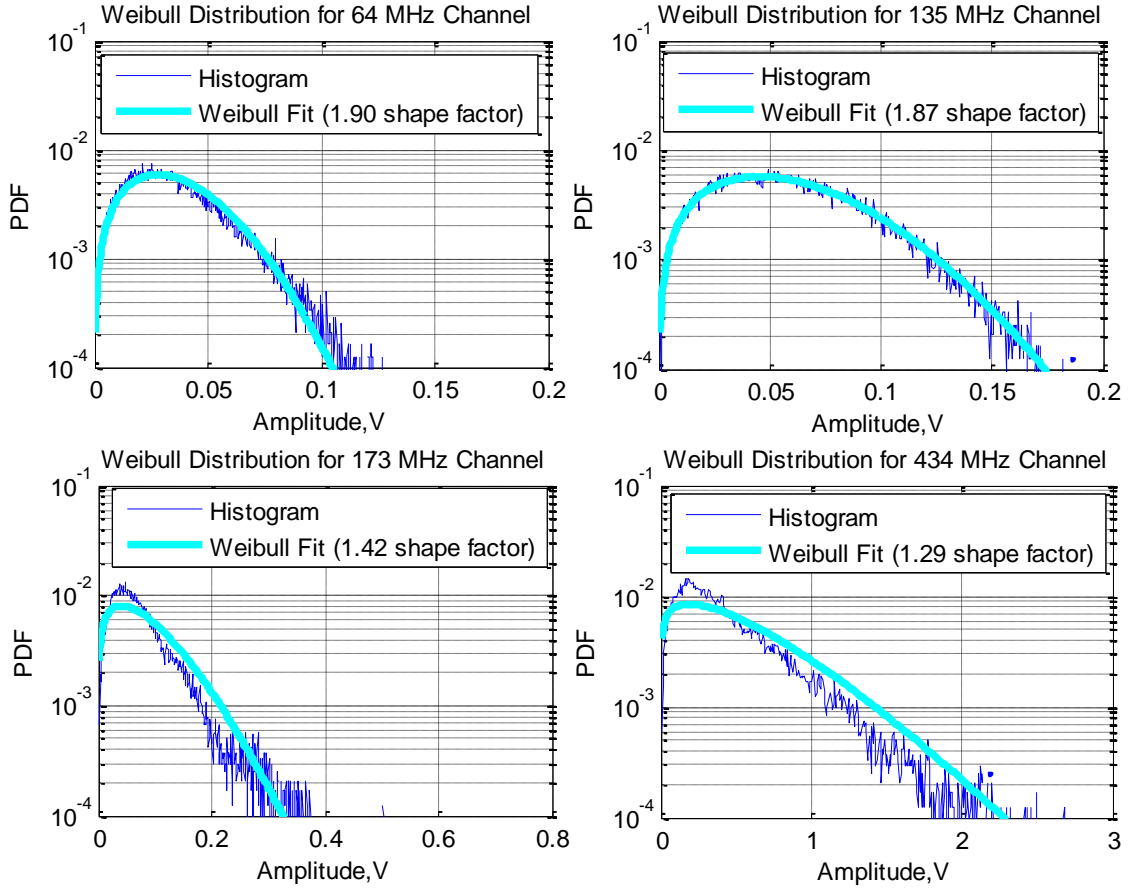


Figure 4.29: Weibull Distribution of a measured clutter at 64 MHz, 135 MHz, 173 MHz and 434 MHz for strong clutter

4.5.4 Doppler Signal Output for Very Strong Wind Speed

The next set of figures shows the result for very strong wind condition taken from the same place at Hornton Grange on 4th September 2009. This file is also chosen because it exhibits the highest clutter from all the files in the data trial. Graphs shown in Figure 4.30 displays the Doppler signal output for all 4 channels. For 64 MHz channel, the maximum amplitude for the channel is 0.18 V and this is followed by 135 MHz channel with maximum amplitude of 0.25 V. While for 173 MHz channel, the maximum amplitude is 0.65V and 3.98 V for 434 MHz channel. We can see that the amplitude for each channel increased when the frequency are increased. These also can be seen clearly in Figure 4.31 where all the amplitudes of the

signal's envelope are displayed in one graph after going through second order LPF with cut-off frequency of 0.08 Hz. All these values are listed in the Table 4.4 including the value for standard deviation, the minimum value for the envelope and also the dynamic range for each of the channels.

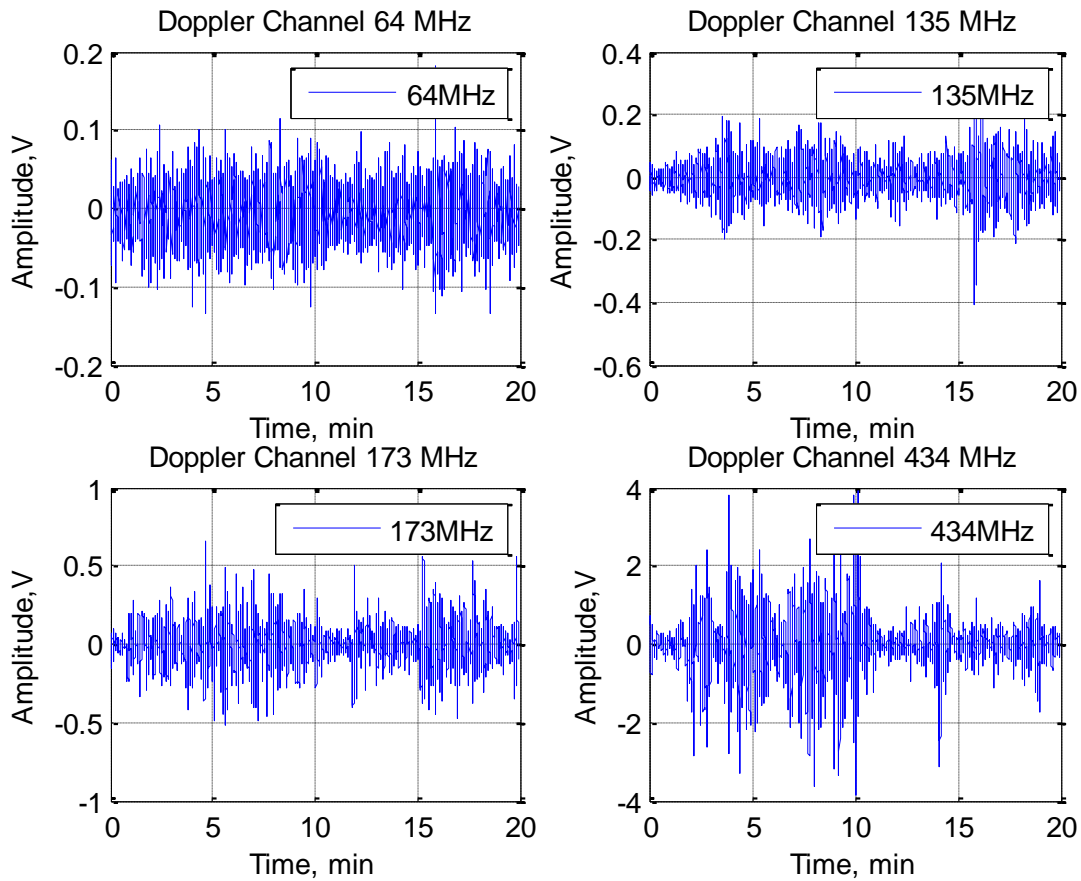
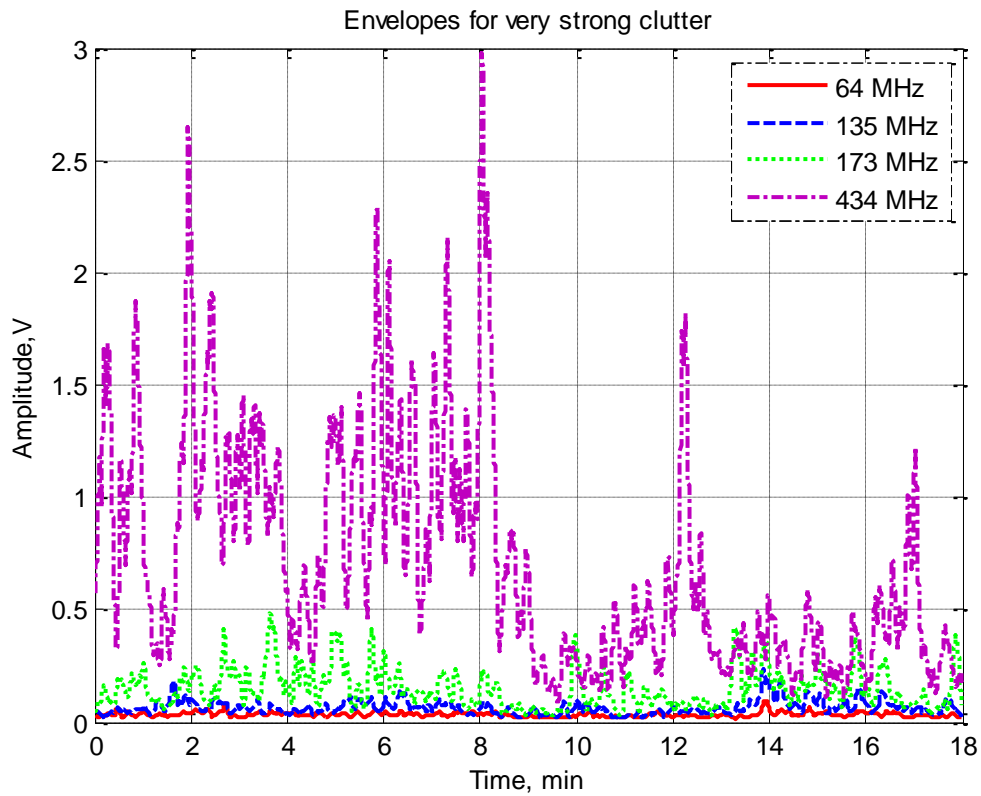


Figure 4.30: Measured Doppler signals at 64 MHz, 135 MHz, 173 MHz and 434 MHz for very strong clutter

Table 4.4: Measured very strong clutter strength for different frequencies

Frequency	Standard Deviation	Envelope		Dynamic Range (dB)
		Min	Max	
64 MHz	0.0275	0.0174	0.0983	7.53
135 MHz	0.0544	0.0195	0.2392	10.89
173 MHz	0.1309	0.0282	0.4875	12.38
434 MHz	0.6707	0.0726	2.9803	16.14

**Figure 4.31: Envelopes for all signal frequencies for very strong clutter**

Again the PSD of the envelopes are calculated and the results are in Figure 4.32 where the graphs show the normalised PSD and also the absolute PSD values. The drop of the PSD slopes is still between 0.005 to 0.01 for all channels. Even though the wind condition are varies from low to very strong wind, the drop of the signal's envelope PSD still within the same range. This proof that the data are taken from the same place which is in this case in Hornton Grange and the wind condition does not affect the PSD values.

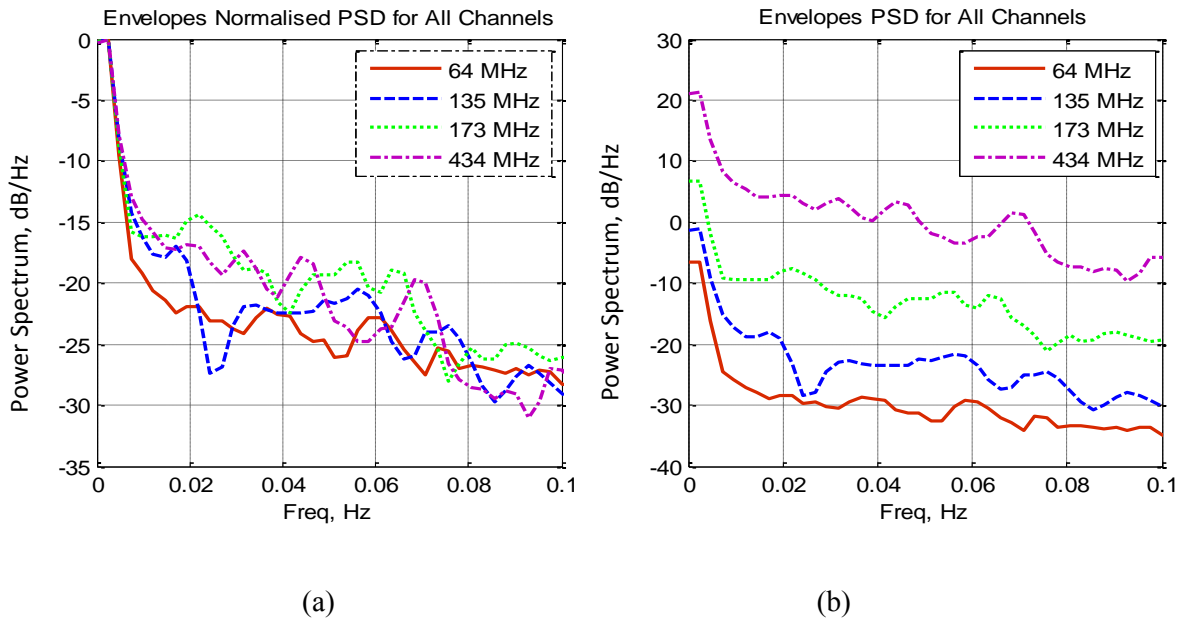


Figure 4.32: Power Spectral Density for clutter envelopes 0.1 cut-off frequency (a) normalized (b) absolute value for very strong clutter.

If we looked into the PSD for the signal in Figure 4.33 and Figure 4.34 (a), we can see it still follow the same trend for all PSD for other wind conditions. The lowest will be 64 MHz channel and the highest is 434 MHz channel. The slopes for all the channels also dropped approximately around 20 dB to 40 dB per decade and the spectrum width for different frequency channels which is defined by 10 dB power drop are about 0.3 to 0.5 Hz.

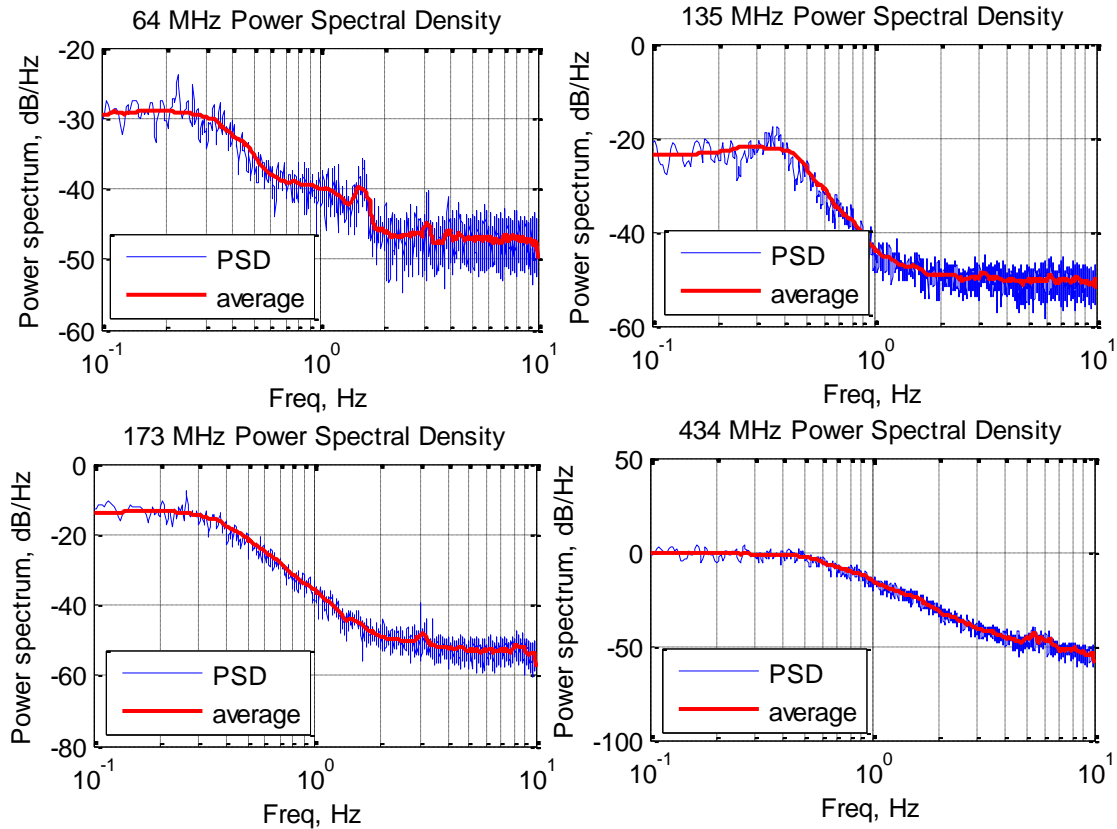


Figure 4.33: PSD of clutter signals for all frequency channels at MHz, 135 MHz, 173 MHz and 434 MHz for very strong clutter

In Figure 4.34 (b), the CDF value for the very strong clutter shows much wider width between 64 MHz channel with 434 MHz channel. For 0.2 CDF value, 64 MHz gives 0.017 V, 135 MHz with 0.028 V, 173 MHz and 434 MHz with 0.063 V and 0.28 V respectively. The PDF distribution in Figure 4.35 also shown Weibull shape with the shape factor ranging from 1.30 to 1.75.

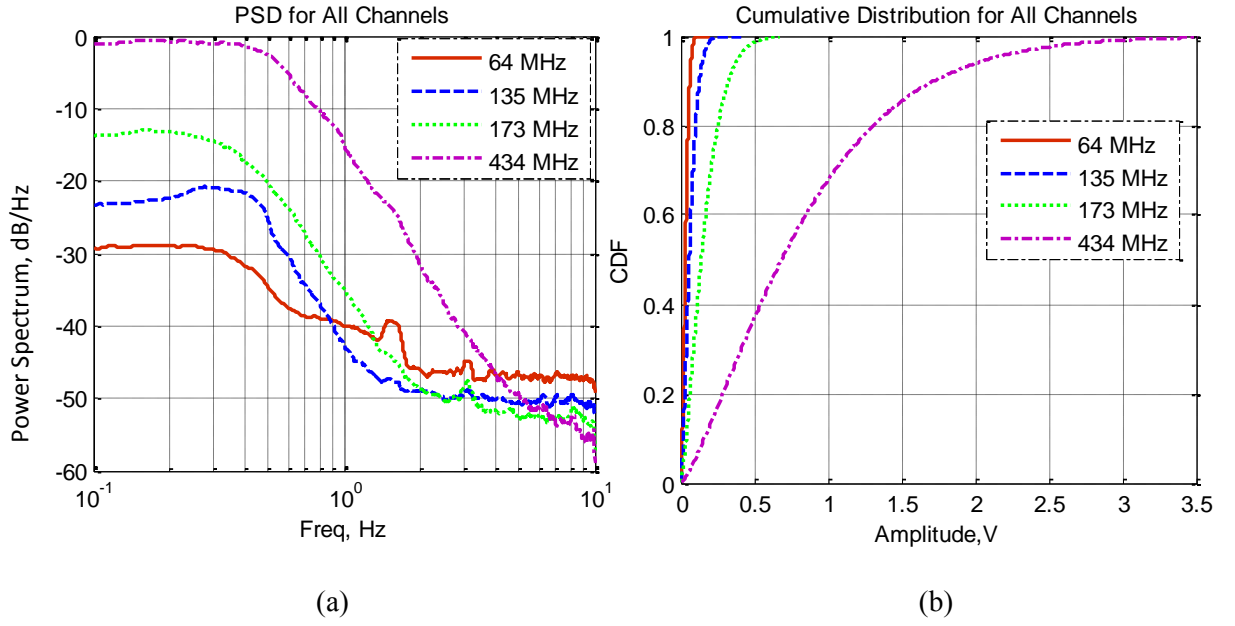


Figure 4.34: (a) PSD comparison for very strong clutter for all frequency channels, (b) Cumulative distribution for all frequency channels.

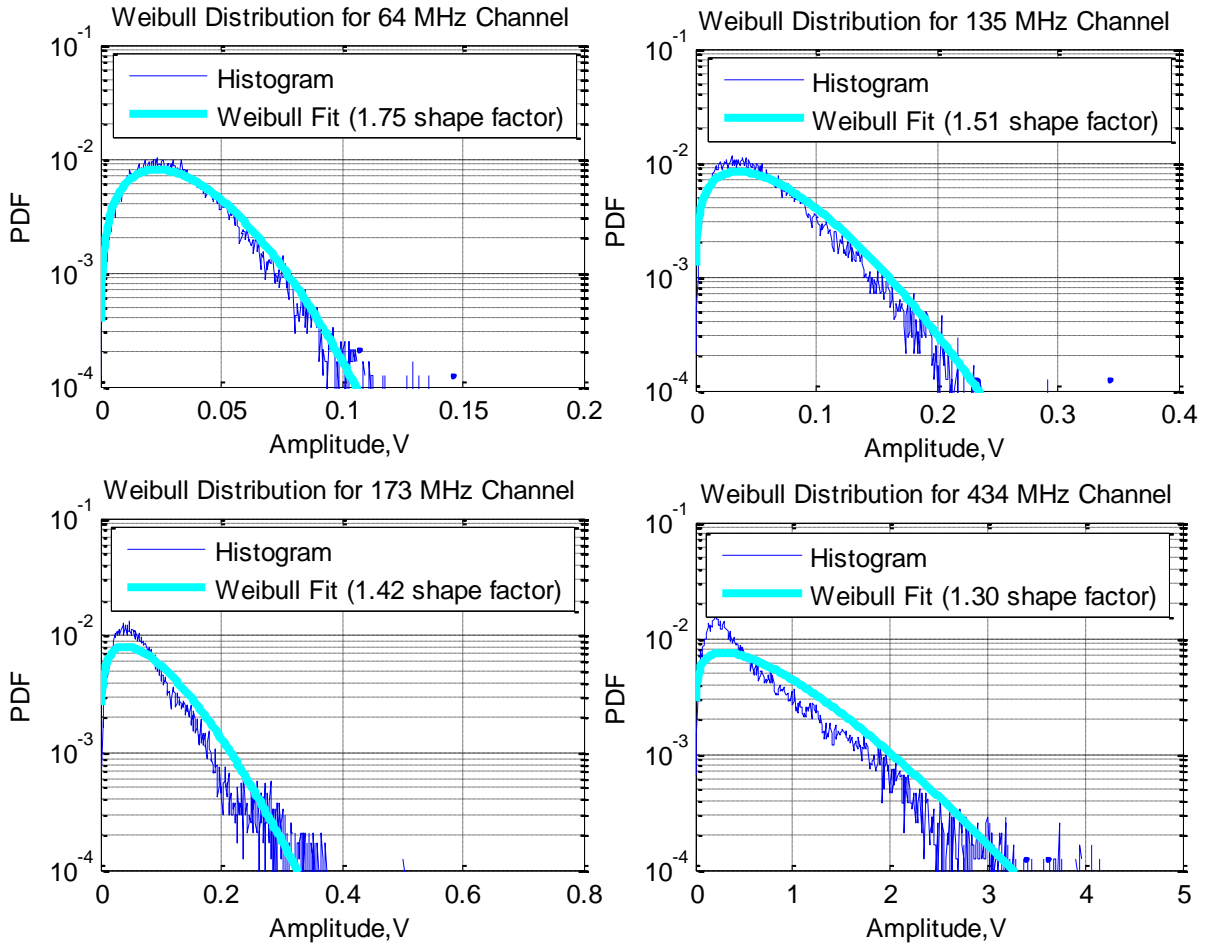


Figure 4.35: Weibull Distribution of a measured clutter at 64 MHz, 135 MHz, 173 MHz and 434 MHz for very strong clutter

4.5.5 Summary of Clutter Results based on Different Wind Speeds

This is the comparison result summary of clutter results based on different wind speeds. Figure 4.36 displayed the STD values for all four different wind speed (low to very strong). The graphs displayed the distribution of clutter STD from 64 MHz to 434 MHz. It shows that the STD is increase when the frequency and wind speed increased. For low wind speed the increment of STD value is just 0.0379 from 64 MHz to 434 MHz. This trend value is increased when the wind speed increased from medium to strong and to very strong with 0.1305, 0.4154 and 0.6432 respectively. These results can be seen clearly in next figure shown in Figure 4.37.

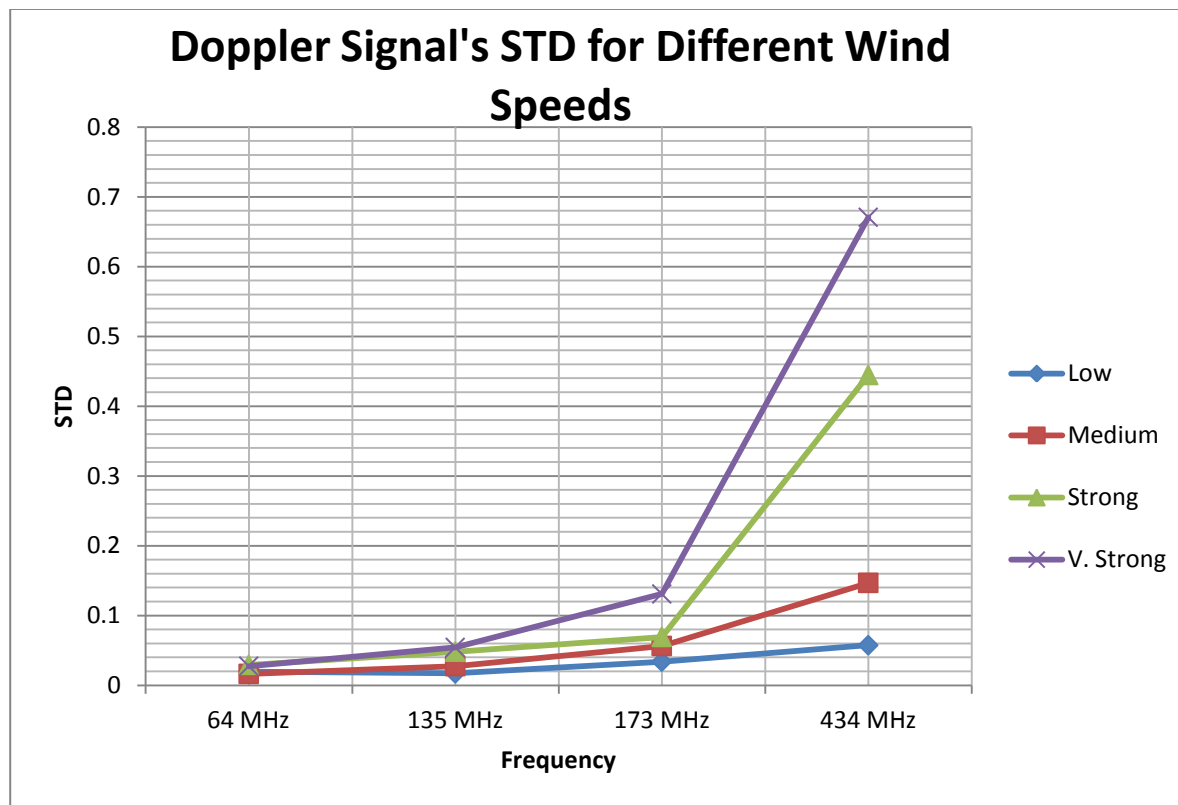


Figure 4.36: Doppler signal's STD value for different wind speeds

In these results, we can see the amplitude of the signals and also the PSD of the signals for different wind speeds for each of frequency channels. From the graphs shows in Figure 4.37, the higher the frequency used and higher clutter strength, the higher will be the amplitude of the clutter's envelope.

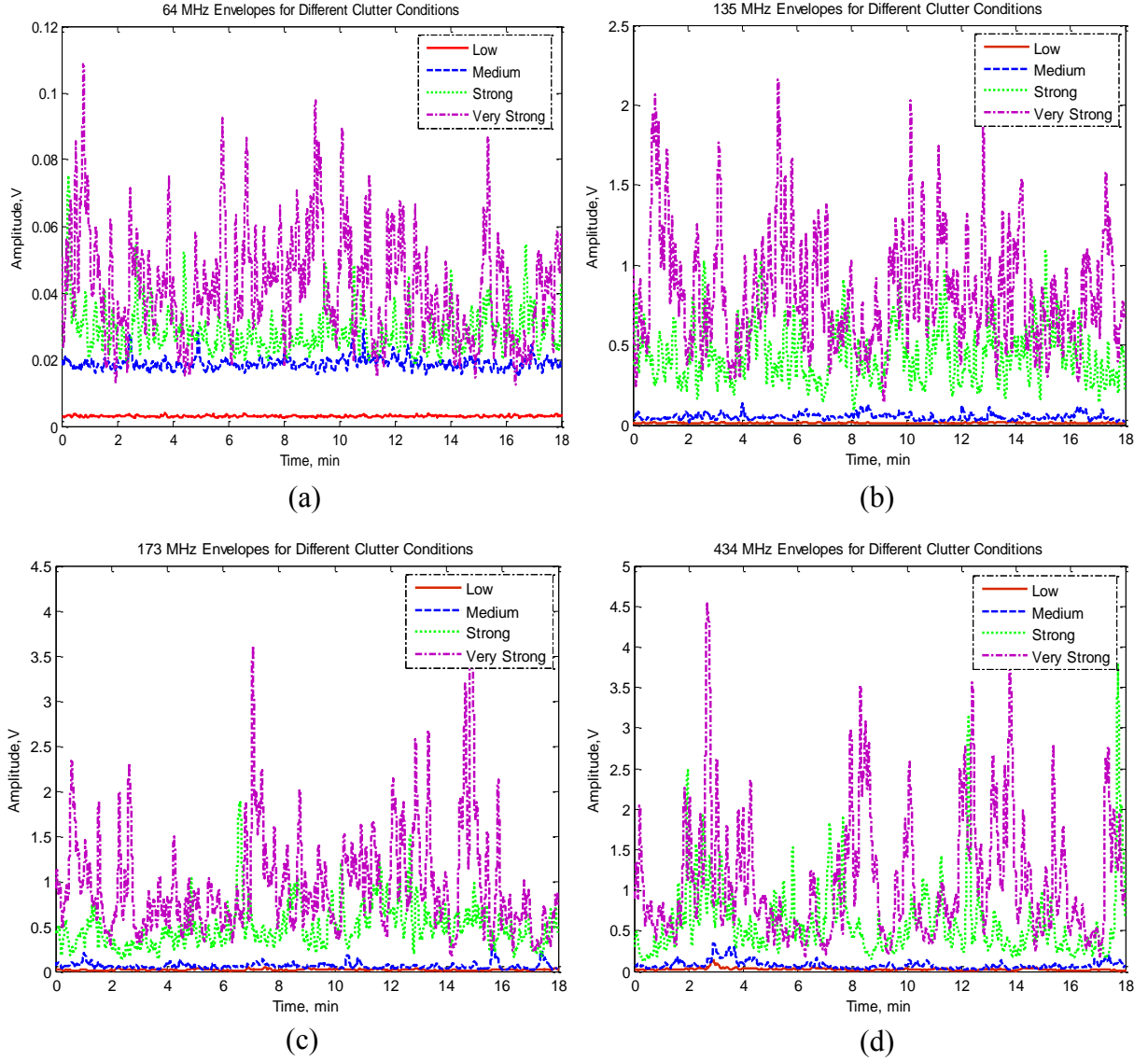


Figure 4.37: Envelopes for all wind conditions for (a) 64 MHz, (b) 135 MHz, (c) 173 MHz, and (d) 434 MHz frequency channel

If we looked into the power spectral density shown in Figure 4.38, it demonstrates the PSD of the signals for different frequencies versus wind speeds. All PSD for all four channels exhibit similar trend even though the wind conditions are varies from low to very strong wind and this shows that the data are taken from the same measurement site. The lowest given PSD is from the low clutter strength and followed to the very strong clutter strength at highest PSD values. The slope shows drop approximately 20 dB to 40 dB per decade and the spectrum width which is defined by 10 dB power drop are about 0.3 to 0.5 Hz.

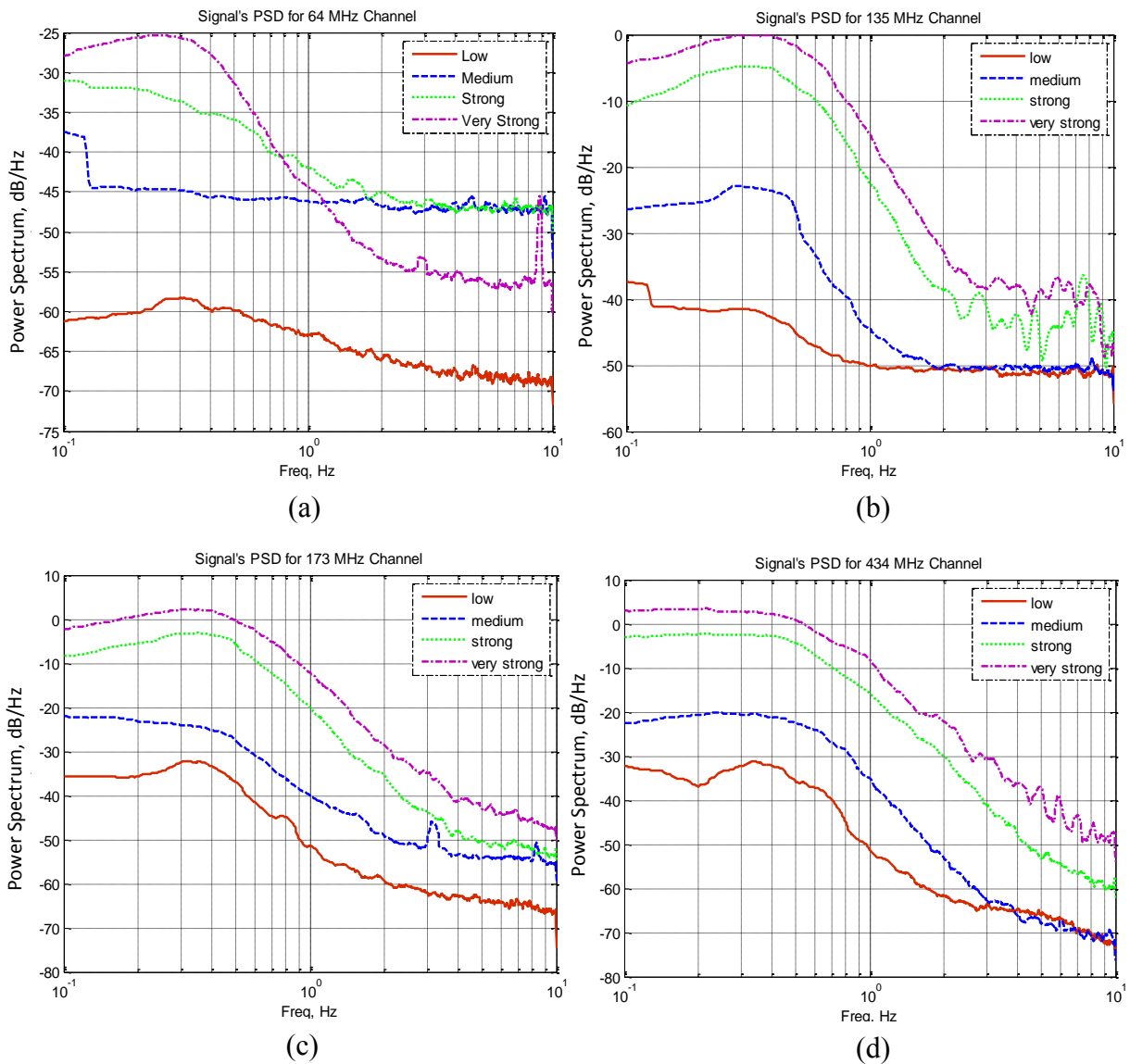


Figure 4.38: PSD comparison for all wind conditions for (a) 64 MHz, (b) 135 MHz, (c) 173 MHz, and (d) 434 MHz frequency channel

It can be concluded from this analysis, that wind speed is the main contribution of clutter strength. It can be seen in the results shown in Table 4.5 below from low to very strong clutter strength all relates to the increased wind speed from low to very strong wind. When the wind is increased, it will blow the surrounding vegetations. This includes bushes and trees with leaves and branches and it will sway. This swaying movement will create Doppler effect and will be detected by the receiver.

Table 4.5: Measured clutter parameters for different clutter strengths (based on wind speed)

Freq (MHz)	Low Clutter				Medium Clutter				Strong Clutter				Very Strong Clutter			
	STD	Envelope		Weibull Fit	STD	Envelope		Weibull Fit	STD	Envelope		Weibull Fit	STD	Envelope		Weibull Fit
		Min	Max			Min	Max			Min	Max			Min	Max	
64	0.0195	0.0138	0.0682	2	0.0163	0.0149	0.0339	1.94	0.0293	0.0188	0.0902	1.9	0.0275	0.0174	0.0983	1.75
135	0.0171	0.0114	0.0767	1.9	0.0275	0.0153	0.1156	1.76	0.0482	0.0196	0.1276	1.87	0.0544	0.0195	0.2392	1.51
173	0.0339	0.0107	0.2132	1.65	0.0564	0.0161	0.2731	1.65	0.0693	0.0211	0.3727	1.42	0.1309	0.0282	0.4875	1.42
434	0.0574	0.0177	0.1926	1.6	0.1468	0.0554	0.5623	1.6	0.4447	0.0803	2.0468	1.29	0.6707	0.0726	2.9803	1.3

4.6 Clutter Results Based on Signal's STD from Long Term Measurement

These are the results from the long term data trials taken from the experiment site in Horton Grange, Birmingham in between 26/08/09 to 13/11/09 which consists of 279 data files with total up to 5940 minutes of record (more than 4 days). The results are presented by different frequency channels. Each frequency channel will have the data for standard deviation (STD), envelope's minimum and maximum value and the shape factor. Based on the results from Section 4.5, it shown that the clutter condition are related to the strength of the wind blown. When the wind speed increased, the clutter strength and the signal's STD risen. Due to this, the main objective in this section is to analysed and categorised all long term measurement data into four different clutter strengths of low, medium, strong and very strong based on the clutter's STD.

All these data will be presented in two ways, the distribution of all numbers of record and histogram format for each frequency. In histogram, it will shows the distribution of each of the parameter and determined the highest and the lowest for each of the parameter (exp: PDF versus signal's STD). While for the distribution; data for STD, Weibull shape factor and envelope's minimum and maximum are to shows the value of the parameters for each number's of record (exp: signal's STD versus number of records). This is to determine which data file contributed from the highest until to the lowest values for each channels frequency. Then this data file are rearranged by following the signal's STD from the lowest upto the highest values. When all the data are gathered, the clutters are divided into four different clutter strengths for each frequency. This is by finding the differences STD value for each clutter strength by using the equations below:

$$D = \frac{H - L}{4} \quad (4.14)$$

and starting value for each clutter can be denoted as:

$$\text{Medium, } M = L + D$$

$$\text{Strong, } S = M + D$$

$$\text{Very strong, } V = S + D$$

where H is the highest STD value and L is the lowest STD value for a given database, and divided into 4 different clutter strengths (low, medium, strong and very strong).

4.6.1 64 MHz Channel

i. Signal's STD, Envelope Minimum and Maximum, and Weibull Shape Factor

For 64 MHz channel as shown in Figure 4.39, it shows all the values for standard deviations, minimum and maximum signal envelopes and the shape factors for all 279 numbers of files. We can see the values for each data record varies from the lowest to the highest values. From here we can see the variations of the wind conditions, where the highest wind blow will create higher clutter with highest signal peak or amplitude.

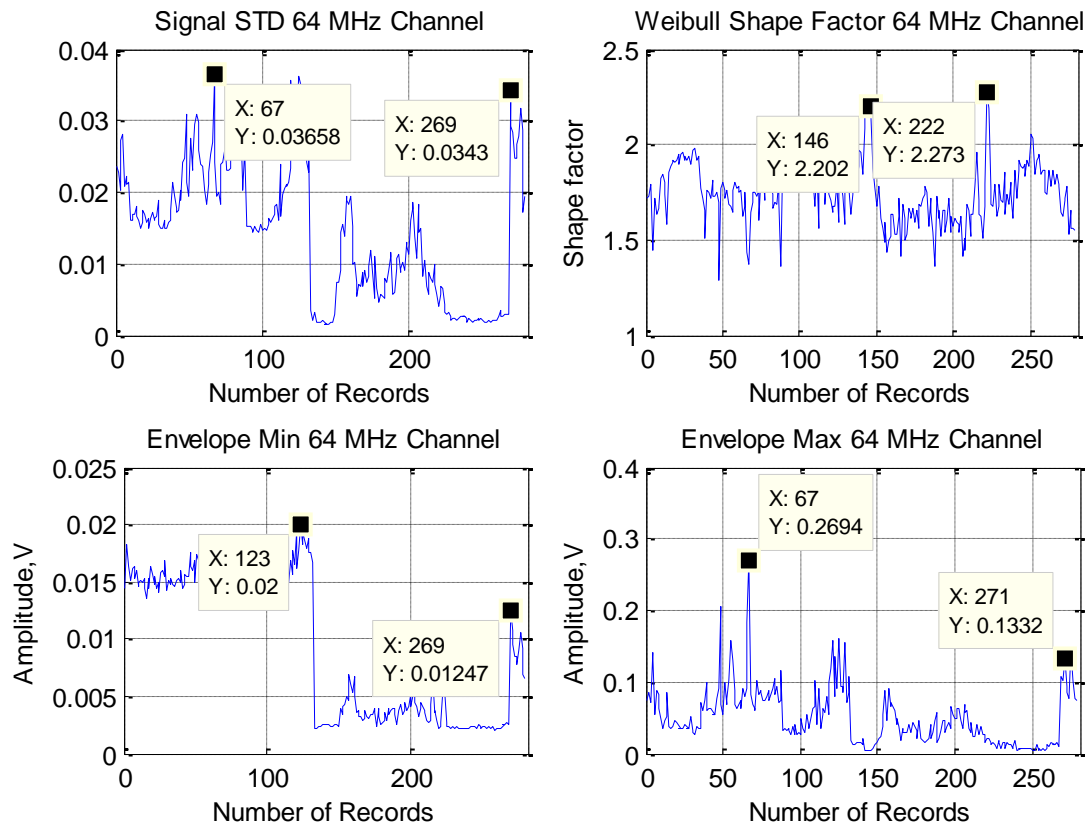


Figure 4.39: Distribution of standard deviation, minimum and maximum signal envelopes and the shape factors for 64 MHz frequency channel

ii. Histogram

In Figure 4.40, it exhibits the histograms for signal's STD, shape factor, envelope's minimum and maximum values. If we looked at the signal standard deviation, the rise in the average of

standard deviation start from 0.035 with most of the standard deviations lies started from 0.0035. While for minimum and maximum values for signal's envelope also shown the distributions are less than 0.02 V for minimum value and 0.28 V for maximum value of the envelopes. The shape factor for all 64 MHz channel's data falls between 1.4 to 2.3 where most of the shape factors are with the value from 1.6 to 2.0. This proof that the lower the frequency, more it tends to exhibit similar to Rayleigh distribution with the shape factor of 2.

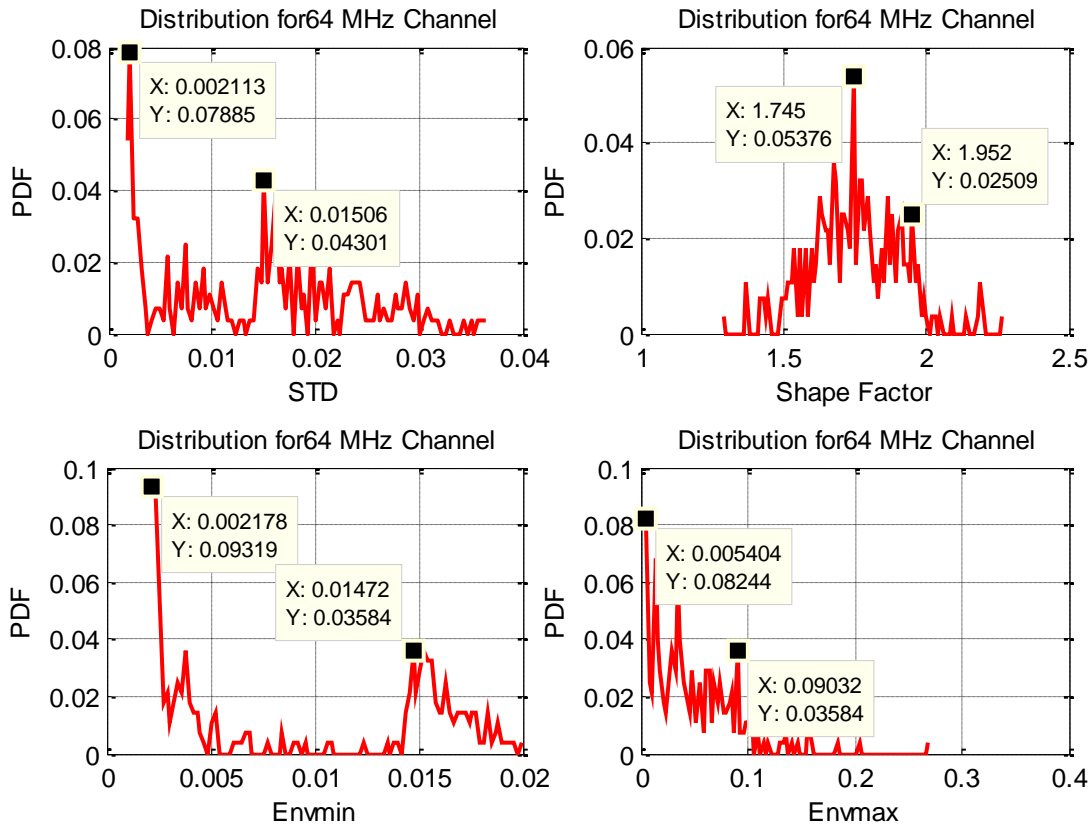


Figure 4.40: Histograms of standard deviation, minimum and maximum signal envelopes and the shape factors for 64 MHz frequency channel

4.6.2 135 MHz Channel

i. Signal's STD, Envelope Minimum and Maximum, and Weibull Shape Factor

The next graph in Figure 4.40, the highest standard deviation values for 135 MHz data are majority lies in between data file 150 to data file 225. Envelope's minimum and maximum amplitudes also show the same trend where the highest peak lies between file 150 to 225.

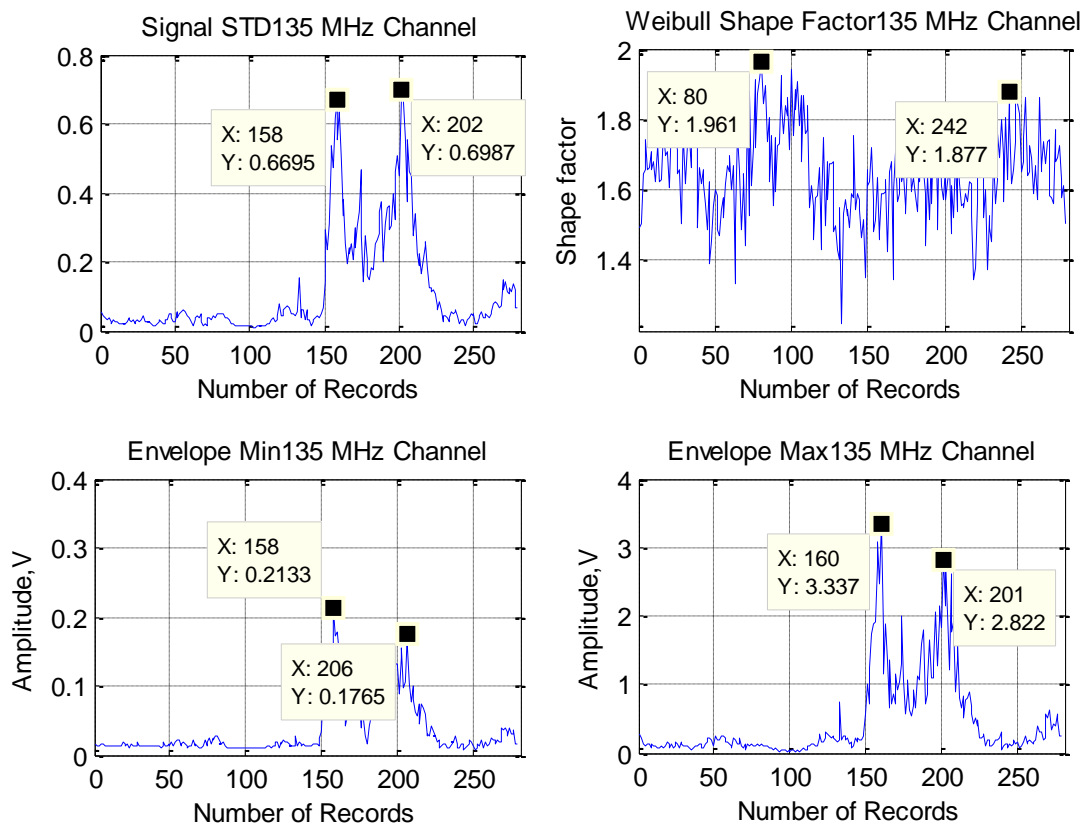


Figure 4.41: Distribution of standard deviation, minimum and maximum signal envelopes and the shape factors for 135 MHz frequency channel

ii. Histogram

The standard deviation's histograms for this channel slightly increased as compared to 64 MHz channel. It is shown in Figure 4.42. This is understandable where all the standard deviations, minimum and maximum values of signal's envelopes will be increased with the

increase of the frequencies. Most of the standard deviation values fall into the range less than 0.03. While the maximum values of the signal's envelopes histogram fall majority less than 0.35 V and minimum values of the signal's envelopes falls less than 0.05 V. The shape factors for this frequency channel lies in between 1.23 to 1.96 with most of it between 1.5 to 1.70.

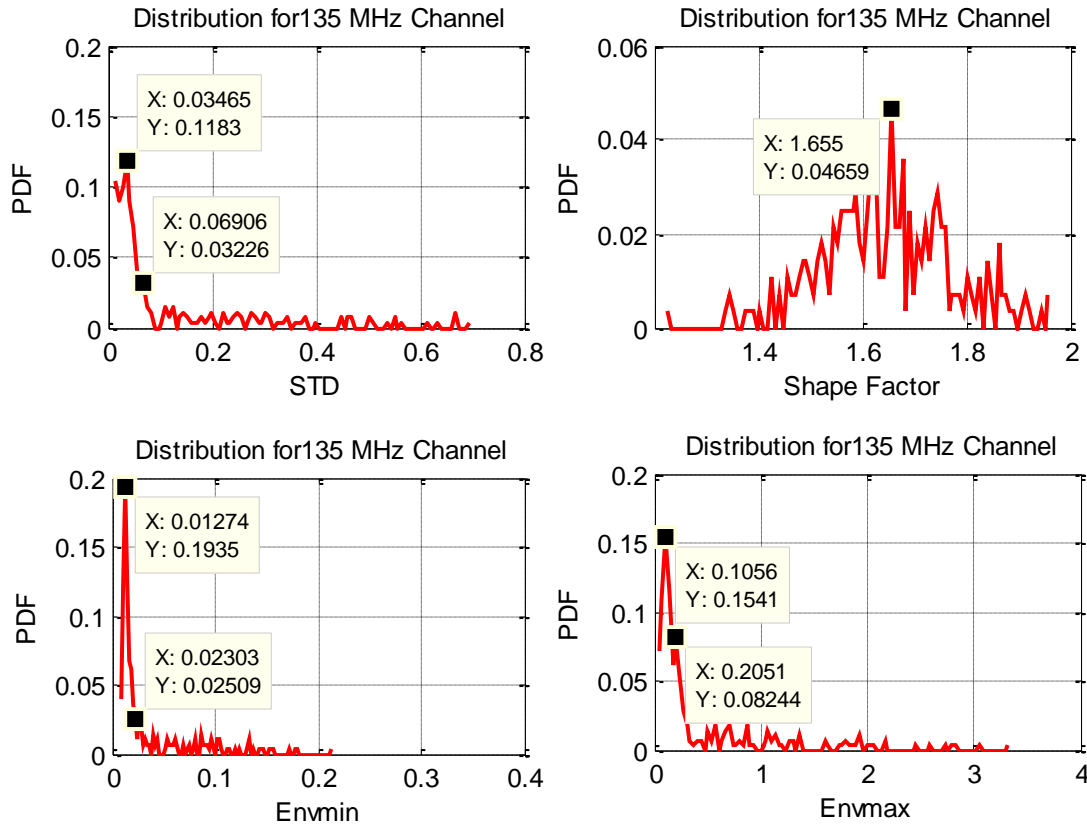


Figure 4.42: Histograms of standard deviation, minimum and maximum signal envelopes and the shape factors for 135 MHz frequency channel

4.6.3 173 MHz Channel

i. Signal's STD, Envelope Minimum and Maximum, and Weibull Shape Factor

Figure 4.43 demonstrates the distributions for 173 MHz channel. The standard deviations, minimum and maximum signal envelopes also exhibit the approximately the same trend with 135 MHz channel where most of the highest amplitude lies in between file number 150 to file

number 220. While the shape factor for the signal ranging from 1.10 to 1.94 which most of it lies between 1.31 to 1.70.

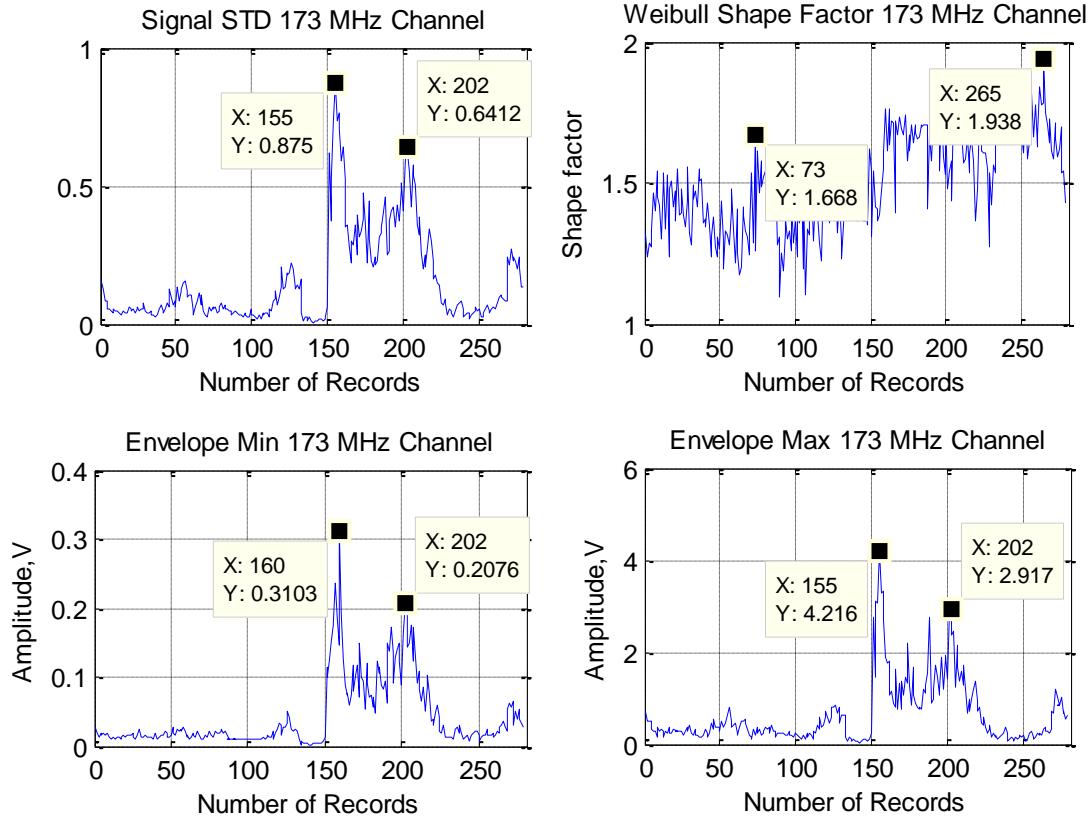


Figure 4.43: Distribution of standard deviation, minimum and maximum signal envelopes and the shape factors for 173 MHz frequency channel

ii. Histogram

The next graphs Figure 4.44, is the histograms for 173 MHz channel. It shows the standard deviation values falls majority less than 0.13 and most of the minimum value of the envelopes are less than 0.04 V. While the maximum value of the envelopes are mostly less than 0.78 V and the shape factor values for the signals are ranging from 1.10 to 1.94.

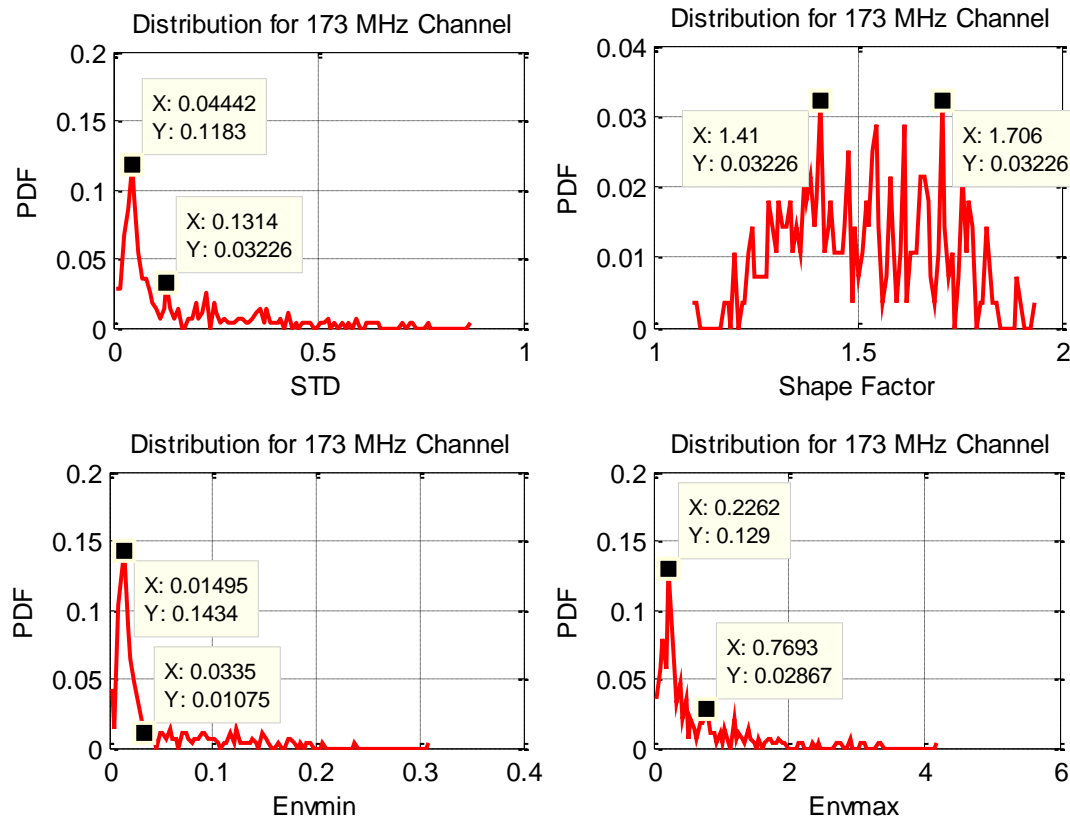


Figure 4.44: Histograms of standard deviation, minimum and maximum signal envelopes and the shape factors for 173 MHz frequency channel

4.6.4 434 MHz Channel

i. Signal's STD, Envelope Minimum and Maximum, and Weibull Shape Factor

For 434 MHz channel, the distributions of all the values are quite unsystematic especially for the standard deviations and the maximum values of the envelopes. There are few highest spikes for the standard deviation such as for the data from file number 56 and 271 with the value of 1.05 and 0.86 respectively. This show that 434 MHz channel is very sensitive to the surrounding that it can pick up every little movement around the area. The highest value for the minimum and maximum signal's envelopes for all 281 data records is 0.24 V from data file number 162 and 5.06 V from file number 52 respectively. As we can see the distribution

for the shape factor is a bit lower than the shape factor for the lower frequency. The higher the frequency, the lower will be the shape factor. All these are shown in Figure 4.45.

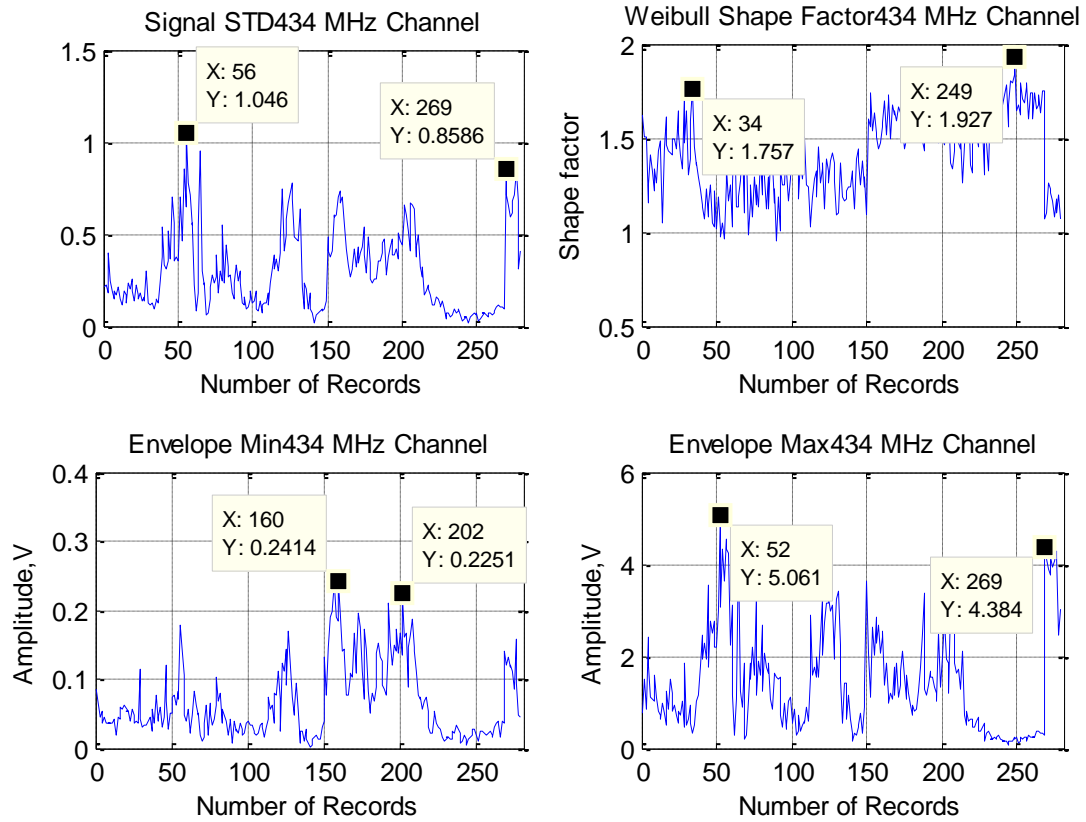


Figure 4.45: Distribution of standard deviation, minimum and maximum signal envelopes and the shape factors for 434 MHz frequency channel

ii. Histogram

The distributions of the histogram also show the same pattern as before, where most of the standard deviations, minimum and maximum values of the envelopes, and the signal's shape factor lies on the left side of the graph. It is shown in Figure 4.46, for standard deviation, all the values are less than 1.05 with the majority less than 0.11. While for the minimum and maximum values of the signal's envelopes are less than 0.25 V and 5 V respectively with the majority are less than 0.05 V for minimum value and less than 2 V for maximum value. The

shape factor distributions for this channel are in between 0.95 to 1.93, where the majority of the shape factors are in between 1.1 to 1.7.

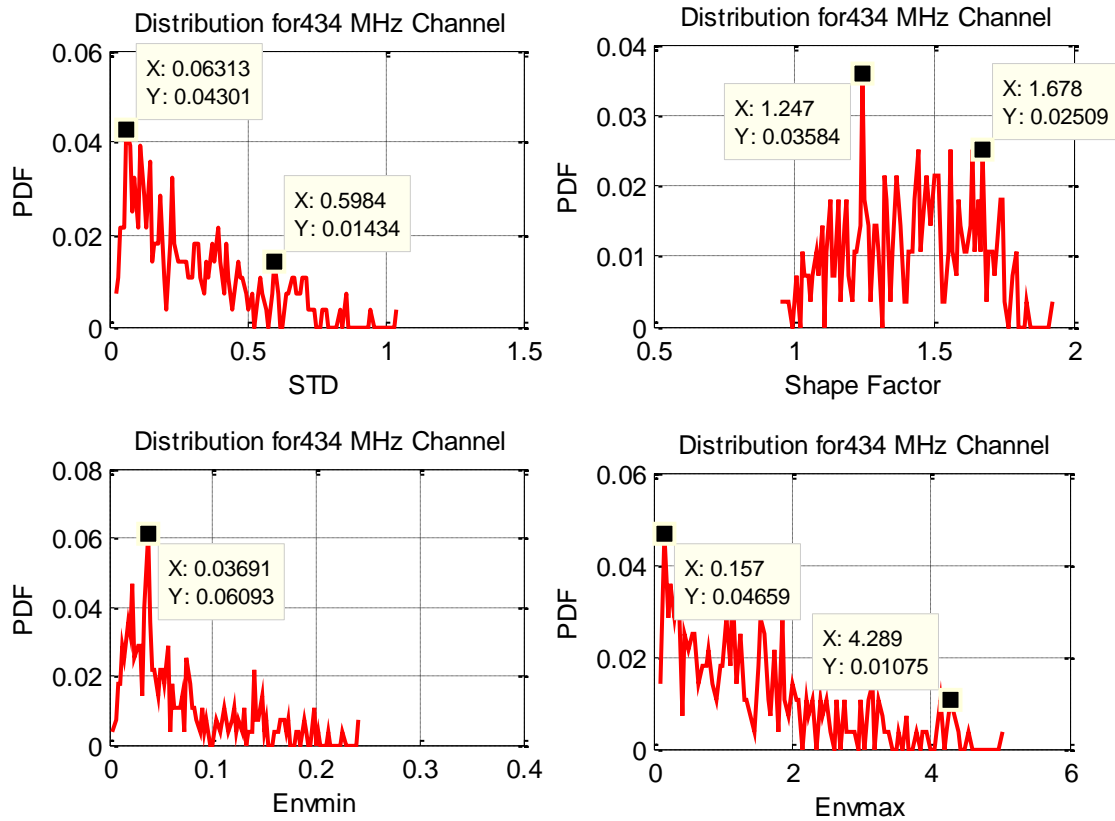


Figure 4.46: Histogram of standard deviation, minimum and maximum signal envelopes and the shape factors for 434 MHz frequency channel

4.6.5 Summary of Clutter Results Based on Signal's STD

Data records written in Table 4.6 below are the summary from four data trials taken from the experiment in Horton Grange. The records are from 279 files which equal to 5940 minutes for a total of approximately 4 days of observations. It has been processed and analysed to find the value for standard deviation, envelope's minimum and maximum, and Weibull's shape factor for different clutter conditions. From the analysis, we can categorised four different clutter conditions such as low, medium, strong and very strong clutter. All the values for four

different parameters are shown in table. It shown that the signal's STD from low to very strong clutter correspond to our finding where the clutter amplitude increased parallel with the increment of clutter strengths. Then these results are compared with the simulated clutter in Chapter 5.

Table 4.6: Measured clutter parameters for different clutter strengths (based on signal's STD)

Freq (MHz)	Low Clutter				Medium Clutter				Strong Clutter				Very Strong Clutter			
	STD	Envelope		Weibull Fit	STD	Envelope		Weibull Fit	STD	Envelope		Weibull Fit	STD	Envelope		Weibull Fit
		Min	Max			Min	Max			Min	Max			Min	Max	
64	0.0016	0.0024	0.0041	2.00	0.0145	0.0148	0.0405	1.95	0.0247	0.0085	0.0939	1.75	0.03658	0.0173	0.2694	1.7
135	0.0106	0.0095	0.0228	1.86	0.2518	0.0861	0.8593	1.71	0.4471	0.1312	1.8141	1.67	0.6673	0.1544	2.7789	1.66
173	0.0252	0.0118	0.0911	1.76	0.3068	0.0912	1.0618	1.64	0.5536	0.143	2.4551	1.44	0.7259	0.1533	3.0868	1.41
434	0.0447	0.0137	0.152	1.67	0.3234	0.0773	1.3007	1.44	0.6561	0.1634	3.2627	1.33	0.9493	0.0834	4.2691	1.19

The maximum and minimum amplitude of the clutter signal is considered as the dynamic range of the clutter amplitude. In Figure 4.47 indicates the dynamic range for all clutter strengths from low to very strong conditions. These specify that with higher clutter power and frequencies used, it gives larger dynamic range.

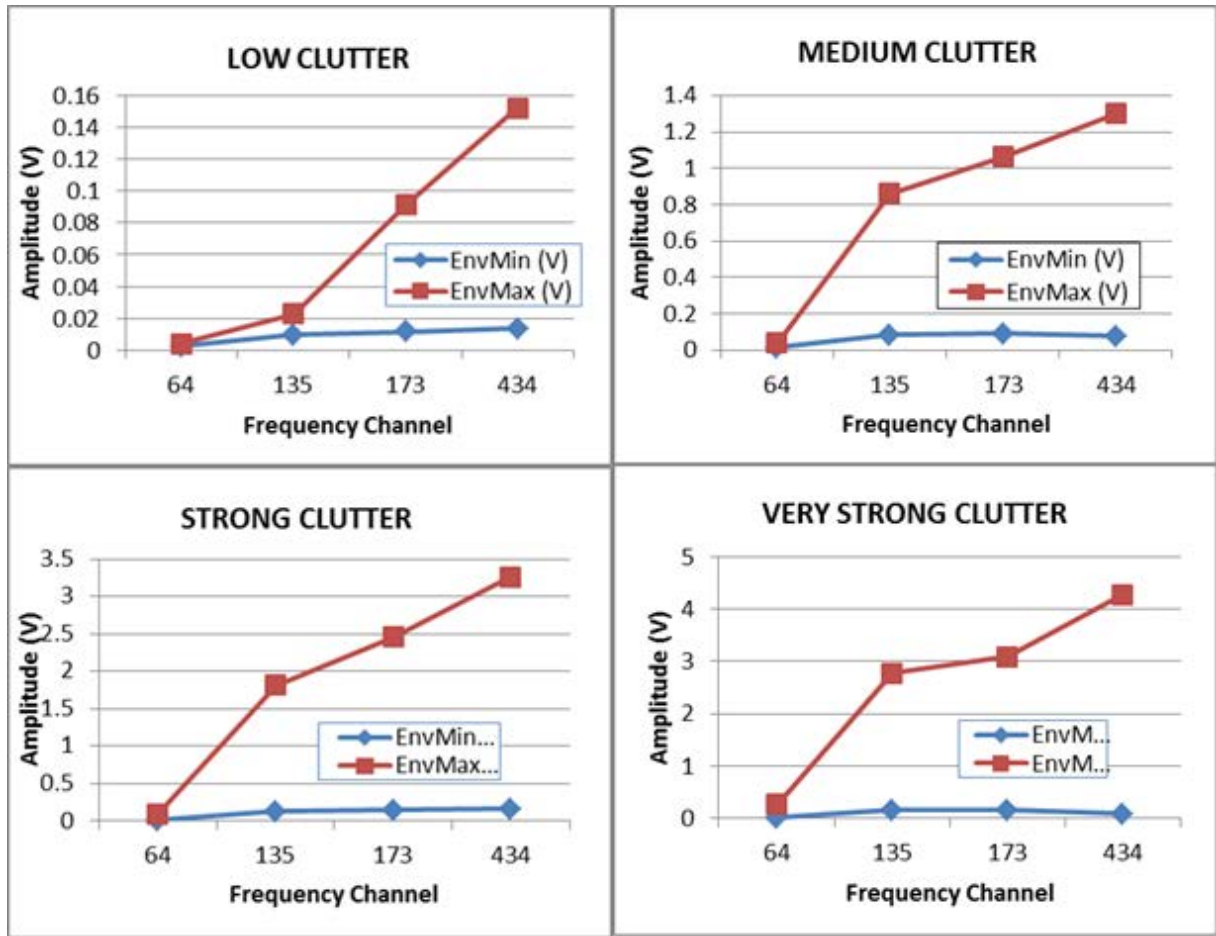


Figure 4.47: Dynamic range for low, medium, strong and very strong clutter signals

The graphs in Figure 4.48 and Figure 4.49 shows all the cumulative distribution function (CDF) parameters for standard deviation, Weibull's shape factor, and envelope's minimum and maximum values. From all these graphs, it shows that 64 MHz channel contributed the lowest CDF amplitude and follows by 135 MHz, 173 MHz and 434 MHz except for the Figure 4.49 (b) for Weibull's shape factor CDF value where the trend of the CDF amplitude is vice versa from the other graphs. In this graph, the highest CDF amplitude is given by the channel 64 MHz channel and the lowest by 434 MHz channel. It is understood that the higher the frequency, the higher will be the CDF values and for the shape factor, the higher the frequency, the lower will be the shape factor value thus gives lower values for CDF.

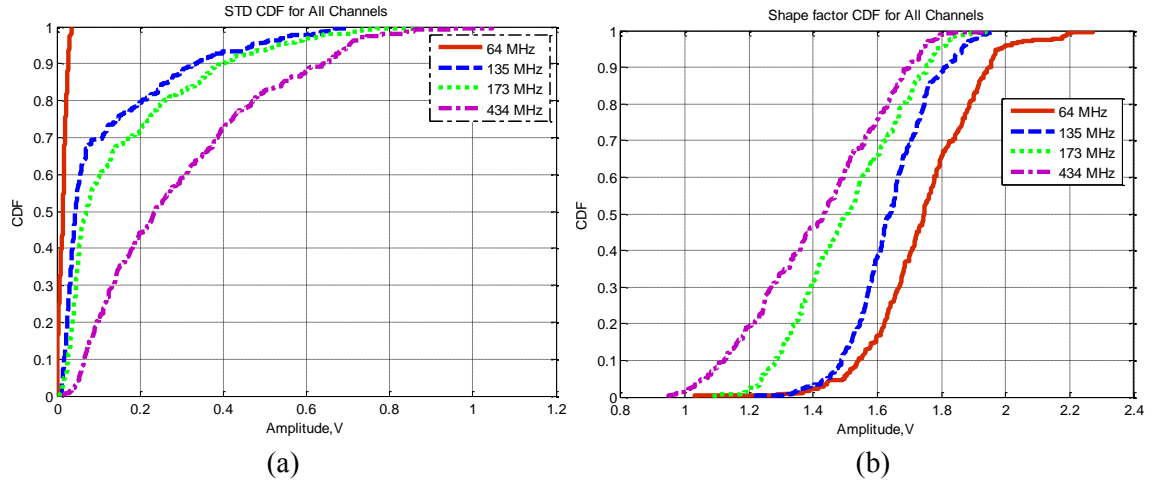


Figure 4.48: (a) Standard deviation CDF for all channels, (b) Weibull shape factor CDF for all channels

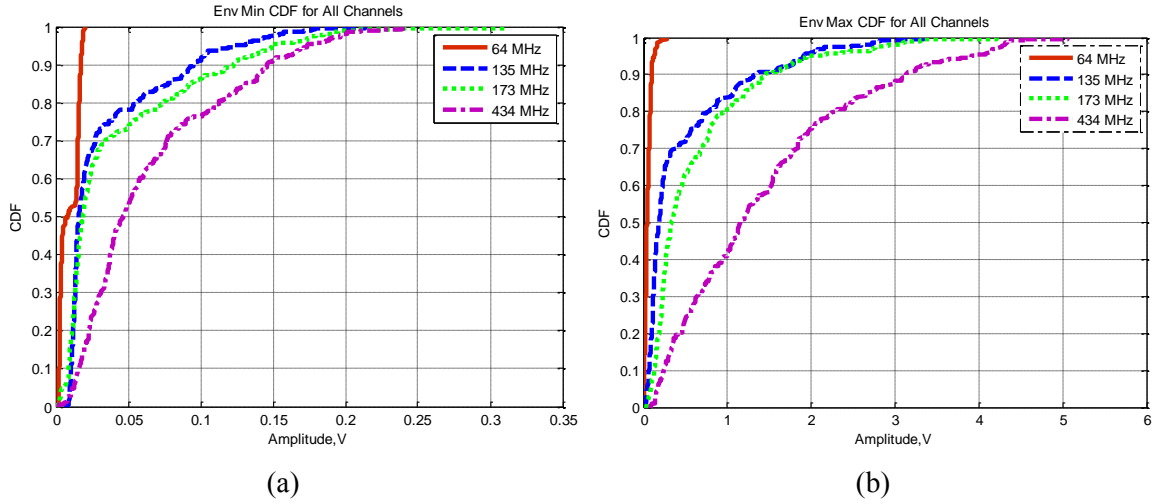


Figure 4.49: (a) Envelope's minimum values CDF for all channels, (b) Envelope's maximum values CDF for all channels

As a result, the average of the standard deviations, minimum and maximum of the signal's envelopes, and also the shape factors of the signals for the data taken follow each other quite well, even though their individual results varied on day to day basis.

4.7 Summary

As a summary, we can summarize that the spectrum of clutter is practically the same. The power dropped approximately around 0.005 Hz to 0.01 Hz with second order LPF and cut-off frequency of 0.1 Hz. The PSD slopes drop approximately around 20 dB to 30 dB per decade for each channel. The spectrum width for different frequency channels which is defined by 10 dB power dropped are about 0.4 to 0.5 Hz.

The amplitude of the Doppler signals is increased with the increased of the operating frequencies and the increment of the wind speed from low to very strong wind. The amplitude of the envelopes which shows the dynamic range of the clutter signal also exhibit the same trend of the clutter pattern, which proof that the signals came from the same place and the same source of clutter.

The clutter distribution which represents the power density function (PDF) of the clutter signals correspond to Weibull distribution with the shape factor ranging from 1.19 for the highest frequency (434 MHz) and up to 2.00 for the lowest frequency (64 MHz). It is understandable that the lower the frequency, the more it tends to exhibit similar to Rayleigh distribution.

The results from the overall data trials (279 data files) shows that the standard deviation, envelope's minimum and maximum amplitude and also the shape factor are depends on the operating frequencies and also the wind speeds. The most probable values for all the parameters are shown in Table 4.6 and these values are used for clutter generation.

CHAPTER 5

EMPIRICAL MODEL OF CLUTTER

5.1 Introduction

After all the analysis on measured clutter are analysed, all the estimated parameter values such as standard deviation, envelope's maximum and minimum are then will be used in this chapter. These parameters are applied to generate clutter in order to have similar characteristics as the measured clutters. Using the simulated clutter with similar characteristic with the measured ones, synthetic environment can be designed to estimate any radar system especially for FSR system. First part of this chapter is the description on empirical model structure of clutter including the flow on how to generate the clutter. This will continue with a simulation process using the Matlab program for clutter generation. Lastly, all the results will be analysed and compared with the measured results.

5.2 The Model Structure

In order to proceed with clutter modelling, first, the signals are analyzed and categorized into four different clutter strengths which can be generally defined as low, medium, strong and

very strong as listed in Table 4.6. The table lists all the parameters used to generate clutter-like signals for different clutter strengths. The estimated parameters from the measured signal from Section 4.6 are then used to generate clutter in order to have similar characteristics as the measured clutter. These include signal's STD, Weibull's shape factor and clutter's envelope.

In this research, the carrier frequencies are considered to varies from 64 MHz to 434 MHz. The procedure of clutter generation is shown in the block diagram in Figure 5.1. This modelling process is divided into three stages. First stage is to generate a “colour” noise using set of random Arbitrary White Gaussian noises (AWGN) passing through a low pass filter (LPF) with cut-off frequency varies around 0.25 to 1 Hz and given spectrum of 0.5 to 1 Hz taken from the measured clutter results. In this stage, the stationary clutter signal is produced.

Second is to generate a time varying envelope of non-stationary clutter using AWGN random clutter. This is to generate a non-stationary signal by taking into accounts different clutter strengths as desired (examples such as low, medium, strong and very strong clutter power) and fit into LPF with cut-off frequency of 0.08 Hz. Then this follows by modulation process of multiplying these two Gaussian clutters from step one and two to develop a time varying non-stationary clutter with adjustment to the given dynamic range from the measured clutter.

While in the third stage, another Gaussian noise clutter will pass through the LPF with cut-off frequency varies from 0.001 to 0.003 Hz. This last stage is to ensure that the simulated clutter-like signal is non-stationary and non-Gaussian clutter with an adjustment of the clutter signal to the measured clutter dynamic range.

Then the procedures of clutter generation are then explained step by step from stage 1 to stage 3 as below in Section 5.2.1 to Section 5.2.3.

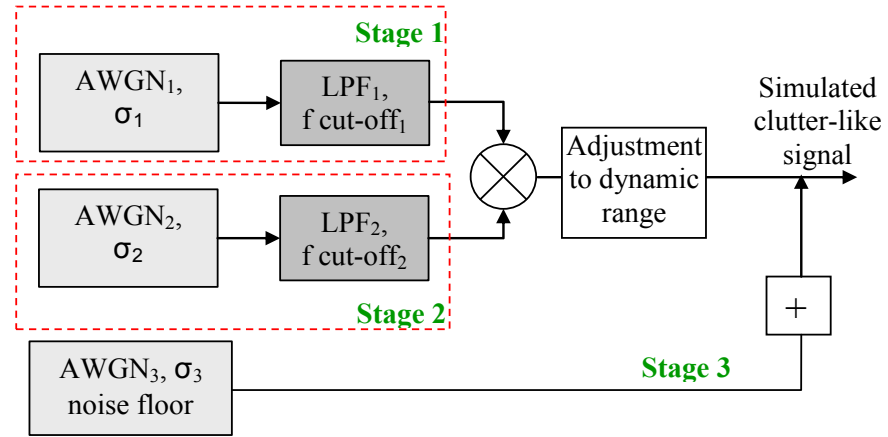


Figure 5.1: Vegetation clutter simulation model block diagram

5.2.1 Stage 1: Generating Stationary Clutter

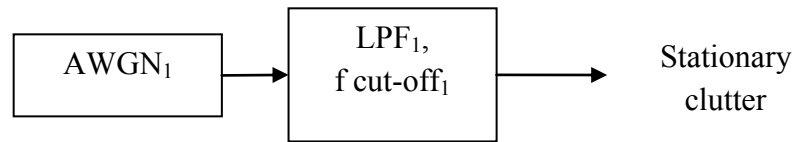


Figure 5.2: Generating stationary clutter

In this process shown in Figure 5.2, AWGN signal is used to generate stationary clutter but first AWGN signal is generated by using given standard deviation of 0.0016 (for example of 64 MHz low clutter) and 24,000 samples (sampling frequency = 20 Hz, time = 1200 seconds). Then this clutter is passing through Butterworth filter with orders varies for different frequencies and clutter power strengths based on the signal's STD. The cut-off frequency used also varies with the strength of clutters and frequencies from 0.4 to 0.5 Hz. Figure 5.3

displayed the result of Stage 1 for stationary clutter simulated for 64 MHz with low clutter power strength characteristic and Figure 5.4 shows the result for all clutter strengths.

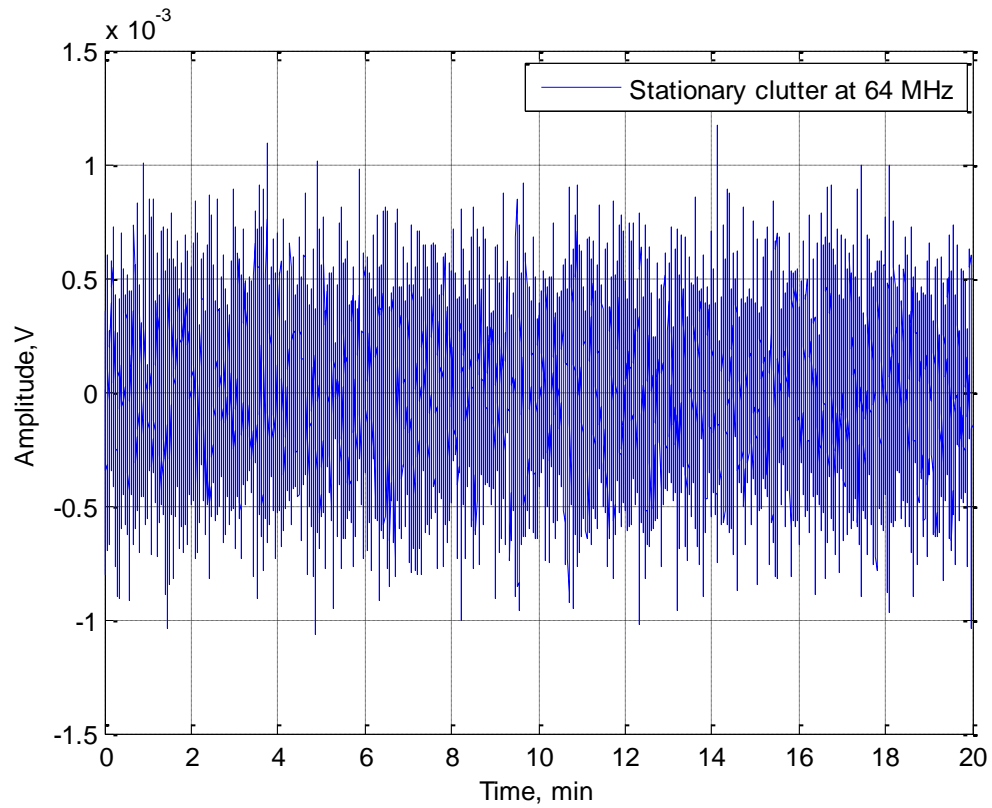


Figure 5.3: Stationary clutter Simulated for 64 MHz

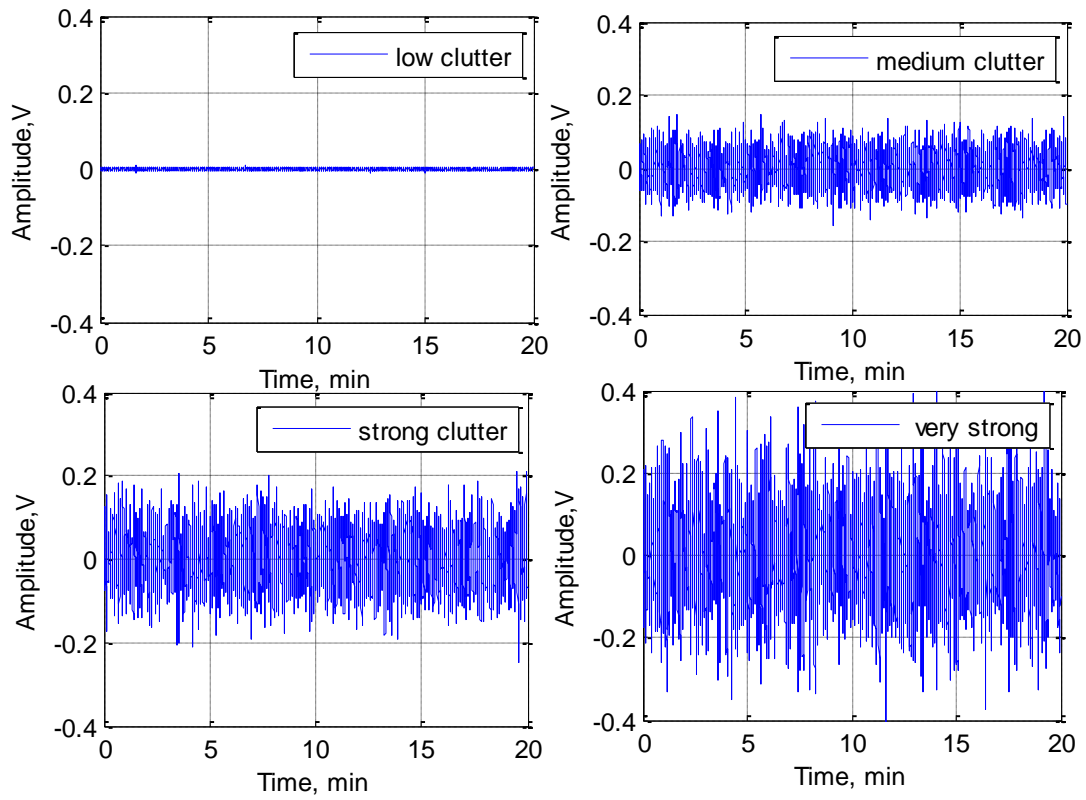


Figure 5.4: Stationary clutter for all clutter conditions

5.2.2 Stage 2: Generating Time Varying Envelope of Non-stationary Clutter

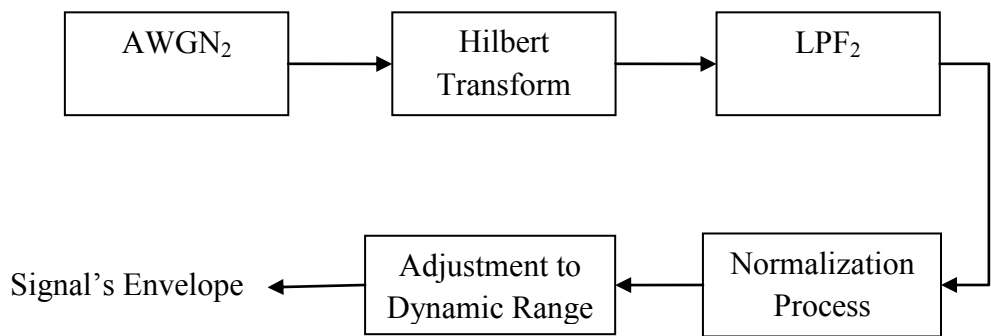


Figure 5.5: Develop clutter's envelope

In this stage, clutter's envelope is generated from another AWGN signal as shown in Figure 5.5. The same process will apply to generate AWGN clutter. This time the standard deviation

of 1 is used as fix value and the number of samples are double than before. This is just to get the same amount of time (20 minutes of data time) after we cut the transient part when the clutter pass through the filter. Then the simulated AWGN clutter will go through Hilbert Transform function. Hilbert transform is a process to calculate the amplitude of the clutter based on four different clutter strengths and create a clutter which only consists of the amplitude of the clutter called as an envelope.

The output clutter is then filtered using 2nd order LPF with cut-off frequency of 0.08 Hz. Figure 5.6 shows the output from the Hilbert transform after passing LPF for 64 MHz of low clutter. Furthermore, Figure 5.7 shows the 64 MHz clutter signals for all clutter strength varies from low to very strong clutter.

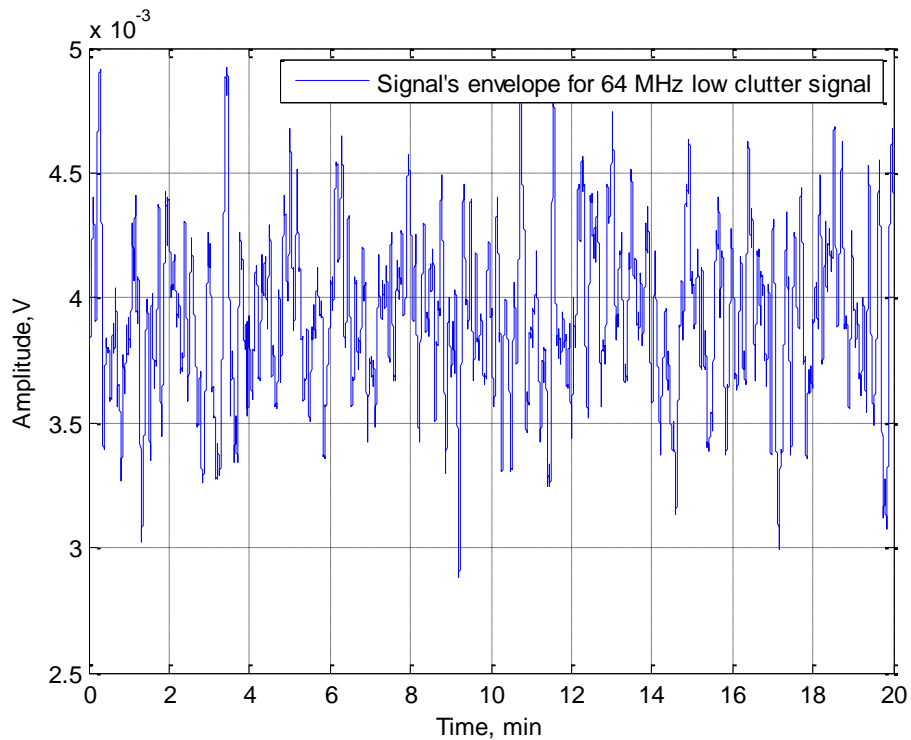


Figure 5.6: Clutter's envelope for 64 MHz low clutter

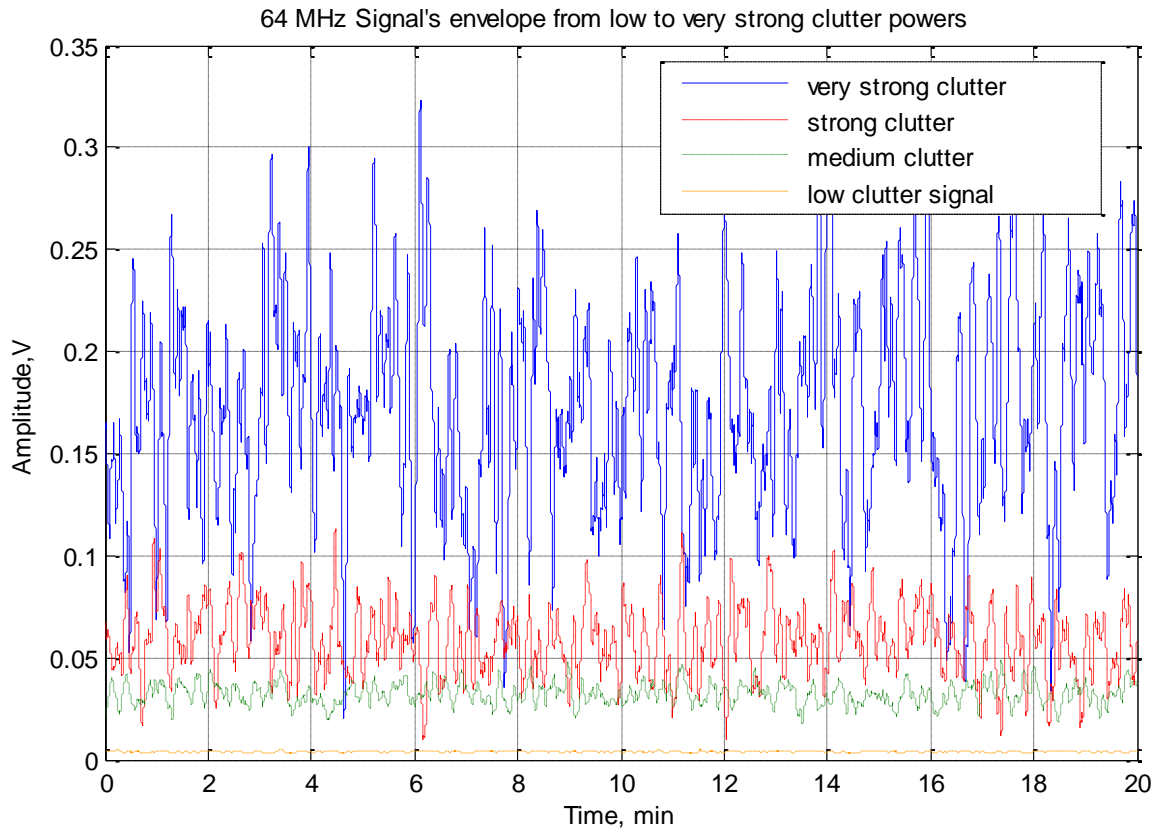


Figure 5.7: 64 MHz clutter's envelope varies from low to very strong clutter powers

Now the next step is to normalise the amplitude of the clutter to produce the non-stationary clutter. Example in Figure 5.8 displayed 64 MHz output clutter signal after normalisation process. From the figure we can see that the highest amplitude of low clutter is 0.0039 V and for very strong clutter at 0.2246 V.

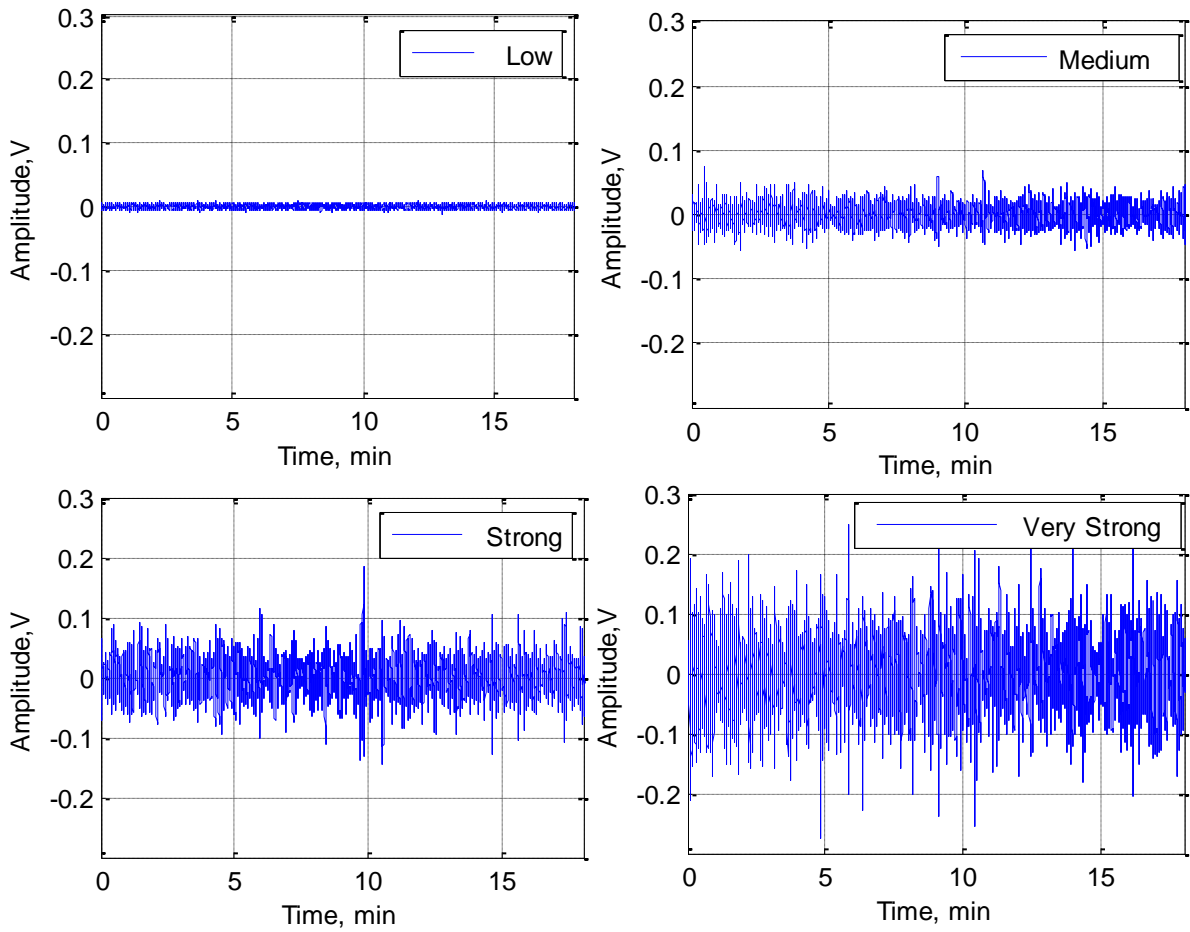


Figure 5.8: 64 MHz normalised non-stationary clutter varies from low to very strong clutter

5.2.3 Stage 3: Generating Gaussian Noise

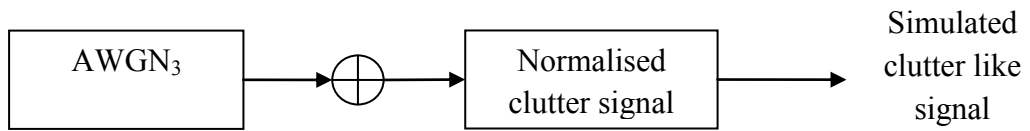


Figure 5.9: Added noise to simulated clutter

In this stage, a random AWGN signal will be added to the normalised non-stationary clutter. This is to generate the similar characteristic as the real measured clutter. The output from this

process is compared with the real measured clutter signal as intended with specific frequencies and clutter strengths. Figure 5.10 displayed the example of 64 MHz clutter for different strengths.

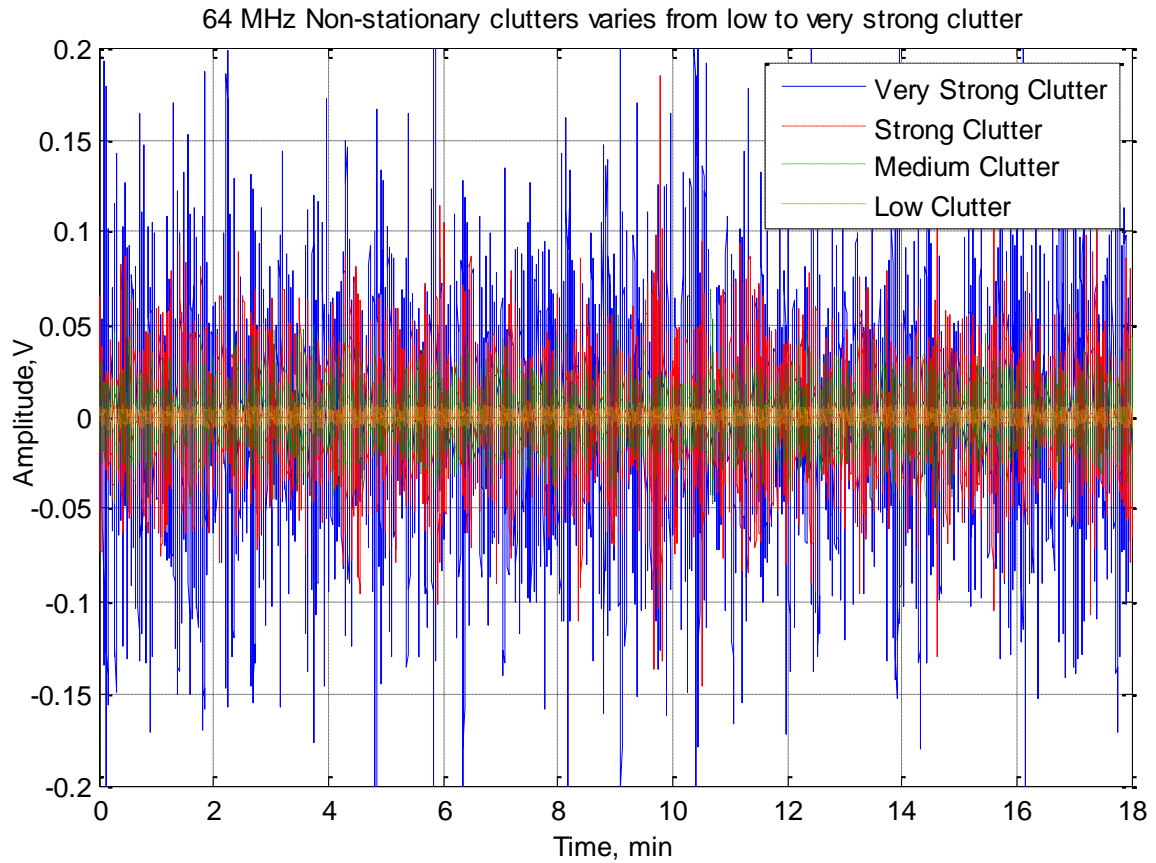


Figure 5.10: 64 MHz Non-stationary clutters varies from low to very strong clutter

5.3 Clutter Generation

Main part in clutter generation involved simulation process using Matlab program which is developed based on clutter generation model explained in previous Section 5.2. Step by step process on how to generate clutter-like signal are explained in detail in Appendix B and the full program can be found in Appendix A.

5.4 Modelled Clutter Parameter Estimation

Based on the estimated parameters from real measured clutter, simulated clutter signals are generated into four different clutter strengths. In this section, the overall results of all simulated non-stationary clutter for all frequencies and clutter levels will be displayed and discussed.

5.4.1 Simulated Low Clutter Strength

Low clutter strength is categories based on the lowest clutter power simulated from the measured parameters. Figure 5.11 shows the distribution of clutter power for four different frequencies ranging from 64 MHz to 434 MHz. It is clearly shown from the amplitude of the clutter, the clutter power increased proportionally with the increase of frequencies. The amplitude ranges from 0.002 V for 64 MHz to 0.18 V for 434 MHz. The overall simulation's result for low clutter strength can be summarised in Table 5.1. The process on how the values are taken are explained in detail in Appendix B.

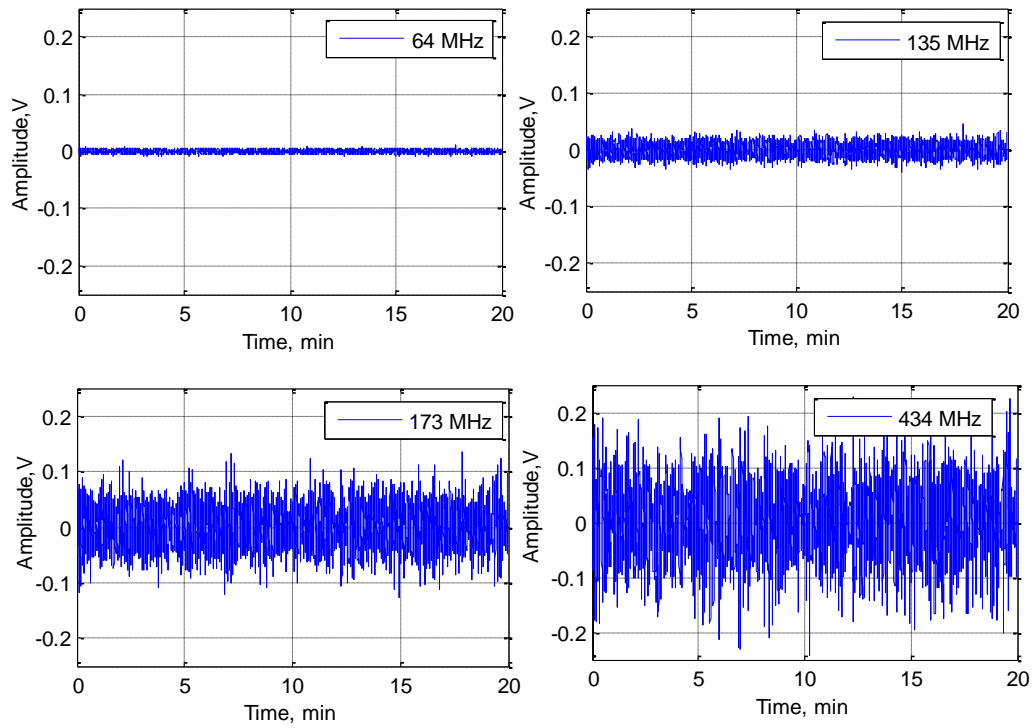


Figure 5.11: Simulated non-stationary low clutter power for all frequency channels

Table 5.1: Simulated low clutter strength for all frequencies

Frequency	Standard Deviation	Weibull Fit	Envelope		Dynamic Range (dB)
			Min	Max	
64 MHz	0.0023	2.00	0.0019	0.0043	3.55
135 MHz	0.0113	1.95	0.0080	0.0239	4.75
173 MHz	0.0334	1.84	0.0147	0.0764	7.16
434 MHz	0.0550	1.75	0.0156	0.1754	10.51

Table 5.1 stated all the parameters for simulated low clutter. The standard deviation, amplitude minimum and maximum values and the dynamic range of the clutter increased in values with the increment of frequencies. From the table, 64 MHz channel frequency

displayed the lowest value of all parameters except for the Weibull fit with the highest value of 2.00. The standard deviation value varies from 0.0023 for 64 MHz to 0.055 for 434 MHz.

The clutter envelopes displayed in Figure 5.12 replicates each other. The difference between 64 MHz maximum amplitude with 434 MHz maximum amplitude is about 0.17 V. If we compared between simulated and measured amplitude, the difference between the lowest amplitude and the highest maximum amplitude of measured clutter is just 0.12V which is 0.04 V differences from the simulated clutter. This shows that the characteristic for both simulated and measured more or less the same.

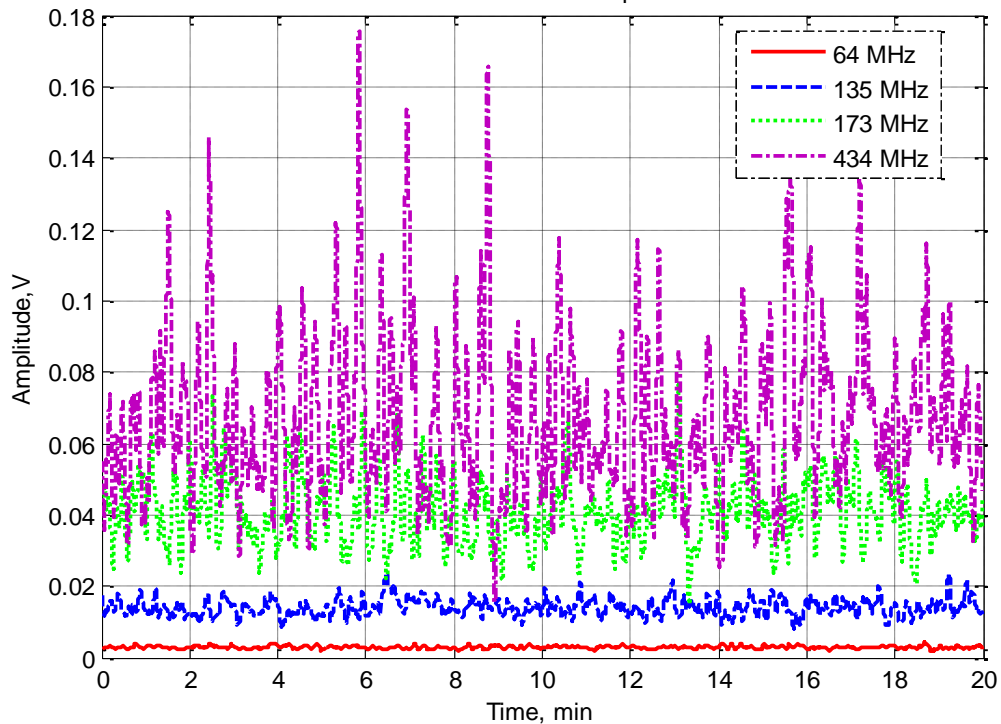


Figure 5.12: Clutter's envelope for all frequency channels

The PSD of low clutter envelopes shown in Figure 5.13 are in normalised and absolute value versions. Both graphs displayed the PSD trend of each frequency increased from 64 MHz to 434 MHz frequencies based on 0.1 Hz cut off frequency and the spectrum of the time- domain envelope of the clutter has a maximum frequency of 0.01 to 0.02 Hz similar. This trend is

replicated again in Figure 5.14 where this time the graph output exhibits the PSD of the clutter signals separately for each frequency and in Figure 5.15 (a) is the comparison for all frequency channels in one graph.

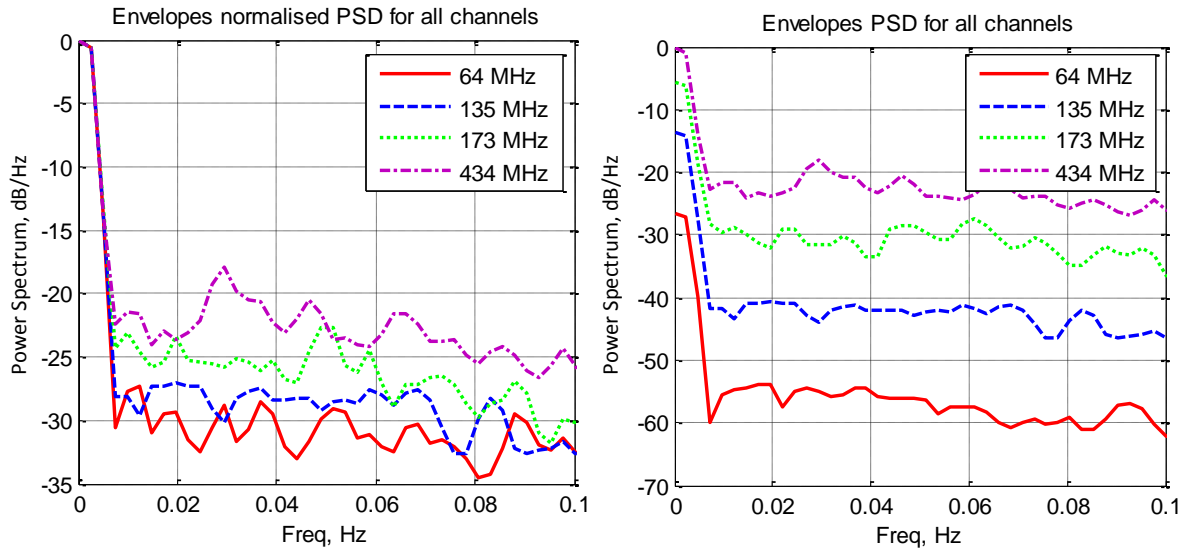


Figure 5.13: Normalised and absolute value clutter's envelope PSD for all frequency channels

If we looked into the power spectrum of the clutter signals in Figure 5.13 and Figure 5.14 (a), we can determine that the spectrum widths for the clutters are varied from 0.4 to 0.5 Hz. This is defined by 10 dB power drop for each channel. This satisfies with the measured low clutter where the values of the spectrum width are the same. The cumulative distribution for low clutter indicates that 64 MHz frequency channel reached the value of 1 at the amplitude of 0.01 V. Then followed by 135 MHz, 173 MHz and 434 MHz frequency channels with the amplitude of 0.03 V, 0.1 V and 0.21 V respectively. All these values are comparable with the low measured CDF with the amplitude range to reach the value 1 for less than 0.3 V.

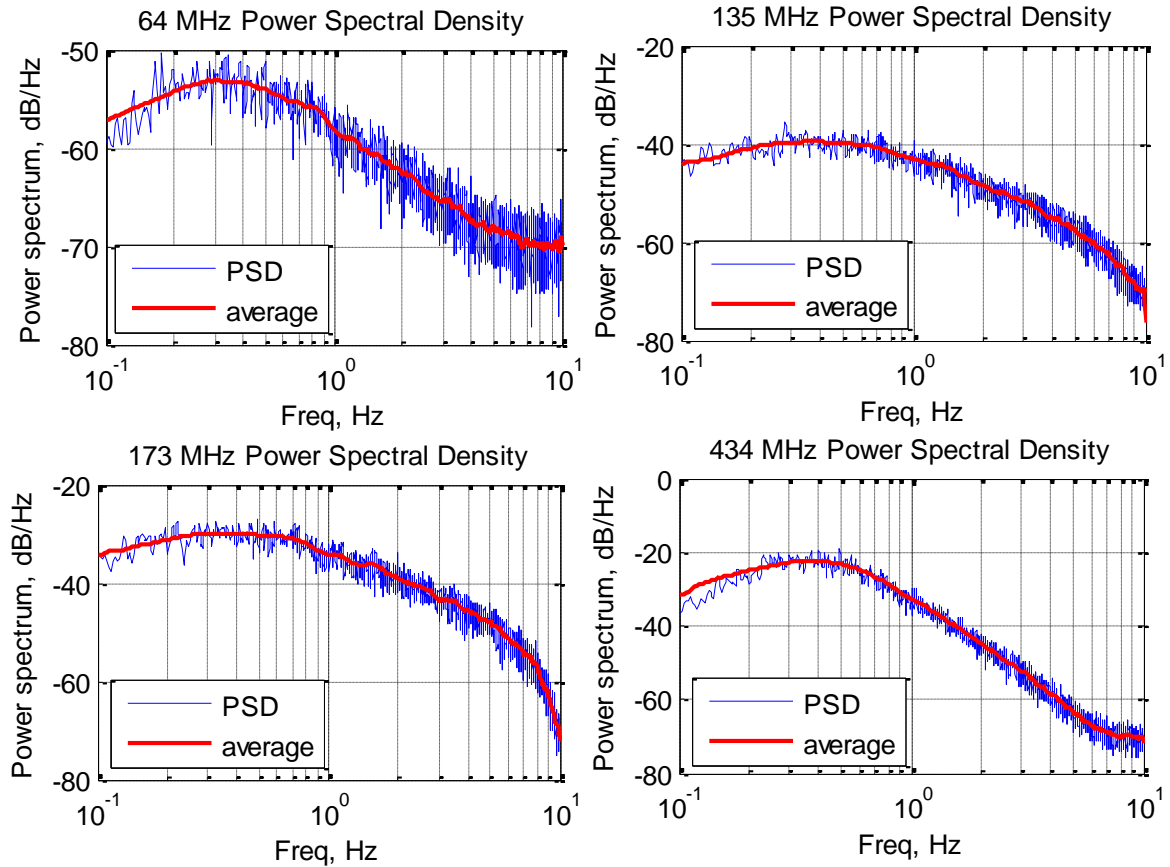


Figure 5.14: PSD for all frequency channels for low clutter.

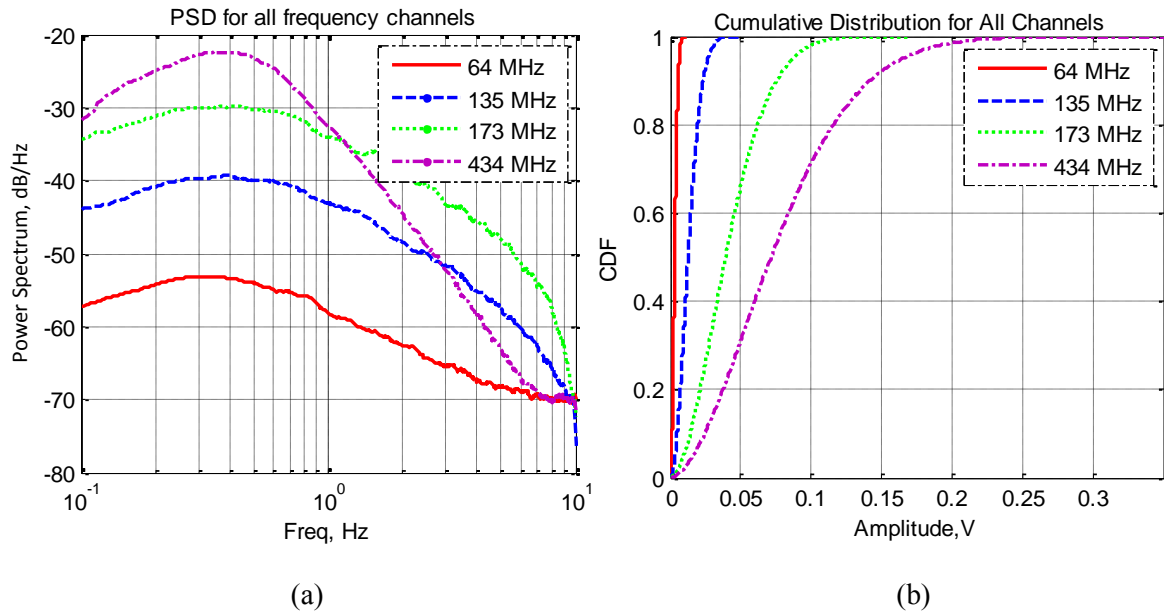


Figure 5.15: (a) PSD comparison for low clutter, (b) Cumulative distribution for all frequencies

Next characteristic is the power density function (PDF) of simulated low clutter as displayed in Figure 5.16. The PDF distributions shown in the figure consist of the histogram of the clutter and the PDF fit. All four different frequencies exhibit Weibull distribution with shape factor ranging from 2.00 for 64 MHz frequency channel and decreased with the increment of frequency to 1.75 for 434 MHz frequency channel. As predicted, the lower the wind, the lower will be the clutter strength and the distribution will become closer to Rayleigh distribution due to distributed thermal noise especially for lower frequency (64 MHz).

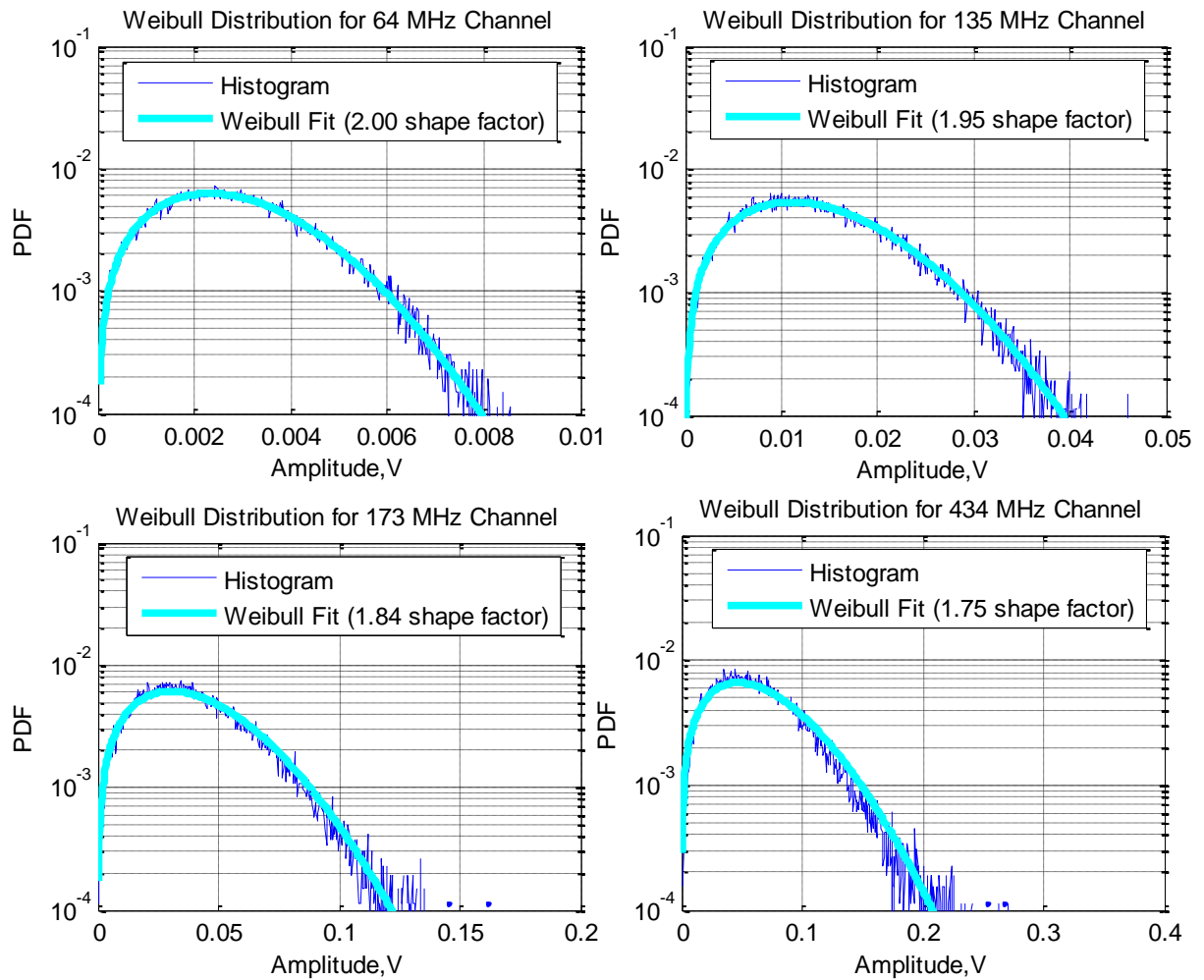


Figure 5.16: Weibull's distribution for all frequencies

5.4.2 Simulated Medium Clutter Strength

Medium clutter is considered as the value where the power lies in between low and strong clutter strengths. The graph shown in Figure 5.17 portrays the amplitude of medium clutter power for all carrier frequencies. All details about the clutter are written in Table 5.2. It can be seen in the table, the dynamic range of the clutter varies from 6.43 dB for 64 MHz to 13.11 dB for 434 MHz. While the standard deviations and the clutter amplitude also varies from low to high value proportional to the rises of the frequencies. For 64 MHz, the standard deviation is about 0.0187 whilst the amplitude varies from 0.0107 V to 0.0471 V. Furthermore, for 434 MHz the standard deviation is 0.45 and the amplitude varies from 0.07 V to 1.41 V. These can be seen clearly in Figure 5.18.

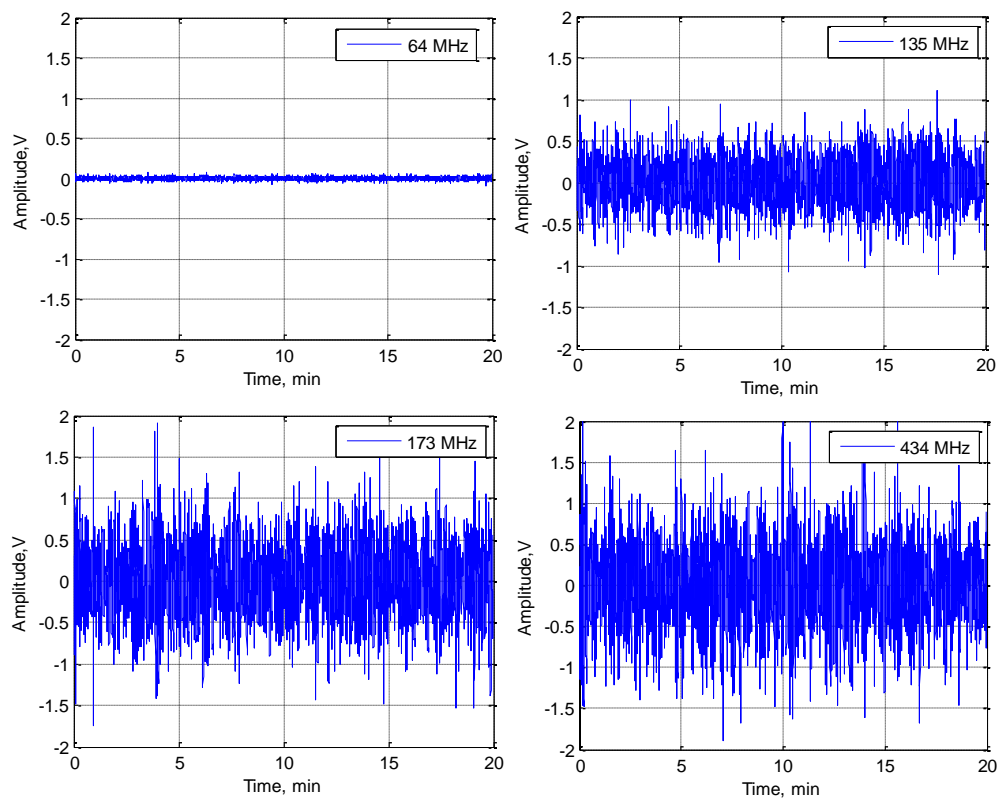


Figure 5.17: Simulated non-stationary medium clutter power for all frequency channels

Table 5.2: Simulated medium clutter strength for all frequencies

Frequency	Standard Deviation	Weibull Fit	Envelope		Dynamic Range (dB)
			Min	Max	
64 MHz	0.0187	1.96	0.0107	0.0471	6.43
135 MHz	0.2577	1.87	0.1045	0.6913	8.20
173 MHz	0.3929	1.76	0.1138	1.1509	10.05
434 MHz	0.4487	1.66	0.0691	1.4127	13.11

If we looked into the value for the Weibull fit, it still follows the trend where the value of the fit decreased when the frequency is increased. For medium clutter strength, the Weibull fit varies from 1.96 for 64 MHz to 1.66 for 434 MHz.

Figure 5.18 displayed the amplitude of the clutter's envelope for different frequencies. Even though the clutters look like overlapping each other but the minimum and the maximum values are still projected the trend of the clutter characteristic, which the lowest frequency 64 MHz gave the lowest minimum and maximum values followed by 135 MHz, 173 MHz and 434 MHz.

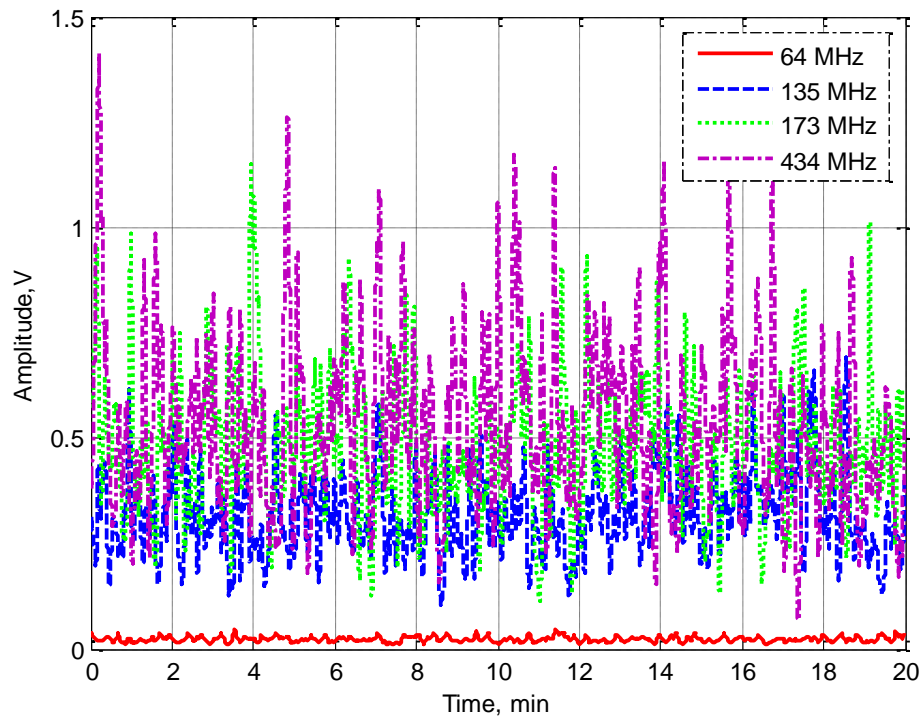


Figure 5.18: Simulated medium clutter's envelope for all frequency channels

The envelope PSD shown in Figure 5.19 for normalised and absolute value for all frequencies indicates the slopes drop approximately between 0.005 to 0.02 and still correspond to 50 to 200 seconds of relative power homogeneity.

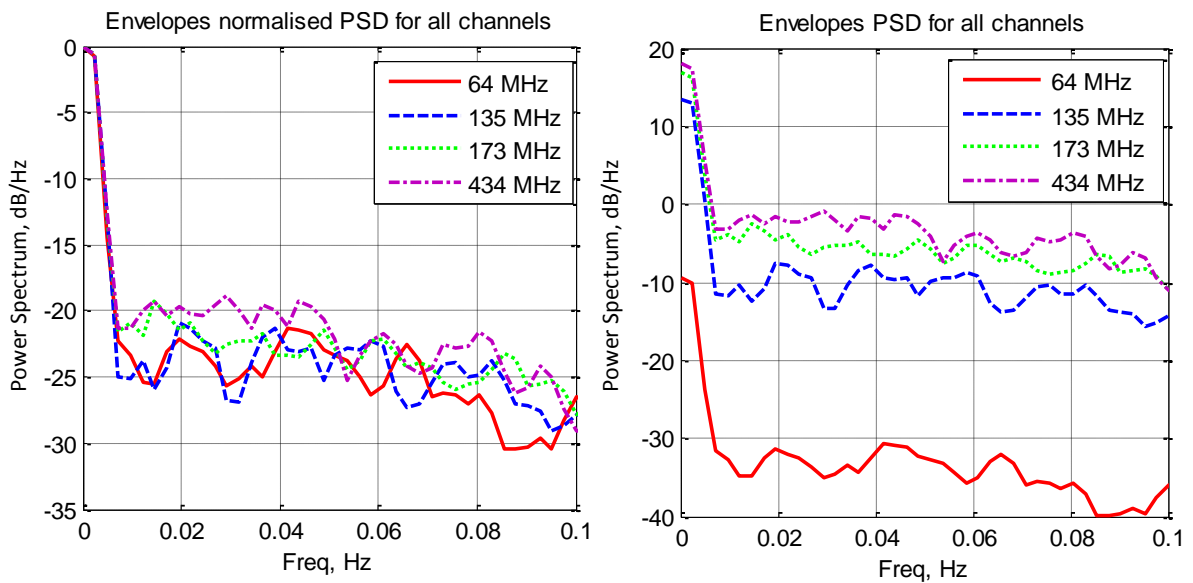


Figure 5.19: Normalised and absolute clutter's envelope PSD for all frequency channels

Next are Figure 5.20 and Figure 5.21 (a) shows the PSD of the clutter for each frequency channels. It can be seen that the clutter's spectrum is independent from the carrier frequencies with a decay of approximately 40 dB per decade and the spectrum width which defined by 10 dB power drop is approximately 0.4 to 0.5 Hz. The cumulative distribution shows in Figure 5.21 (b) displayed the distribution of medium clutter for all channel frequencies.

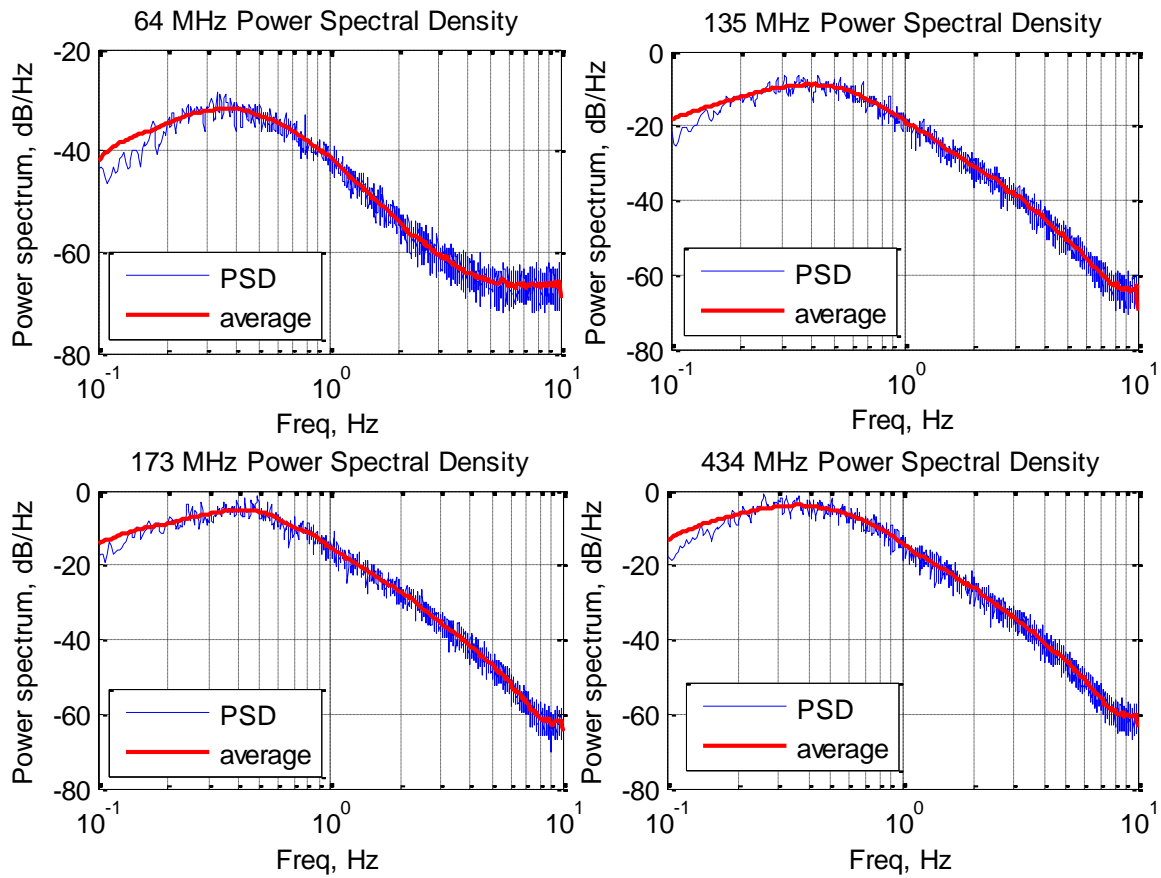


Figure 5.20: PSD for all frequency channels for medium clutter.

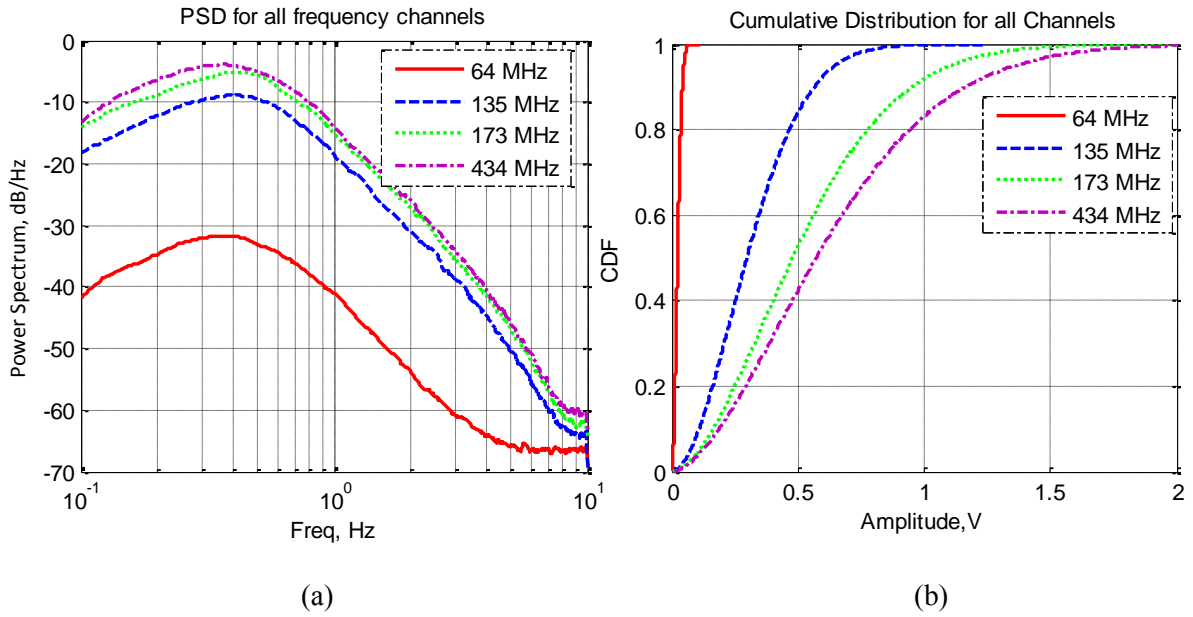


Figure 5.21: (a) PSD comparison for medium clutter, (b) Cumulative distribution for all frequencies

Clutter amplitude distribution for medium clutter strength shown in Figure 5.22 is not much different from low clutter strength. The Weibull fit shape factor for each frequency drop a little bit but still with the same trend as before. The lowest frequency of 64 MHz with 1.96 shape factor and the highest frequency of 434 MHz with the lowest value shape factor of 1.66.

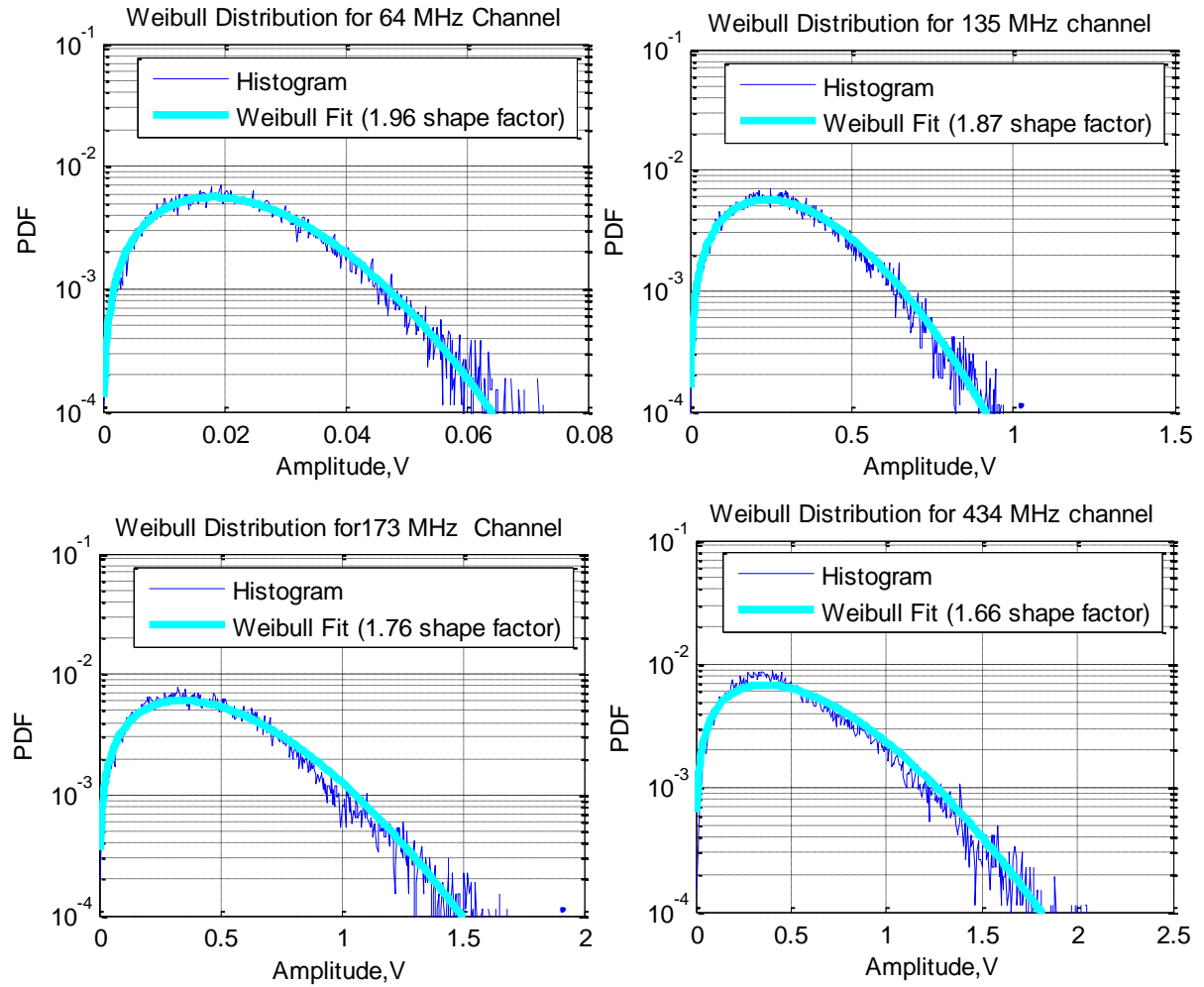


Figure 5.22: Weibull's distribution for all frequencies

5.4.3 Simulated Strong Clutter Strength

In Figure 5.23 is the simulated non-stationary strong clutter strength generated for 20 minutes. The distribution of the clutter signal for each frequency can be summarized into Table 5.3 where it shown the value for standard deviation (STD), Weibull shape factor, envelope's minimum and maximum values, and the dynamic range of the clutter signal.

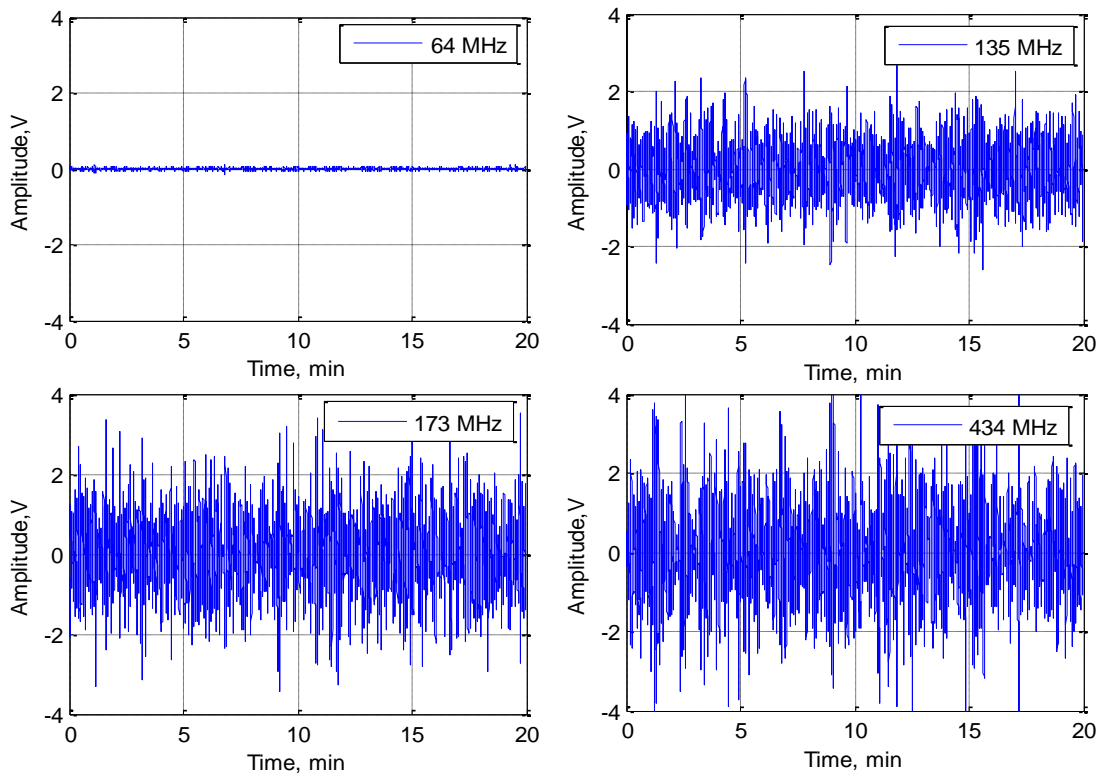
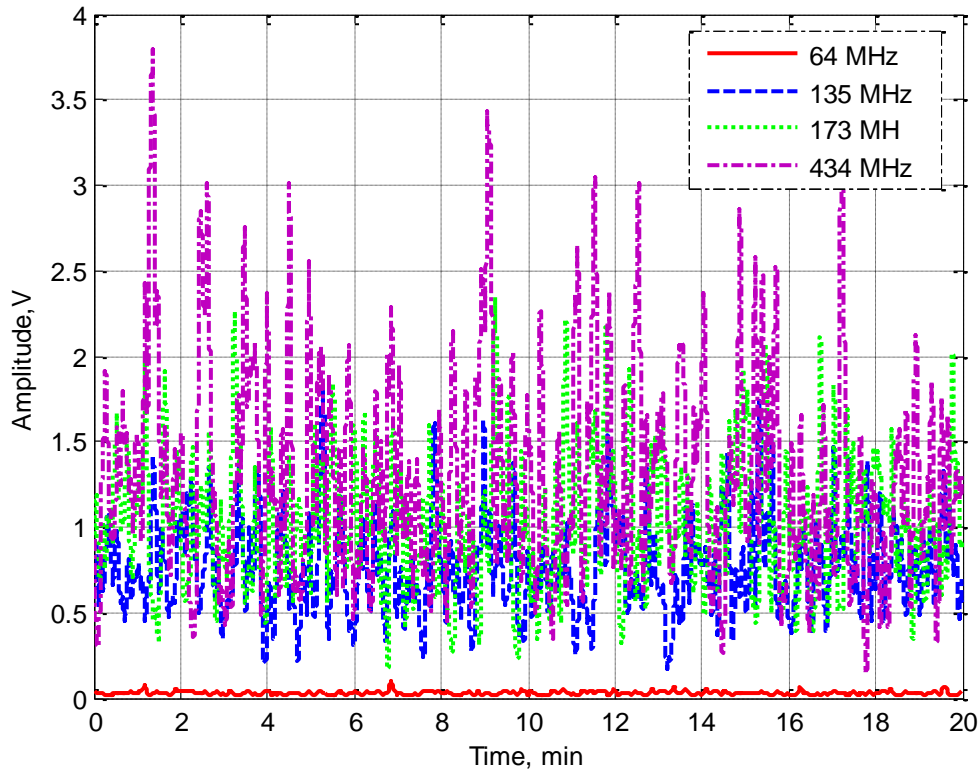


Figure 5.23: Simulated non-stationary strong clutter power for all frequency channels

It stated in the table clearly that the amplitude of the clutter envelopes increased when the frequency increase. The amplitude varies from 0.012 V to 0.10 V for 64 MHz, 0.17 V to 1.83 V for 135 MHz, 0.17 V to 2.35 V for 173 MHz and 0.14 V to 3.80 V for 434 MHz. The amplitude of the envelopes is visibly displayed in Figure 5.24. The standard deviation for strong clutter strength varies from 0.025 to 1.1. This value is increased slightly about 0.006 for 64 MHz and about 0.65 for 434 MHz. This increment is already predicted as the frequency increased and the clutter strength increased from low to very strong clutter, the value of standard deviation and the amplitude of the clutter signal will also increase. The raised of the amplitude are written in the form of dynamic range value which ranging from 9.12 dB for lower frequency (64 MHz) and 14.22 dB for higher frequency (434 MHz). This can be seen in Figure 5.24 for better view.

Table 5.3: Simulated strong clutter strength for all frequencies

Frequency	Standard Deviation	Weibull Fit	Envelope		Dynamic Range (dB)
			Min	Max	
64 MHz	0.0245	1.81	0.0118	0.0964	9.12
135 MHz	0.6273	1.75	0.1667	1.8279	10.40
173 MHz	0.8472	1.68	0.1701	2.3507	11.40
434 MHz	1.1008	1.60	0.1437	3.7959	14.22

**Figure 5.24: Simulated strong clutter's envelope for all frequency channels**

If we looked into the envelope's PSD for strong clutter signal in Figure 5.25 it still indicates similar drop between 0.005 to 0.02 Hz. It shows that the spectrum of clutter does not depend on the wind which is the main influence of the clutter strength. No matter how strong the wind and the clutter strength, the spectrum will always be within the same range.

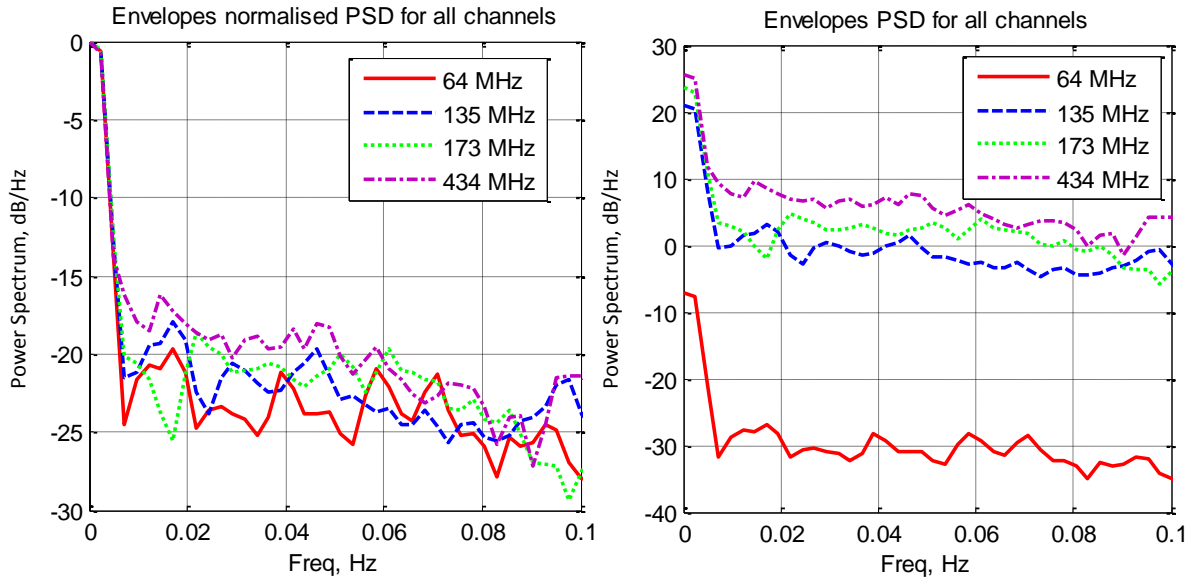


Figure 5.25: Normalised clutter's envelope PSD for all frequency channels

Figure 5.26 (a) and Figure 5.27 shows the PSD of the clutter signal in one graph and separately for all frequencies respectively. It clearly demonstrates that the PSD slopes corresponds to 0.3 to 0.5 Hz for 10 dB power drop. This shows that it is invariant of carrier frequencies and the clutter strengths. While for cumulative distribution for this clutter strength are shown in Figure 5.27 (b).

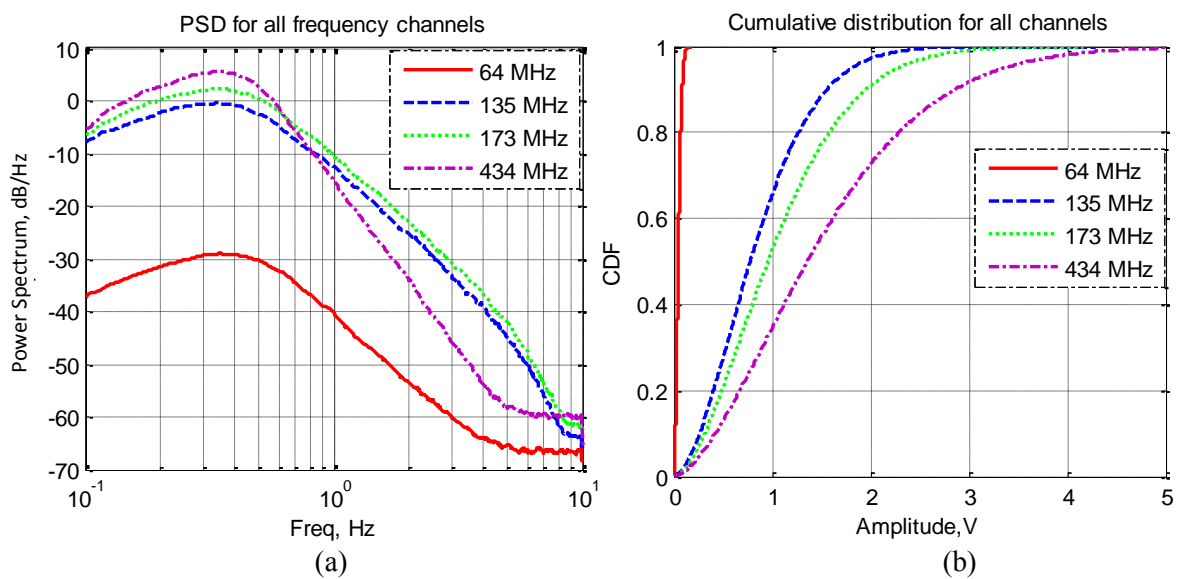


Figure 5.26: (a) PSD comparison for strong clutter, (b) Cumulative distribution for all frequencies

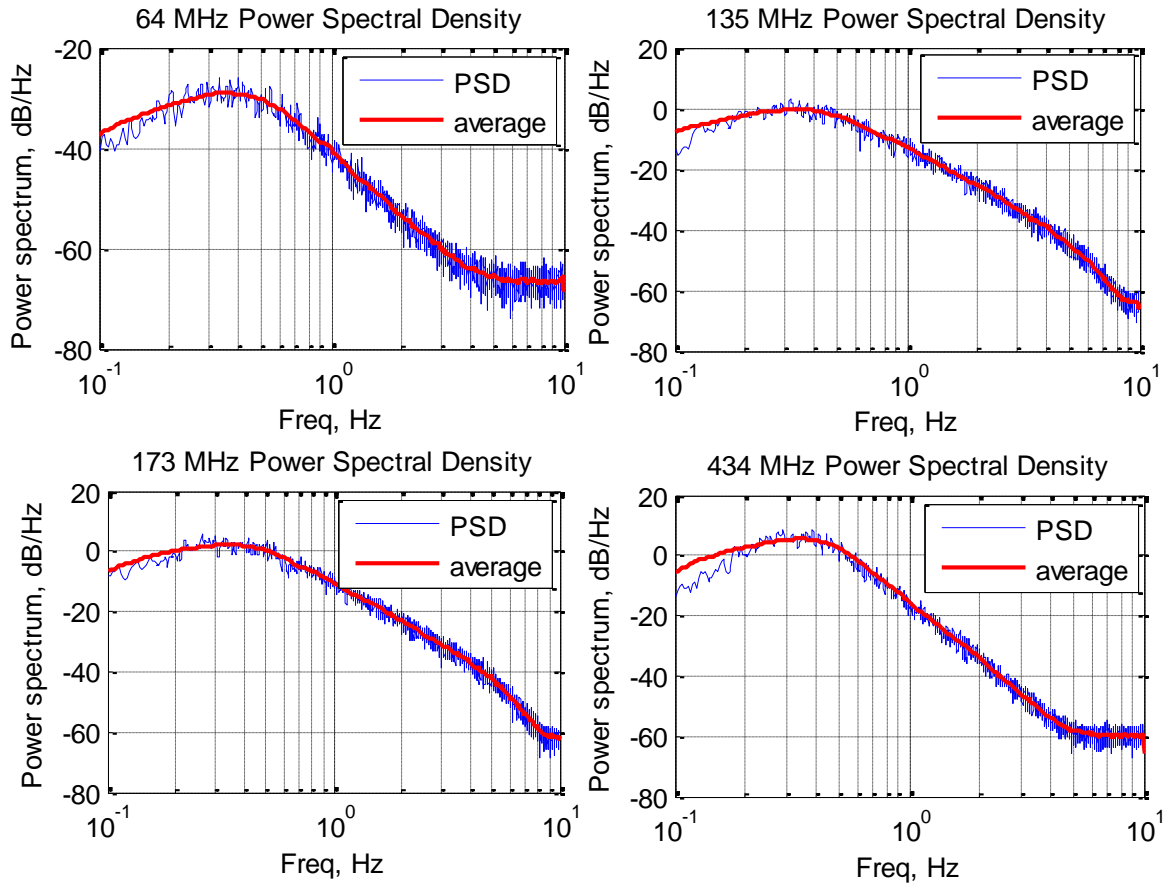


Figure 5.27: PSD for all frequency channels for strong clutter.

By comparison with the different carrier frequencies, clutter amplitude distribution for strong clutter strength still close to Weibull distribution as shown in Figure 5.28. The shape factor varies from 1.81 for 64 MHz to 1.60 for 434 MHz. The lower the wind the closer it will be to Rayleigh distribution and vice versa.

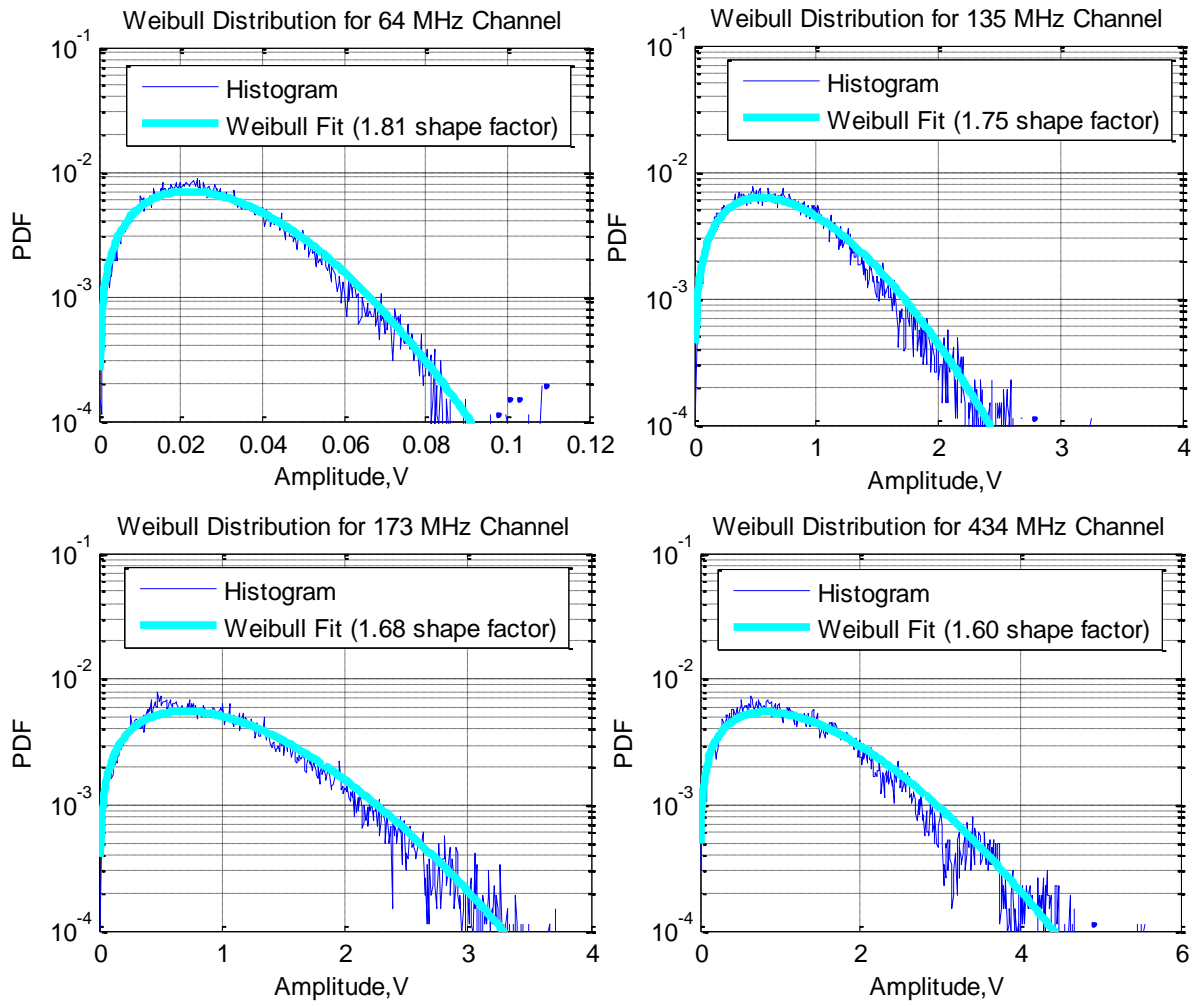


Figure 5.28: Weibull's distribution for all frequencies

5.4.4 Simulated Very Strong Clutter Strength

Very strong clutter power strength normally due to high wind speed (gale). In our measured experiment, only a few data consists a very strong clutter power signal. All important parameters in the data are recorded and used in this simulated clutter analysis to generate similar clutter signal with the same characteristic as very strong clutter strength. In Figure 5.29, very strong clutter power signal generated for 20 minutes is shown for different carrier frequencies.

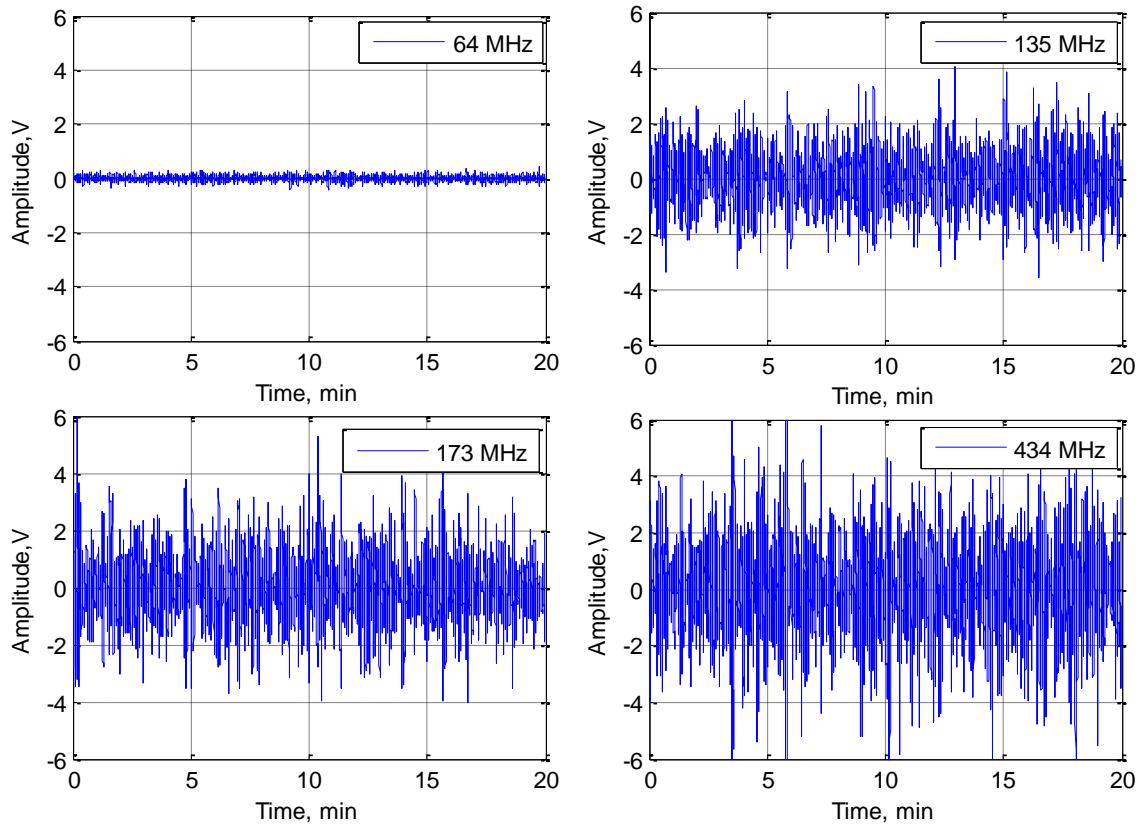


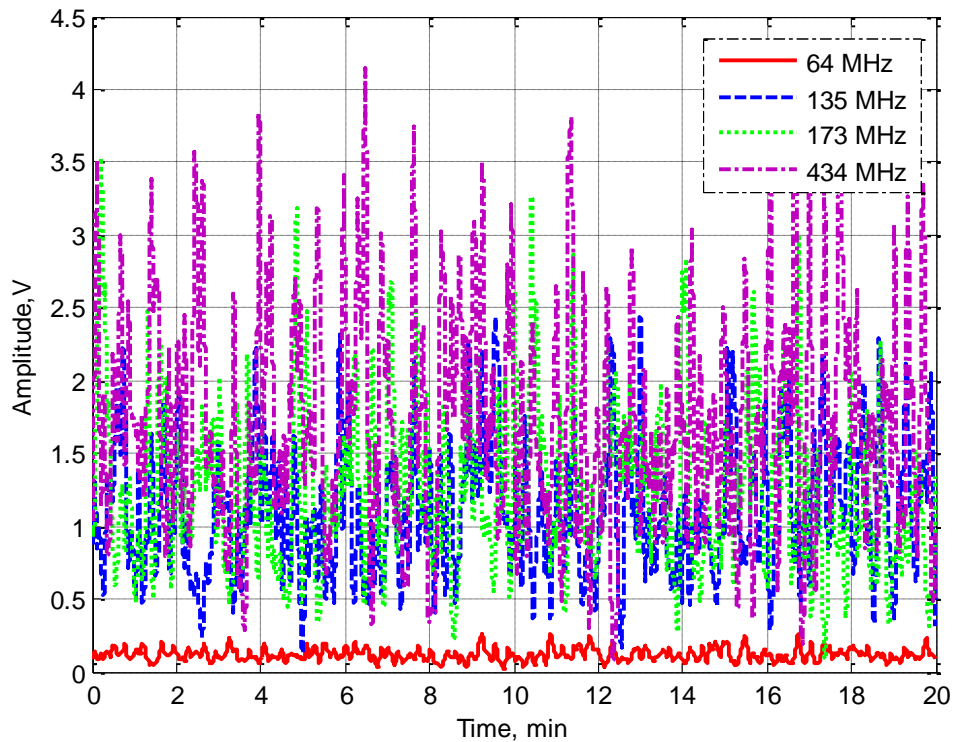
Figure 5.29: Simulated non-stationary very strong clutter power for all frequency channels

Table 5.4 displayed all the characteristics of the clutter signal for 64 MHz to 434 MHz carrier frequencies. Again it shows the increment of the value of standard deviation, envelope's minimum and maximum values and the dynamic range of the clutter signal except for the Weibull shape factor which is decreased as predicted when the frequency is increased. It can be summarized that when the operating frequency varies from 64 MHz to 434 MHz, the value of standard deviation varies from 0.10 to 1.45, the amplitude of the envelope varies from 0.03 V to 4.14 V, the dynamic range varies from 10.09 to 17.60 and the Weibull shape factor (fit) decreased from 1.77 to 1.57.

Table 5.4: Simulated very strong clutter strength for all frequencies

Frequency	Standard Deviation	Weibull Fit	Envelope		Dynamic Range (dB)
			Min	Max	
64 MHz	0.0967	1.77	0.0259	0.2643	10.09
135 MHz	0.9131	1.67	0.1260	2.4431	12.88
173 MHz	1.0638	1.61	0.0898	3.5329	15.95
434 MHz	1.4475	1.57	0.0720	4.1419	17.60

Figure 5.30 shows the amplitude distribution of the clutter envelopes for all frequencies. The lowest amplitude (red) is always the lowest frequency (64 MHz) and the highest amplitude is always from the highest frequency of 434 MHz in purple colour line.

**Figure 5.30: Very strong clutter's envelope for all frequency channels**

Envelope PSD for very strong clutter strength does not have much different with other clutter strength as explain before. The spectrum dropped still within the range of 0.005 to 0.02 Hz shown in Figure 5.31. Same goes for the clutter signal PSD in Figure 5.32 and Figure 5.33 (a).

The spectrum width for 10 dB power drops is varies from 0.3 to 0.5 Hz and the differences between each frequency are approximately 2 to 3 dB except for 64 MHz where the difference with 135 MHz frequency is about 20 dB. As stated before, at low frequency the clutter power is mainly from the thermal noise which contributes very low clutter power. As for the cumulative distribution, it is shown in Figure 5.33 (b).

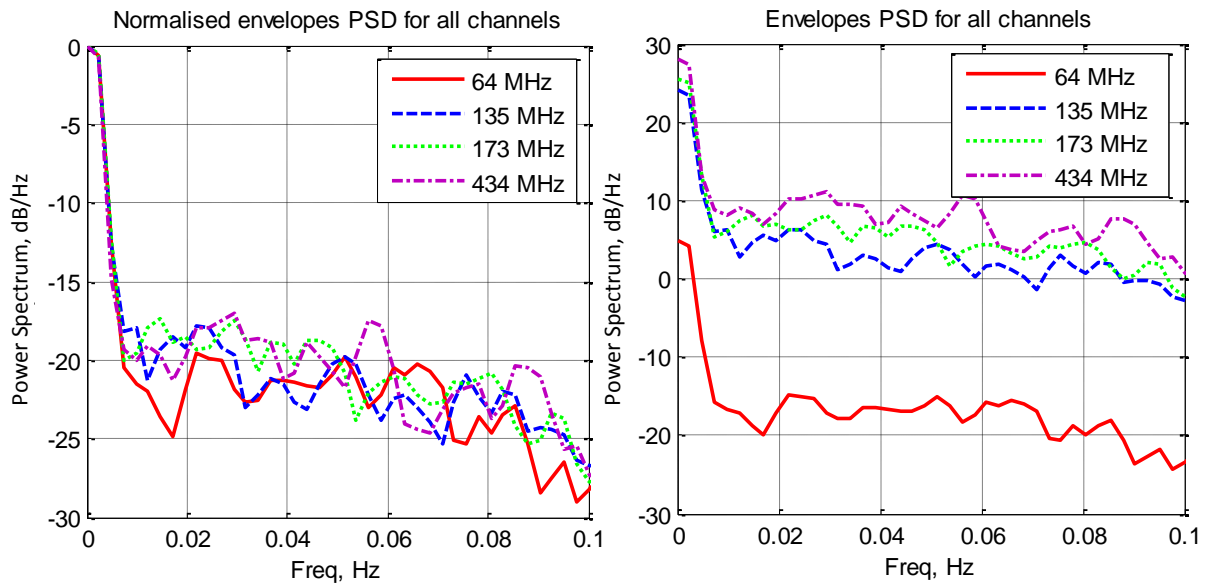


Figure 5.31: Normalised clutter's envelope PSD for all frequency channels

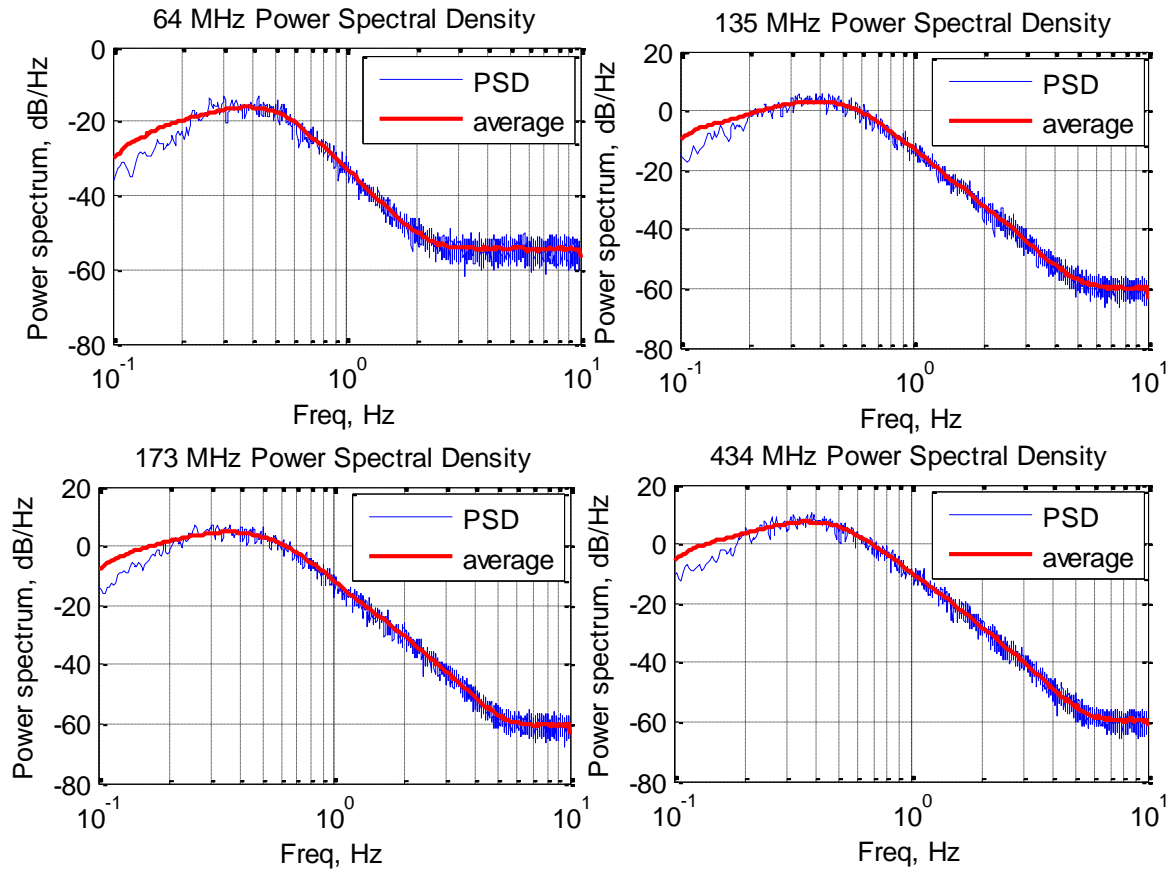


Figure 5.32: PSD for all frequency channels for very strong clutter.

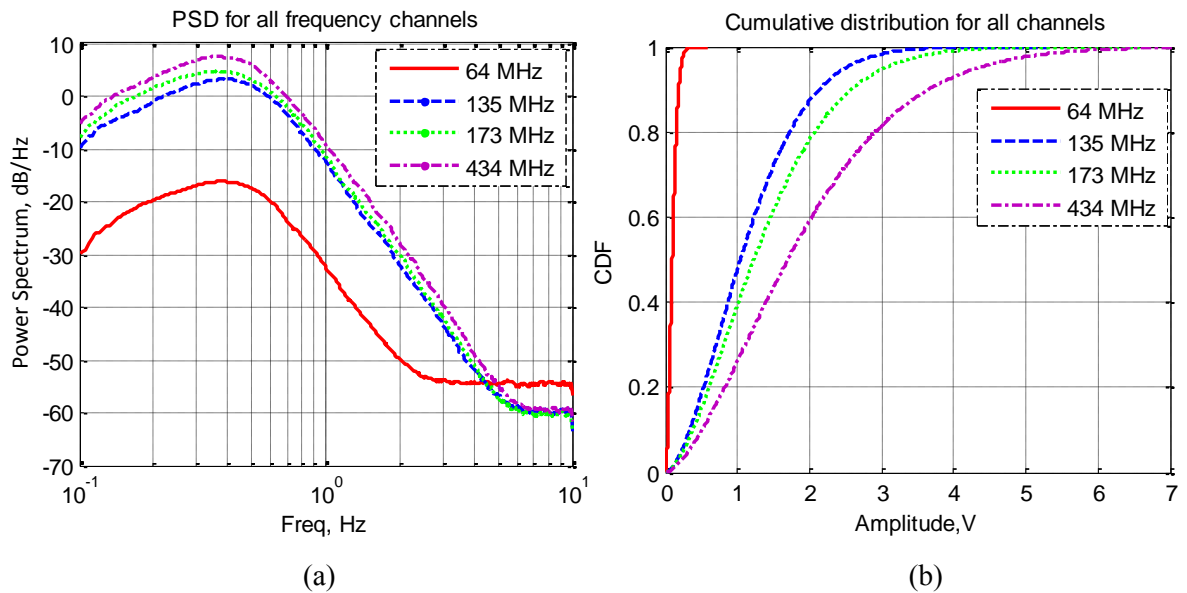


Figure 5.33: (a) PSD comparison for very strong clutter, (b) Cumulative distribution for all frequencies

Figure 5.34 shows the distribution of the clutter signal. For very strong clutter strength the shape factor is 1.77, 1.67, 1.61 and 1.57 for each frequency from 64 MHz to 434 MHz respectively. This value is much lower than the value in lower clutter strengths.

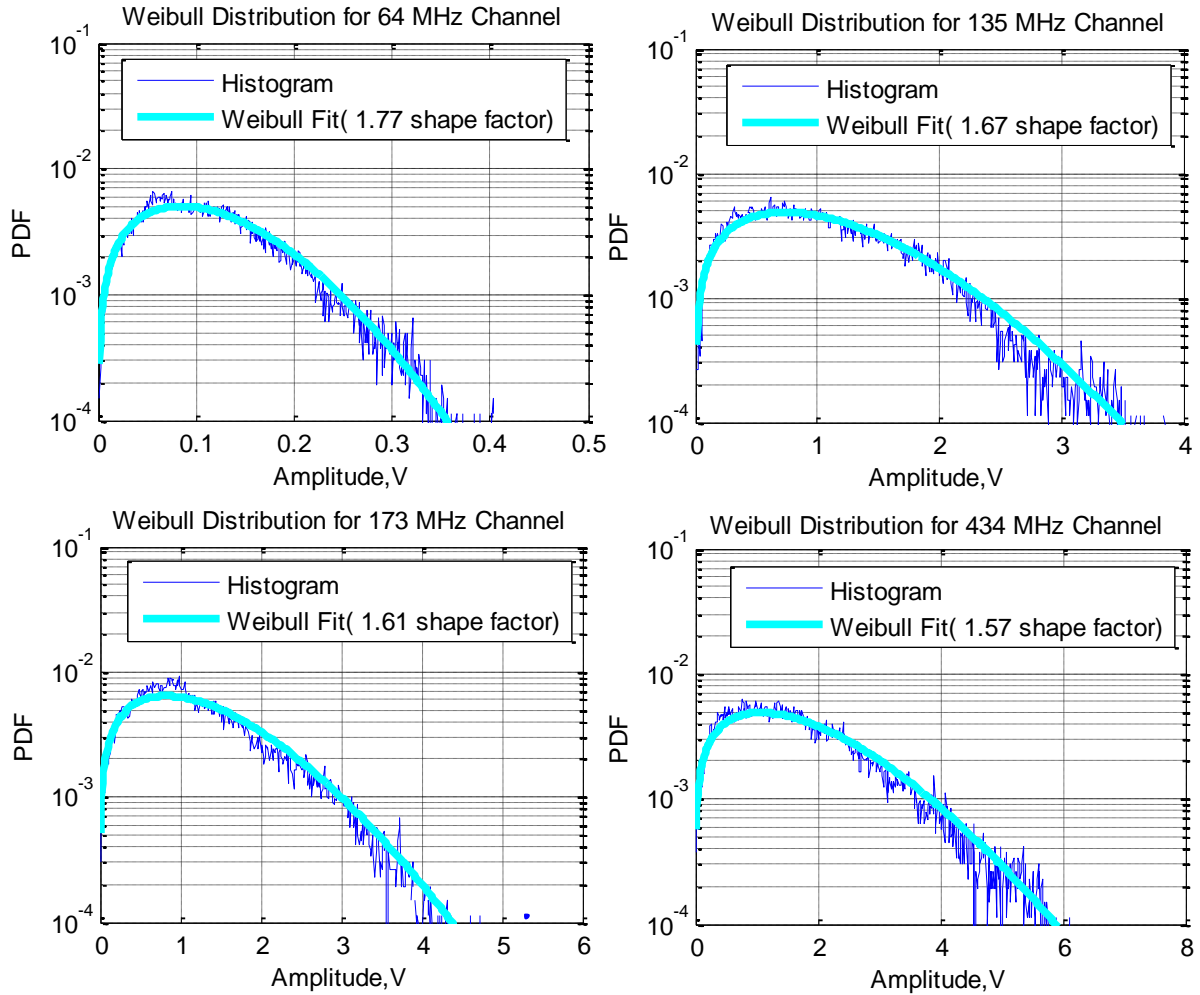


Figure 5.34: Weibull's distribution for all frequencies

5.5 Comparison of The Empirical Model and The Recorded Clutter

In this stage, measured clutter and simulated clutter are compared. This is to make sure that the generated clutter signals approximately the same as measured clutter signals. These can be shown in the next sections on which the comparisons are divided into two parts. The first part is the comparison of simulated clutter versus measured clutter for different clutter strengths

form low to very strong clutter. The second part is the comparison of simulated and measured clutter for different carrier frequencies from 64 MHz to 434 MHz.

5.5.1 Simulated Versus Measured Clutter for Different Clutter Strengths

As described before, clutter is divided into four different strengths from low, medium, strong to very strong clutter strength. In this analysis, the received data from the experiments are analysed and divided into these different clutter strengths. All the characteristics are estimated and written in Table 5.1. Then these parameters are used to generate clutter-like signal and the results are described in Section 5.4.1 to Section 5.4.4. Furthermore the results are then summarized in Table 5.6. In this table all the characteristics of simulated clutter signals are described for low to very strong clutter strength. The parameters include clutter standard deviation (STD) values, envelope's minimum and maximum values and the Weibull shape factor (fit) for all carrier frequencies.

If we compared between simulated and measured parameters, the differences between each value are very small. Bear in mind, the simulated clutter signal is based on the random generated signal. So the exact clutter signal similar to measured signal cannot be generated.

Table 5.5: Simulated clutter parameters for different clutter strengths

Freq (MHz)	Low Clutter				Medium Clutter				Strong Clutter				Very Strong Clutter			
	STD	Envelope		Weibull Fit	STD	Envelope		Weibull Fit	STD	Envelope		Weibull Fit	STD	Envelope		Weibull Fit
		Min	Max			Min	Max			Min	Max			Min	Max	
64	0.0023	0.0019	0.0043	2.00	0.0187	0.0107	0.0471	1.96	0.0245	0.0118	0.0964	1.81	0.0967	0.0259	0.2643	1.77
135	0.0113	0.0080	0.0239	1.95	0.2577	0.1045	0.6913	1.87	0.6273	0.1667	1.8279	1.75	0.9131	0.1260	2.4431	1.67
173	0.0334	0.0147	0.0764	1.84	0.3929	0.1138	1.1509	1.76	0.8472	0.1701	2.3507	1.68	1.0638	0.0898	3.5329	1.61
434	0.0550	0.0156	0.1754	1.75	0.4487	0.0691	1.4127	1.66	1.1008	0.1437	3.7959	1.60	1.4475	0.0720	4.1419	1.57

Figure 5.35 shows the clutter envelopes for both simulated and measured 64 MHz frequency for 20 minutes measurement time. It can be seen clearly that the range of amplitude is approximately the same for low, medium and strong clutter strength except for very strong clutter strength, where the distribution of simulated clutter amplitude is slightly increased to a value around 0.03 V to 0.26 V for the whole 20 minutes. While for measured clutter the maximum amplitude for very strong clutter only reached 0.1 V starting from the last 10 minutes. This is based on real measured data where the amplitude of the clutter can be unpredictable due to wind conditions.

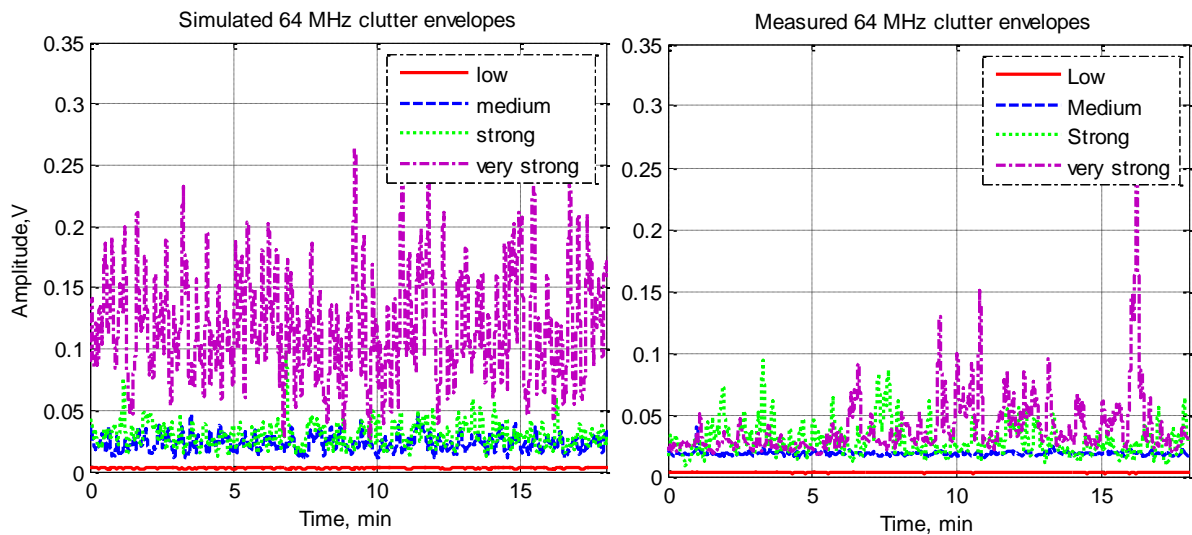


Figure 5.35: 64 MHz simulated and measured clutter envelopes

Next will be envelope's amplitude distribution for 135 MHz, 173 MHz and 434 MHz carrier frequency as shown in Figure 5.36, Figure 5.37 and Figure 5.38 respectively. From all the figures, it can be summarised that the envelopes exhibit approximately similar trend for all measured and simulated clutter strengths.

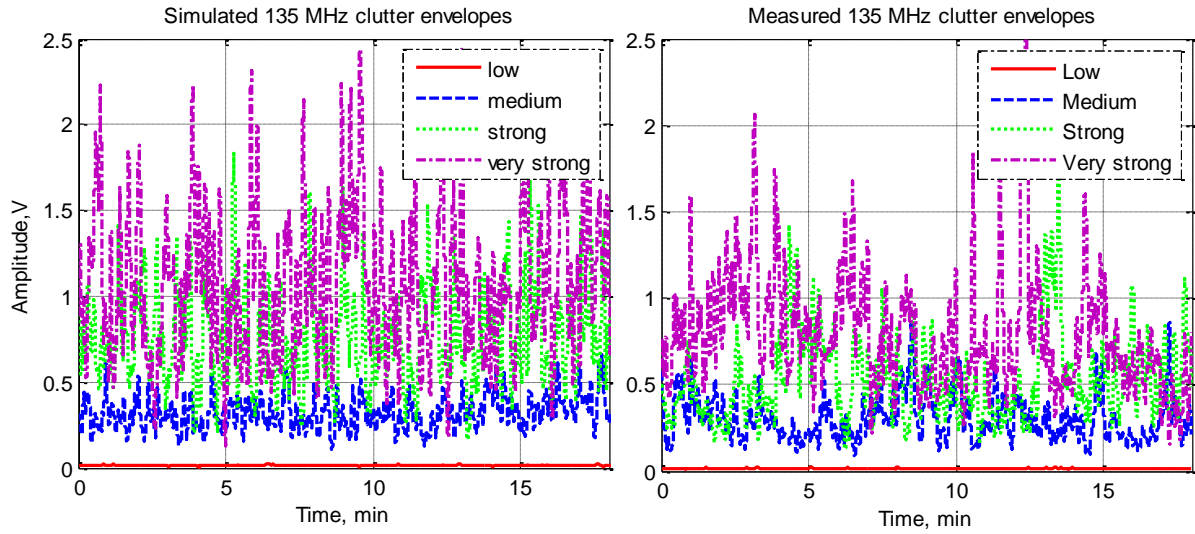


Figure 5.36: 135 MHz simulated and measured clutter envelopes

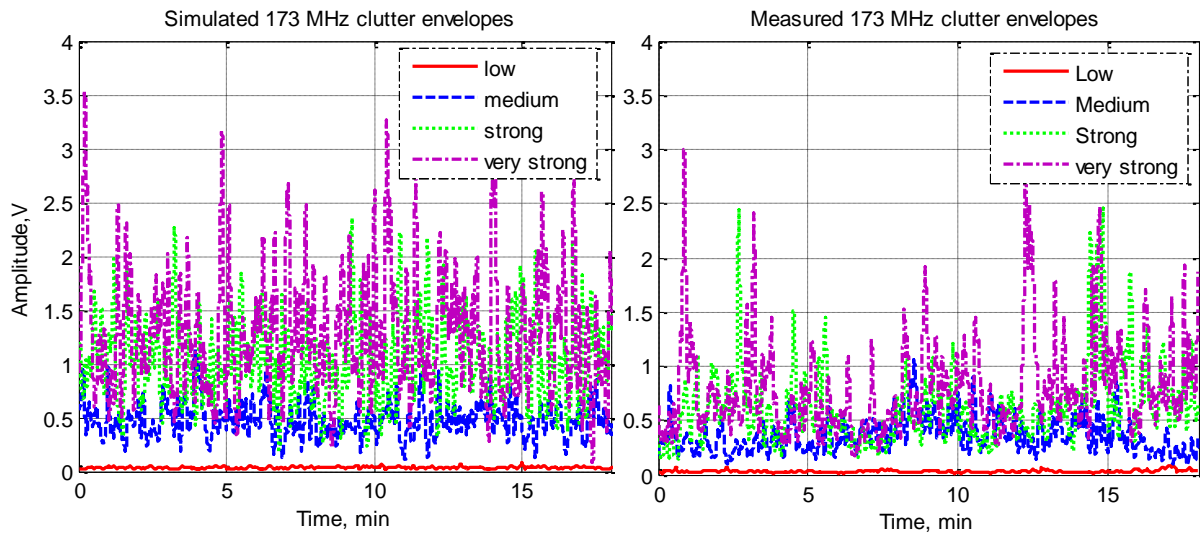


Figure 5.37: 173 MHz simulated and measured clutter envelopes

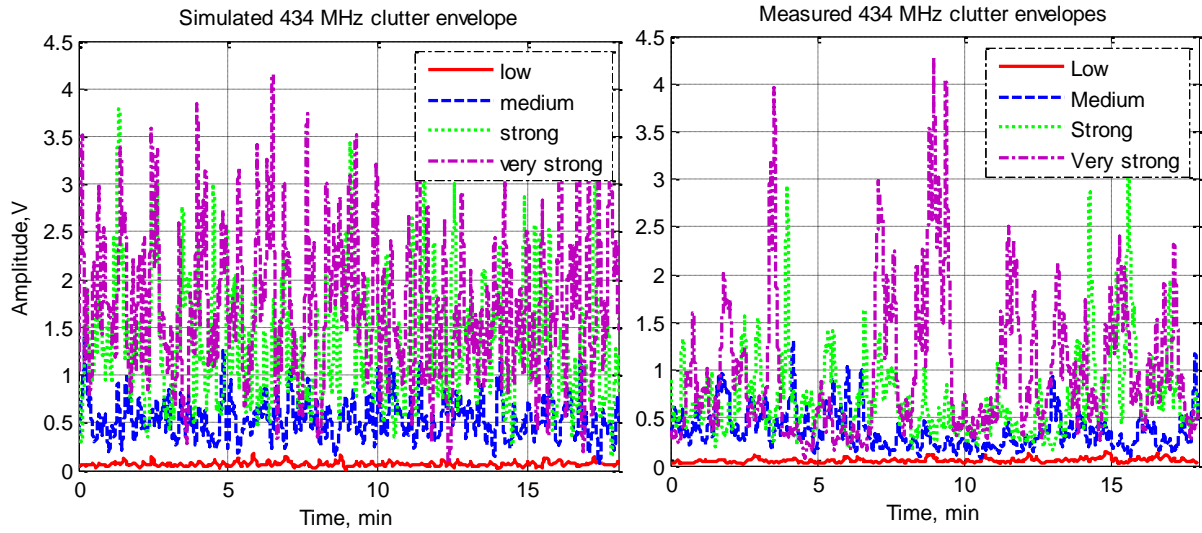


Figure 5.38: 434 MHz simulated and measured clutter envelopes

The clutter power spectral density shows in Figure 5.39 to Figure 5.42 are the normalised power spectral density for simulated and measured clutter's envelope for each frequency for different clutter conditions. The trends of the envelope PSD are approximately the same for both simulated and measured graphs. It can be seen in the graphs below for 64 MHz, 135 MHz, 173 MHz and 434 MHz carrier frequencies.

The spectrum of the clutter envelopes seen in Figure 5.39 for 64 MHz carrier frequency is about 0.01 to 0.02 Hz for all clutter strengths. This characteristic also resembles to other channels frequencies. This corresponds to 50 - 100 seconds of relative power homogeneity.

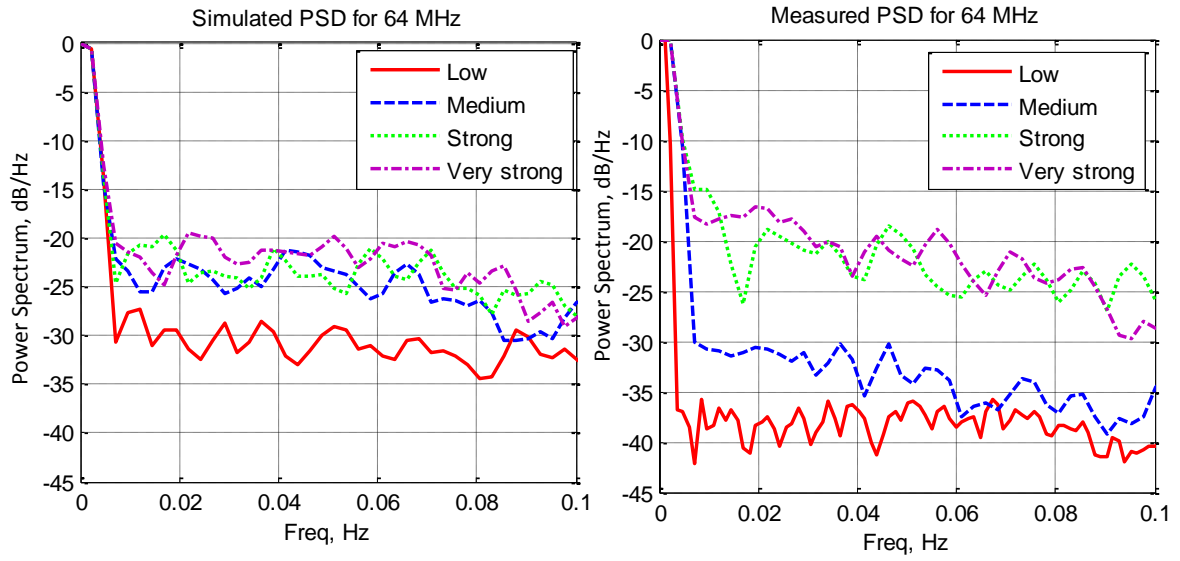


Figure 5.39: Simulated and measured clutter PSD for 64 MHz

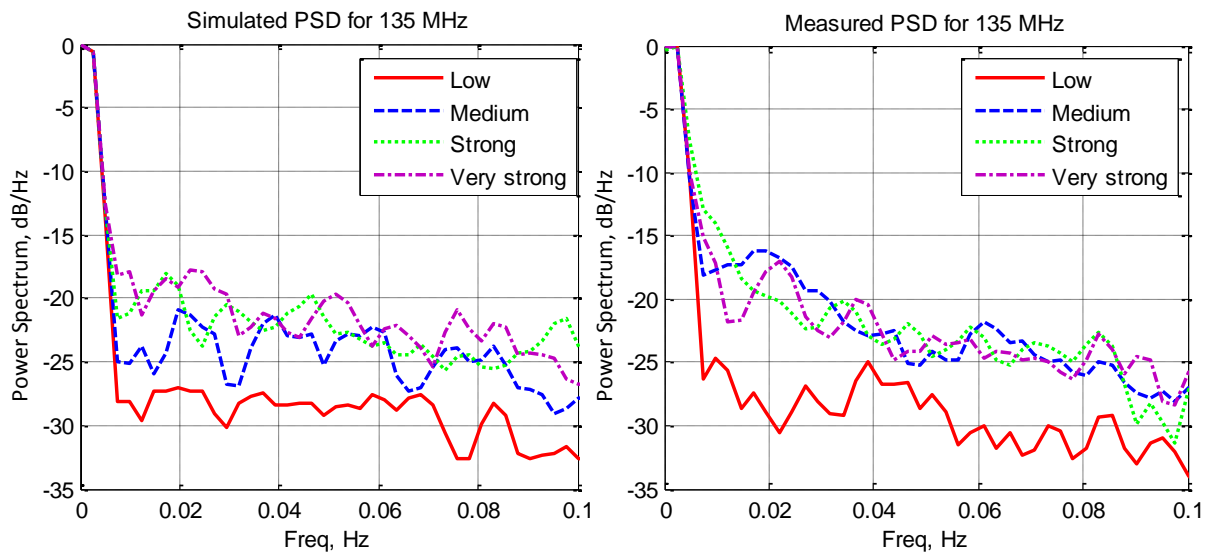


Figure 5.40: Simulated and measured clutter PSD for 135 MHz

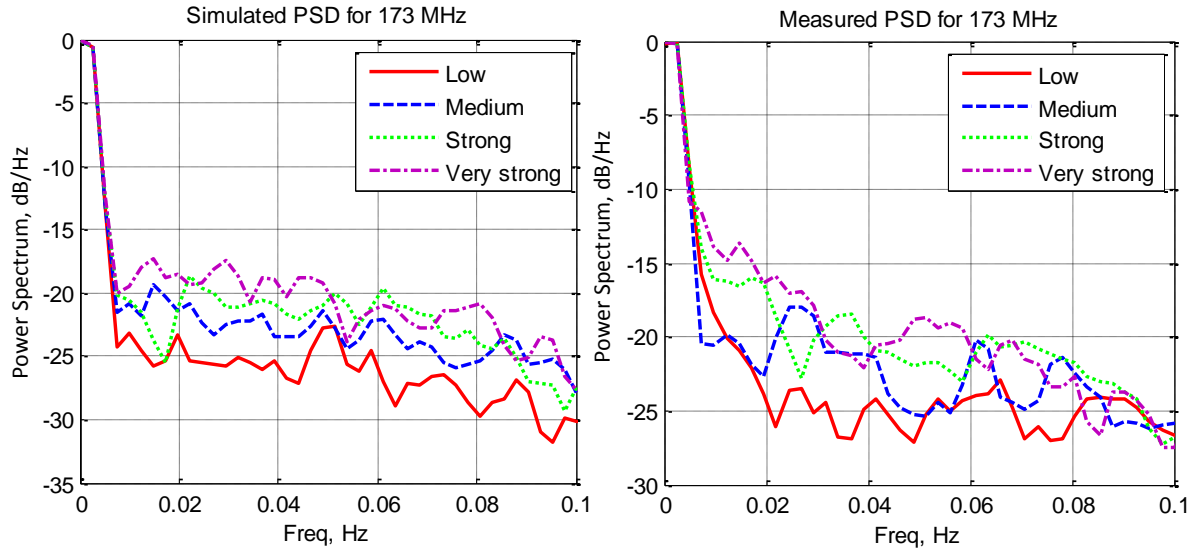


Figure 5.41: Simulated and measured clutter PSD for 173 MHz

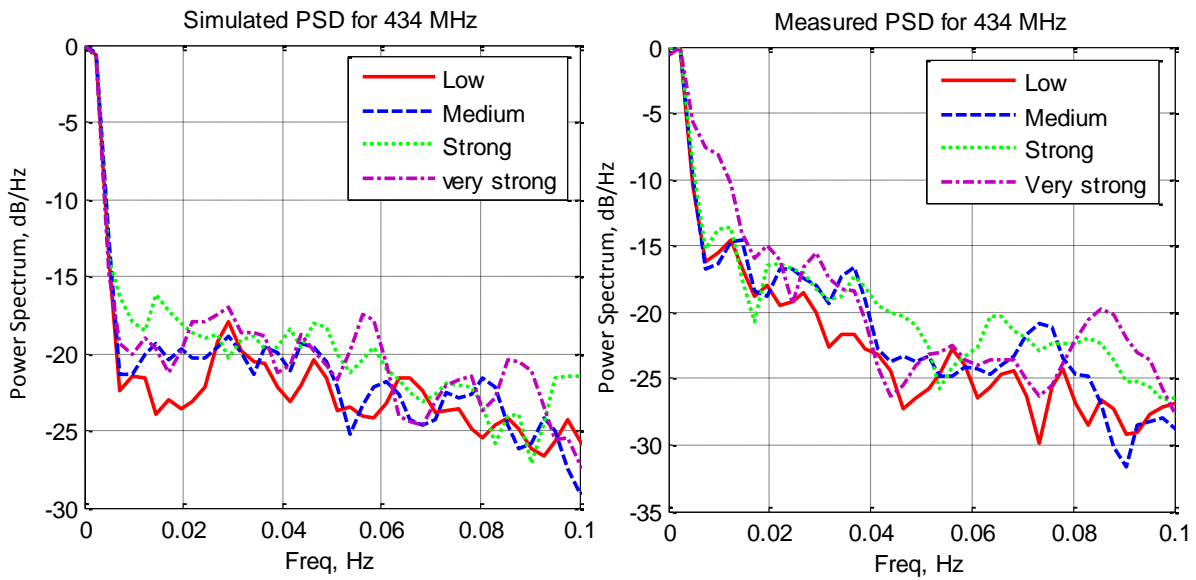


Figure 5.42: Simulated and measured clutter PSD for 434 MHz

5.5.2 Simulated Versus Measured Clutter for Different Frequencies

In this part, the comparison of simulated and measured clutter signal are based on different channel frequencies which varies from 64 MHz, 135 MHz, 173 MHz to 434 MHz. Only the

lowest and the strongest clutter strengths will be discussed in this part as other clutter strengths such as medium and strong clutter strength also portrays similar trends of results.

Figure 5.43 and Figure 5.44 shows the simulated and measured low clutter signal respectively. It can be seen in the figures that the clutter amplitude for both simulated and measured are within the same range of clutter voltage from 0.0041 V to 0.17 V, and the increased of clutter power from the lowest frequency of 64 MHz to the highest clutter power range of 434 MHz. This tells us that the clutter power increased with the increases of frequency.

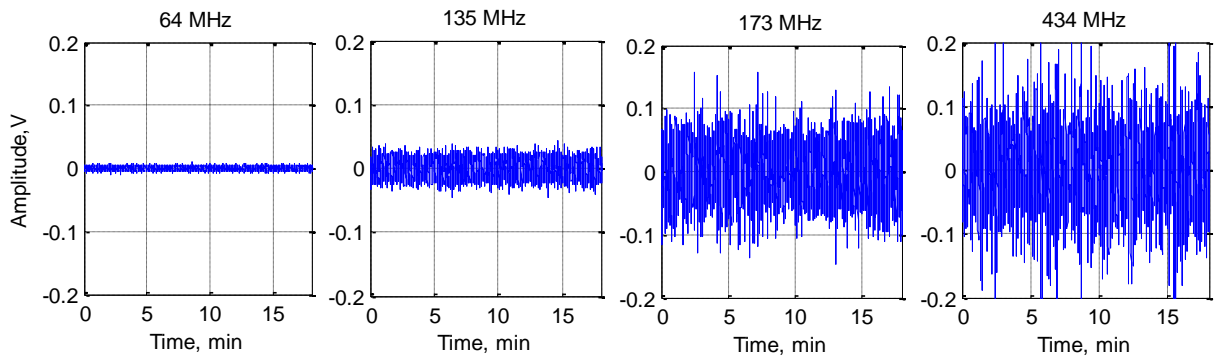


Figure 5.43: Simulated low clutter for different frequency channels

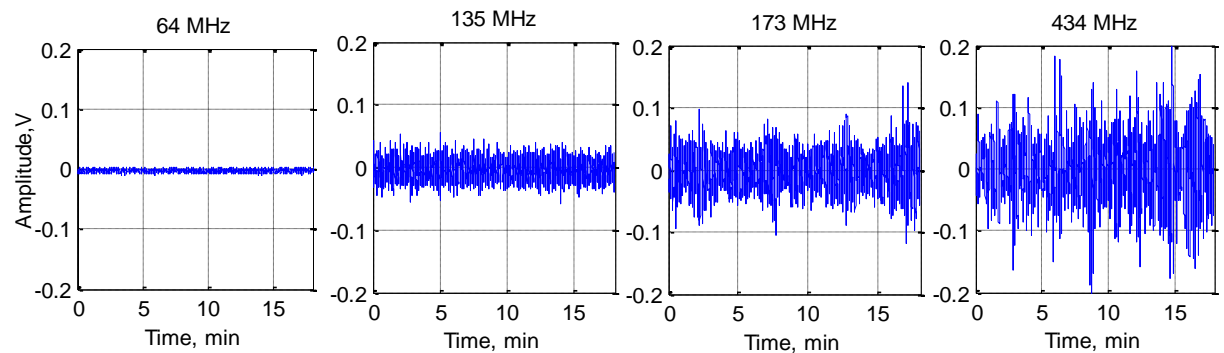


Figure 5.44: Measured low clutter for different frequency channels

Furthermore, the power spectral densities for simulated and measured low clutter are approximately within the same trends. The frequency channel that contributed the highest PSD is 434 MHz and the lowest is from 64 MHz channel frequency with the spectrum width of 10 dB power drop of 0.3 to 0.5 Hz for both simulated and measured clutters shown in Figure 5.45.

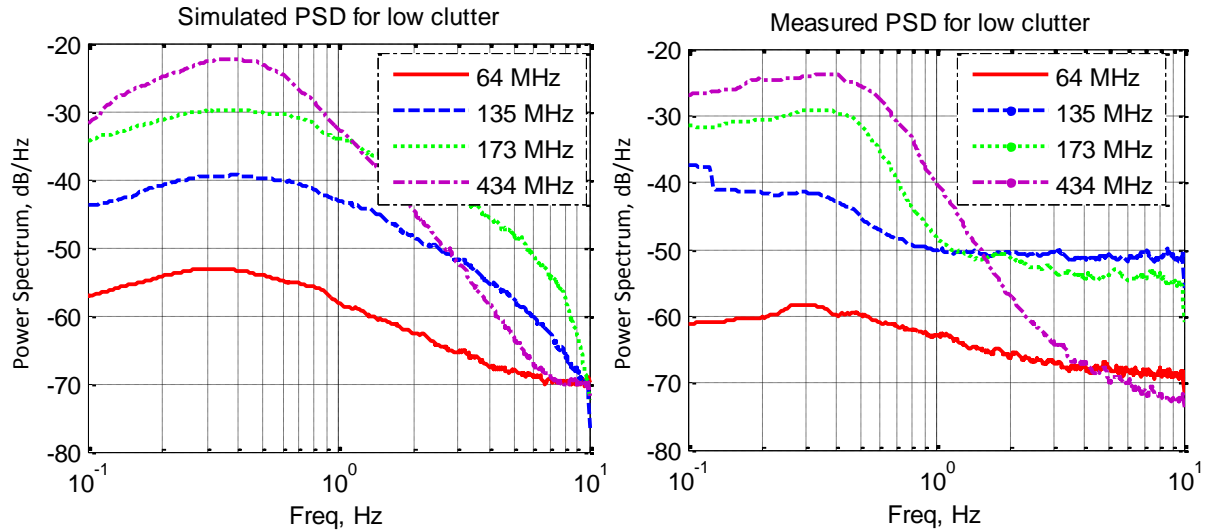


Figure 5.45: Simulated and measured low clutter PSD

Next is the comparison between the simulated and measured of very strong clutter strength for different frequency channels. As said earlier, the trend of the results for all clutter strengths are the same which can be seen clearly from Figure 5.46 and Figure 5.47 for clutter amplitude displayed. The clutter amplitude for both simulated and measured very strong clutter also lies within the same range to as low as 0.26V for 64 MHz frequency channel to as high as 4.27 V for 434 MHz frequency channel. When the operating frequency is increased, the clutter amplitude will also increase.

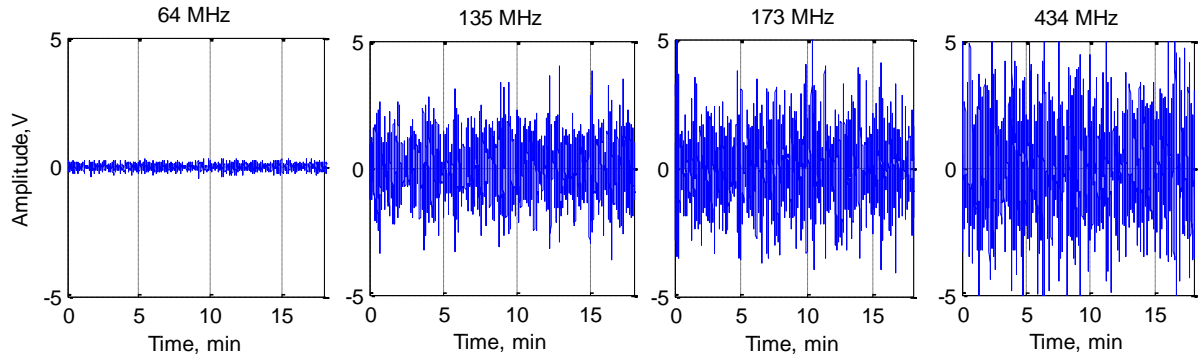
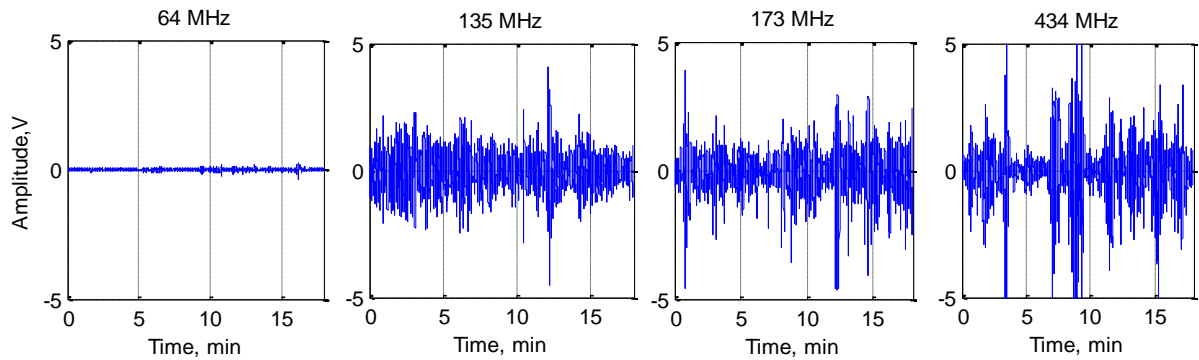


Figure 5.46: Simulated very strong clutter for different frequency channels



As for the clutter PSD shown in Figure 5.48 the trend between both simulated and measured are approximately the same. The differences between each frequency are around 2 dB for 135 MHz to 173 MHz and 434 MHz. While for 64 MHz, the signal PSD a bit low around -25 dB to -30 dB which is about 20dB less from 135 MHz frequency channel's PSD for both simulated and measured clutter signals. In 64 MHz frequency channel, the main contribution of noise is from the thermal noise. We can see from all clutter strengths from low to very strong clutter, the clutter amplitude of 64 MHz frequency channel is always at the lowest which is ranging from 0.0041 V to 0.2694 V. While for 135 MHz frequency channel, it is ranging from 0.024 V to 2.779 V which is about dB difference from 64 MHz channel.

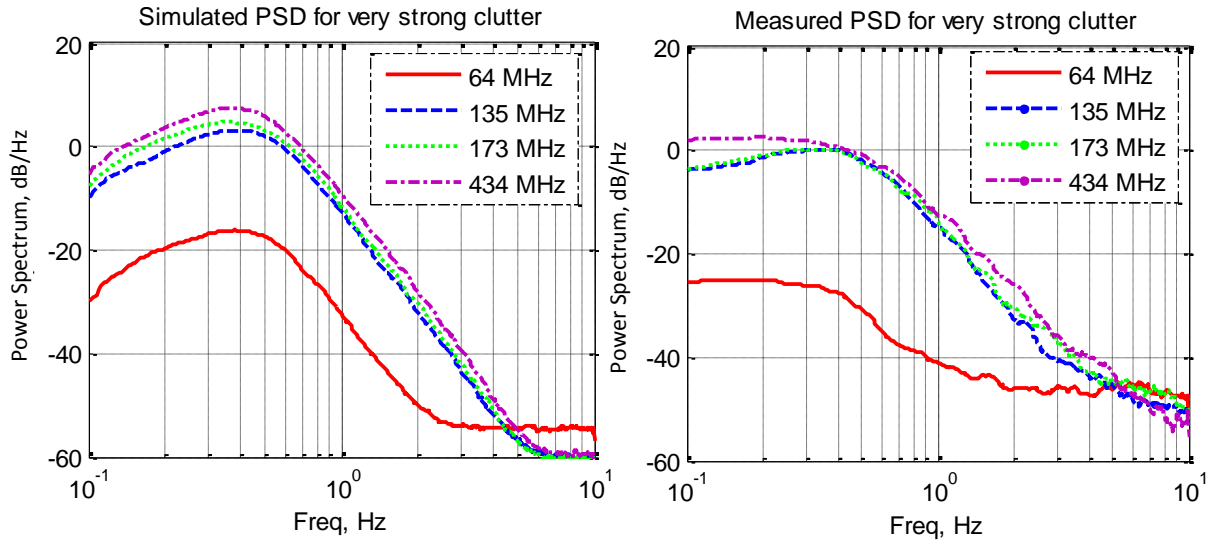


Figure 5.48: Simulated and measured very strong clutter PSD

5.6 Summary

In this chapter, methods of simulation process are described step by step. Then the results for each clutter strength such as low, medium, strong and very strong clutter are described in detailed which include the statistical results and the amplitude distributions. Then the results are compared with the measured result in two parts; one is by comparing with different clutter strength and; two is by comparing simulated and measured clutter for different frequencies. Detailed of the simulation programs using Matlab software are attached in the Appendix A.

It can be summarized from the results that the simulation and measured clutter signal are approximately the same for all characteristics that have been analysed. This is shown clearly from the results that amplitude distribution exhibit Weibull distribution with the shape factor decreased with the increased of the frequency and clutter strength, the PSD trend and the clutter power increased with the increased of the frequency.

CHAPTER 6

CONCLUSION AND FUTURE WORKS

In this thesis, the clutter analysis of Forward Scatter Micro Radar has been carried out for VHF and UHF frequency bands. There are two methods of measurement used; the short term measurement and long term measurement. All measurements were taken from several places with different landscapes varying from concrete runway to dense woodlands.

Earlier in the thesis, the specific research subjects have been outlined in Chapter 1 including the motivation for the present work and the problem statement of the research. The literature review of FSR has been presented in Chapter 2. The basic principles of radar and FSR which includes the configuration of radar for monostatic and bistatic, introduction of FSR and basic equations of FSR have been discussed. The theory of radar clutter has been introduced in this chapter which include literature survey of clutter especially for FSR.

Chapter 3, has given detailed description of the equipment used and the measurement set up. All data processing and analysis have been described in detailed. There are two method of measurements have been used in this research which are the short term measurement and long

term measurement. The short term measurement involved with measurements that contains separate data with 20 minutes each. While for the long term measurement, the measurement are conducted in several days. There are 279 data files for a total of 5940 minutes that have been analysed for this analysis. Each data are recorded continuously from four data trials.

Chapter 4 is dedicated for the analysis of the results. In this chapter, the results have been discussed detailing for short term measurement and long term measurement. In short term measurement, this measurement is done in order to confirm that the main influence to clutter build up is the wind speed. From the data trials, four wind conditions are identified from low (up to 5 mph), medium (6 – 15 mph), strong (16 - 24 mph) and very strong (gale > 25 mph) wind conditions. It is shown from the analysis, the clutter STD increases when the frequency and wind speed increased. The higher the frequency, the higher will be the clutter strength and the amplitude of the clutter's envelope. The PSD of all frequencies also exhibits the same trend for all wind conditions, with the lowest PSD for the lowest frequency and low wind speed. While the highest PSD for high frequency and very strong wind speed. The characteristic of the clutter also have been identified, where the spectrum of the clutter is practically the same for all frequency channels with the power dropped around 0.005 Hz to 0.01 Hz using second order LPF and cut-off frequency of 0.1 Hz. While the PSD slopes drop approximately 20 dB to 30 dB per decade and the spectrum width defined by 10 dB power dropped are about 0.4Hz to 0.5 Hz.

In the long term measurement, the results are presented by different frequency channels. Each frequency channel will have the data for standard deviation, envelope's minimum and maximum value and also the shape factor in histogram format and also for different number

of records. From the analysis, it shows that the standard deviation, envelope's minimum and maximum amplitude and also the shape factor are depends on the operating frequencies and also the wind speeds. As from the analysis, four main clutter conditions are then categories such as low, medium, strong and very strong clutter. These values are then used for clutter generation.

Chapter 5 has been focused on the generation of simulated clutter-like signals based on the empirical model. The empirical model of clutter was generalised from the estimated measured clutter characteristics. With this model, the clutter-like signals are simulated for different clutter strengths and compared with the measured clutter. It shows that the results from the measured and simulated clutter signal are approximately similar for all characteristics that have been analysed.

The aim of this research to analyse the ground clutter for Forward Scatter Micro-sensor has been achieved. All the analysis done in this research are clearly explained and described. However future work can be carried out for further improvements which include:

Analysis on bigger database: In this research there are two main analysis of clutter; short term measurement with 180 data files and long term measurement with 279 data files both are from the same measurement site (Horntorn Grange, UK). More measurements need to be done which covers the whole possible scenarios that may involve in radar target detection especially for FSR network. The possible scenarios may include database for different ground landscapes, weather and many more. With bigger database, the system performance are much better which can cover all possibilities.

Include more parameters: Besides STD, PSD, the dynamic range and Weibull's shape factor, other parameters should be added. More parameters used, it can justify more accurate and precise clutter signals analysis.

False alarm: False alarm is one of the weakness in target detection. Need to find the solutions on how to minimize the false alarm.

Create Synthetic Environment (SE) system: Synthetic environment system will be the next aim. With bigger database, the system will be more accurate for the analysis of radar system performance and to test the radar system itself. This has been done in [63] where near-field technique is used for phased array radar system. Instead of testing the radar system in far-field ranges with large radar antennas, larger distances, an uncontrolled outdoor environment with limited test equipments; the test can only be done indoor in anechoic chamber. Another research on synthetic environment is in [64] where it stated that the synthetic environment is used to replace the needs of conducting the experiments several times. This some sort of simulator can be used to produce an accurate synthetic replacement to the data a radar would actually collect. All these explained the significant of synthetic environment for FSR system.

Further analysis on the clutter distributions: based on the previous studies, the most suitable distribution for FSR ground clutter is by using Weibull distribution. This is stated in [60, 61]. Additional analysis on this has been made and the results will be presented in conference later. It shown from the analysis, the best distribution based on the data used in this research, is Gamma distribution for VHF frequency and Log-logistic distribution for UHF.

REFERENCES

- [1] N. J. Willis and H. D. Griffiths, "Advances in Bistatic radar," *Scientec Publisher*, 2007.
- [2] A. B. Blyakhman and I. A. Runova, "Forward scattering radiolocation bistatic RCS and target detection," in *Radar Conference, 1999. The Record of the 1999 IEEE*, 1999, pp. 203-208.
- [3] M. A. Richards, W. A. Holm, and J. A. Scheer, Eds., *Principles of Modern Radar: Basic Principles v. 1*. Raleigh, NC: SciTech Publishing Inc, 2009.
- [4] M. Cherniakov, Ed., *Bistatic Radar, Principles and Practice*. John Wiley & Sons, 2007.
- [5] V. Sizov, M. Gashinova, M. Antonio, and M. Cherniakov, "Signature Modelling and Coherent Target Detection for FSR Sensors," in *IRS 2009*, Hamburg Germany, 2009.
- [6] H. R. Raemer, "Radar System Principle," *CRC Press LLC*, 1997.
- [7] M. Antoniou, V. Sizov, H. Cheng, P. Jancovic, R. Abdullah, N. E. A. Rashid, *et al.*, "The concept of a forward scattering micro-sensors radar network for situational awareness," in *Radar, 2008 International Conference on*, 2008, pp. 171-176.
- [8] M. I. Skolnik, *Radar Handbook, Third Edition*, 3 edition. New York: McGraw-Hill Professional, 2008.
- [9] N. E. A. Rashid, P. Jancovic., M. Gashinova, *et al.*, "The effect of clutter on the automatic target classification accuracy in FSR," in *Radar Conference, 2010 IEEE*, 2010, pp. 596-602.
- [10] M. Cherniakov, M. Gashinova, N. A. Zakaria, V. Sizov, "Empirical model of vegetation clutter in forward scatter radar micro-sensors, " in *Radar Conference 2010*, Washington, DC, 2010, pp. 899-904.
- [11] V. Sizov, C. Hu, M. Antoniou, and M. Cherniakov, "Vegetation clutter spectral properties in VHF/UHF bistatic doppler radar," in *Radar Conference, 2008. RADAR '08. IEEE*, 2008, pp. 1-6.
- [12] M. Cherniakov, M. Salous, V. Kostylev, and R. Abdullah, "Analysis of forward scattering radar for ground target detection," in *Radar Conference, 2005. EURAD 2005. European*, 2005, pp. 145-148.
- [13] A. B. Blyakhman, A. V. Myakinkov, and A. G. Ryndyk, "Tracking algorithm for three-dimensional bistatic forward scattering radar with weighting of primary measurements," in *Radar Conference, 2005. EURAD 2005. European*, 2005, pp. 153-156.

-
- [14] R. S. A. Raja Abdullah, M. F. A. Rasid, M. W. Azis, and M. Khalafalla, "Target prediction in Forward Scattering Radar," in *Asia-Pacific Conference on Applied Electromagnetics, 2007. APACE 2007*, pp. 1-5.
- [15] M. I. Skolnik, *"Introduction to Radar Systems"*, 3 edition. Boston: McGraw-Hill Higher Education, 2002.
- [16] P. Z. Peebles, *"Radar Principles"*, 1 edition. New York: Wiley-Blackwell, 1998.
- [17] V. S. Chernyak, *Fundamentals of Multisite Radar Systems: Multistatic Radars and Multistatic Radar Systems*. Amsterdam, The Netherlands: CRC Press, 1998.
- [18] Willis, N.J., "Bistatic Radar", technology Service Cooperation, 1995.
- [19] D. K. Barton, "Radars Volume 5: Radar Clutter, *Artech House*, 1975.
- [20] V. Sizov, M. Cherniakov, and M. Antoniou, "Forward scattering radar power budget analysis for ground targets," *Radar, Sonar & Navigation, IET*, vol. 1, 2007, pp. 437-446.
- [21] V. C. Chen, F. Li, S. S. Ho, and H. Wechsler, "Micro-Doppler effect in radar: phenomenon, model, and simulation study," *Aerospace and Electronic Systems, IEEE Transactions on*, vol. 42, 2006, pp. 2-21.
- [22] D. K. Barton, *Modern Radar System Analysis*. Artech House, 1988.
- [23] Physics Classroom, "The Doppler Effect", [Online]. Available: <http://www.physicsclassroom.com/class/waves/Lesson-3/The-Doppler-Effect>, [Access: 15 June 2014].
- [24] N. E.A. Rashid, "Automatic Vehicle Classification in a Low Frequency Forward Scatter Micro-Radar," Ph.D. dissertation, University of Birmingham, Birmingham, United Kingdom, 2011.
- [25] Christian Wolff, "Radar Cross Section," Available from the website: <http://www.radartutorial.eu/18.explanations/ex09.en.html>, Last access date: March 2012.
- [26] M. A. Richards, "Fundamentals of Radar Signal Processing", Second Edition, 2 edition. New York: McGraw-Hill Professional, 2014.
- [27] V. Sizov, M. Cherniakov, "Netted Forward Scattering Micro Radars for Ground Target," in *3rd Annular technical EMRS/DTC Conference*, Edinburg, UK, 2006.
- [28] M. Cherniakov, R. S. A. R. Abdullah, P. Jancovic, M. Salous, and V. Chapursky, "Automatic ground target classification using forward scattering radar," *Radar, Sonar and Navigation, IEE Proceedings -*, vol. 153, 2006, pp. 427-437.
- [29] V. Sizov, M. Cherniakov, and M. Antoniou, "Forward scatter RCS estimation for ground targets," in *Microwave Conference, 2007. European*, 2007, pp. 1700-1703.
- [30] V. Sizov, M. Gashinova, N. E. Rashid, J. Chen, and M. Cherniakov, "Forward Scattering Micro Radar efficiency analysis for different landscapes " in *6th EMRS DTC Technical Conference* Edinburgh, 2009.
- [31] M. Cherniakov, R. S. A. R. Abdullah, P. Jancovic, M. Salous and V. Kostylev, "Forward Scattering Radar for Ground Targets detection and Recognition," in *2nd EMRS DTC Technical Conference* Edinburgh, 2005.
-

-
- [32] R. S. A. R. Abdullah and A. Ismail, "Forward Scattering Radar: Current and Future Applications," in *International Journal of Engineering and Technology*, vol. 3, no. 1, 2006, pp 61-67.
 - [33] C. W. Fareez, K. A Othman, N. E. Rashid, et. al., " Forward Scattering Radar (FSR) ground target signal processing using wavelet technique (WT)," *16th International Radar Symposium (IRS)*, Dresden, Germany, 2015, pp. 646-65 .
 - [34] M. Cherniakov, R. S. A. R. Abdullah, P. Jancovic and M. Salous, "Forward Sacttering Micro Sensor for Vehicle Classification," in *Radar Conference, 2005. RADAR '05. IEEE*, 2008, pp. 184-189.
 - [35] R. S. A. R. Abdullah, et. al., "Target Classification In Forward Scattering Radar," in *World Engineering Congress*, Penang, Malaysia, 2007, pp. 201-208.
 - [36] N. E. Rashid, N. Ahmad, N. F. A. Nor, N. Ismail," The effect of different ground characteristic to the stability and similarity of target spectra in FSR micro-sensor network," *IEEE Student Conference on Research and Development (SCOREd)*, Penang, Malaysia, pp. 23-228, 2012.
 - [37] M. Salah, M.F.A. Rasid and R. S. A. R. Abdullah, " Speed Estimation in Forward Scattering Radar by Using Standard Deviation Method," in *Modern Applied Science*, vol. 3, no. 3, 2009, pp. 16-25.
 - [38] M. Cherniakov, Cheng Hu, M. Gashinova, M. Antoniou, V. Sizov and L.Y. Daniel, " Ultra-Wideband Forward Scattering Radar: Definition and Potential," in *4th EMRS DTC Technical Conference*, Edinburgh, 2007, pp. A2.
 - [39] M. Gashinova, V. Sizov, N. A. Zakaria, and M. Cherniakov, "Signal Detection in Multi-frequency Forward Scatter Radar," in *Radar Conference (EuRAD) 2010 European* Paris, France, 2010, pp. 276 - 279.
 - [40] N. E. A. Rashid, M. Gashinova, V. Sizov M. Cherniakov and N. Ismail," The influence of different baseline lengths to ground target signature in a FS micro-radar network," in *IEEE 9th International Colloquium on Signal Processing and Applications (CSPA)*, Kuala Lumpur, 2013, pp. 21-26.
 - [41] V. Sizov, M. Gashinova, N. E. A. Rashid, N. A. Zakaria, P. Jancovic, and M. Cherniakov, "FSR Sensor Network: Performance and Parameters," in *7th EMRS DTC technical Conference*, Edinburg, UK, 2010, pp. A13.
 - [42] Radar Tutorial, "Radar Basic: Radar Clutter", [Online]. Available: <http://www.radartutorial.eu/11.coherent/co04.en.html>: [Access: 20 June 2014].
 - [43] L. Sevgi, "Synthetic Radar-Signal Environment: Computer Generation of Signal, Noise, and Clutter," *Antennas and Propagation Magazine, IEEE*, vol. 49, 2007, pp. 192-198.
 - [44] X. Li and X. Xu, "A Statistical Model for Correlated K-distributed Sea Clutter," in *Image and Signal Processing, 2008. CISP '08. Congress on*, 2008, pp. 408-412.
 - [45] K. D. Ward, R. J. A. Tough, and S. Watts, "Sea Clutter: Scattering, The K Distribution and Radar Performance," vol. 20. *London: The Institution of Engineering and Technology*, 2006.
-

-
- [46] M. Gashinova, K. Kabakchiev, L. Daniel, E. Hoare, V. Sizov, and M. Cherniakov, "Measured forward-scatter sea clutter at near-zero grazing angle: analysis of spectral and statistical properties," *IET Radar Sonar Navig.*, vol. 8, no. 2, pp. 132–141, Feb. 2014.
 - [47] K. D. Ward, R. J. A. Tough, and S. Watts, *Sea clutter scattering, the K distribution and radar performance*. Stevenage, U.K.: Institution of Engineering and Technology, 2013.
 - [48] K. Kabakchiev, L. Y. Daniel, E. G. Hoare, M. Gashinova, and M. Cherniakov, "Near zero grazing angle forward-scatter sea clutter measurement statistical properties," in *Radar Symposium (IRS), 2013 14th International*, 2013, vol. 2, pp. 620–624.
 - [49] M. Gashinova, K. Kabakchiev, L. Daniel, E. Hoare, V. Sizov, and M. Cherniakov, "Measured forward-scatter sea clutter at near-zero grazing angle: analysis of spectral and statistical properties," *IET Radar Sonar Navig.*, vol. 8, no. 2, pp. 132–141, Feb. 2014.
 - [50] J. B. Billingsley, "Low-angle Radar Land Clutter: Measurements and Empirical Models", *William Andrew Publishing*, United State, 2002.
 - [51] D. K. Barton, "Land clutter models for radar design and analysis," *Proceedings of the IEEE*, vol. 73, 1985, pp. 198-204.
 - [52] G. P. Kulemin, "Millimeter-wave Radar targets and Clutter", Artech House, 2003.
 - [53] J. B. Billingsley, A. Farina, F. Gini, M. V. Greco and L. Verrazzani, "Statistical analyses of measured radar ground clutter data," *IEEE Trans. AES*, vol. 35, no. 2, April 1999, pp. 579-593.
 - [54] M. sekine and Y. Mao, *Weibull Radar Clutter*, *Peter Peregrinus Ltd.*, 1990.
 - [55] N. E. A. Rashid, P. Jancovic, M. Gashinova, *et al.*, "The effect of clutter on the automatic target classification accuracy in FSR," in *Radar Conference, 2010 IEEE*, 2010, pp. 596-602.
 - [56] N. A. Zakaria, M. Gashinova, and M. Cherniakov, "Synthetic Environment for Forward Scattering Radar Detection," in *Asia Pacific Defence and Security Technology Conference 2009*, Kuala Lumpur, Malaysia, 2009.
 - [57] N. A. Zakaria, M. Gashinova, and M. Cherniakov, "Statistical Forward Scattering Radar Detection," in *Asia Pacific Defence and Security Technology Conference 2009*, Kuala Lumpur, Malaysia, 2009.
 - [58] N. E. A. Rashid, M. Antoniou, P. Jancovic, V. Sizov, R. Abdullah, and M. Cherniakov, "Automatic target classification in a low frequency FSR network," in *Radar Conference, 2008. EuRAD 2008. European*, 2008, pp. 68-71.
 - [59] V. Sizov, M. Cherniakov, and M. Antoniou, "Forward scatter RCS estimation for ground targets," in *Microwave Conference, 2007. European*, 2007, pp. 1700-1703.
 - [60] M. Skolnik, *Radar Handbook*, *Mc Graw-Hills Education*, 3rd edition, 2008.
 - [61] J.P. Cusumano, "The Power Spectral Density and the Autocorrelation," Available from the website: <http://mcise.uri.edu/chelidze/courses/mce567/handouts/psdtheory.pdf>, Last access date: 1 Aug 2011.
-

- [62] S. Sayama and H. Sekine, "Weibull, log-Weibull and K-distributed ground clutter modeling analyzed by AIC," *Aerospace and Electronic Systems, IEEE Transactions on*, vol. 37, 2001, pp. 1108-1113.
- [63] J. B. Billingsley, A. Farina, F. Gini, M. V. Greco, and L. Verrazzani, "Statistical analyses of measured radar ground clutter data," *Aerospace and Electronic Systems, IEEE Transactions on*, vol. 35, 1999, pp. 579-593.
- [64] W. Wallace, C. New, and J. Branson, "Demonstrating the concept of using synthetic environments in radar acceptance and procurement," in *Radar Systems, 2007 IET International Conference on*, 2007, pp. 1-5.
- [65] F. E. Nathanson, J. P. Reilly, and M. N. Cohen, *Radar Design Principles*, 2 edition. Mendham, N.J.: SciTech Publishing, 1999.
- [66] A. J. Gatesman, T. Goyette, J. C. Dickinson, J. Waldman, J. Neilson, and W. E. Nixon, "Physical scale modeling the millimeter-wave backscattering behavior of ground clutter," pp. 141-151, 2001.

APPENDIX A

1. HARDWARE DESCRIPTION

TX and RX channels are built from the standard short-range radio modules by Radiometrix¹. Types of RX and TX modules used for each carrier frequency are shown in Tab. A1.3.

Standard Panorama² helical monopole antennas are used for different frequencies in transmitters and receivers (Tab. A1.3 and Fig. A1.3). Directional Yagi antenna with 9dB gain can be used for some specific measurements at 434MHz, as well (Fig. A1.8)

Table A1.3

Channel, MHz	TX module	RX module	Antenna
64-1, 64-2	TX1M-64-5	RX1M-64-5	MXSK-BNC (64.5 MHz)
135-1, 135-2	LMT1-135-5	LMR1-135-5*	MFX-H3-BNC (135 MHz)
144	LMT1-144-5	LMR1-144-5*	MFX-H4-BNC (144 MHz)
173	LMT1-173-5	LMR1-173-5*	MFX-H7-BNC (173 MHz)
434-1, 434-2	TX2M-433-5	LMR2-434-5	MQ-U-BNC (434 MHz) or directional Yagi antenna

* These RX modules are modified to increase dynamic band of input signal.

The use of unified RX and TX modules gives it possible to change carrier frequencies in the equipment easily according to the goal of trials. All modules have also carrier frequency adjustment in a band around 1-2 MHz (depending on the type of module). This feature can be used for tune the frequency if the narrow-band interference signal is received.

The block-diagram of 3LT_TX is shown on Fig. A1.4.

¹ <http://www.radiometrix.com/our-products/narrow+band>

² http://www.panorama.co.uk/uk/products/pmr_portables.html

The 3LT_TX transmitter is built from different frequencies Radiometrix's TX modules. The four-channel transmitter 4N_TX has the similar structure, except the number of TX modules and antennas. Required carriers are installed by frequency selection switchers.

Battery state indicator (LED) shows TX "Power ON" state and "Battery low" (flashing LED) state as well. The battery could be charged by use of suitable charger connected to the external socket.

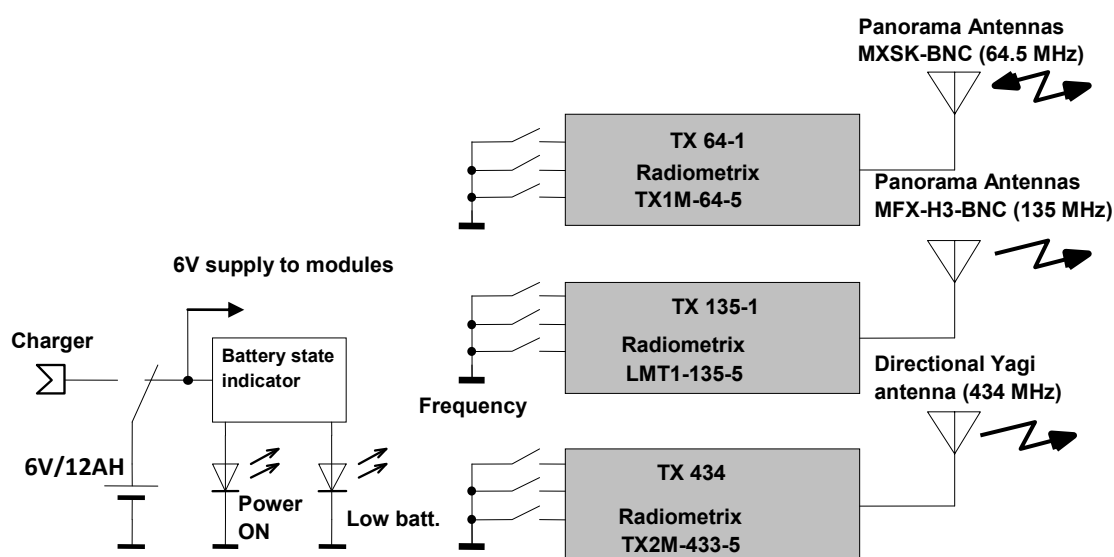


Figure A1.4: 3LT_TX. Block diagram

The block-diagram of the 4LT_RX receiver is shown in Fig. A1.5.

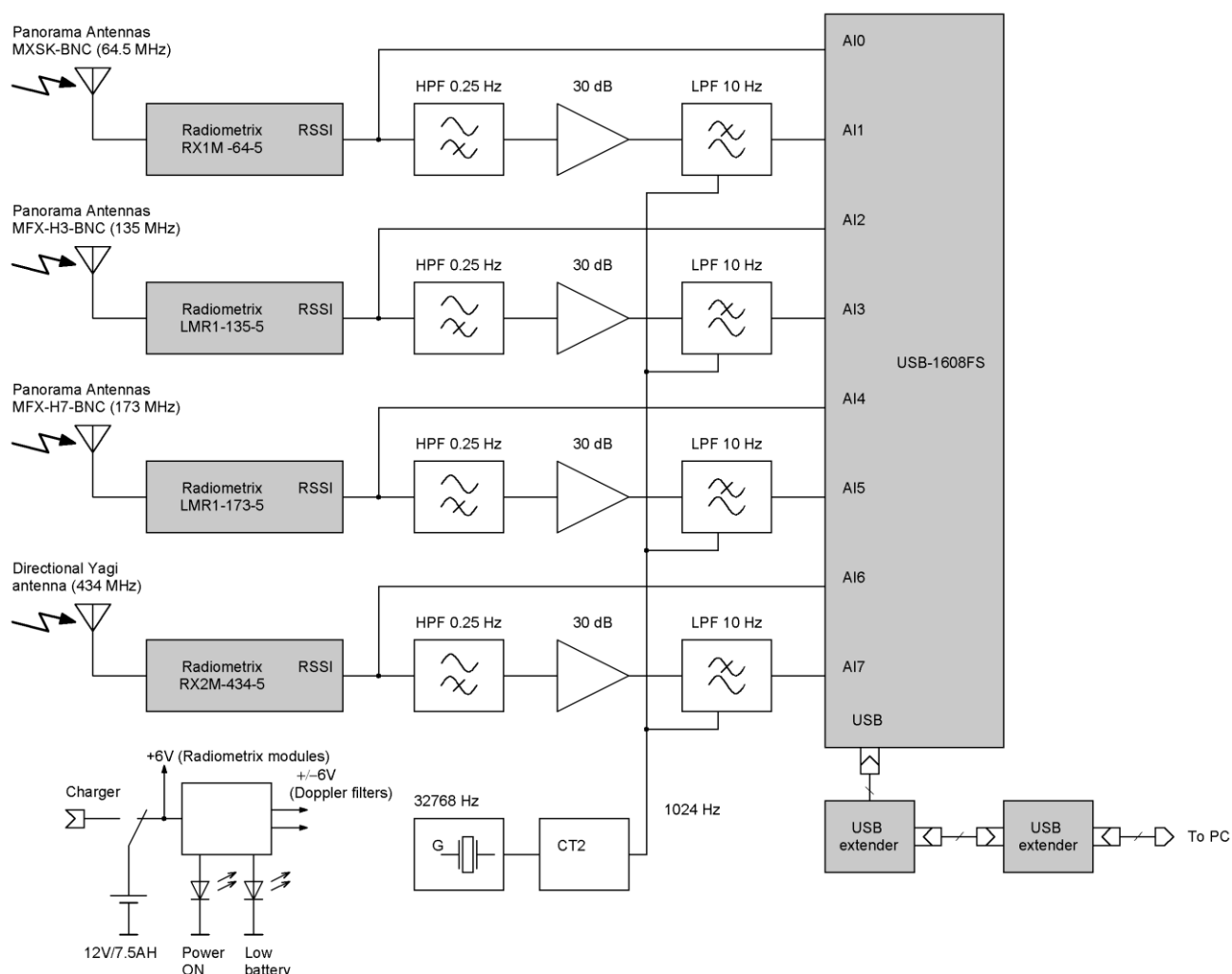


Figure A1.5: 4LT_RX block-diagram

The receiver is built from Radiometrix's RX modules (Tab. A1.3). The received signal strength indicator (RSSI) output of the modules has logarithmic dependence of output voltage from input power in a wide dynamic band. RSSI output voltages are converted by ADC into digital data rate and sent to PC by USB connection.

The average value of the output voltage corresponds to direct leakage power. It is converted by ADC and transferred to PC. The mix of target signal, clutter and Noise are much less (up to 20-40 dB) than leakage power, so that, it can be seen as small variations of the RSSI voltage. In order to use full ADC resolution for target Doppler signature, additional Doppler channels are created. The DC component in each channel RSSI output is rejected by 1st order high pass filter (HPF); and Doppler variations are amplified with constant gain of 30dB. After anti-aliasing low-pass filters (LPF, 5th order switched capacitors filters, LM1063

by Linear Technology³) the Doppler signature of target signals is also converted to digital form and transferred to PC by USB protocol. Two USB extenders are used to increase the cable length up to 30m from the central post and make small the influence of operator movements in measured signals.

The cut-off frequencies, limited Doppler band, are 0.25Hz for HPF and 10.24 Hz for LPF.

Receiver has the same battery state LED indicator as transmitter.

The 3-channel receiver has the similar block-diagram, except the number and types of RX modules (3 instead 4).

1.4. ADC sampling frequency

The LPF cut-off is optimized for using ADC sampling frequency of 20Hz, Not less (Nyquist–Shannon sampling theorem. The value of sampling frequency is set by data acquisition software.

It is possible to set less values of sampling frequency (30–50 Hz) for the signals with very limited spectrum bandwidth width like human and foliage clutter. For higher speed target (car) measurement sampling frequency should be increased to 100Hz.

1.5. Receivers sensitivity and dynamic range

All RX channels are built from unified modules and have similar sensitivity and linear detection range approximately from $-(60...70)$ dBm to $-(120...130)$ dBm (Fig. A1.7).

Concrete detection range for every channel is defined by calibration procedure and used in data acquisition and data visualization software.

³ <http://cds.linear.com/docs/Datasheet/1063fa.pdf>

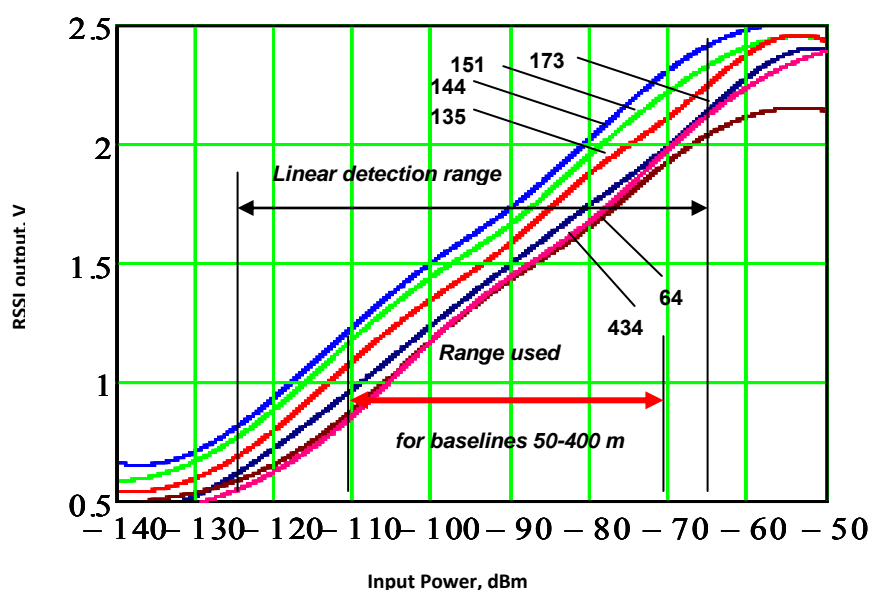


Figure A1.7: Receivers detection range

1.6. Current consumption

- 3N_RX: 70mA from 12V@7.5Ah battery
- 3N_TX: <250mA from 6V@12Ah battery
- 4N_RX: <150mA from 6V@12Ah battery
- 4N_TX: <200mA from 6V@12Ah battery

Gelled lead-acid batteries are used in the modules. Fully charged batteries provide the long term measurement for at least 48 hours.

1.7. Antennas

Helical monopole antennas are used for all channels (Fig. A1.3). Theoretical value of full quarter wavelength monopole antenna installed directly on perfect electrical conductive ground is 2.3 dB.

Real helical antennas are shorter than $\lambda/4$ and they installed above the real ground, which is characterized by some values of dielectric permittivity and loss. Thus, the gain of such antennas should be less than ideal antenna gain. In case the modules installed directly on the ground surface the antennas gains are estimated as:

- 64 MHz: 0dB;
- 135...173 MHz: +0...1dB;
- 434 MHz: +1...1.5dB.

With these values of the gain measured and calculated propagation loss well coincide at baseline length from 20 to 300m.

Effective antenna's heights are dependent on the antenna's lengths and module dimensions:

- 3N_RX: 64-1 – 32 cm; 135-1 and 434 – 29cm.
- 3N_TX: 64-1 – 20 cm; 135-1 and 434 – 15cm
- 4N_RX and 4N_TX: 64-2 – 22 cm; 135-2; 144 and 173 – 17cm.

Every extra BNC-type attenuator installed to the antenna adds 5 cm to antenna's effective height.

These antennas' height values should be taken into account for power budget calculations.

For some specific measurements, which require directional antennas, Yagi antennas with 9.5dB gain can be used at 434MHz. The installed height of Yagi antenna is 80cm (in waterproof container – Fig. A1.6) or 1m (on tripod - Fig.A1.8).

1.8. Hardware assembling

The example of equipment assembly is presented on Fig. A1.5.

RX and TX modules are mounted on special carrier boards and connected to power supply. Receiver has an extra PCB with Doppler filters and amplifiers and ADC as well. All PCBs and batteries are mounted in waterproof metal boxes. BNC connectors are used for antenna's connection.

Being waterproof, the transmitter and the receiver could be installed directly on ground surface.

While making long-term measurements in all-weather conditions, the additional waterproof containers are used (Fig. A1.6). Transmitter and receiver are installed on the bottom of the container, and the 434MHz directional antenna is mounted on the top of container.

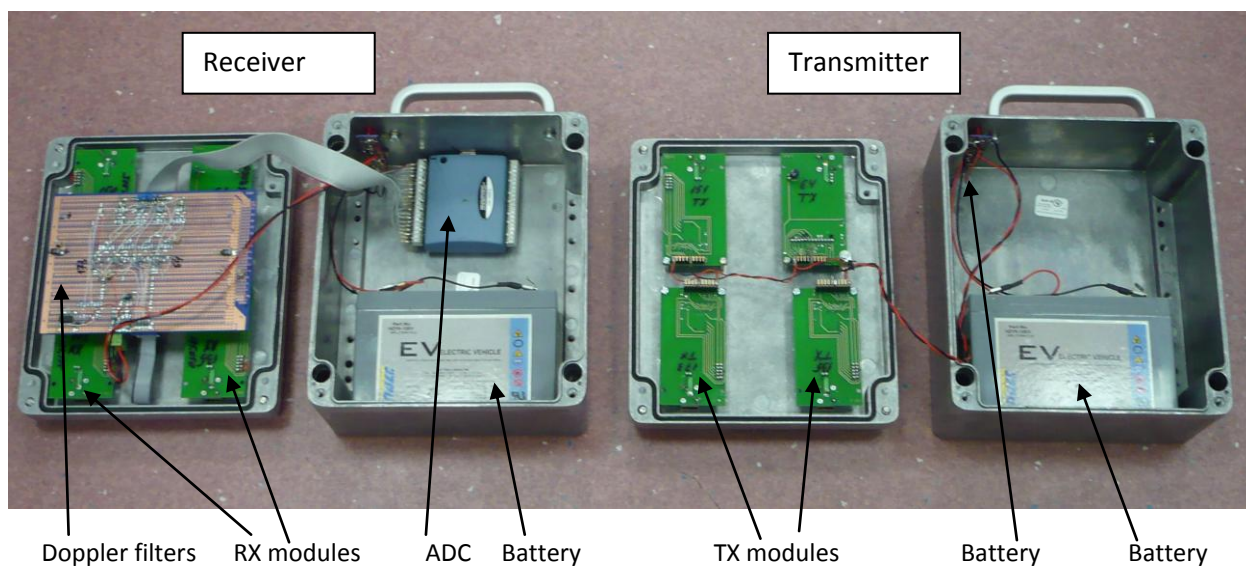


Figure A1.5: 4LT_ equipment assembly

2. Generate_clutter.m Program

```

%% creating clutter
%% using random addaptive white gaussian noise and then filter it
%% this program is created for anaylsing 1 frequency at a time
%% filter characteristics:
%%
%% butterworth filter
%% cutoff freq of 0.7...1Hz
%% created by emileen
%% edited by Ayu
%% date 1st May 2010

%-----

clear all;
close all;

%% Input value
%-----

% randn('state', 0);
clLevel = 1;      % clutter level: 1 = weak; 2 = medium; 3 = strong; 4 =
very strong;
Nfrequency1 =1;   % Frequency used:1 = 64 MHz, 2= 135 MHz, 3= 173 MHz, 4=
434 MHz

cutFEnv=0.08;     % cutoff frequency for hilbert in 2nd stage
orderFEnv=2;      % 2nd order filter for hilbert in 2nd stage
sRate = 20;       % sampling Rate

%-----
%% Parameter
%-----

% frequency step

vlight= 3*10.^8;   % speed of light
fs=sRate;         % sampling frequency
fs2=fs/2;         % nyquist
dt = 1/(fs);
time = 20;
totTime = time * 60; % time in sec
nSamples=(totTime*fs)+ 2400; % number of samples for the channel , ns=
time.60.fs

freq=[64 135 173 434]*10^6;
frequency =freq(Nfrequency1);

CluttLevel=[1 2 3 4];
ClutterLevel =CluttLevel(clLevel);

```

```

strFreq=strcat(num2str(frequency*10^-6),blanks(1),' MHz')
strCLevel=strcat(num2str(ClutterLevel),blanks(1))
nSamples2=nSamples*2;          % number of samples for non stationary envelope
t=1/sRate*(1:nSamples);

% Distribution parameters

bin = 500;                      % number of bins for histogram

%-----
%% stage 1 : generating coloured noise
%-----

%% Clutter and noise std deviation based on real clutter measurements
%%%%%%%%%%%%%%%%%%%%%%%%%%%%%%%%%%%%%%%%%%%%%%%%%%%%%%%%%%%%%%%%%%%%%%%%

%% measured clutter parameters

CutF0=[0.4 0.5 0.5 0.5; 0.5 0.5 0.5 0.5; 0.4 0.4 0.4 0.4;0.5 0.5 0.5 0.5];
%(row - clutter strength,column - freq)
fNoise0=[0.001 0.001 0.001 0.001; 0.0015 0.002 0.0025 0.003; 0.0015 0.002
0.0025 0.003;0.006 0.003 0.003 0.003;];

envRangeMin0=[0.0024 0.0095 0.0118 0.0137; 0.0148 0.0861 0.0912
0.0773;0.0085 0.1312 0.143 0.1634; 0.01731 0.1544 0.1533 0.08341;]*3.2;

envRangeMax0=[0.0041 0.0228 0.0911 0.152; 0.0405 0.8593 1.0618 1.3007;
0.0939 1.8141 2.4551 3.2627; 0.2694 2.7789 3.0868 4.2691;]*2.4;

stdClutter0=[0.0016 0.0106 0.0252 0.0447; 0.1446 0.2518 0.3068 0.3234;
0.0247 0.4471 0.5536 0.6561; 0.03658 0.6673 0.7259 0.9493];

fOrder0=[1 1 1 2; 2 2 2 2; 2 2 2 3;3 3 3 3];

stdNoise=fNoise0(clLevel,Nfrequency1);
stdClutter=stdClutter0(clLevel,Nfrequency1);
envRangeMin=envRangeMin0(clLevel,Nfrequency1);
envRangeMax=envRangeMax0(clLevel,Nfrequency1);
cutF=CutF0(clLevel,Nfrequency1);
fOrder=fOrder0(clLevel,Nfrequency1);

%-----
%% clutter + noise generation
%-----

randn('state', 0);
AWG=normrnd(0,stdClutter,1,nSamples);          % generate random noise using
AWGN
ScaleAWG=AWG;

```

```

% AWG=normrnd(0,stdClutter,1,nSamples);          % generate random noise using
AWGN
% ScaleAWG=AWG;                                  % clutter after scaled to
real noise amplitude *(realsqrt(2)*(stdClutter))

coh=0.25;
[b2,a2] = butter(fOrder,coh/fs2,'high');          % Butterworth filter
coefficients for hardware HPF
clutterH = filter(b2,a2,ScaleAWG);

col=9.9;
[b1,a1] = butter(fOrder,col/fs2,'low');           % Butterworth filter
coefficients for hardware LPF
clutterL = filter(b1,a1,clutterH);

[b3,a3] = butter(fOrder,cutF/fs2,'low');          % Butterworth filter
coefficients for software LPF
clutter = filter(b3,a3, clutterL);

% y = randsample(clutter,1)

StatClutter = clutter;
figure (1)
plot(t/60,StatClutter),grid on;                   % plotting stationary clutter
xlabel('Time, min');
ylabel('Amplitude,V');
legend(strcat('Stationary clutter at',blanks(1),strFreq))

%-----
%%      Stage 2 modulation
%-----

[envF]=envelope3(nSamples2,nSamples,orderFEnv,cutFEnv,fs2,envRangeMax,envRa
ngeMin);%#ok<NASGU> % pre-envelope

NormStatClutter=StatClutter/max(StatClutter);      % Normalised to 1

NonStatClutter1= (envF.*NormStatClutter.*max(NormStatClutter)); % modulate
stationary clutter to the envelope

figure (100)
plot(t/60,NonStatClutter1),grid on;               % plotting stationary
clutter
xlabel('Time, min');
ylabel('Amplitude,V');
legend(strcat('Normalised non-stationary clutter at',blanks(1),strFreq))

hgsave(strcat(strFreq,' Simulated Clutter'))

noise=normrnd(0,stdNoise,1,nSamples);             % generate random noise using
AWGN
% noise floor
NonStatClutter= NonStatClutter1+noise;            % coloured noise/stationary
clutterStatClutter=clutter+noise;                 % coloured
noise/stationary clutter=clutter+noise;           % coloured

```

```

noise/stationary clutter=clutter+noise;           % coloured
noise/stationary clutter

stdNonClutter= std(NonStatClutter);               % stdev of Non Stationary
clutter

%% generating envelope for nonstatclutter

env5 = abs(hilbert(NonStatClutter));              % find envelope for
non-stationary clutter

[b4,a4] = butter(orderFEnv,cutFEnv/fs2,'low');     % Butterworth filter
coefficients
envF11 = filter(b4,a4,env5);                      % envelope for non-
stationary clutter

signal = NonStatClutter(2401:length(NonStatClutter)); % cut the transient
part of the LPF
envelope = envF11(2401:length(envF11));

n1 = length (signal);                             % length of signal
after cut
t1=[0:dt:(n1-1)*dt];

figure (101)
plot(t1/60,signal),grid on;                       % plotting stationary clutter
xlabel('Time, min');
ylabel('Amplitude,V');
legend(strcat('Non-stationary Signals for ',blanks(1),strFreq))

hgsave(strcat(strFreq,' Non-stationary Simulated Clutter'))

minenvF11 = min (envelope)                         % min value of the envelope
maxenvF11 = max(envelope)                         % max value of the envelope
stdsignal = std(signal)
maxsignal = max (signal)
d_range = 10*log10 (maxenvF11/minenvF11) % signal dynamic range

min_envF11= min(envF11(3001:length(envF11)));      % to get rid of transient
part
max_envF11= max(envF11(3001:length(envF11)));

%-----
--
% PSD
%-----
---

[d f ] = pwelch(NonStatClutter,[],[],[],fs);      % to find the PSD for the
non stat clutter

x = f;                                             % freq in x-axis
y = d;                                             % data in y-axis

```

```

y1 = smooth(y,101); % smooth fxn for the data, Z
= SMOOTH(Y,SPAN) smooths data Y using SPAN as the number of points used to
compute each element of Z.

%-----
% Envelope's PSD
%-----

col = 0.1;

order1 = 2;
[b5,a5] = butter(order1,col/fs2,'low'); % Butterworth filter
coefficients
envF12 = filter(b5,a5,env5);

[d1 f1 ] = pwelch(envF12,[],[],[],fs); % to find the PSD for the
signal
xx = f; % freq in x-axis
yy = d; % data in y-axis

y2 = smooth(yy,101);

%-----
-----
%% Distributions
%-----
signal1 = StatClutter; % stationary clutter
signal2 = NonStatClutter; % Non Stationary clutter
Samp_length1 = length (signal1); % calculated the length of the
stationary clutter
Samp_length2 = length (signal2); % calculated the length of the non
stationary clutter

%% Random Distribution
%-----

%-----
%% Weibull Distribution
%-----

% signal3 = normrnd(0,1,1,10000);
%
% Samp_length3 = length (signal3);
% bin1=500;

% Stationary-----

% [weibull1,b,normHist,Fitw]= weibull_dist_uni(signal3, bin);

% Non_Stationary-----

[weibull2,b2,normHist2,Fitw2, A]= weibull_dist_uni(signal2, bin);

% CDF -----

```

```

p2 = wblcdf(b2,A,Fitw2);

figure (100)

plot(b2,p2,'g','linewidth',2), grid on, hold on, % plot
histogram with weibull distribution fit for stationary
% plot histogram with normrnd distribution fit
legend(strcat(strFreq))
title(strcat( 'Cumulative Distribution for ', strFreq, ' Signal '))
xlabel('Amplitude,V');
ylabel('CDF');
xlim([0 0.5]);

hgsave (strcat(strFreq, ' CDF'))

%% Plot all graphs

figure (3)

subplot(221)

plot(t1/60,signal,'b'), grid on, hold on, %
plotting envelope for non-stationary clutter
plot(t1/60,envelope,'r','linewidth',2);
title(strcat(strFreq, 'Clutter with envelope'))
legend('NonStatClutter','Envelope')
xlabel('Time, min');
ylabel('Amplitude,V');

subplot(222)

plot(f1,10*log10(d1), 'linewidth', 2), grid on,hold on,
% plotting stationary clutter
title(strcat(strFreq, ' PSD for Clutter Envelope '))
legend('PSD with 0.1 Hz')
xlabel('Freq, Hz');
ylabel('Power spectrum, dB');
xlim([0 0.1]);

subplot (223)

semilogx(f,10*log10(d)), grid on, hold on,
% plotting PSD for the signal
semilogx(f,10*log10(y1),'r', 'linewidth',2)
% plotting the smooth PSD for the signal
title(strcat(strFreq, ' Power Spectral Density '))
legend('PSD with 0.08 Hz')
xlabel('Freq, Hz');
ylabel('Power spectrum, dB');
xlim([10^-1 10^1]);

sprintf('%5.2f ' ,Fitw2) ;
strwbl=strcat(num2str(sprintf('(%5.2f' ,Fitw2)), ' shape factor)');

```

```

subplot (224)

semilogy(b2,normHist2),grid on, hold on,
semilogy(b2,weibull2,'c','LineWidth',3); % plot
histogram with weibull distribution fit for stationary
% plot histogram with normrnd distribution fit
title(strcat( 'Weibull Distribution for ', strFreq,' Channel '))
legend ('Histogram',strcat('Weibull Fit', strwbl))
xlabel('Amplitude,V');
ylabel('PDF');
ylim([10^-4 10^-1]);

hgsave (strcat(strFreq, ' All graph'))

%
figure (6)

sprintf('%5.2f ' ,Fitw2) ;
strwbl=strcat(num2str(sprintf('(%5.2f' ,Fitw2)), ' shape factor)');

subplot(121)

semilogy(b2,normHist2), grid on, hold on, %
plot histogram with weibull distribution fit for stationary
% plot histogram with normrnd distribution fit
semilogy(b2,weibull2,'c','LineWidth',3);
title(strcat( 'Weibull Distribution for ', strFreq,' Channel '))
legend ('Histogram',strcat('Weibull Fit', strwbl))
xlabel('Amplitude,V');
ylabel('PDF');
ylim([10^-4 10^-1]);

subplot (122)

bar(b2,normHist2);grid on, hold on;
plot(b2,weibull2,'c','LineWidth',3);
title(strcat( 'Weibull Distribution for ', strFreq,' Channel '))
legend ('Histogram',strcat('Weibull Fit', strwbl))
xlabel('Amplitude,V');
ylabel('PDF');

hgsave (strcat(strFreq, ' weibull'))

```

3. real_signal_processing.m Program

```
% load file from real signal for distribution analysis
% created by ayu
% date 15 May 2010

function [signal,storedy, storeenvmin, storeenvmax, storestdsignal,
storefitb,SA,PA,QA,RA,intS,intP,intQ,intR,fitb,strFreq] =
real_signal_processing2(listFileFull,freqUsed,sRate)
%-----

dataDir = listFileFull{1}(1:max(findstr(listFileFull{1},'\')));
nFiles = length(listFileFull);
% stdsignalall = [dirCara 'std.mat']; % .mat file
directory
%% Read the estimated velocity from .mat file

switch (freqUsed)
    case 1,
        freqUsedInd = 2;
    case 2,
        freqUsedInd = 4;
    case 3,
        freqUsedInd = 6;
    case 4,
        freqUsedInd = 8;
end

%% Process the target signals for the current directory

for j=1:nFiles;
    %% Read the binary file containing 8 target signals
    fileName = listFileFull{j};
    fileNameShort = fileName(max(findstr(fileName,'\'))+1:end);
    [data] = readTargetSignalBin(fileName, 8);
    td = data(freqUsedInd,:);
    % if length(td)<num_signal
    %     td(end+1:num_signal)=0;
    % else
    %     td=td(1:num_signal);
    % end

    %% Input value
    %-----

    time= 20; % time in minute
```

```

co2 = 0.08; % signal's
envelope cut off freq in hz
order2 =2;
co3 = 0.1; % cut off freq
for PSD's filtered envelope
order3 = 2;
sRate = 20; % sampling Rate
vlight= 3*10.^8; % speed of
light
fs=sRate; % sampling
frequency
fs2=fs/2;
bin = 100;
dt = 1/(fs);
%% Load file
%-----

freq=[64 135 173 434]*10^6; % carrier freq that are
used in matrix form
frequency =freq(freqUsed);
strFreq=strcat(num2str(frequency*10^-6),blanks(1),' MHz')

signal1 = td; % rename the
doppler signal

Samp_length = length ( signal1); % samples
length for the whole signal

%% Envelope
%-----

S1 = abs(hilbert(signal1)); % envelope of
the signal

[b4,a4] = butter(order2,co2/fs2,'low'); % Butterworth
filter coefficients for the signal
envF = filter(b4,a4,S1); % filtered
envelope

%% Find the signal's std, min and max of the envelope
%-----

signal = signal1(2401:length(signal1)); % cut the
transient part of the LPF
envelope = envF(2401:length(envF));

n1 = length (signal); % length of
signal after cut
t1=[0:dt:(n1-1)*dt];

```

```

        envmin = min(envelope)
% min value of the envelope
        envmax = max(envelope)
% max value of the envelope

        stdsignal = std(signal)
        dynamicrange = 10*log10 (envmax/envmin);

        storedy(j,1:length(dynamicrange)) = (dynamicrange);
% save and store all data in diff file name: exp; dynamic range = storedy
        storestdsignal(j,1:length(stdsignal))= (stdsignal);
% save storestdsignal
        storeenvmin(j,1:length(envmin))= (envmin);
        storeenvmax(j,1:length(envmax))= (envmax);

        Samp_length2 = length (storestdsignal);

%%-----
%% PSD
%%-----

S1 = abs(hilbert(signal)); % envelope of the
signal % signal
[b5,a5] = butter(order3,co3/fs2,'low'); % Butterworth
filter coefficients for the envelope's psd
envF1 = filter(b5,a5,S1); % filtered
envelope

[d f] = pwelch(signal,[],[],[],fs); % to
find the PSD for the non stat clutter = [data freq]= pwelch ()

[d1 f1 ] = pwelch(envF1,[],[],[],fs); % to
find the PSD for the signal's envelope

%
% figure (100)
% plot (f, 10*log10(d),'b'), grid on, hold on,

% smooth PSD-----

        x = f;
% freq in x-axis
        y = d;
% data in y-axis

        y1 = smooth(y,101);
% smooth fxn for the data, Z = SMOOTH(Y,SPAN) smooths data Y using SPAN as
the number of points used to compute each element of Z.

% plot (f,10*log10(y1),'r')

%% Distributions
%%-----

```

```

%% histogram

S = storestdsignal; %
histogram for signal std
[intS,SA]= Histogram_uni(S, bin);

P = storeenvmin; %
histogram for signal env min
[intP,PA]= Histogram_uni(P, bin);
% Horizontal concatenation

Q = storeenvmax; %
histogram for signal env max
[intQ,QA]= Histogram_uni(Q, bin);

%% Weibull Distribution
%-----

%
[FF2,int2,Q3,fitb]= weibull_dist_uni(signal, n1, bin); % weibull pdf
distribution sub-function
%
storefitb(j,1:length(envmax))= fitb;

sprintf('%5.2f ' ,fitb) ;
strwbl=strcat(num2str(sprintf('(%5.2f' ,fitb)), ' shape factor)');
% to include the value of shape factor in the legend
% %
R = storefitb; %
histogram for signal shape factor
[intR,RA]= Histogram_uni(R, bin);

%-----
%% Plot all graphs

% figure (1)

% subplot(222)
% plot(f1,10*log10(d1), 'linewidth', 2), grid on,hold on,
% plotting PSD for the envelope
% title(strcat(strFreq, ' PSD for the Filtered Envelope '))
% legend('PSD with 0.1 Cut-off ')
% xlabel('Freq, Hz');
% ylabel('Power spectrum, dB');
% xlim([0 0.1]);
%
% subplot (223)

```

```

%           semilogx(f,10*log10(d)), grid on, hold on,
% plotting PSD for the signal
%           semilogx(f,10*log10(y1),'r','linewidth',2)
% plotting the smooth PSD for the signal
%           title(strcat(strFreq, ' PSD '))
%           legend('PSD with 0.08 Cut-off ')
%           xlabel('Freq, Hz');
%           ylabel('Power spectrum, dB');
%           xlim([10^-1 10^1]);
%
%           sprintf('%5.2f ',fitb) ;
%           strwbl=strcat(num2str(sprintf('(%5.2f ',fitb)), ' shape factor)');
%
%
%           figure (4)
%
%           semilogx(f,10*log10(y1),'g-','LineWidth',2.0), grid on,
%           xlim([10^-1 10^1]);
%           legend(strcat(strFreq,'PSD'))
%           xlabel('Freq, Hz');
%           ylabel('Power spectrum');
%           title(strcat( 'PSD for', blanks(1), strFreq,' Signal '))
%           hgsave (strcat(strFreq, ' PSD'))
%
end
a=[storestdsignal storeenvmin storeenvmax storedy storefitb];

savefile = 'test.mat';
save(savefile, 'a')

```

4. run_all_measured_clutter.m program

```

% load file from real signal for distribution analysis
% created by ayu
% date 2 July 2010

clear;
close all;

randn('state', 0);

%% Read the list of files to be processed
[listFileFull{1}, listFileShort{1}] = readListFile('radiodatalistnew.txt');

```

```

%% Parameters

Nfrequency1 = 1;                                % Frequency
used:1 = 64 MHz, 2= 135 MHz, 3= 173 MHz, 4= 434 MHz
sRate = 20;                                     % sampling Rate
vlight= 3*10.^8;                                % speed of
light
fs=sRate;                                       % sampling
frequency
fs2=fs/2;                                       % nyquist
dt = 1/(fs);
bin = 500;

%% Get data from list of files in subfunction
%-----

[signal,storedy, storeenvmin, storeenvmax, storestdsignal,
storefitb,SA,PA,QA,RA,intS,intP,intQ,intR,Fitw,strFreq,R,g1,m1,q1,r1] =
real_signal_processing_4Aug10(listFileFull{1},Nfrequency1,sRate);

Samp_length = length (signal);
Samp_length2 = length (storestdsignal);

%-----
%% Plot all graphs

figure (1)

subplot(221)
plot(storestdsignal);
title(strcat('Signal STD', blanks(2), strFreq,' Channel '));
xlabel('Number of Records');
xlim ([0 281])
grid on;

% minenv = sprintf('%15.4f ',storeenvmin);

subplot(223)

plot (storeenvmin)
title(strcat('Envelope Min ', blanks(2), strFreq,' Channel '));

```

```

xlabel('Number of Records');
ylabel('Amplitude,V');
grid on;
xlim ([0 281])

% maxenv = sprintf('%15.4f ' ,storeenvmax);

subplot(224)

plot (storeenvmax)
title(strcat('Envelope Max ', blanks(2), strFreq,' Channel '));
xlabel('Number of Records');
ylabel('Amplitude,V');
grid on;
xlim ([0 281])

subplot(222)

plot (storefitb)
title(strcat('Weibull Shape Factor ', blanks(2), strFreq,' Channel '));
ylabel('Shape factor');
xlabel('Number of Records');
xlim ([0 281])
grid on;

hgsave (strcat(strFreq, ' Signal all'))
% drange = abs (storedy);

figure (2)

plot (storedy)
title(strcat('Dynamic Range ', blanks(2), strFreq,' Channel '));
xlabel('Number of Records');
ylabel('dB');
grid on;

hgsave (strcat(strFreq, ' Dynamic Range'))

figure (3)

subplot (221)

% [G w] = hist(storestdsignal,bin);
% built histogram; Q = frequency counts, b = bin locations.
%             hbinWidth = w(2) - w(1);
% bin width
%             htotCount = sum(G);
%             Hist = G/htotCount;
%

```

```

plot(intS,SA,'r','linewidth',2), hold on, grid on,
% plot(w,Hist,'r','linewidth',2), hold on, grid on,
% std plot histogram with normrnd distribution fit for the signal
title(strcat( ' Distribution for ', strFreq,' Channel '))
xlabel('STD');
ylabel('PDF');

subplot (223)

plot(intP,PA,'r','linewidth',2), hold on, grid on,
% envmin plot histogram with normrnd distribution fit for the signal
title(strcat( ' Distribution for ', blanks(1), strFreq,' Channel '))
xlabel('Envmin');
ylabel('PDF');

subplot (224)

plot(intQ,QA,'r','linewidth',2), hold on, grid on,
% envmax plot histogram with normrnd distribution fit for the signal
title(strcat( ' Distribution for ', blanks(1), strFreq,' Channel'))
xlabel('Envmax');
ylabel('PDF');

subplot (222)

plot(intR,RA,'r','linewidth',2), hold on, grid on,
% shape factor histogram with normrnd distribution fit for the signal
title(strcat( ' Distribution for ', blanks(1), strFreq,' Channel '))
xlabel('Shape Factor');
ylabel('PDF');

hgsave (strcat(strFreq, ' Histograms'))

figure (4)

subplot (221)
plot(intS,g1,'g','linewidth',2), grid on, hold on, %
plot histogram with weibull distribution fit for stationary
% plot histogram with normrnd distribution fit
legend(strcat(strFreq))
title(strcat( 'STD CDF for ', strFreq,' Channel '))
xlabel('Amplitude,V');
ylabel('CDF');

subplot (222)
plot(intR,r1,'b','linewidth',2), grid on, hold on,
legend(strcat(strFreq))
title(strcat( 'Shape factor CDF for ', strFreq,' Channel '))
xlabel('Amplitude,V');
ylabel('CDF');

subplot (223)

```

```

plot(intP,m1,'m','linewidth',2), grid on, hold on,
legend(strcat(strFreq))
title(strcat( 'Env Min CDF for ', strFreq,' Channel '))
xlabel('Amplitude,V');
ylabel('CDF');

subplot (224)
plot(intQ,q1,'b','linewidth',2), grid on, hold on,
legend(strcat(strFreq))
title(strcat( 'Env Max CDF for ', strFreq,' Channel '))
xlabel('Amplitude,V');
ylabel('CDF');

hgsave (strcat(strFreq, ' cdf'))

figure (5)

[h,r] = ecdf(storestdsignal);

subplot (221)

plot (r,h,'g', 'LineWidth',3), grid on, hold on,

cdfplot(storestdsignal), grid on, hold on, % plot
histogram with weibull distribution fit for stationary
% plot histogram with normrnd distribution fit
legend(strcat(strFreq))
title(strcat( 'STD CDF for ', strFreq,' Channel '))
xlabel('Amplitude,V');
ylabel('CDF');

subplot (222)
cdfplot(storefitb), grid on, hold on,
legend(strcat(strFreq))
title(strcat( 'Shape factor CDF for ', strFreq,' Channel '))
xlabel('Amplitude,V');
ylabel('CDF');

subplot (223)
cdfplot(storeenvmin), grid on, hold on,
legend(strcat(strFreq))
title(strcat( 'Env Min CDF for ', strFreq,' Channel '))
xlabel('Amplitude,V');
ylabel('CDF');

subplot (224)
cdfplot(storeenvmax), grid on, hold on,
legend(strcat(strFreq))

```

```

title(strcat( 'Env Max CDF for ', strFreq, ' Channel '))
xlabel('Amplitude,V');
ylabel('CDF');

```

```

hgsave (strcat(strFreq, ' empirical cdf'))

```

5. readListFile.m Program

```

%%
%% function [listFile] = readListFile(fileName_listFile)
%%
%% Reads the list of files to be processed and stores in the variable
%% listFile
%%
%% Input:
%%
%% Returns: listFile
%%
%% created by Peter Jancovic, 12 Feb 2008
%%

function [listFileFull, listFileShort] = readListFile(fileName_listFile)

fid = fopen(fileName_listFile, 'rt');

i=1;
while feof(fid)==0
    fn_inp = fscanf(fid,'%s',1);
    fn_inp = strrep(fn_inp,'/','\');
    listFileFull{i} = fn_inp;
    %% Extract only the name of the file (no directory, no extension);
    %% assuming the extension is 3 letters long
    fn_inp_short = fn_inp(max(findstr(fn_inp,'\'))+1:end-4);
    listFileShort{i} = fn_inp_short;
    i=i+1;
end

fclose(fid);

```

APPENDIX B

1. Data Processing Real Measurement

Data processing will be explained in detail in this appendix. This is used for short term and long term measurement. The process includes the analysis to check the power level, power spectrum density, amplitude distribution and many more. It is divided into two main stages:

- iii. Stage 1: Data acquisition
- iv. Stage 2: Data analysis

Stage 1: Data Acquisition

This stage is the first stage of data processing part. The entire received signal will be stored in computer database that connected to the receiver. To collect the data, first the equipment (3 channels or 4 channels equipment) is connected to the computer. Install Calc program is used to detect the equipment. After the equipment has been detected, the Data Collection program is used to monitor the received signals. This Data Collection program is developed by MISL group using Mathcad Software and is used in this research. Layout of the program is displayed in Figure 1. There are few input value that need to be enter in this program such as the file name, the sampling frequency and the numbers of samples in data acquisition box (all shown in Figure 2(a) and 2 (b)). After all the input values are keyed in, then the program can be run. The output result of the signals from all the channels will be displayed as in Figure 3.

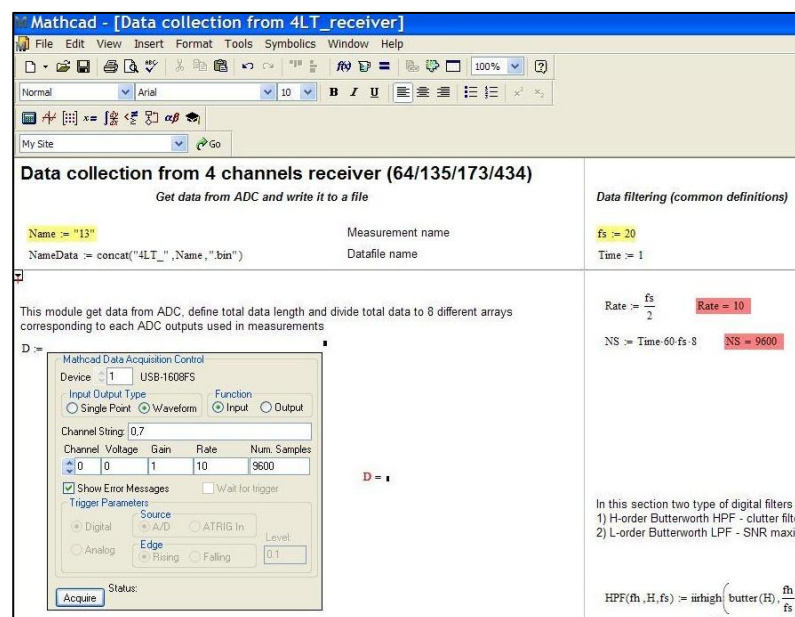
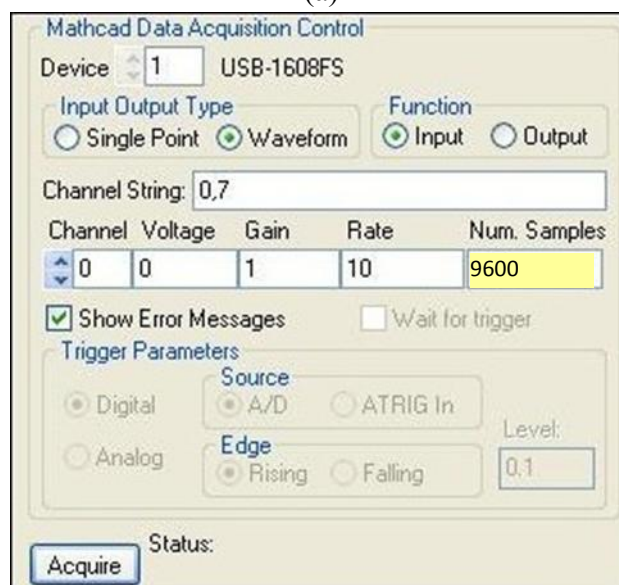


Figure 1: Data collection program layout

Name := "13"	Measurement name	fs := 20
NameData := concat("4LT_", Name, ".bin")	Datafile name	Time := 1

(a)



Mathcad Data Acquisition Control

Device: 1 USB-1608FS

Input Output Type: ☐ Single Point ☒ Waveform

Function: ☒ Input ☐ Output

Channel String: 0,7

Channel	Voltage	Gain	Rate	Num. Samples
0	0	1	10	9600

☒ Show Error Messages ☐ Wait for trigger

Trigger Parameters:

Source: ☒ Digital ☐ A/D ☐ ATRIG In

Edge: ☒ Rising ☐ Falling

Level: 0.1

Acquire Status:

(b)

Figure 2: (a) Insert file name and sampling frequency (fs), (b) Data Acquisition table to include number of samples

The Receive Signal Strength Indicator (RSSI) signals are displayed in this program to view the power strength of each received signal. The power level for each channel output is used to estimate the power of direct leakage signal that are collected during the experiment. Receiver gain that attained by extra attenuators are installed between antenna and channel input connector. This is to keep the signal in linear detection range. Refer to Figure 3 to view the linear detection range level.

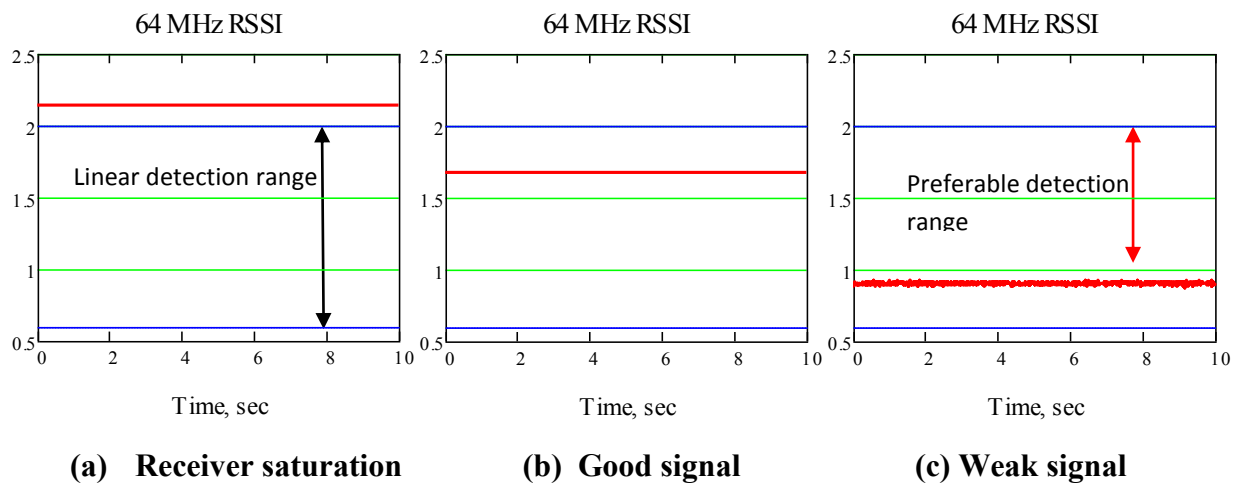


Figure 3: RSSI level estimation examples

Figure 3 shows the examples of 64 MHz received signal in the program with three different results. It is a voltage versus time (in second) graph. If the RSSI signal level (voltage, marked in red colour line) exceeds the saturation level for linear detection band (marked in blue), normally the signal is having receiver saturation and there is distortion to the signal. An extra attenuator should be added to the equipment at particular frequency to prevent this from happening (Figure 3 (a)). When the RSSI signal level is a bit spiky and nearly to the minimum value of linear detection range, this signal is considered as weak signal where there is strong background noise are picked up from surrounding area (Figure 3 (c)). Good signal is when the RSSI level is more or less 80% from the linear detection range (Figure 3 (b)). This is the first process to check the incoming signal from the equipment. After this process, the next received signals will be kept as database in the computer in different file name for the next process.

Then in the next process, all the signals that are kept in the database are viewed using Data Visualization program. This program also developed by MISL Group and used in this research. In this program, all RSSI signals and Doppler signals will be viewed for all frequencies. The signals are displayed in power versus time (sec) in Figure 4. Further analysis of all the signals are continued with the next stage.

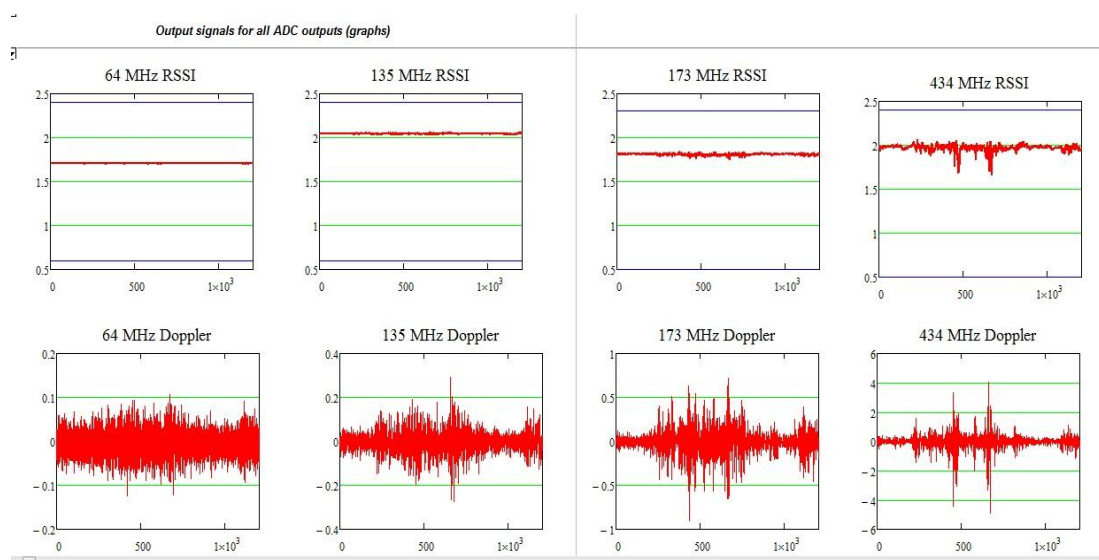


Figure 4: RSSI and Doppler signals in Data Visualization program for all channel frequencies.

Stage 2: Data Analysis

There are two types of data that are analysed. One is the short measurement data and another set of data is the long term measurement data.

i. Short Term Measurement

Short term measurement is set in several places with 20 minutes long for each data. In these measurement, there are two main analyses need to be done. The first one is to carried out analysis for target detection and second is for clutter analysis.

a. Target Detection Analysis

In this analysis, Mathcad software is used to display and analyse the received signal. The program is called as Target_Det_only program. This program contained non-coherent and cross-correlation processing for target detection. Step by step on how to use this program is as below:

Step 1: Open program file with the name of Target_Det_only. The program will be displayed as in Figure 5.

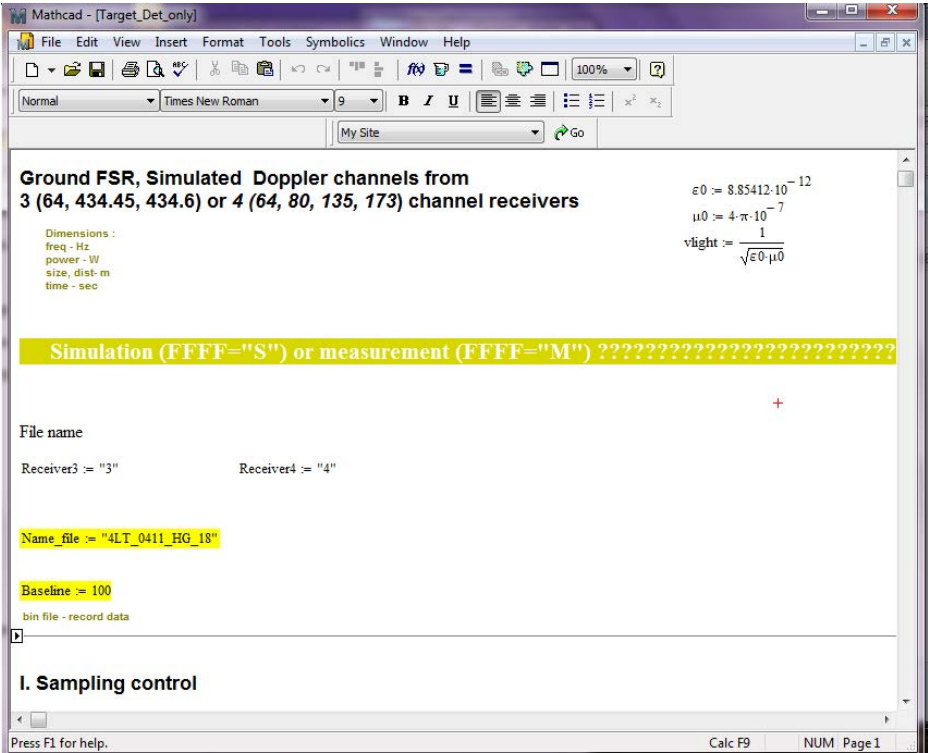


Figure 5: Target_Det_only program using Mathcad software

Step 2: Then insert the file name and the sampling frequency used as example shown in Figure 6 where file 4LT_0411_HG_18 is used with 40 Hz sampling frequency.

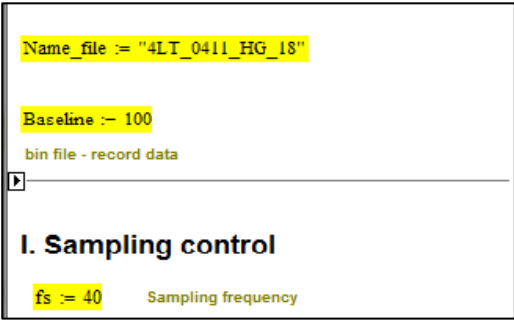


Figure 6: Insert file name and sampling frequency

Step 3: After everything is keyed in, all signals will be displayed. Desired signal display starting point and stop point also can be inserted here in yellow highlight shown in Figure 7.

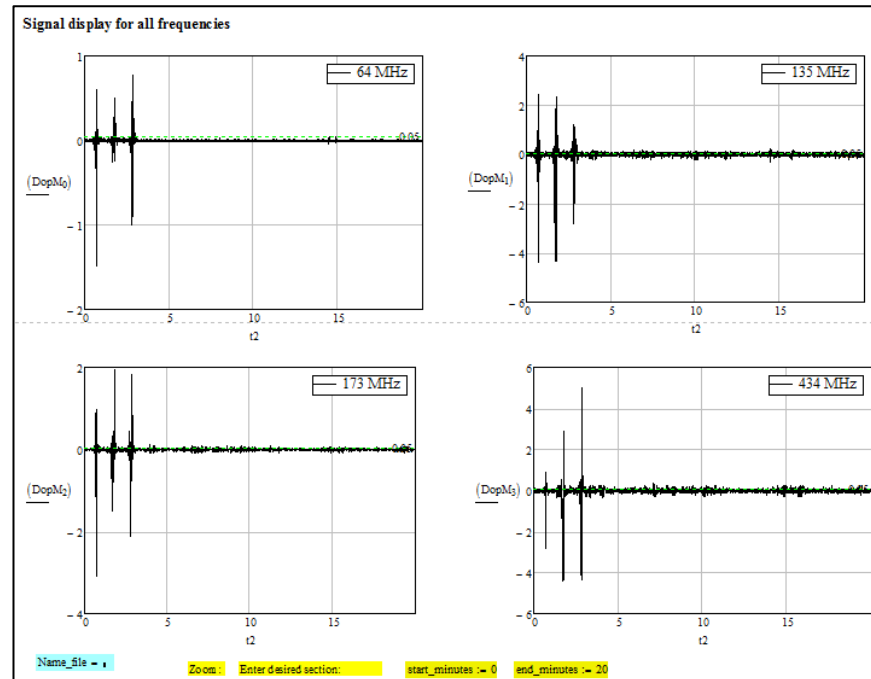


Figure 7: Signal displayed for 64 MHz, 135 MHz, 173 MHz and 434 MHz

Step 4: Finally the detected signal using non-coherent and cross-correlation processing are displayed as shown in Figure 8. In this example the non-coherent graph is displaying 434 MHz channel frequency. The required channel frequency is displayed according to the number entered in the yellow highlighted box. Numbers 0 to 3 represent frequency use. For non-coherent process; 0 is for 64 MHz, 1 is for 135 MHz, 2 is for 173 MHz and 3 is for 434 MHz frequency. While for cross-correlation process numbers represent pair of frequencies such as 0 for 64 MHz and 135 MHz, 1 is for 135 MHz and 173 MHz, 2 is for 173 MHz and 434 MHz and last number 3 is for 64 MHz and 173 MHz.

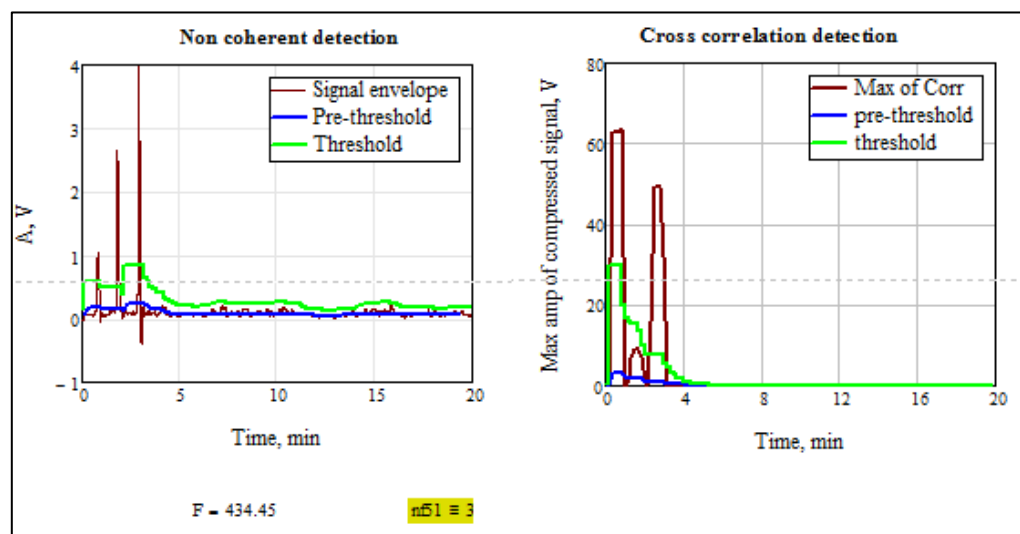


Figure 8: Detection results using non-coherent and cross correlation process

b. Clutter Analysis

In short measurement clutter analysis, all data are processed using Real Signal Processing program developed by using MATLAB Software. The layout of the program is shown in Figure 9. In this program all parameters such as operating frequency, equipment module (3 channels or 4 channels), sampling rate, time for each data, cut-off frequency for the filters and number of bins used for Weibull distribution are keyed in. Step-by-step instructions on how to process the data are described below

Step 1: Open `real_signal_processing.m` file using MATLAB software. Program layout will be displayed as Figure 9.

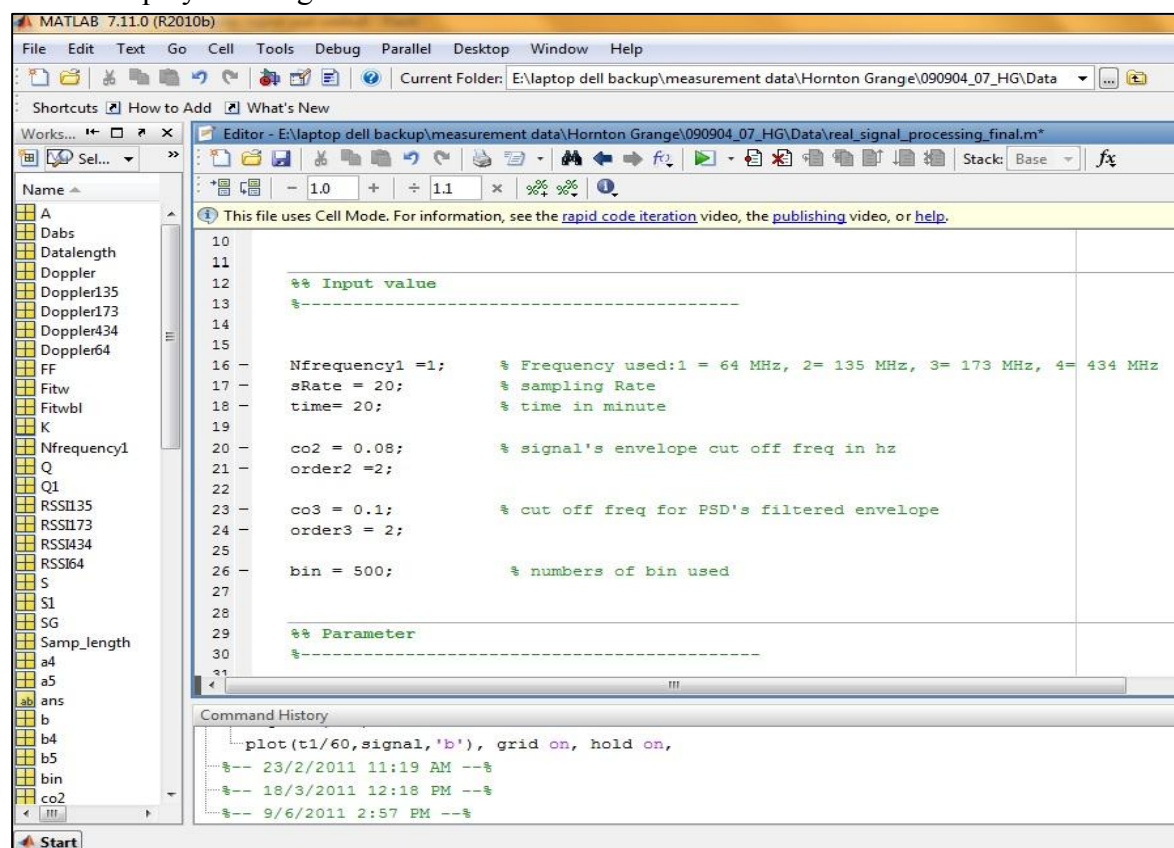


Figure 9: Real signal processing program layout using MATLAB Software

Step 2: Insert the operating frequency (`Nfrequency1`) used such as 1 for 64 MHz, 2 for 135 MHz, 3 for 173 MHz and 4 for 434 MHz.

Step 3: Insert the sampling rate (`sRate`) and the time duration of each file (normally `sRate` is 20 Hz and time is 20 minutes) as shown in Figure 10.

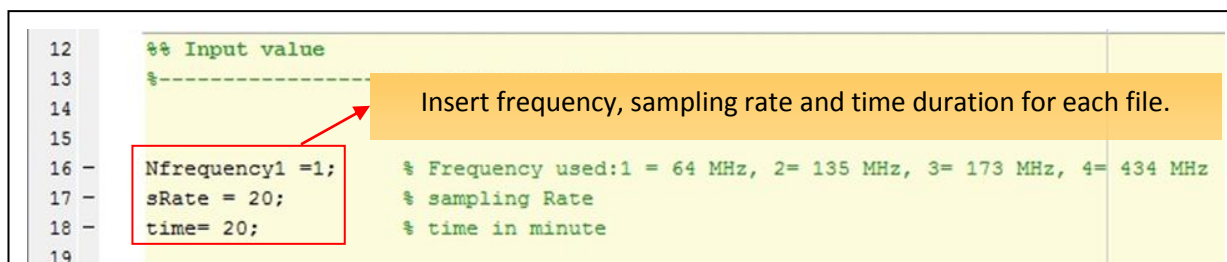


Figure 10: Input value for the operating frequency used

Step 4: Then the filename is inserted in the program. The filename is depend on which module that is used; 4LT for 4 channels and 3LT for 3 channels module and followed by file number. This data file is using bin extension file (.bin). The MATLAB function is shown in Figure 11.

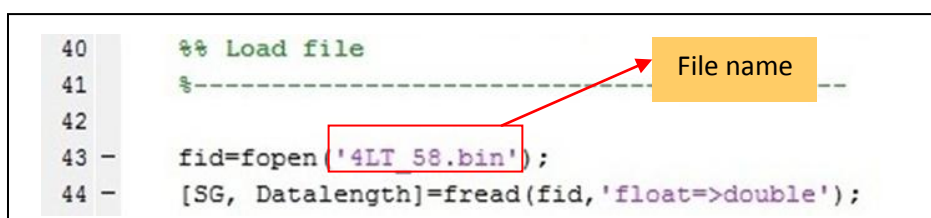


Figure 11: Load filename

Step 5: Next step is to display all the signals in the data file which include 64 MHz, 135 MHz, 173 MHz and 434 MHz. This is just to make sure that the signal is good for the next process (signal is not corrupted by noise or interference). See Figure 12 for the example of signals displayed.

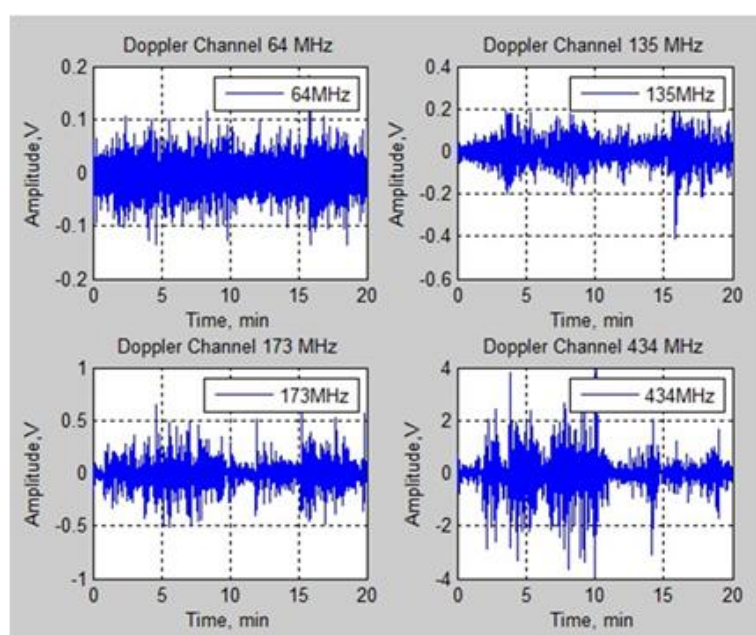


Figure 12: Doppler signal for 64 MHz, 135 MHz, 173 MHz and 434 MHz

Step 6: Now the next step is to find envelope's minimum and maximum value, (envmin, envmax), signal's standard deviation (stdsignal), signal's dynamic range of the envelope (d_range) and the mean value (mu). Refer Figure 13 for the coding in MATLAB.

```

143      %% Find the signal's std, min and max of the envelope
144      %-----
145
146      envmin = min (envelope)           % average minimum
147      envmax = max (envelope)           % average maximum
148      stdsignal = std(signal)           % signal STD
149      d_range = 10*log10 (envmax/envmin) % signal dynamic range
150      mu = mean (signal);               % mean value

```

Figure 13: Signal's STD, dynamic range, mean value, envelope's minimum and maximum input value

Step 7: Power Spectral Density (PSD). The signal's envelope is filtered using Butterworth filter using cut-off frequency of 0.1 Hz. Then the Pwelch function is used to find PSD of non-stationary clutter signal and the envelope of the signal as displayed in Figure 14.

```

153      %% PSD
154      %-----
155
156
157      [b5,a5] = butter(order3,co3/fs2,'low'); % Butterworth filter
158      envF1 = filter(b5,a5,S1);               % filtered envelope
159
160      [d f] = pwelch(signal,[],[],[],fs);      % PSD of non-stationary
161
162      [d1 f1] = pwelch(envF1,[],[],[],fs);    % PSD for envelope
163

```

Filter the envelope with 0.1 Hz

PSD of non-stationary

PSD for envelope

Figure 14: Signal's power spectral density input value

Step 8: Weibull Distribution will be the next step in this stage. In this distribution function which already developed in MATLAB function, Hilbert transform is used to find the envelope of the Doppler signal. Then the absolute value of the Hilbert Transform is used to build the histogram with the number of bin specified earlier in this program (Figure 15). Now the Weibull fit is include in the histogram graph with the fit is automatically search using Weibull fit function (wblfit). Last both the histogram and the Weibull fit is displayed in a graph as shown in Figure 17.

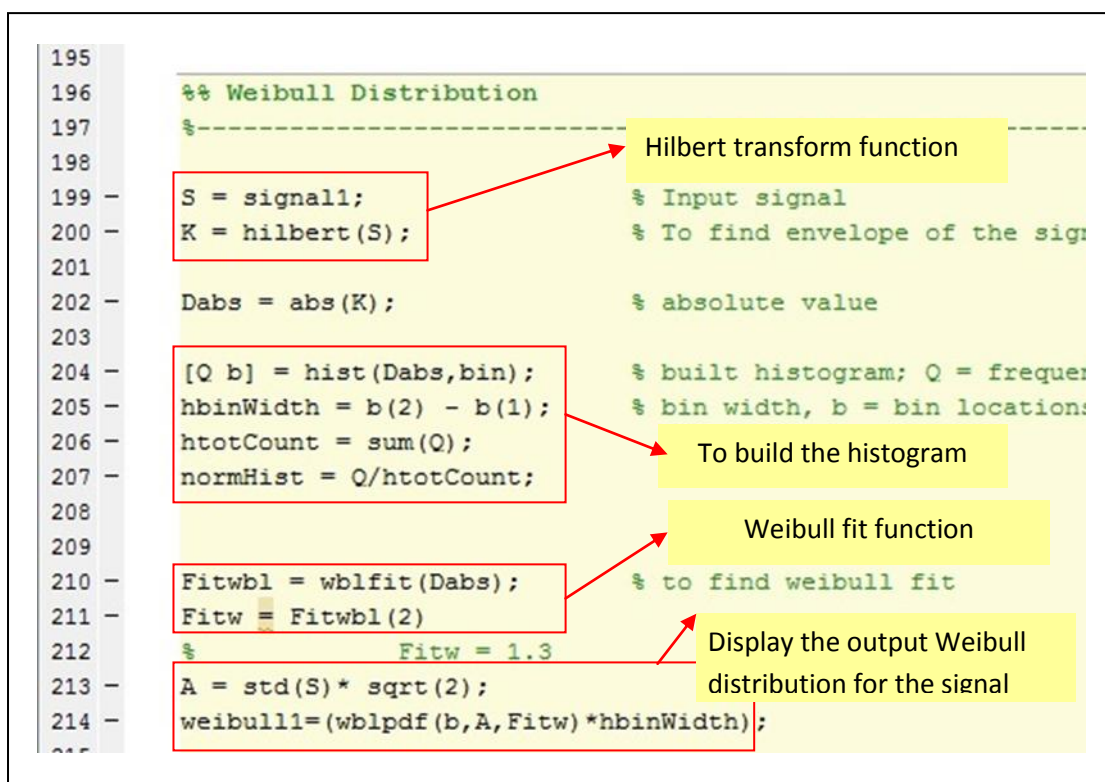


Figure 15: Weibull distribution

Step 9: This step is to find the Cumulative Distribution using build function in MATLAB (Figure 16).

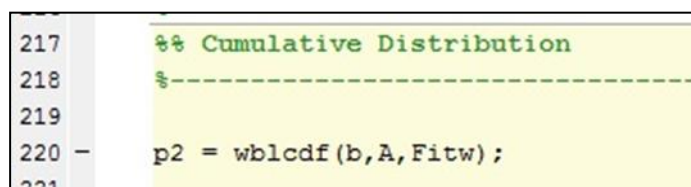


Figure 16: Cumulative distribution

Step 10: Last step is to display all the main graphs in the program which include non-stationary signal with envelope, PSD for the filtered envelope with 0.1 Hz cut-off and PSD for the signal and last the Weibull distribution with Weibull fit. Figure 17 shows the example of all the graphs for 64 MHz signal.

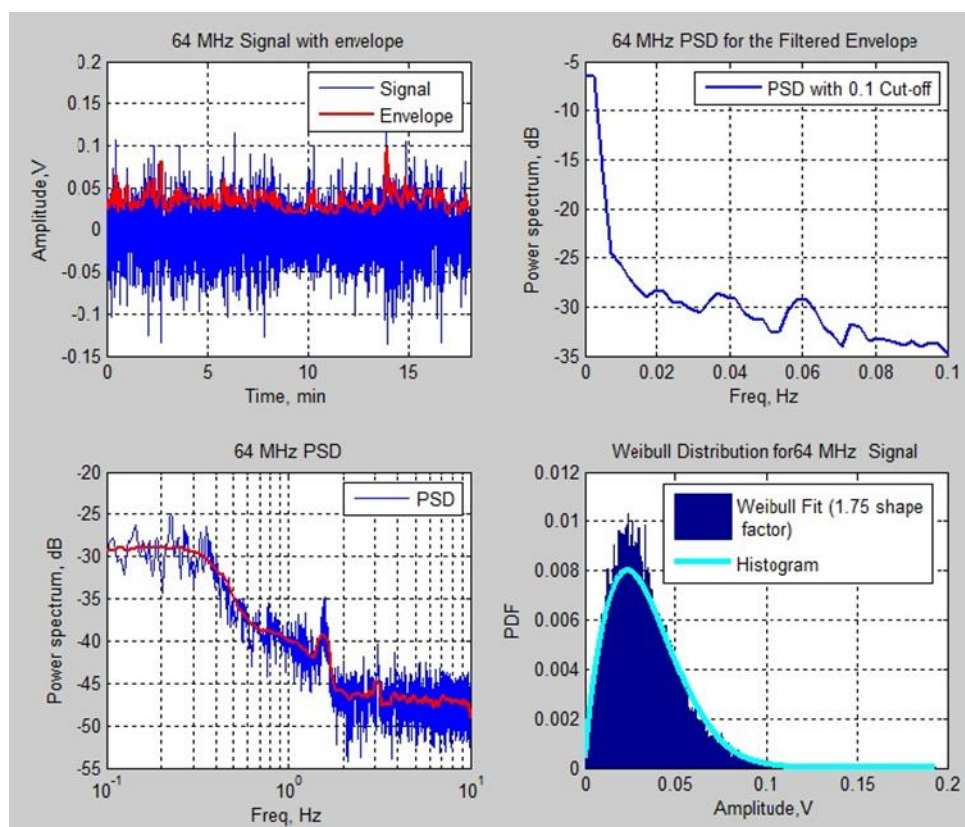


Figure 17: All output signals

ii. Long Term Measurement

In long term measurement the program is a bit different even though there are some part of it is still the same. In this measurement program, it is developed to read all the data files in one time. There is one main program and two main sub-functions. The main program is used to call the two main sub-functions and to display all the output graphs. Step-by-step instructions on how to process the data are described below (long term measurement full program can be view in detail in Appendix A):

Step 1: Open the long term measurement main program (run_all_measured_cluttersignal.mat). Insert all the input value such as the frequency used, sampling rate and numbers of bin used. Figure 18 displayed the main layout of the program with two sub-functions and input values are highlighted in red boxes.

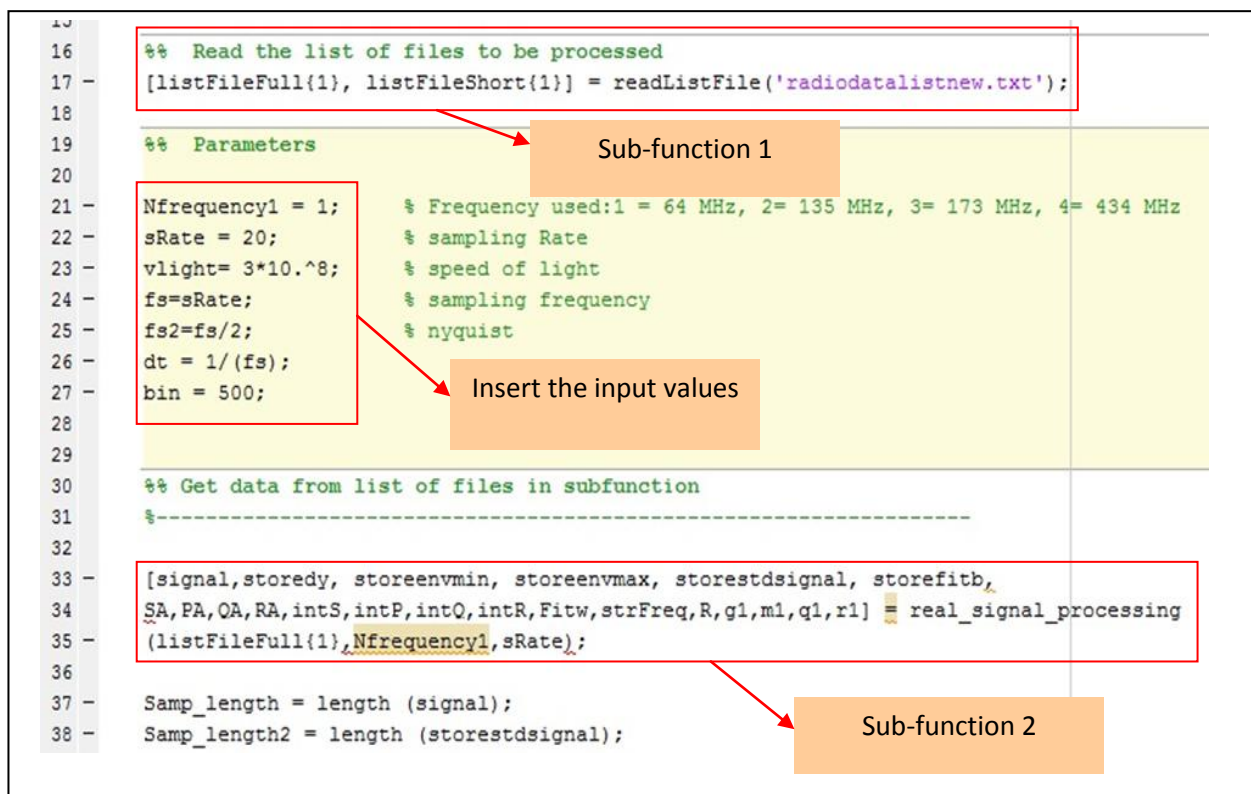


Figure 18: Main program of long term measurement (run_all_measured_cluttersignal.mat)

Other steps will be continued in the next sub-function part.

The two main sub-functions used are:

a. readListFile.mat (Sub-function 1)

This sub-function was created earlier by one of the group member in MISL Group. I used this function to call all the data file in my database. This is much simpler rather than open and analyse each files one by one. In this sub-function it will read all the data file name that is written in radiodatalist.txt file that is saved in the same folder. Radiodatalist file content all the data filenames that need to be process. This is shown in Figure 19 and Figure 20.

```

15 function [listFileFull, listFileShort] = readListFile(fileName_listFile)
16
17 fid = fopen(fileName_listFile, 'rt');
18
19 i=1;
20 while feof(fid)==0
21     fn_inp = fscanf(fid, '%s', 1);
22     fn_inp = strrep(fn_inp, '/', '\');
23     listFileFull{i} = fn_inp;
24     %% Extract only the name of the file (no directory, no extension);
25     %% assuming the extension is 3 letters long
26     fn_inp_short = fn_inp(max(findstr(fn_inp, '\'))+1:end-4);
27     listFileShort{i} = fn_inp_short;
28     i=i+1;
29 end
30
31 fclose(fid);

```

Figure 19: Read list file function

Step 2: In this step, the program will go to sub-function 1 (readListFile.mat). In this sub-function it will read all the data filenames that have been written in radiodatalist.txt file before it sent all the data to sub-function 2.

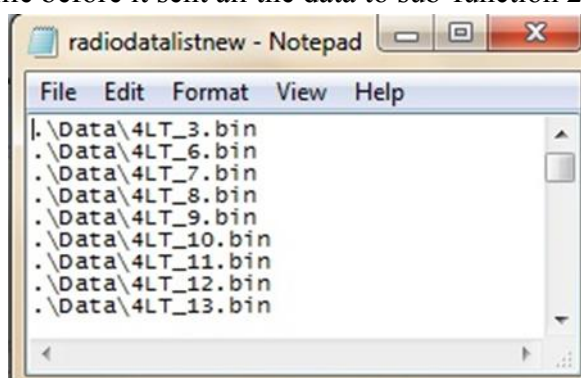


Figure 20: Radiodatalist file (.txt file format)

b. real_signal_processing.mat (Sub-function 2)

In this sub-function (Figure 21), it processes all the data file for the current directory one by one in one time. In here, the signal's STD, envelope minimum and maximum, PSD and the shape factor will be analysed same as in short measurement program. The only difference in here is the data signals are combined among few hundreds of data files and run simultaneously. All the results will then transfer back to the main program in run_all_measured_cluttersignal.mat.

```

9      function [signal,storedy, storeenvmin, storeenvmax, storestdsignal,
10              storefitb,SA,PA,OA,RA,intS,intP,intQ,intR,Fitw,strFreq, R,g1,m1,q1,r1]
11      = real_signal_processing(listFileFull,freqUsed,co2, co3, bin, sRate)
12
13      %% Input value
14      %-----
15
16
17      order2 =2;
18      order3 = 2;
19
20      vlight= 3*10.^8; % speed of light
21      fs=sRate;      % sampling frequency
22      fs2=fs/2;
23      dt = 1/(fs);
24
25      dataDir = listFileFull{1}(1:max(findstr(listFileFull{1},'\')));
26      nFiles = length(listFileFull);

```

Figure 21: Real_signal_processing sub-function program

Step 3: All data files are combination of Doppler signal and RSSI of 8 signals (for 4 channels equipment, 2 signals for each frequency). In this step, shown in red box in Figure 22, the Doppler signal is extract and analyse. Then the Doppler signal is renamed as signal1 for next process.

```

44      %% Process the target signals for the current directory
45
46      for j=1:nFiles;
47          %% Read the binary file containing 8 target signals (doppler, RSSI)
48          fileName = listFileFull{j};
49          fileNameShort = fileName(max(findstr(fileName,'\'))+1:end);
50          [data] = readTargetSignalBin(fileName, 8);
51          doppler = data(freqUsedInd,:);
52
53          %% Load file
54          %-----
55
56          freq=[64 135 173 434]*10^6; % carrier freq that are used in matrix form
57          frequency =freq(freqUsed);
58          strFreq=strcat(num2str(frequency*10^-6),blanks(1),' MHz')
59
60          signal1 = doppler; % rename the doppler signal
61          Samp_length = length ( signal1); % samples length for the whole signal

```

Figure 22: Function to extract Doppler signal from the data file

Step 4: Hilbert function is used to find the envelope of the signal. Then the envelope will go through filtering process with cut-off frequency of 0.08 Hz (Figure 23).

```

63 %% Envelope
64 %-----
65
66 - S1 = abs(hilbert(signal1));
67
68 - [b4,a4] = butter(order2,co2/fs2,'low');
69 - envF = filter(b4,a4,S1);

```

Figure 23: To find envelope using Hilbert Transform

Step 5: First part of this section shown in Figure 24 is a function to cut the transient part of the signal after going through low pass filter. The second section is to find the envelope's minimum and maximum value (envmin and envmax respectively), standard deviation (std) of the signal and the dynamic range of the signal's envelope.

```

72 %% Find the signal's std, min and max... of the envelope
73 %-----
74
75 - signal = signal1(2401:length(signal1)); % cut the transient part of the L
76 - envelope = envF(2401:length(envF));
77
78 - n1 = length (signal); % length of signal after cut
79 - t1=[0:dt:(n1-1)*dt];
80
81 - envmin = min(envelope) % min value of the envelope
82 - envmax = max(envelope) % max value of the envelope
83 - stdsignal = std(signal)
84 - dynamicrange = 20*log10 (envmax/envmin);

```

Cut the transient part

Find envmin, envmax, std and dynamic range

Figure 24: Function to find signal's envelope minimum and maximum, STD and the dynamic range

Step 6: The next step is to stored all the data in a file (test.mat) for further analysis and for database collection (Figure 25).

```

86 - storey(j,1:length(dynamicrange)) = (dynamicrange);
87 - storestdsignal(j,1:length(stdsignal))= (stdsignal);
88 - storeenvmin(j,1:length(envmin))= (envmin);
89 - storeenvmax(j,1:length(envmax))= (envmax);

233 - a=[storestdsignal storeenvmin storeenvmax storedy
234     storefitb storefitbinWidth storemaxbinwidth
235     storeminbinWidth storestdbinwidth];
236
237 - savefile = 'test.mat';
238 - save(savefile, 'a')

```

Figure 25: Store all the data in text file for further analysis

Step 7: This step will be the same as short measurement program. First the signal (without the transient part) will go through again the Hilbert function to find the envelope of the signal. Then it will be passed to the low pass filter with cut-off frequency of 0.1 Hz before it is transferred to Pwelch command to find the power spectral density of the signal and for the envelope (Figure 26).

```

94 %% PSD
95 %-----
96
97 - S1 = abs(hilbert(signal));
98 - [b5,a5] = butter(order3,co3/fs2,'low');
99 - envF1 = filter(b5,a5,S1);
100
101 - [d f] = pwelch(signal,[],[],[],fs);
102
103 - [d1 f1] = pwelch(envF1,[],[],[],fs);
104

```

Figure 26: To find signal's PSD

Step 8: This step is a distribution process. In this process, it is used to find the histogram and cumulative distribution function (cdf) of the signal. Figure 27 shows the distribution process for standard deviation values. In here standard deviation value for all the data is process to find the histogram and the cdf. Then this process will be continued for envelope's minimum value, envelope's maximum value and the shape factor of Weibull distribution for all data.

```

121 % Distributions
122 %-----
123 %% histogram and CDF
124
125 % STD Histogram
126 %-----
127 S = storestdsignal;
128 [g intS] = hist(S,bin);
129 stdbinwidth = intS(2) - intS(1);
130 htotCount = sum(g);
131 SA = g/htotCount;
132
133 storestdbinwidth(j,1:length(stdbinwidth)) = (stdbinwidth);
134
135 % STD CDF
136 %-----
137 Fitwbl1 = wblfit(storestdsignal);
138 Fitw1 = Fitwbl1(2);
139 A1 = std(storestdsignal)* sqrt(2);
140 g1 = wblcdf(intS,A1,Fitw1);

```

Figure 27: Function to find histogram and CDF for overall signal's STD

Step 9: All the data are sent back to main program for graph display. After all the steps are followed, the result will be displayed as in Figure 28, Figure 29, Figure 30 and Figure 31. Further descriptions about the results are described in next chapter.

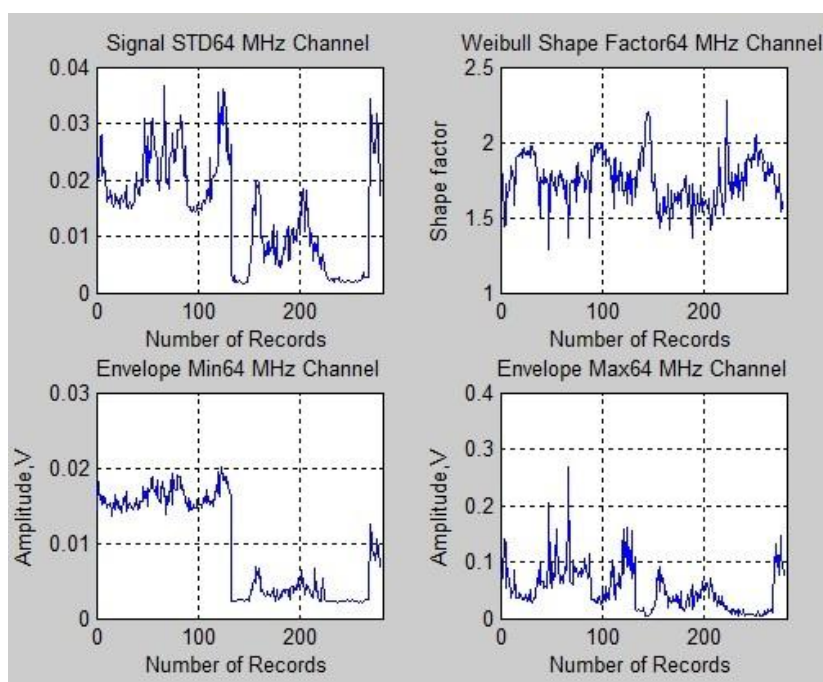


Figure 28: STD, envelope's minimum and maximum, shape factor values for each of the data for 278 data altogether

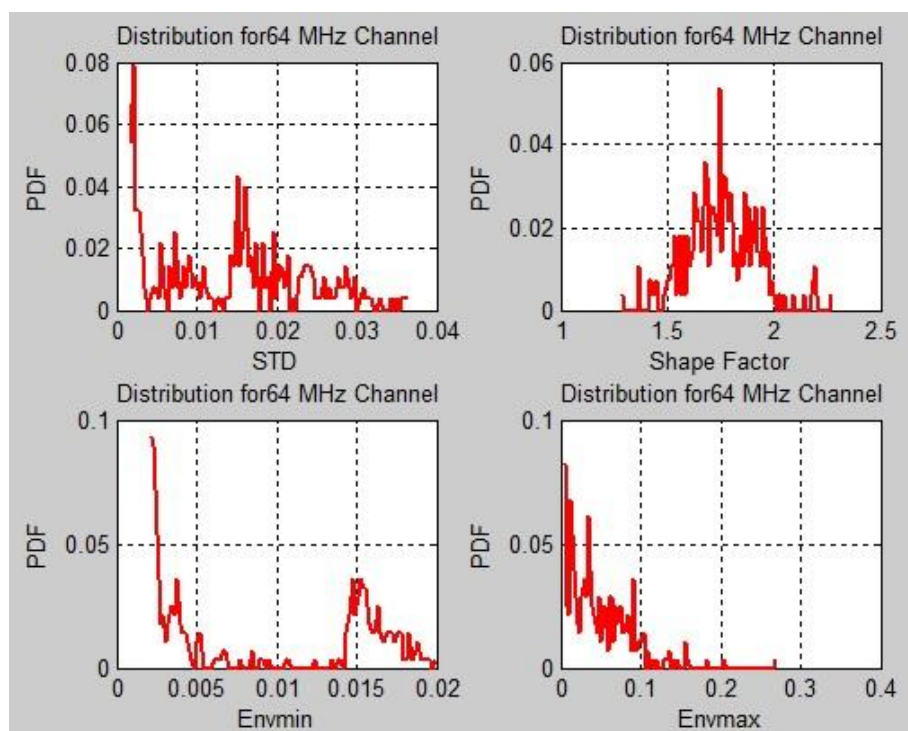


Figure 29: Histograms for STD, envelope's minimum and maximum, shape factor for all data

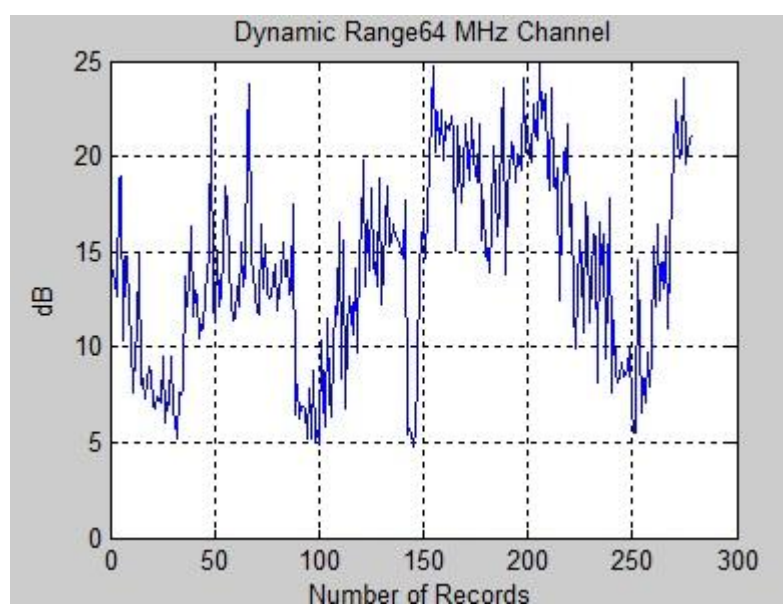


Figure 30: Dynamic range for 64 MH channel

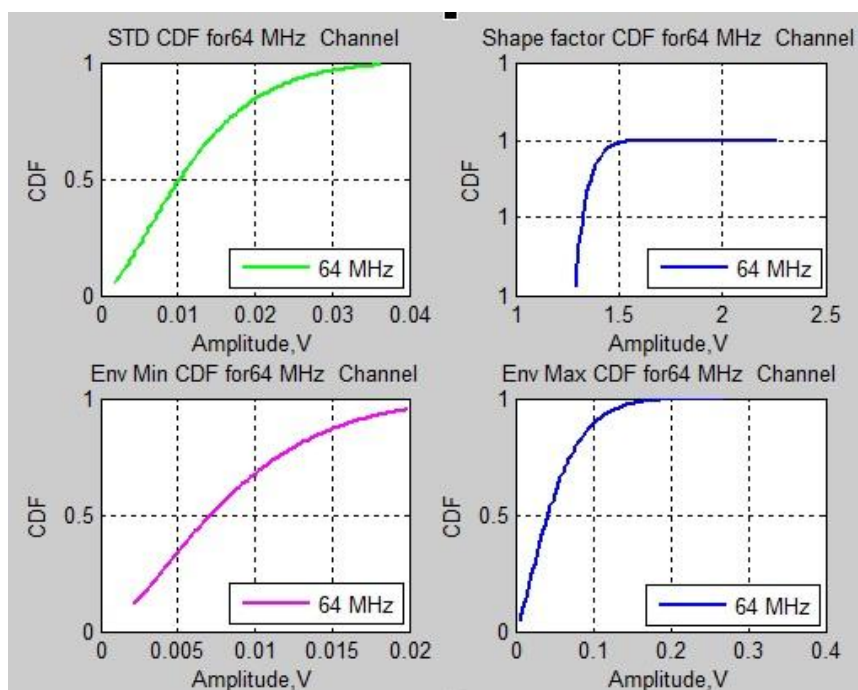


Figure 31: Cumulative distribution function for STD, envelope's minimum and maximum, shape factor for all data

2. Database Description

All collected raw data from the measurements are kept in computer databases in bin file format. The example of the file database that is stored in a folder is shown in Figure 32. This is the example from Horton Grange long term measurement folder from the measurement taken on 4th September 2009. The folder consists of 180 bin files. These are stored from the data collection program in the first stage.

Measurement's date		Name	Type	Size	Date modified
04.09.09 HG	26.08.09 HG	4LT_1.bin	BIN File	750 KB	4/9/2009 6:08 PM
		4LT_2.bin	BIN File	750 KB	4/9/2009 6:28 PM
		4LT_3.bin	BIN File	750 KB	4/9/2009 6:48 PM
	
		4LT_178.bin	BIN File	750 KB	7/9/2009 5:09 AM
		4LT_179.bin	BIN File	750 KB	7/9/2009 5:29 AM
		4LT_180.bin	BIN File	750 KB	7/9/2009 5:49 AM

File name

Figure 32: File database

A proper database records for each measurement are then written in Excel. Each database will have date, location, wind speed, time for each file start, baseline range, description for each file (such as any target detected), sampling frequency and many more. Layout of the description is shown in Figure 33. All databases for each measurement can be viewed in Appendix B. Figure 33 shown the example of long term measurement database taken in Horton Grange on several date. The layout only displayed the database for measurement taken on 13 to 16 November 2010.

1	Task:	Long term Clutter measurement			
2	Location:	Hornton Grange			
3	Date:	13-16/11/09			
4	Prog. Started at	13/11/09 (19:10)			
5	Prog. Finished at	16/11/09 (07:14)			
6	Total Data Record:	60 hours, 180 files each 20 minutes			
7	Wind Speed each day:	13/11/09 wind: 3 - 9 m/h (low),)			
8		14/11/09 wind: 1-13 m/h (low and medium), 15/11/09 wind:			
9		0 - 4 m/h (low), 16/11/09 wind: 0 - 4 m/h (low)			
10	Sampling Freq:	20 Hz			
11	Attenuators:	30dB 64RX; 10dB 135RX; 10dB 173RX; 20dB 434RX (directional antennas)			
12					
15		File	File Start	Descriptions	
16		(4LT_HG_)	Time		
17	Date			Target	BL Range (m)
18	13/11/2009	4LT_RSSI_5	19:10	Leakage level (RSSI)	1 min testing. 100
19		1	19:13	Clutter Measurement	100
20		2	19:33	Clutter Measurement	100
21		3	19:53	Clutter Measurement	100
22		4	20:13	Clutter Measurement	100
23		5	20:33	Clutter Measurement	100
24		6	20:53	Clutter Measurement	100
25		7	21:13	Clutter Measurement	100
26		8	21:33	Clutter Measurement	100
27		9	21:53	Clutter Measurement	100
<div> <div>13-16 Nov09</div> <div>03-04-Sept09</div> <div>04-07 Sept09</div> <div>21-22 Aug09</div> <div>26 Aug09</div> <div>04-09</div> </div>					

Other measurements from the same site

Figure 33: Long term measurement database

The next stage is the signal analysis results. This is done in the first stage of data processing in Data Visualization process. In this process, each the data signal is view to check any detections or the signal is pure clutter signal without any interference or detections. The results of the analysis are kept in database as shown in Figure 34 and Figure 35.

3. Clutter Generation Data Processing

This is the main part in clutter generation involved simulation process using Matlab program which is developed based on clutter generation model explained in previous Subtopic 7.2 in main thesis. Step by step process on how to generate clutter-like signal in Matlab program are explained as below:

Step 1: Need to key in all the input parameters such as the desired clutter level to be produced, frequency used, cut-off frequency for the envelope, sampling rate and time duration for each data in unit seconds or minutes (Figure 1).

```

22      %% Input value
23      %-----
24
25 -    clLevel = 1;      % clutter level: 1 = weak; 2 = medium; 3 = strong; 4 = very strong;
26 -    Nfrequency1 = 3; % Frequency used:1 = 64 MHz, 2= 135 MHz, 3= 173 MHz, 4= 434 MHz
27
28 -    cutFEnv=0.08;     % cutoff frequency for hilbert in 2nd stage
29 -    orderFEnv=2;     % 2nd order filter for hilbert in 2nd stage
30 -    sRate = 20;      % sampling Rate

```

Figure 1: Insert input values

Step 2: Insert all the parameters estimated from measured experiment including the cut-off frequency (CutF0), clutter standard deviation (stdClutter0), envelope's maximum (envRangeMax0), minimum (envRangeMin0) range and noise STD (fnoise0). All shown in Figure 2. Then all these parameters are rearranged to different 'name' for frequency and clutter strength insertion values (Figure 3).

```

67      %% measured clutter parameters
68
69 -    CutF0=[0.4 0.5 0.5 0.5; 0.5 0.5 0.5 0.5; 0.4 0.4 0.4 0.4;0.5 0.5 0.5 0
70 -    fNoise0=[0.001 0.001 0.001 0.001; 0.0015 0.002 0.0025 0.003; 0.0015 0.
71
72
73 -    envRangeMin0=[0.0024 0.0095 0.0118 0.0137; 0.0148 0.0861 0.0912 0.0773;
74
75 -    envRangeMax0=[0.0041 0.0228 0.0911 0.152; 0.0405 0.8593 1.0618 1.3007;
76
77 -    stdClutter0=[0.0016 0.0106 0.0252 0.0447; 0.1446 0.2518 0.3068 0.3234;
78

```

Figure 2: Measured clutter parameters

```

82 - stdNoise=fNoise0 (clLevel,Nfrequency1);
83 - stdClutter=stdClutter0 (clLevel,Nfrequency1);
84 - envRangeMin=envRangeMin0 (clLevel,Nfrequency1);
85 - envRangeMax=envRangeMax0 (clLevel,Nfrequency1);
86 - cutF=CutF0 (clLevel,Nfrequency1);
87 - fOrder=fOrder0 (clLevel,Nfrequency1);

```

Figure 3: All parameters are rearrange to new name for clutter level and frequency insertion

Step 3: this step is to generate stationary clutter. First is the generation of random AWGN with specific STD values (for different clutter strength and frequency) and numbers of samples. Then it will go through hardware and software filters using Butterworth filter (Figure 4).

```

93 - AWG=normrnd(0,stdClutter,1,nSamples);
94 - ScaleAWG=AWG;
95 -
96 - coh=0.25;
97 - [b2,a2] = butter(fOrder,coh/fs2,'high');
98 - clutterH = filter(b2,a2,ScaleAWG);
99 -
100 - col=9.9;
101 - [b1,a1] = butter(fOrder,col/fs2,'low');
102 - clutterL = filter(b1,a1,clutterH);
103 -
104 - [b3,a3] = butter(fOrder,cutF/fs2,'low');
105 - clutter = filter(b3,a3, clutterL);

```

Figure 4: Stationary clutter generation using AWGN clutter and the filters

Step 4: Generate clutter's envelope from the stationary clutter in step 3 for creating non-stationary clutter with real measured clutter parameter. In this stage (shown in Figure 5), the clutter is passing through sub-program (envelope3). In this program, Hilbert transform function is used. This is already described in Subtopic 7.2.2 in main thesis. Then the output clutter from this program (clutter's envelope) will modulated with normalised stationary clutter.

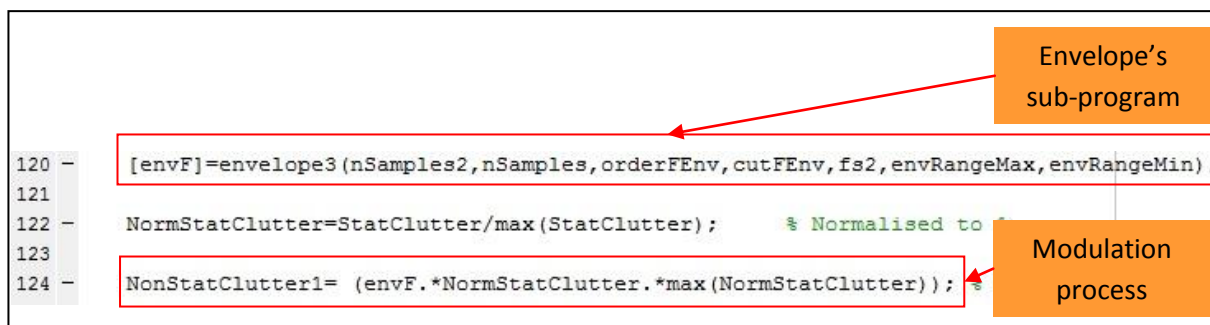


Figure 5: Modulation process of normalised stationary clutter with the clutter's envelope

Step 5: Adding random noise to non-stationary clutter Figure 6 to create real non-stationary clutter.

```

127 - noise=normrnd(0,stdNoise,1,nSamples);
128 -
129 - NonStatClutter= NonStatClutter1+noise;

```

Figure 6: Adding noise

Step 6: Generating non-stationary's envelope and then filter it. Then cutting the transient part of the clutter after going through LPF (Figure 7).

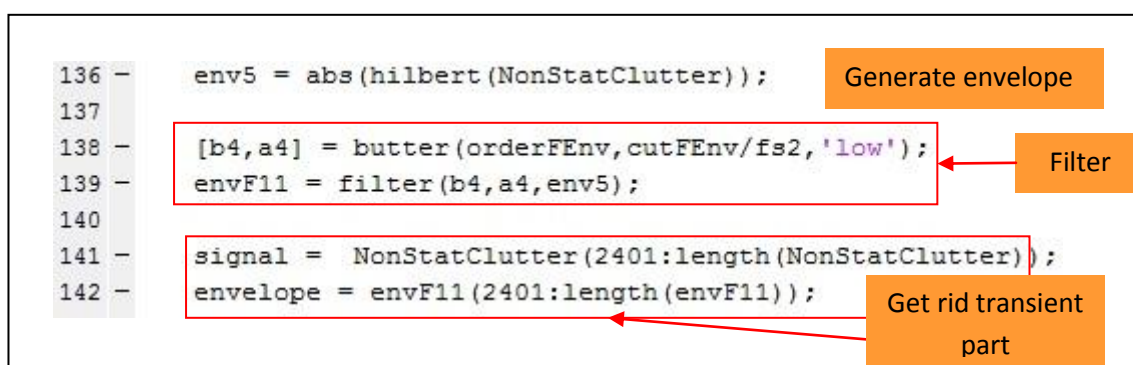


Figure 7: Generating envelope for the non-stationary clutter

Step 7: To find the clutter STD and envelope minimum and maximum values (Figure 8).

```

147 - stdNonClutter= std(NonStatClutter);
148 - minenvF11 = min(envelope)
149 - maxenvF11 = max(envelope)

```

Figure 8: determine clutters STD, envelope's minimum and maximum values

Step 8: This step is to find PSD of non-stationary clutter using Pwelch function and using smooth function to make the clutter smooth.

```

158 - [d f] = pwelch(NonStatClutter,[],[],[],fs);
159
160 - x = f;
161 - y = d;
162
163 - y1 = smooth(y,101);

```

Figure 9: Clutter's PSD

Step 9: Next is to find the PSD of the clutter with different cut-off frequency of 0.1 Hz. Then again go through pwelch and smooth function (Figure 10).

```

169 - co1 = 0.1;
170
171 - order1 = 2;
172 - [b5,a5] = butter(order1,co1/fs2,'low');
173 - envF12 = filter(b5,a5,env5);
174
175 - [d1 f1] = pwelch(envF12,[],[],[],fs);
176 - xx = f;
177 - yy = d;
178
179 - y2 = smooth(yy,101);

```

Figure 10: Clutter's PSD with cut-off frequency of 0.1 Hz

Step 10: This step is to display the amplitude distribution of non-stationary clutter. Weibull distribution is used in the analysis shown in Figure 11 for stationary and non-stationary clutters.

```

203 % Stationary-----
204
205 - [weibull1,b,normHist,Fitw]= weibull_dist_uni(signal3, bin);
206
207 % Non_Stationary-----
208
209 - [weibull2,b2,normHist2,Fitw2]= weibull_dist_uni(signal2, bin);

```

Figure 11: Weibull distribution function

Step 11: The final step is to plot the entire output graph (Figure 12).

```

211 %% Plot all graphs
212
213 - figure (3)
214
215 - subplot(221)
216
217 - plot(t1/60,signal,'b'), grid on, hold on,
218 - plot(t1/60,-envelope,'r','linewidth',2);
219 - title(strcat(strFreq, 'Clutter with envelope'))
220 - legend('NonStatClutter','Envelope')
221 - xlabel('Time, min');
222 - ylabel('Amplitude,V');
223
224 - subplot(222)
225
226
227 - plot(f1,10*log10(d1), 'linewidth', 2), grid on,hold on,
228 - title(strcat(strFreq, ' PSD for Clutter Envelope '))
229 - legend('PSD with 0.1 Hz')
230 - xlabel('Freq, Hz');
231 - ylabel('Power spectrum, dB');
232 - xlim([0 0.1]);

```

Figure 12: Plot all output graphs

4. Example of Long Term Database

All other databases will be in the CD

Task: Long term Clutter measurement

Location: Hornton Grange

Date: 03-04/11/09

Prog. Started at 03/11/09 (15:47)

Prog. Finished at 04/11/09 (10:27)

Total Data Record: 18 hours, 28 files each 40 minutes

Wind Speed: 03/11/09 wind: 0 - 13 m/h (low), 04/11/09 wind: 3 - 11 m/h (low)

Sampling Freq: 20 Hz

Attenuators: 30dB 64RX; 10dB 135RX; 10dB 173RX; 20dB 434RX (directional antennas)

Date	File (4LT_HG_)	File Start Time	Descriptions		BL Range (m)
			Target	Comments	
11/3/2009	4LT_RSSI_HG_1	15:36	Leakage level (RSSI)	1 min testing.	100
	0311HG_1	15:47	Clutter Measurement		100
	0311HG_2	16:27	Clutter Measurement		100
	0311HG_3	17:07	Clutter Measurement		100
	0311HG_4	17:47	Clutter Measurement		100
	0311HG_5	18:27	Clutter Measurement		100
	0311HG_6	19:07	Clutter Measurement		100
	0311HG_7	19:47	Clutter Measurement		100
	0311HG_8	20:27	Clutter Measurement		100
	0311HG_9	21:07	Clutter Measurement		100
	0311HG_10	21:47	Clutter Measurement		100
	0311HG_11	22:27	Clutter Measurement		100
	0311HG_12	23:07	Clutter Measurement		100
	0311HG_13	23:47	Clutter Measurement		100
11/4/2009	0311HG_14	0:27	Clutter Measurement		100
	0311HG_15	1:07	Clutter Measurement		100
	0311HG_16	1:47	Clutter Measurement		100
	0311HG_17	2:27	Clutter Measurement		100
	0311HG_18	3:07	Clutter Measurement		100
	0311HG_19	3:47	Clutter Measurement		100
	0311HG_20	4:27	Clutter Measurement		100
	0311HG_21	5:07	Clutter Measurement		100
	0311HG_22	5:47	Clutter Measurement		100
	0311HG_23	6:27	Clutter Measurement		100
	0311HG_24	7:07	Clutter Measurement		100

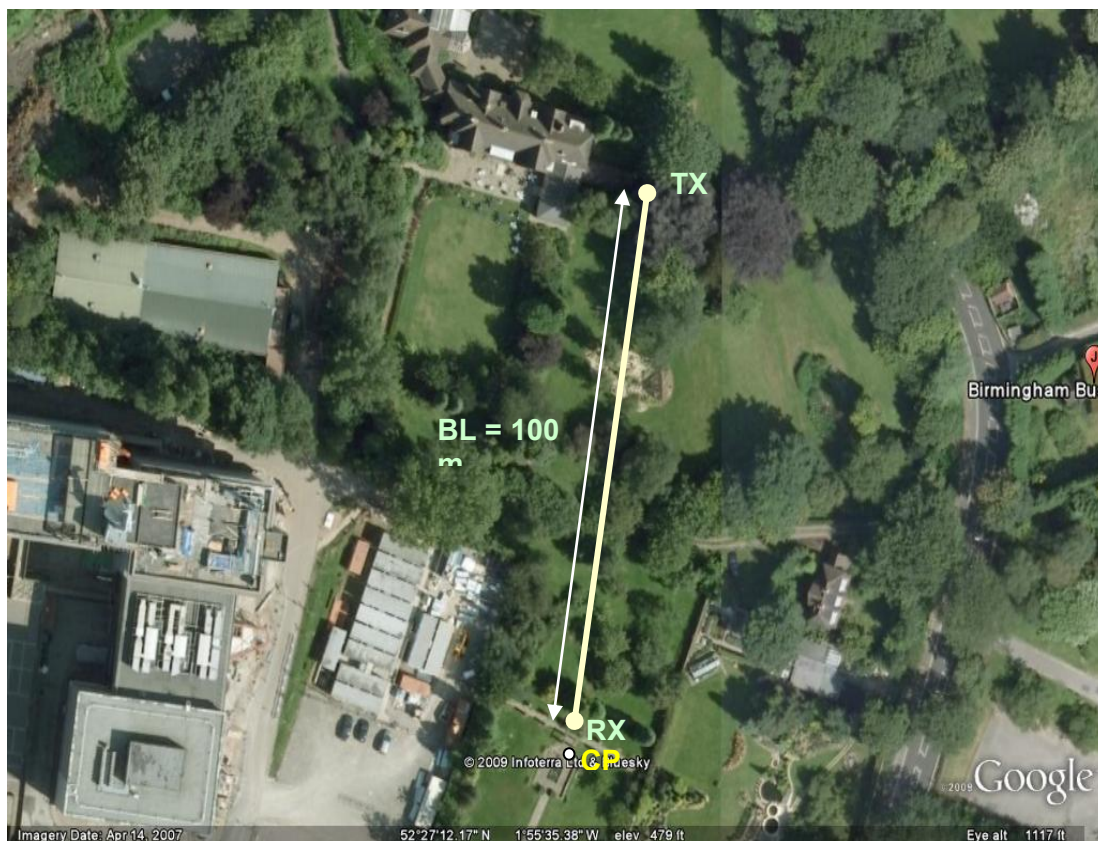
Extra Notes:**4C equipment:****Antennas:**

64 MHz - helical, elevated at 15cm (TX) and 34 cm (RX) above the ground

135 MHz - helical, elevated at 15cm (TX) and 29 cm (RX) above the ground

173 MHz - helical, elevated at 15cm (TX) and 29 cm (RX) above the ground

434.45 - directional, installed 90 cm (TX) and 90 cm (RX) above the ground



5. Example of Short Term Database

All other databases will be in the CD

Task: Short term Measurement

Location: Talesford Airfield (Short Term Measurement)

Date: 12/02/09

Wind Speed: 10-15 km/h

Sampling Freq: 100 Hz


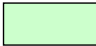
Targets: Human, car (LR); humans in a convoy; cars and human in a convoy

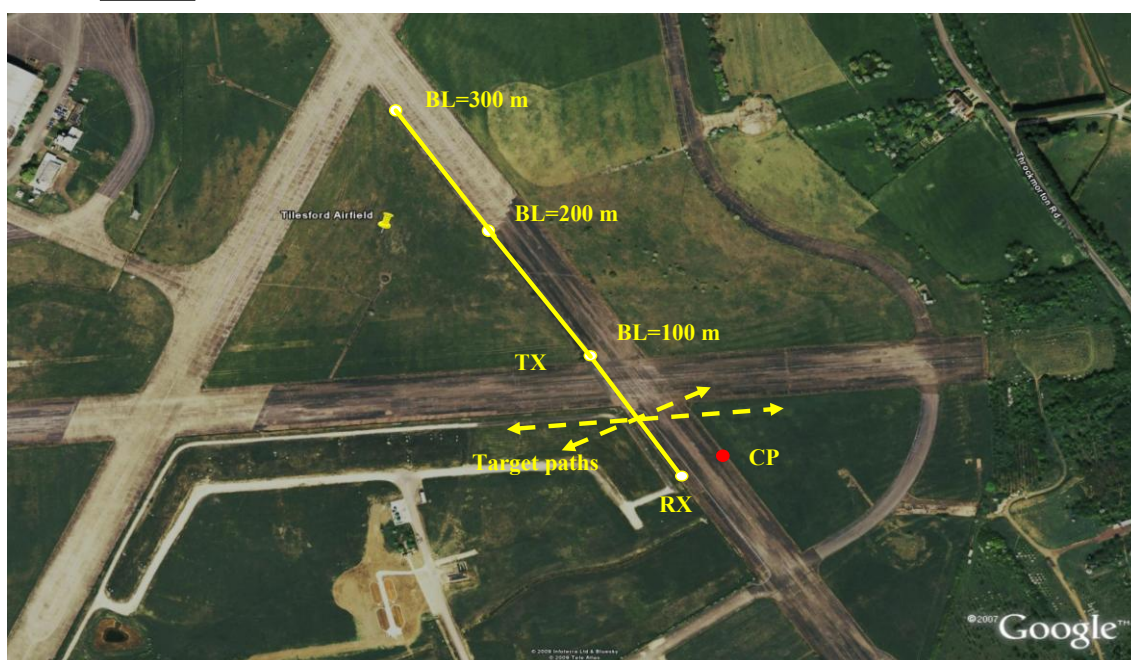
Task: Measure signatures of different moving humans and convoys

File	Descriptions		BL Range (m)	Attenuators (dB)						
				3 Channels (MHz)			4 Channels (MHz)			
	Target	Comments		64.125	434.60 (D)	434.45 (O)	135.05	144.05	151.23	173.28
1	Leakage level (RSSI)	Antennas on ground	100	20 RX	0 and (10+10 ant)	0	Not working	Not working		Not used
2	Human run left	Speed ~ 12km/h	100	20 RX	0 and (10+10 ant)	0			0	
3	Human run right				0 and (10+10 ant)	0			0	
4	Leakage level (RSSI)	4C installed on stools (67 cm add to ant height)	100	20 RX	0 and (10+10 ant)	0			0	
5	Human run left		100	20 RX	0 and (10+10 ant)	0			0	
6	Human run right				0 and (10+10 ant)	0			0	
7	Leakage level (RSSI)	Same as 4, testing the interference from power generator (Switched off)	100	20 RX	0 and (10+10 ant)	0			0	
8	Leakage level (RSSI)	Power generator switched on	100	20 RX	0 and (10+10 ant)	0			0	
9	Leakage level (RSSI)		200	20 RX	0 and (10+10 ant)	0			0	
10	Human run right	100 m target path length	200	20 RX	0 and (10+10 ant)	0			0	
11	Human run left	200 m target path length				0			0	
12	Human walk right	200 m target path length				0			0	
13	Human walk left	100 m target path length				0			0	
14	Human walk right	4C RX&TX installed on stools	200	20 RX	0 and (10+10 ant)	0			0	
15	Human walk left	4C RX&TX installed on stools	200	20 RX	0 and (10+10 ant)	0			0	
16	Human walk right	3C RX&TX installed on stools			0 and (10+10 ant)	0			0	
17	Human walk left	All equipment installed on ground	300	20 RX	0 and (10+10 ant)	0			0	
18	Human walk left	3C RX 4C TX installed on stools	300	20 RX	0 and (10+10 ant)	0			0	
19	Human walk right	3C RX&TX installed on stools			0 and (10+10 ant)	0			0	
20		Unrecognized signal			0 and (10+10 ant)	0			0	
21	2 humans move right	CD=5 m, perpendicular to baseline direction	100	20 RX	0 and (10+10 ant)	0			0	
22	2 humans move left		100	20 RX	0 and (10+10 ant)	0			0	
23	2 humans move right	CD=2 m, perpendicular to baseline direction	100	20 RX	0 and (10+10 ant)	0			0	
24	2 humans move left		100	20 RX	0 and (10+10 ant)	0			0	
25	2 humans move right	CD=10 m, perpendicular to baseline direction	100	20 RX	0 and (10+10 ant)	0			0	
26	2 humans move left		100	20 RX	0 and (10+10 ant)	0			0	
27	2 humans move right	CD=10 m, 60° to baseline direction	100	20 RX	0 and (10+10 ant)	0			0	
28	2 humans move left		100	20 RX	0 and (10+10 ant)	0			0	
29	2 humans move left	CD=5 m, 60° to baseline direction			0 and (10+10 ant)	0			0	
30	2 humans move right				0 and (10+10 ant)	0			0	
31	2 humans move left	CD=2 m, 60° to baseline direction	100	20 RX	0 and (10+10 ant)	0			0	
32	2 humans move right		100	20 RX	0 and (10+10 ant)	0			0	
33	3 humans move left	CD=2 m, 60° to baseline direction	100	20 RX	0 and (10+10 ant)	0			0	

3 humans move right	CD=2+5 m, 60° to baseline direction	100	20 RX	0 and (10+10 ant)	0				0		
3 humans move left	CD=5+5 m, 60° to baseline direction				0				0		
3 humans move right	CD=5+10 m, 60° to baseline direction				0	↓		↓	0		↓
LR + human move right	CD=5 m, 60° to baseline direction	100	20 RX	0 and (10+10 ant)	0	Not working		Not working	0		Not used
LR + human move left	CD=5 m, 60° to baseline direction	100	20 RX	0 and (10+10 ant)	0	↓		↓	0		↓
LR + human move right	CD=10 m, 60° to baseline direction				0	↓		↓	0		↓
LR + human move left	CD=10 m, 60° to baseline direction				0	↓		↓	0		↓

Remarks:

	Channel not in used, loaded by attenuators
	Damaged/ Not working

**Notes:**

[3C \(64-2x434\) - has 3C *.bin in files names](#)

Doppler amplifier gain: 30 dB for all channels (64; 2x434).

Cut-off freq for Doppler hardware **LPF** are (5th order Butterworth) 40 Hz all channels.

Cut-off freq for Doppler hardware **HPF** are (1st order Butterworth): 0.1 Hz (4.7 uF*330 k) all channels.

Antennas: 64 MHz - helical, elevated at 15cm (TX) and 34cm (RX) above the ground
 434.45 - helical, installed 15 cm (TX) and 29 cm (RX) above the ground
 434.60 - directional Yagi with 10 dB attenuator both in RX and TX

[4C \(x-x-151-x\) - has 4C *.bin in files names.](#)

Doppler amplifier gain: 30 dB for all channels (64 2x434, 135, 144, 151, 173).

Cut-off freq for Doppler hardware **LPF** are (5-th order Butterworth) 40 Hz all channels.

Cut-off freq for Doppler hardware **HPF** are (1-th order Butterworth): 0.1 Hz (4.7 uF*330 k) all channels.

Antennas: All channels - helical, elevated 17 cm (both TX and RX).

Channels 135 and 144 MHz are not working.

6. Measurement Data (All data will be in the CD)

Example of measured data in database for long term measurement

Name	Date modified	Type
4LT_1.bin	05-Sep-09 1:08 AM	BIN File
4LT_1_1.bin	22-Aug-09 1:34 AM	BIN File
4LT_1_2.bin	22-Aug-09 1:54 AM	BIN File
4LT_1_3.bin	22-Aug-09 2:14 AM	BIN File
4LT_1_4.bin	22-Aug-09 2:34 AM	BIN File
4LT_1_5.bin	22-Aug-09 2:54 AM	BIN File
4LT_1_6.bin	22-Aug-09 3:14 AM	BIN File
4LT_1_7.bin	22-Aug-09 3:34 AM	BIN File
4LT_1_8.bin	22-Aug-09 3:54 AM	BIN File
4LT_1_9.bin	22-Aug-09 4:14 AM	BIN File
4LT_1_10.bin	22-Aug-09 4:34 AM	BIN File
4LT_1_11.bin	22-Aug-09 4:54 AM	BIN File
4LT_1_12.bin	22-Aug-09 5:14 AM	BIN File
4LT_1_13.bin	22-Aug-09 5:34 AM	BIN File
4LT_1_14.bin	22-Aug-09 5:54 AM	BIN File
4LT_1_15.bin	22-Aug-09 6:14 AM	BIN File
4LT_1_16.bin	22-Aug-09 6:34 AM	BIN File
4LT_1_17.bin	22-Aug-09 6:54 AM	BIN File
4LT_1_18.bin	22-Aug-09 7:14 AM	BIN File
4LT_1_19.bin	22-Aug-09 7:34 AM	BIN File
4LT_1_20.bin	22-Aug-09 7:54 AM	BIN File
4LT_1_21.bin	22-Aug-09 8:14 AM	BIN File
4LT_1_22.bin	22-Aug-09 8:34 AM	BIN File

APPENDIX C

PUBLICATIONS

Synthetic Environment for Forward Scattering Radar Detection

N. A. Zakaria⁽¹⁾, M. Gashinova⁽¹⁾, M. Cherniakov⁽¹⁾


⁽¹⁾ University of Birmingham, Edgbaston, Birmingham, nxz809@bham.ac.uk

Phone: + (44) 121 414 4286, fax: + (44) 121 414 4291

Web: <http://www.eee.bham.ac.uk/misl/>

Abstract

This paper describes an experiment into the use of a Synthetic Environment in a radar acceptance and procurement procedure. The concepts and benefits of using synthetic environment are discussed and a suite of models algorithm which can produce realistic synthetic radar data is described. The experiment involved with real data measurements and modeled signal with added clutter. These two results are compared to see the performance of detection. Non-stationary clutter is modeled in order to obey spectral and probabilistic characteristics of measured clutter in arbitrary environment. For target detection; coherent, quasi-coherent (multi-channel correlation) and non-coherent detection approaches are used.



the 1990s, the number of people in the UK who are employed in the public sector has increased by 1.5 million (from 2.5 million in 1980 to 4 million in 1999). The public sector has become a major employer in the UK, and this has implications for the way in which the public sector is managed and the way in which it is funded.

The public sector is a complex organisation, and it is difficult to understand how it works. This paper aims to provide a brief overview of the public sector in the UK, and to discuss the challenges that it faces. The paper is divided into three main sections: the first section discusses the structure of the public sector, the second section discusses the challenges that the public sector faces, and the third section discusses the ways in which the public sector can be improved.

The public sector is a complex organisation, and it is difficult to understand how it works. This paper aims to provide a brief overview of the public sector in the UK, and to discuss the challenges that it faces. The paper is divided into three main sections: the first section discusses the structure of the public sector, the second section discusses the challenges that the public sector faces, and the third section discusses the ways in which the public sector can be improved.

The public sector is a complex organisation, and it is difficult to understand how it works. This paper aims to provide a brief overview of the public sector in the UK, and to discuss the challenges that it faces. The paper is divided into three main sections: the first section discusses the structure of the public sector, the second section discusses the challenges that the public sector faces, and the third section discusses the ways in which the public sector can be improved.

The public sector is a complex organisation, and it is difficult to understand how it works. This paper aims to provide a brief overview of the public sector in the UK, and to discuss the challenges that it faces. The paper is divided into three main sections: the first section discusses the structure of the public sector, the second section discusses the challenges that the public sector faces, and the third section discusses the ways in which the public sector can be improved.

The public sector is a complex organisation, and it is difficult to understand how it works. This paper aims to provide a brief overview of the public sector in the UK, and to discuss the challenges that it faces. The paper is divided into three main sections: the first section discusses the structure of the public sector, the second section discusses the challenges that the public sector faces, and the third section discusses the ways in which the public sector can be improved.

The public sector is a complex organisation, and it is difficult to understand how it works. This paper aims to provide a brief overview of the public sector in the UK, and to discuss the challenges that it faces. The paper is divided into three main sections: the first section discusses the structure of the public sector, the second section discusses the challenges that the public sector faces, and the third section discusses the ways in which the public sector can be improved.

The public sector is a complex organisation, and it is difficult to understand how it works. This paper aims to provide a brief overview of the public sector in the UK, and to discuss the challenges that it faces. The paper is divided into three main sections: the first section discusses the structure of the public sector, the second section discusses the challenges that the public sector faces, and the third section discusses the ways in which the public sector can be improved.

The public sector is a complex organisation, and it is difficult to understand how it works. This paper aims to provide a brief overview of the public sector in the UK, and to discuss the challenges that it faces. The paper is divided into three main sections: the first section discusses the structure of the public sector, the second section discusses the challenges that the public sector faces, and the third section discusses the ways in which the public sector can be improved.

the 1990s, the number of people in the UK who are aged 65 and over has increased by 1.5 million, and the number of people aged 75 and over has increased by 1.2 million (Office for National Statistics 1999). The number of people aged 85 and over has increased by 0.5 million in the same period.

There is a growing awareness of the need to develop services to meet the needs of the ageing population. The Department of Health (1999) has published a strategy for ageing, which sets out the government's commitment to improve the lives of older people. The strategy is based on three main principles: (1) to ensure that older people have the opportunity to live independently; (2) to ensure that older people have access to the services they need; and (3) to ensure that older people are treated with respect and dignity.

The strategy is based on the following assumptions: (1) that older people are a valuable resource; (2) that older people have the right to live independently; (3) that older people have the right to access the services they need; and (4) that older people should be treated with respect and dignity. The strategy is based on the following principles: (1) to ensure that older people have the opportunity to live independently; (2) to ensure that older people have access to the services they need; and (3) to ensure that older people are treated with respect and dignity.

The strategy is based on the following principles: (1) to ensure that older people have the opportunity to live independently; (2) to ensure that older people have access to the services they need; and (3) to ensure that older people are treated with respect and dignity. The strategy is based on the following principles: (1) to ensure that older people have the opportunity to live independently; (2) to ensure that older people have access to the services they need; and (3) to ensure that older people are treated with respect and dignity.

The strategy is based on the following principles: (1) to ensure that older people have the opportunity to live independently; (2) to ensure that older people have access to the services they need; and (3) to ensure that older people are treated with respect and dignity. The strategy is based on the following principles: (1) to ensure that older people have the opportunity to live independently; (2) to ensure that older people have access to the services they need; and (3) to ensure that older people are treated with respect and dignity.

The strategy is based on the following principles: (1) to ensure that older people have the opportunity to live independently; (2) to ensure that older people have access to the services they need; and (3) to ensure that older people are treated with respect and dignity. The strategy is based on the following principles: (1) to ensure that older people have the opportunity to live independently; (2) to ensure that older people have access to the services they need; and (3) to ensure that older people are treated with respect and dignity.

The strategy is based on the following principles: (1) to ensure that older people have the opportunity to live independently; (2) to ensure that older people have access to the services they need; and (3) to ensure that older people are treated with respect and dignity. The strategy is based on the following principles: (1) to ensure that older people have the opportunity to live independently; (2) to ensure that older people have access to the services they need; and (3) to ensure that older people are treated with respect and dignity.

The strategy is based on the following principles: (1) to ensure that older people have the opportunity to live independently; (2) to ensure that older people have access to the services they need; and (3) to ensure that older people are treated with respect and dignity. The strategy is based on the following principles: (1) to ensure that older people have the opportunity to live independently; (2) to ensure that older people have access to the services they need; and (3) to ensure that older people are treated with respect and dignity.

The strategy is based on the following principles: (1) to ensure that older people have the opportunity to live independently; (2) to ensure that older people have access to the services they need; and (3) to ensure that older people are treated with respect and dignity. The strategy is based on the following principles: (1) to ensure that older people have the opportunity to live independently; (2) to ensure that older people have access to the services they need; and (3) to ensure that older people are treated with respect and dignity.

Empirical Model of Vegetation Clutter in Forward Scatter Radar Micro-Sensors

M. Gashinova, M. Cherniakov, N. A. Zakaria

School of Electronic, Electrical and Computer Engineering
University of Birmingham
Birmingham, United Kingdom
gashinms@bham.ac.uk

V. Sizov

Department of Radio-Electronics
Moscow Institute of Electronic Technology
Moscow, Russian Federation
sizov_vi@rambler.ru

Abstract — Spectral and statistical properties of measured vegetation clutter are analyzed for ground-based forward scatter radar (FSR) sensors operating in VHF/UHF bands employing omni-directional antennas. The empirical computer simulation model of vegetation clutter is proposed.

the 1990s, the number of people in the world who are under 15 years of age has increased by 1.2 billion, from 1.1 billion in 1980 to 2.3 billion in 1999. The number of people aged 15 years and over has increased by 1.1 billion, from 1.1 billion in 1980 to 2.2 billion in 1999.

There are a number of reasons why the world population is growing so rapidly. One of the main reasons is that the number of children born to each woman has increased. In 1980, the average woman in the world had 2.5 children. In 1999, the average woman in the world had 2.7 children.

Another reason why the world population is growing so rapidly is that the number of people who are surviving to old age has increased. In 1980, the average person in the world lived for 55 years. In 1999, the average person in the world lived for 65 years.

There are a number of reasons why the number of people who are surviving to old age has increased. One of the main reasons is that the number of people who are surviving to old age has increased. In 1980, the average person in the world lived for 55 years. In 1999, the average person in the world lived for 65 years.

Another reason why the number of people who are surviving to old age has increased is that the number of people who are surviving to old age has increased. In 1980, the average person in the world lived for 55 years. In 1999, the average person in the world lived for 65 years.

There are a number of reasons why the number of people who are surviving to old age has increased. One of the main reasons is that the number of people who are surviving to old age has increased. In 1980, the average person in the world lived for 55 years. In 1999, the average person in the world lived for 65 years.

Another reason why the number of people who are surviving to old age has increased is that the number of people who are surviving to old age has increased. In 1980, the average person in the world lived for 55 years. In 1999, the average person in the world lived for 65 years.

There are a number of reasons why the number of people who are surviving to old age has increased. One of the main reasons is that the number of people who are surviving to old age has increased. In 1980, the average person in the world lived for 55 years. In 1999, the average person in the world lived for 65 years.

Another reason why the number of people who are surviving to old age has increased is that the number of people who are surviving to old age has increased. In 1980, the average person in the world lived for 55 years. In 1999, the average person in the world lived for 65 years.

There are a number of reasons why the number of people who are surviving to old age has increased. One of the main reasons is that the number of people who are surviving to old age has increased. In 1980, the average person in the world lived for 55 years. In 1999, the average person in the world lived for 65 years.

Another reason why the number of people who are surviving to old age has increased is that the number of people who are surviving to old age has increased. In 1980, the average person in the world lived for 55 years. In 1999, the average person in the world lived for 65 years.

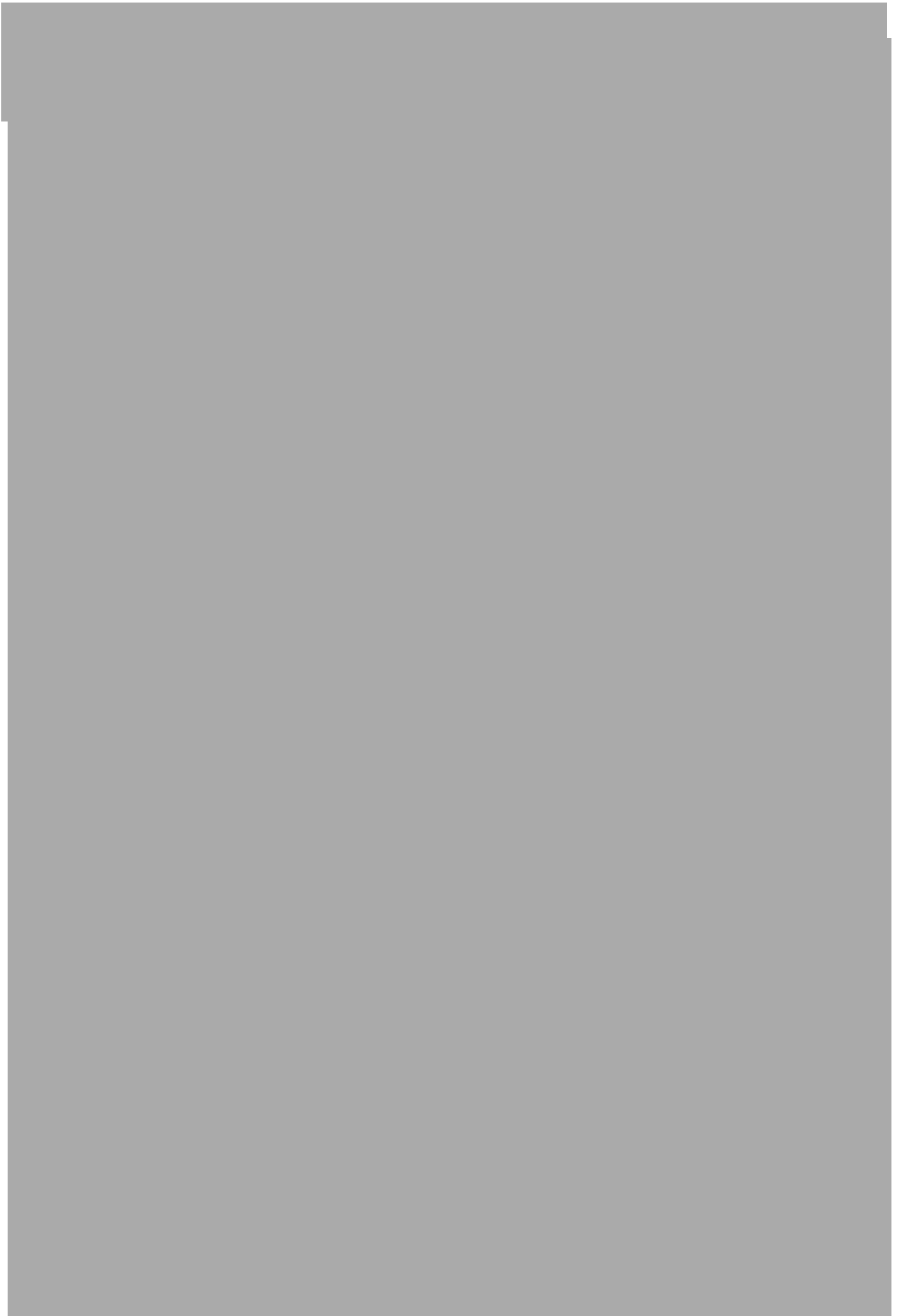
There are a number of reasons why the number of people who are surviving to old age has increased. One of the main reasons is that the number of people who are surviving to old age has increased. In 1980, the average person in the world lived for 55 years. In 1999, the average person in the world lived for 65 years.

Another reason why the number of people who are surviving to old age has increased is that the number of people who are surviving to old age has increased. In 1980, the average person in the world lived for 55 years. In 1999, the average person in the world lived for 65 years.

The first of these is the *Journal of the Royal Society of Medicine*, which was founded in 1849 and is the oldest of the three. It is a peer-reviewed journal that covers a wide range of medical topics, including clinical medicine, public health, and medical law. The journal is published by the Royal Society of Medicine, which is a professional body that represents the interests of the medical profession in the United Kingdom. The journal is known for its high quality and its focus on original research.

The second of the three journals is the *British Medical Journal*, which was founded in 1844. It is a peer-reviewed journal that covers a wide range of medical topics, including clinical medicine, public health, and medical law. The journal is published by the British Medical Association, which is a professional body that represents the interests of the medical profession in the United Kingdom. The journal is known for its high quality and its focus on original research.

The third of the three journals is the *Lancet*, which was founded in 1823. It is a peer-reviewed journal that covers a wide range of medical topics, including clinical medicine, public health, and medical law. The journal is published by the Lancet Publishing Group, which is a professional body that represents the interests of the medical profession in the United Kingdom. The journal is known for its high quality and its focus on original research.



Empirical Clutter Analysis for Forward Scatter Micro-Sensors

N. A. Zakaria

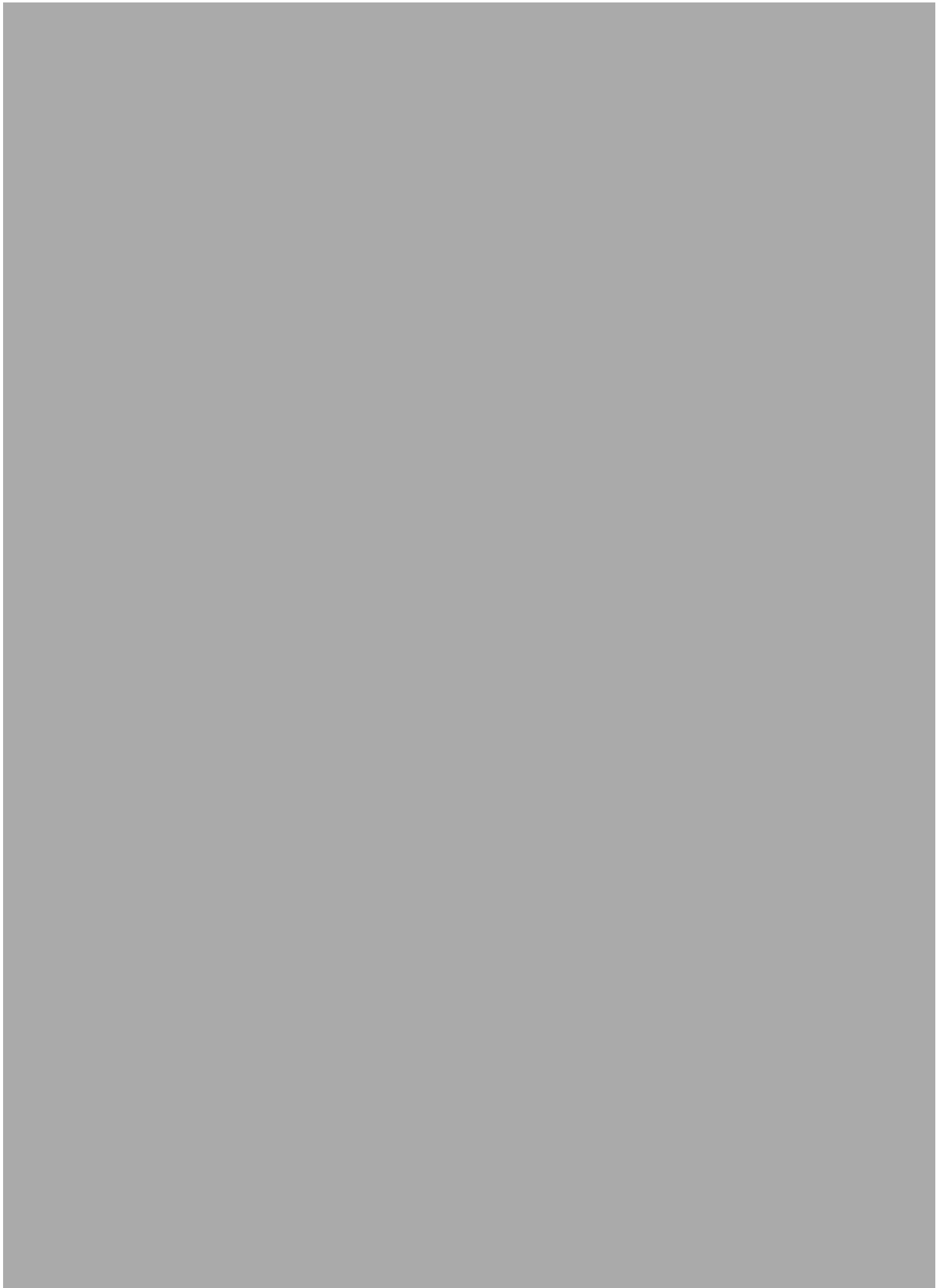
Faculty of Electrical Engineering
University of Technology MARA,
Shah Alam, Selangor, Malaysia
norayu713@salam.uitm.edu.my

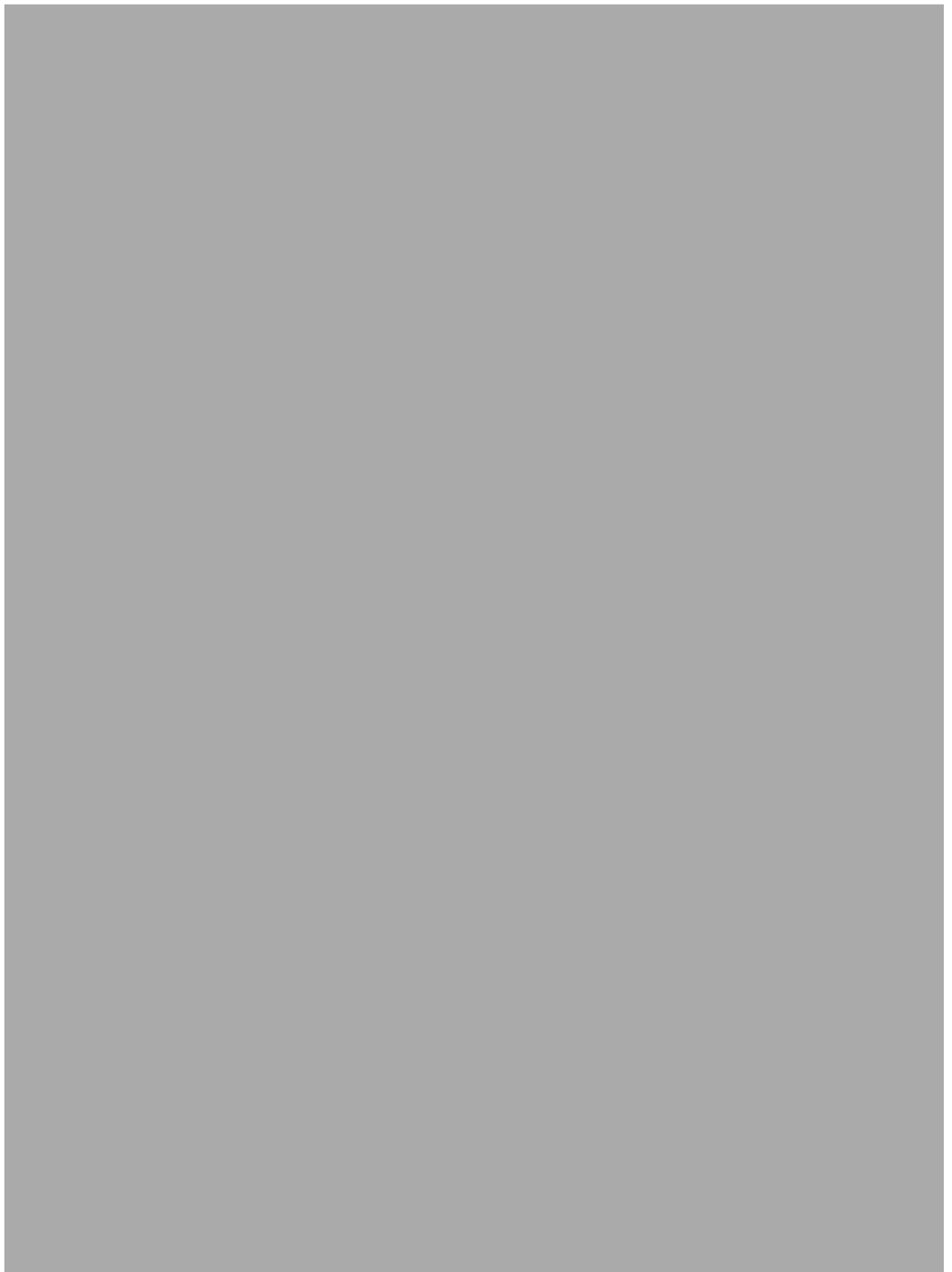
M.Cherniakov, M. Gashinova, V. Sizov

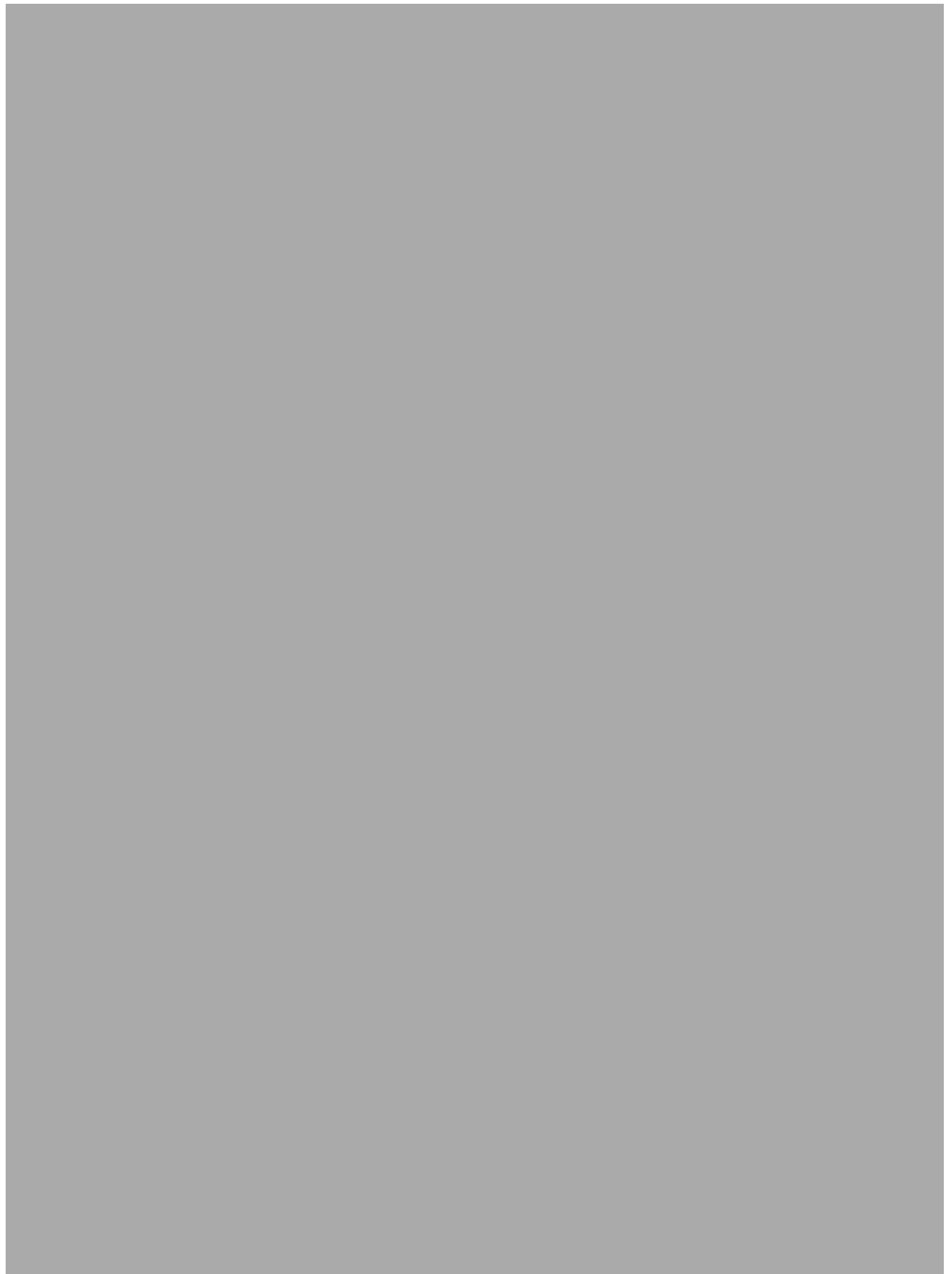
School of Electronic, Electrical and Computer Engineering
University of Birmingham
Birmingham, United Kingdom
gashinms@bham.ac.uk

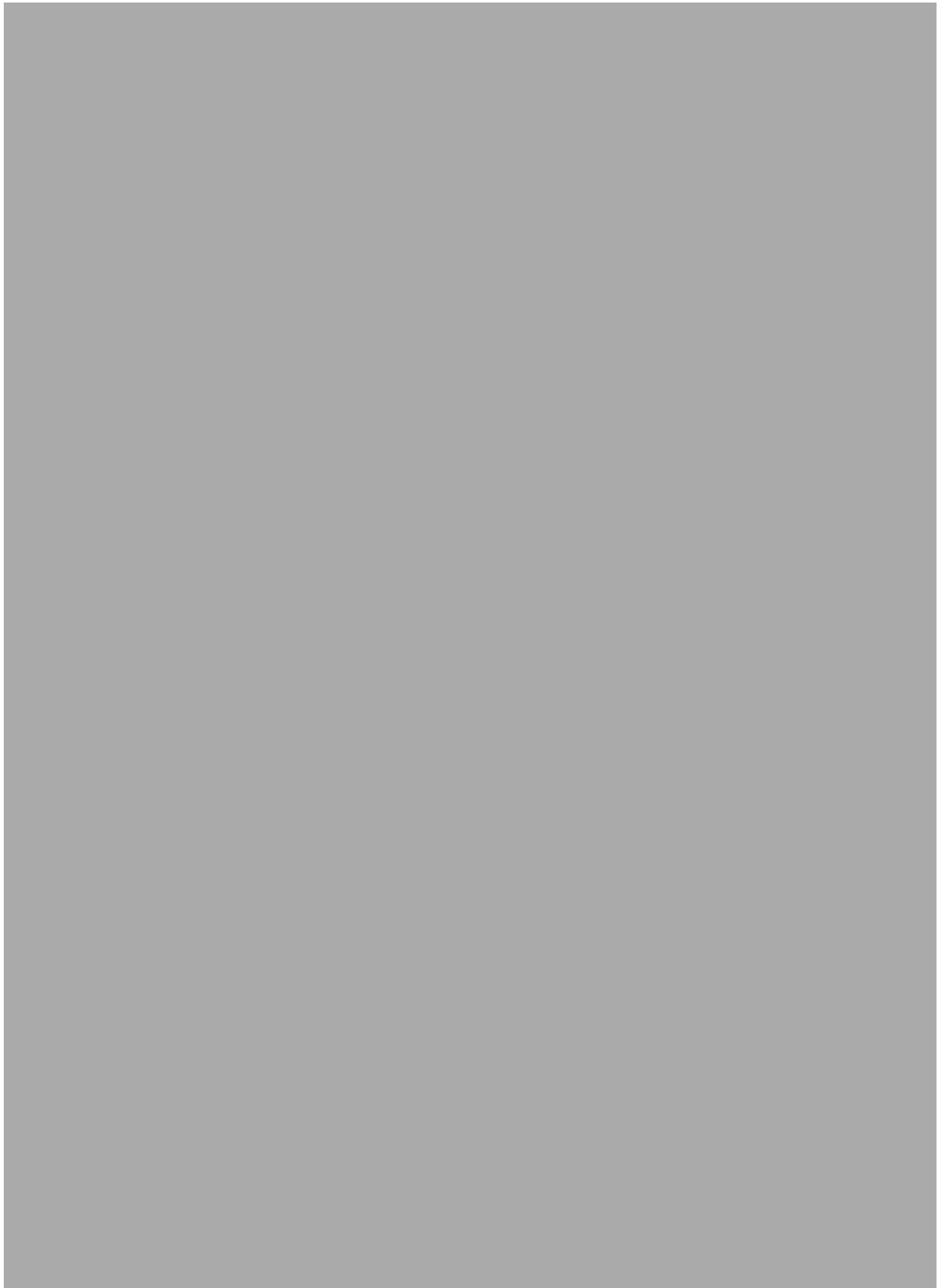
Abstract— Vegetation clutter is a significant factor that limit the performance of ground-based Forward Scatter Radar. The clutter experimental and statistical analysis of Forward Scatter Micro-sensors is presented in this paper. The analysis involved different parameters: different operating frequencies, wind speed and different baseline length to see the effect of the parameters to clutter. The clutter characteristics are then discussed.

Keywords— clutter, FSR, VHF/UHF, radar









Signal Detection in Multi-Frequency Forward Scatter Radar

M. Gashinova^{*1}, V. Sizov^{#2}, N.A.Zakaria^{*3}, M. Cherniakov^{*4}

Figure 1. ^{*}*School of Electronic, Electrical and Computer Engineering*

Figure 2. *University of Birmingham*

Figure 3. *Birmingham, United Kingdom*

¹gashinms@bham.ac.uk

⁴cherniam@bham.ac.uk

Figure 4. [#]*Department of Radio-Electronics*

Figure 5. *Moscow Institute of Electronic Technology*

Figure 6. *Moscow, Russian Federation*

²sizov_vi@rambler.ru

Abstract — The peculiarity of Forward Scatter Radar (FSR) is the absence of range resolution. As a consequence, possible low signal-to-clutter ratio is the most limiting factor in FSR detection. In this paper we will discuss non-coherent and coherent FSR Doppler signal processing and consider an alternative cross-correlation approach, which could be called 'quasi-coherent' processing. Multi-frequency radar enables correlation of Doppler output from two different channels which can be considered as the matching waveform, or the reference signal, to the first signal. This leads to a compression of the FSR return by cross-correlation with enhanced processing gain, and, consequently, enhanced detection.

